Cryogenic Surface Electrode Ion Traps with Integrated Superconducting Microwave Resonators for Polar Molecular Ion Spectroscopy

by

Paul Bogdan Antohi

M.S. Physics
Case Western Reserve University, 2004

S.B. Physics
Alexandru Ioan Cuza University, 1999

Submitted to the Department of Physics
in partial fulfillment of the requirements for the degree of

Doctor of Philosophy in Physics

at the

MASSACHUSETTS INSTITUTE OF TECHNOLOGY

June 2011

Author .....
Department of Physics
May 23, 2011

Certified by .....
Isaac L. Chuang
Professor of Physics and
Professor of Electrical Engineering and Computer Science
Thesis Supervisor

Accepted by .....
Krishna Rajagopal
Professor of Physics, Associate Head for Education

Cryogenic Surface Electrode Ion Traps with Integrated Superconducting Microwave Resonators for Polar Molecular Ion Spectroscopy

by

Paul Bogdan Antohi

Submitted to the Department of Physics
on May 23, 2011, in partial fulfillment of the
requirements for the degree of
Doctor of Philosophy in Physics

Abstract

Trapped cold molecules open the possibility of studying ultracold chemistry and astrophysical processes in laboratory settings. Their rich internal structure also makes them suitable for quantum information manipulation or for tests of fundamental laws of nature. These experiments require precise control over the molecular internal degrees of freedom. There are few present proposals for trapping and cooling molecules. One proposal is based on confining neutral polar molecules in DC Stark shift traps, but this approach presents some issues. An attractive alternative is to confine polar molecular ions in RF Paul ion traps, which is the focus of this thesis.

The objectives here are to develop the theoretical models and to devise the experimental components and methods to investigate the coupling of polar molecular ions' rotational states to the microwave radiation. The new approach presented here is based on co-trapping Sr^+ atomic ions together with $SrCl^+$ molecular ions in a cryogenic surface electrode RF ion trap and on using the coupling of the molecular ion's rotational states to an integrated superconducting microwave line or cavity either as a cooling method or for precise rotational spectroscopy.

The first part of the thesis describes two theoretical methods for observing the coupling of the microwave radiation to the rotational levels of a molecule. The first method proposed is based on the enhancement of the molecular rotational transition rates by the co-trapped molecular-atomic ions Coulomb collisions. The second method is based on microwave cavity assisted heating or cooling of the molecular ions. The second part of the thesis presents the development of a cryogenic surface electrode RF ion trap with an integrated microwave transmission line/resonator. The ion trap is operated in a 4.2 K closed cycle cryostat.

Thesis Supervisor: Isaac L. Chuang
Title: Professor of Physics and
Professor of Electrical Engineering and Computer Science

Acknowledgments

This thesis would not have been possible without the support of many people at MIT. I thank my advisor, Professor Isaac Chuang, for his tremendous support. Working in his lab has been an invaluable learning experience. I appreciated the opportunity to work on both the theoretical and experimental aspects of my project. I am also grateful to Ike for his continuous efforts to secure the funds essential for the lab. Furthermore, I really appreciate his high standards in the communication of scientific information, as they have been very valuable in my training to write and speak about physics. I also want to thank all members of my committee, including Professor Vladan Vuletic and Professor Pablo Jarillo-Herrero, for their great insights and feedback on my project.

I owe a lot to my lab mates. I thank Waseem Bakr for bringing me up to speed on the workings of the lab and for his assistance in setting up the first cryogenic ion trapping system in the lab. Robert Clark has been a great colleague and friend to have around. I thank him for his design of the trap on which I made the first forays into my project. I appreciate our conversations over the years. His humor has lightened many long days of work in the lab. In addition, I learned a lot about the hardware side of lasers through my conversations with Jaroslaw Labaziewicz and by studying the lasers that he built. David Schuster was instrumental in our collaboration on setting up the first stages of the experiment described in this thesis. I thank Stephan Schulz for his help in investigating the first Nb based superconducting microwave resonators in our lab. I am very grateful to Yufei Ge for her help on the trap wirebonding and in fabricating the traps used at the beginning of this project, and to Adam McCaughan for building the later Nb surface electrode ion traps, which were essential for this project. I thank David Meyer for his help in setting up the microwave delivery components. I thank Anders Mortensen and Arolyn Conwill for their help in a series of calculations and experimental measurements of the cryostat heat loading.

I thank my mom and dad for their encouragements and tremendous support from the early beginnings of my interests in science. I dedicate this thesis to them.

Contents

List of Figures

List of Tables

Chapter 1

Introduction

1.1 Cold polar molecules

1.1.1 Why polar molecular ions?

Molecules have a rich internal structure which makes them suitable candidates for, among others, quantum information manipulation [ADD+06, DeM02, RDD+06], tests of the fundamental laws of nature [DCM+08, ZKY08], or low temperature chemical reactions [CDKY09, HTS+06]. A key factor in the realization of any of these experiments is the precise control over the molecular internal degrees of freedom, which in most cases requires ultracold molecules in their internal ground state. One difficulty in producing ultracold molecules is that most molecules do not possess closed optical transitions and, as such, well established laser cooling techniques are inapplicable.

Cold polar molecules in their electronic and vibration ground states are particularly attractive for quantum information manipulation. They posses very long (100's of days) life time rotational states, that make them suitable candidates as quantum memory. Their high permanent electric dipole moment ($\sim$10 Debye) permits to strongly couple their rotational transitions to microwave fields in general and to microwave cavities in particular, and opens the possibility to use microwave circuits as quantum data buses. Present proposals for using the rotational levels

as memory qubits are based on neutral polar molecules confined in DC Stark shift traps [ADD+06, DeM02, RDD+06]. Confining neutral molecules in DC Stark shift traps presents a series of issues: a) the traps have low trap depths ($\sim 10^{-5}$ eV) which requires a source of translationally cold molecules, b) only the low field seeking states are trapped conducing to a loss of trapped molecules, and c) the trapped states are dephased by the trapping fields.

The molecular ions present an attractive alternative to neutral molecules, as some difficulties associated with manipulating neutral molecules are not significant for molecular ions. Ions in any internal state can be easily trapped in RF Paul traps with trap depths of the order of 1 eV [KRS07, OZW+06]. Moreover, in RF Paul traps, the ion internal degrees of freedom are not directly involved in the trapping process. Since RF Paul traps can trap concomitantly few species of ions, the molecular ions are sympathetically cooled by Doppler cooled co-trapped atomic ions. Experiments have shown that in cold mixed ion Wigner crystals the molecular ions internal degrees of freedom decouple from the external motion and reach thermal equilibrium with the surrounding black body radiation [BJD06, KRS07]. Therefore the internal cooling must be addressed separately. Trapping in a cryogenic environment is the most straightforward approach.

1.1.2 Cooling of neutral and ionic molecules

Over the past decade many approaches for preparing cold neutral or charged molecules have been developed. In the case of the neutral molecules, most cooling techniques have been concentrated in the following areas: Stark deceleration [BBM99, HBL+04, SHMvdM09], photoassociation of laser cooled atoms [LHP+93, MCH93, SSBD05], and buffer gas cooling [DFKP95, WdG+98]. More recently, a laser cooling method for strontium monofluoride has been demonstrated experimentally [SBD10]. The Stark deceleration and the laser cooling methods are capable of cooling only the translational motion of the neutral molecules. The photoassociation is applicable only when the constituent atoms can be laser cooled individually. The buffer gas cooling technique has the advantage of being applicable to any molecule, while cooling both

the external and the internal degrees of freedom, although not to the ground state of a typical molecule.

For cooling the molecular ions, several methods have also been developed and perfected. The most successful approach to date, has been the sympathetic cooling of the molecular ions through the Coulomb interaction with co-trapped laser-cooled atomic ions. The sympathetic cooling allows for the molecular ions to reach motional temperatures in millikelvin range [MD00, DMM$^+$04, BRF$^+$05, OZW$^+$06], with the highly localized co-trapped ions forming Wigner crystals. However, in the sympathetic cooling method, the molecular ion's internal degrees of freedom remain mostly unaffected, since due to the Coulomb repulsion, the co-trapped atomic ions cannot interact with molecular ions at sufficiently short range [BJD06, KRS07]. As in the case of neutral molecules, buffer gas cooling is another method which can be applied to molecular ions also, yet the final internal and external temperatures that can be reached are limited to the kelvin range [POHDL95, Ger95]. In order to address the the problem of cooling the molecular ions to their internal ground states a few schemes based on direct optical cooling have been proposed [VMD02, VMD04b, VMD04a]. Recently, two of these optical cooling methods have been demonstrated experimentally. In one method based on optical pumping with two continuous wave lasers, hydrogen deuteride molecular ions trapped in a room temperature system have been cooled to a rovibrational ground-state population of 78%, corresponding to an internal temperature of 26 K [SRD$^+$10]. In the other method using a laser cooling scheme based on excitation of a single rovibrational transition, MgH^+ molecular ions sympathetically cooled by co-trapped Mg^+ atomic ions had their rovibrational ground-state population increased 15 fold, which corresponds to a drop in their internal temperature from 300 K to 20 K [SHS$^+$10].

1.2 Contributions of this work

The objectives of this thesis are to develop the theoretical models necessary to investigate the coupling of polar molecular ions rotational states to the microwave

radiation, and to devise the experimental components and methods necessary to accomplish these goals. The new approach I present here is based on co-trapping Sr^+ atomic ions together with $SrCl^+$ molecular ions in a cryogenic surface electrode RF ion trap, and to use the coupling of the molecular ion's rotational states to the integrated superconducting microwave line or cavity either as a cooling method or for precise rotational spectroscopy.

1.2.1 Theoretical work

In order to observe the microwave coupling, two issues must be addressed first. Since the polar molecular ions have no closed optical transitions their internal states cannot be detected directly. The second issue is that the long lived rotational states make any coupling signal vanishingly small. A method which solves the detection problem is to couple rotational states to the translational motion of the molecular ions and to use sympathetic heating spectroscopy [CGD+10, DMM+04] to monitor the translational temperature of the molecular ions and, implicitly, their internal rotational states. In sympathetic heating spectroscopy a mixture of co-trapped atomic ions and molecular ions due to strong Coulomb interactions reaches thermal translational equilibrium and the temperature of the ion ensemble is monitored with laser induced florescence (LIF) on the atomic ions.

To address the second detection issue, the molecular rotational transition rates must be increased to experimentally manageable values for which I envision two approaches. One method is based on the fact that in a mixed ion cloud the non-radiative molecular rotational transition rates are enhanced by Coulomb collisions taking place between the co-trapped molecular and atomic ions. In this approach a mixed ion cloud of Sr^+ and $SrCl^+$ is trapped in a surface electrode ion trap with integrated microwave transmission line. Due to Coulomb collisions between atomic and molecular ions, the molecular rotational populations are thermalized to the ion cloud external degrees of freedom through non-radiative rotational transitions. The first rotational transition of the molecular ions is excited with microwave radiation and produces a population inversion among the first two rotational levels, which leads

to the ion cloud heating, while the temperature is monitored through the laser induced fluorescence on the atomic ions.

In the second method, the molecular ions trapped in the presence of a microwave cavity have their radiative transition rates enhanced by the cavity Purcell factor. In a CPW based superconducting microwave cavity the electromagnetic field can be confined to a very small volume compared with its physical dimensions ($\sim 10^{-6}$), which in conjunction with its high quality factor ($\sim 10^6$), puts the vacuum Rabi frequency in kHz range. In the mixed ion crystal of Sr^+ and $SrCl^+$ trapped in a surface electrode ion trap with integrated microwave cavity, the rotation levels of the molecular ions are modulated by the harmonic motion of the ions (side bands). The molecular ions are pumped with microwave radiation tuned on the first red rotational side band transition, while the microwave cavity is tuned on the natural rotational transition frequency the molecular ions. In each such excitation - de-excitation cycle the molecular ions gain one translational phonon, thus increasing the ion crystal temperature. Again, the co-trapped atomic ions are used to monitor the Wigner crystal temperature.

1.2.2 Experimental work

The hardware side of the experiment requires to develop a RF Paul trap with an integrated microwave transmission line/ resonator. Specifically, for this experiment I design a surface electrode ion trap with the ground electrode acting as a microwave coplanar waveguide, a trap which I operate in a 4.2 K closed cycle cryostat [ASA+09]. The planar aspect of this trap has two advantages compared with other geometries: the ion traps are fabricated in house with lithographic methods, and the good thermal contact to the cryostat cold head allows us to implement high-Q superconducting microwave cavities. As polar molecular ion I use $SrCl^+$ which has a theoretical permanent electric dipole of 9.6 Debye, and the first rotational transition frequency of 6.52 GHz [Gau]. To sympathetically cool the molecular ions and monitor their temperature I use Sr^+, which can be laser cooled with commercially available diode lasers [LRB+07]. Both the atomic and the molecular ions are produced through the

laser ablation of a $SrCl_2$ target.

1.3 Thesis outline

The reminder of this thesis explores the experimental and theoretical aspects involved in the microwave spectroscopy of polar molecular ions confined in cryogenic surface electrode RF ion traps.

Chapter 2 introduces two of the main experimental components: the RF ion traps and the microwave cavities. It begins with an overview of various RF ion trap geometries capable of supporting integrated microwave transmission lines or cavities. The second part of the chapter reviews the theory of ion confinement in RF quadrupole traps, and also addresses practical aspect of numerical modeling of the RF ion traps properties. The chapter concludes with a theoretical description at the classical level of CPW based microwave resonators.

Chapter 3 presents the theoretical analysis of the two microwave - molecular ion coupling detection methods proposed anterior. The chapter begins with a review of the atomic and molecular structures, and the principles of laser cooling and detection. The reminder of the chapter is dedicated to an in depth study of the trapped polar molecular ions dynamics in the two cases: in the presence of atom - molecule Coulomb collisions, and in the presence of a microwave cavity.

Chapter 4 describes the experimental setup built around a closed cycle cryostat capable of reaching 4.2 K temperatures. The components and the particular requirements necessary to build a cryogenic ion trapping system are presented in the first part of the chapter, while in the second part I describe a cryogenic compatible atomic and molecular ion source based on a laser ablation method.

Chapter 5 presents in detail the surface electrode ion trap with integrated CPW microwave resonator. It starts with a review of various ion trap geometries I investigated experimentally before deciding on a surface electrode ion trap design. The main part of the chapter describes the surface electrode ion trap design and fabrication, and a number of experimental issues as electrical shorting and charging. The chapter

concludes with the experimental characterization of the surface electrode ion traps.

Chapter 6 concludes the thesis with a summary of the results and with an outlook on future experiments.

1.4 Co-workers contribution and published results

While most of the work presented in this thesis it is my own contribution, many colleagues assisted me in this project. The surface electrode ion trap (Bastille), in which I showed that loading molecular ions by laser ablation is possible, was design by Robert Clark, a former Ph.D. student in our group. Another two former post-docs in our group helped with the project along the way: David Schuster developed the microwave slot line based ion trap, while Stephan Schulz designed the microwave strip (plate) line based ion trap, both of which are presented in Chapter 5. With very few exceptions, the niobium surface electrode ion traps were fabricated by Ph.D. students Adam McCaughan and David Meyer, who are still currently involved in the project. Towards the end of my work on this project, two more members joined the project. The post-doc Anders Mortensen helped with the calculations of the cryostat heat loads, while the Ph.D. student Arolyn Conwill provided some of the experimentally measured heat loads.

Below is a list of publications I have co-authored during my Ph.D. work.

1. David R. Leibrandt, Robert J. Clark, Jaroslaw Labaziewicz, *Paul B. Antohi*, Waseem Bakr, Kenneth R. Brown, and Isaac L. Chuang, Laser ablation loading of a surface-electrode ion trap, PHYSICAL REVIEW A, 76, 055403 (2007).

2. Jaroslaw Labaziewicz, Yufei Ge, *Paul B. Antohi*, David Leibrandt, Kenneth R. Brown, and Isaac L. Chuang, Suppression of Heating Rates in Cryogenic Surface-Electrode Ion Traps, PHYSICAL REVIEW LETTERS, 100, 013001 (2008).

3. *Paul B. Antohi*, David Schuster, Gleb M. Akselrod, Jaroslaw Labaziewicz, Yufei Ge, Ziliang Lin, Waseem S. Bakr, and Isaac L. Chuang, Cryogenic ion trapping

systems with surface-electrode traps, REVIEW OF SCIENTIFIC INSTRUMENTS, 80, 013103 (2009).

Chapter 2

Ion traps with integrated microwave resonators

This chapter starts by introducing a few trap geometries capable of supporting integrated microwave transmission lines or resonators and also gives a theoretical overview of the two trap components. The second part reviews the principles of ion trapping in RF quadrupole traps, and addresses the practical problem of numerical modeling of the ion trap behavior. In the final section, I present the theoretical description of the microwave resonators based on coplanar waveguides (CPW).

2.1 RF ion traps with integrated microwave resonators

There are various designs for microwave resonators, but particularly suitable for integration with RF ion traps are those based on microwave transmission lines. Three easy geometries to implement are constructed around the slot line, strip line, and coplanar waveguide microwave transmission lines [Wad91, Sim01, MYJ80]. The slot line and strip line based RF ion traps are three dimensional structures, while the CPW based RF ion trap has a two dimensional structure, although all three designs operate on the principles of the surface electrode ion traps. Unlike the three dimensional

ion traps, the surface electrode ion traps contain all the electrodes in a single plane. Surface electrode ion traps were first suggested by by Chiaverini *et al.* [CBB+05] and subsequently implemented by several groups [PLB+06, SCR+06].

All the RF ion traps with integrated microwave transmission lines presented in the following, were design and fabricated at MIT. For internal bookkeeping, most of the trap designs we fabricate in our lab receive names.

2.1.1 Slot line RF ion trap (Azkaban traps)

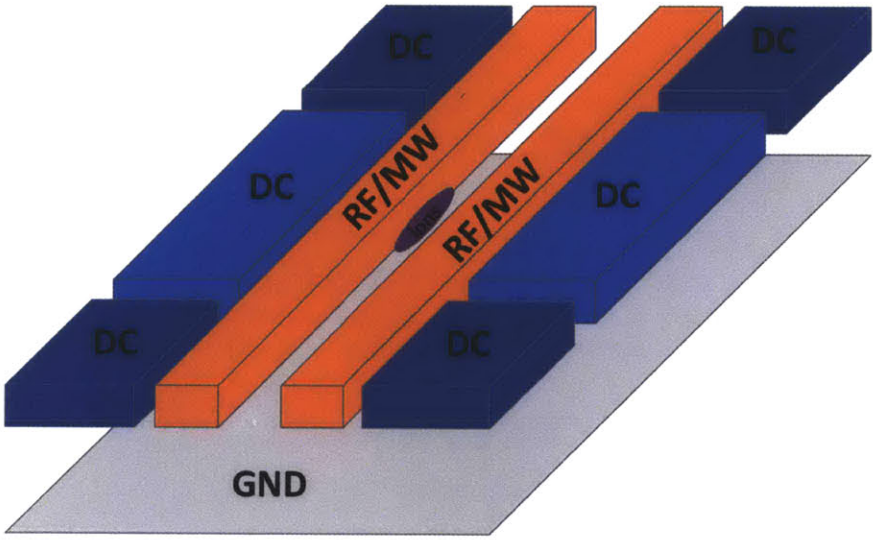

Figure 2-1: RF ion trap with integrated microwave slot transmission line (Azkaban trap series).

The slot line ion trap (Figure 2-1) has a two layer structure (Azkaban trap series). The top layer contains the microwave slot line and the main ion trap electrodes. The bottom layer acts as ground electrode and aids in ion confinement. The spacing between the two layers determines the ion position along the normal to the ion trap plane, and as such the ion position can be adjusted at will. In order to operate the slot line RF ion trap it is necessary to mix the RF trapping voltage with the microwave signal, which in practice becomes quite challenging.

2.1.2 Strip line RF ion trap

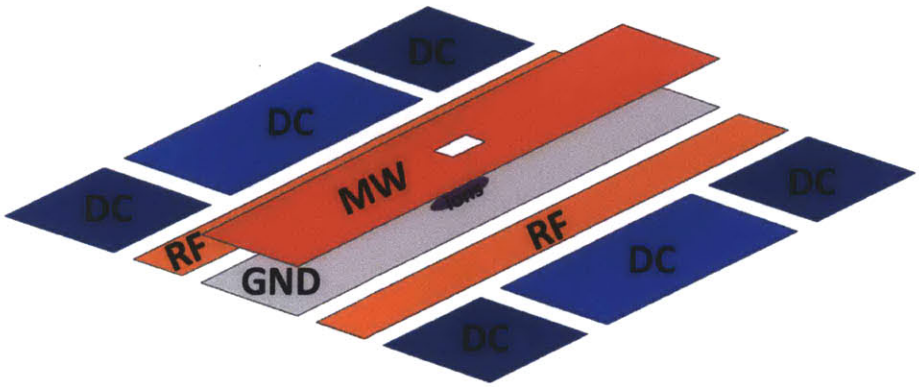

Figure 2-2: Rf ion trap with integrated microwave strip transmission line. The pinhole in the microwave electrode allows for ion imaging.

The strip line ion trap is another two layer ion trap design. This geometry eliminates the problem encounter in the slot line ion trap by keeping the ion trap electrodes separated from the microwave transmission line. The top layer contains only a rectangular shaped microwave electrode, while the bottom layer contains the ion trap (Figure 2-2). In order to allow for the trapped ions imaging the microwave electrode includes a pinhole, which size is matched to the numerical aperture of the imaging system. The strip line RF ion trap presents a number of problems with the ion loading and ion imaging. But most important issue with both slot line and strip line RF ion trap structures is that the microwave electrodes cannot be efficiently thermally sunk to the cryogenic substrate, thereby making the the superconducting regime very difficult to achieve.

2.1.3 CPW line RF ion trap (Giants traps)

The CPW RF ion trap is a single layer structure, where all the trap and microwave electrodes electrodes lay in one single plane as shown in Figure 2-3 (Giants trap series). In this geometry the central DC electrode together with the two lateral RF electrodes naturally form a coplanar waveguide structure (CPW), which can be used

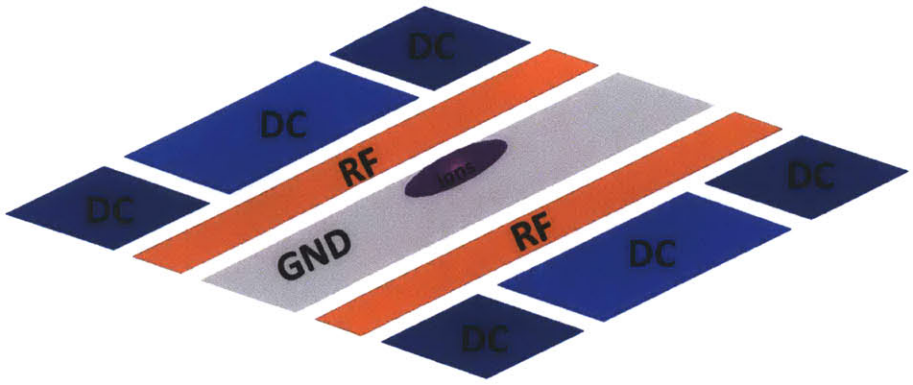

Figure 2-3: RF ion trap with integrated microwave coplanar waveguide (Giants trap series).

for microwave radiation delivery (Figure 2-4). An RF ion trap built around a CPW alleviates all the problems presented by the previous two structures, with the added benefit that it can be developed in house with well established lithographic techniques. All three trap designs will be presented again in more detail in Chapter 4.

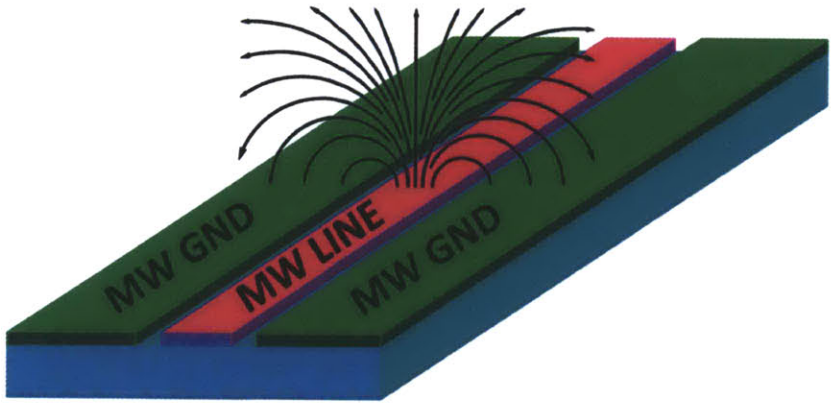

Figure 2-4: Microwave electric field distribution above a CPW transmission line.

2.2 Theory of ion trapping in RF quadrupole traps

Earnshaw's theorem forbids the trapping of the ions in a stable configuration with just static electric fields. With a combination of static and RF electric fields is possible to form a dynamically stable trap for charged particles. The theory of the RF ion

traps has been covered in depth in many publications before [Gho96, MGW05]. Here I review only the main mathematical results concerning the ion confinement in RF ion traps.

2.2.1 Mathieu equations and the adiabatic approximation

Consider a charged particle of mass m and charge Q interacting with a set of DC and RF electric quadrupole fields (Figure 2-5). Assuming that the particle trajectory is confined around the saddle points of the two fields, the corresponding electric potentials can be approximated by series expansion up to the second order in coordinates around the saddle points:

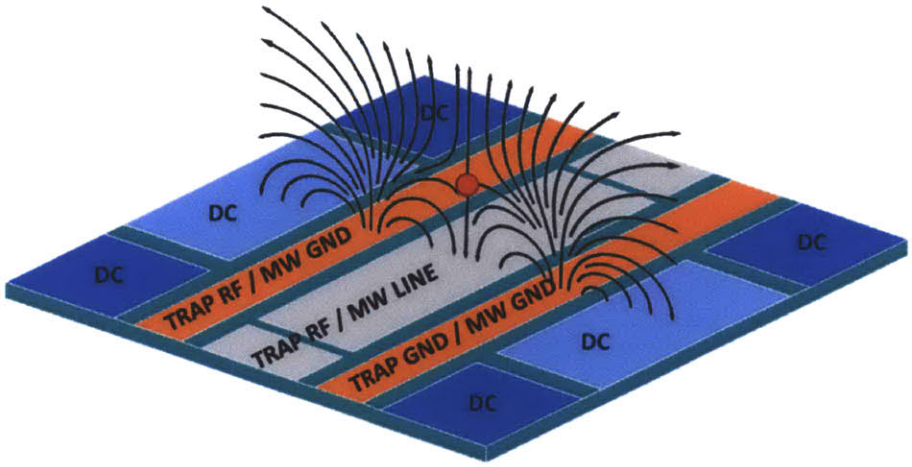

Figure 2-5: RF electric field distribution in a surface electrode ion trap. The ions are trapped at the RF field null (red dot).

$$\Phi_{\mathrm{DC}}(\vec{x}) \simeq U_0 \left(1 + \sum_{i=1}^{3} a_i^{\mathrm{DC}} x_i + \sum_{i,j=1}^{3} b_{\mathrm{ij}}^{\mathrm{DC}} x_i x_j + \ldots\right), \tag{2.1a}$$

$$\Phi_{\mathrm{RF}}(\vec{x}, t) \simeq V_0 \left(1 + \sum_{i=1}^{3} a_i^{\mathrm{RF}} x_i + \sum_{i,j=1}^{3} b_{\mathrm{ij}}^{\mathrm{RF}} x_i x_j + \ldots\right) \cos(\Omega \mathrm{t}), \tag{2.1b}$$

where Ω is the RF field angular frequency. If the saddle points of the two fields coincide (experimentally known as compensation) and taking them as the coordinates system origin, the linear terms in the series expansions become zero ($\partial_i \Phi(\vec{x})\,|_{x_j=0} = 0$, $\forall$i,j):

$$\Phi_{\mathrm{DC}}(\vec{x}) \simeq U_0 \left(1 + \sum_{i,j=1}^{3} b_{\mathrm{ij}}^{\mathrm{DC}} x_i x_j + \ldots\right), \tag{2.2a}$$

$$\Phi_{\mathrm{RF}}(\vec{x}, t) \simeq V_0 \left(1 + \sum_{i,j=1}^{3} b_{\mathrm{ij}}^{\mathrm{RF}} x_i x_j + \ldots\right) \cos(\Omega \mathrm{t}). \tag{2.2b}$$

We note that, without loss of generality, the coefficients b can be taken to be symmetric under the permutation of their indices, and thus forming two real symmetric traceless matrices (traceless because $\nabla^2 \Phi(\vec{x}) = 0$). With the above expressions for the potentials (2.2) the motion of the charged particle is described by the Lagrangian:

$$L = \frac{m}{2} \sum_{i=1}^{3} \dot{x}_i{}^2 - QU_0 \left(1 + \sum_{i,j=1}^{3} b_{\mathrm{ij}}^{\mathrm{DC}} x_i x_j + \ldots\right) - QV_0 \left(1 + \sum_{i,j=1}^{3} b_{\mathrm{ij}}^{\mathrm{RF}} x_i x_j + \ldots\right) \cos(\Omega \mathrm{t}), \tag{2.3}$$

from which the equations of motion are readily determined:

$$m\ddot{x}_i + 2\mathrm{QU}_0 \sum_{j=1}^{3} b_{\mathrm{ij}}^{\mathrm{DC}} x_j + 2\mathrm{QV}_0 \sum_{j=1}^{3} b_{\mathrm{ij}}^{\mathrm{RF}} x_j \cos(\Omega \mathrm{t}) = 0, \; i = 1, 2, 3. \tag{2.4}$$

The system of differential equations (2.4) can be decoupled only if the two matrices $\left\{b_{\mathrm{ij}}^{\mathrm{DC}}\right\}$ and $\left\{b_{\mathrm{ij}}^{\mathrm{RF}}\right\}$ commute, i.e the DC and RF potentials bilinear expansions have the same principal axes. Assuming that the commutation condition is satisfied, after the diagonalization of b matrices the equations of motion (2.4) become:

$$m\ddot{X}_i + 2\mathrm{QU}_0 b_i^{\mathrm{DC}} X_i + 2\mathrm{QV}_0 b_i^{\mathrm{RF}} X_i \cos(\Omega \mathrm{t}) = 0, i = 1, 2, 3, \tag{2.5}$$

where X_i are the principal axes and $b_i^{\mathrm{DC,RF}}$ are the corresponding eigenvalues. By introducing the notations:

$$a_i = \frac{8\mathrm{QU}_0 b_i^{\mathrm{DC}}}{m\Omega^2}, \; q_i = -\frac{4\mathrm{QV}_0 b_i^{\mathrm{RF}}}{m\Omega^2}, \; \tau = \frac{1}{2}\Omega \mathrm{t}, \tag{2.6}$$

the equations of motion (2.5) take the form of the standard homogenous Mathieu's differential equations:

$$\frac{d^2X_i}{d\tau^2} + [a_i - 2q_i\cos(2\tau)]\,X_i = 0. \tag{2.7}$$

According to Floquet's theorem (or Bloch's theorem), the solutions to the Mathieu's equation have the form:

$$u_1(\tau) = e^{\mu\tau} f(\tau),\ u_2(\tau) = e^{-\mu\tau} f(-\tau), \tag{2.8}$$

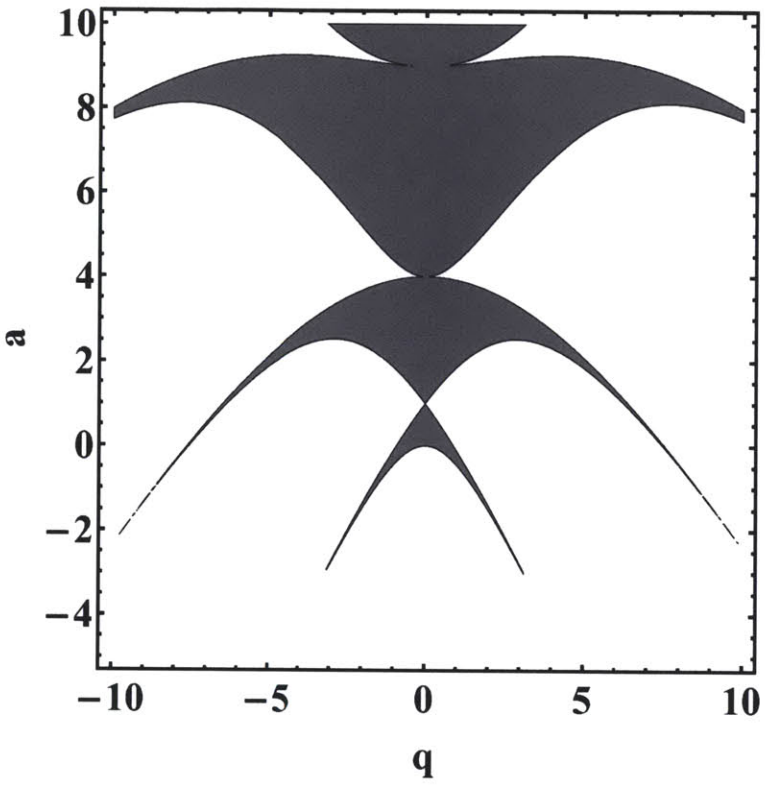

Figure 2-6: Stability map of Mathieu's equation (stable regions are shaded).

where f is a periodic function of period π and the characteristic exponent $\mu = \alpha + i\beta$ is a complex function of the parameters a, q. If $\alpha \neq 0$, or $\alpha = 0 \wedge \beta \notin \mathbb{Z}$ the two solutions (2.8) are linear independent, but only the case $\alpha = 0 \wedge \beta \notin \mathbb{Z}$ provides stable solutions as $\tau \to \infty$ (Fig. 2-6). For the case in which $\alpha = 0 \wedge \beta \in \mathbb{Z}$ (but $q \neq 0$) the two solutions (2.8) become linear dependent and it can be shown that the second linear independent solution is unstable as $\tau \to \infty$. If the condition $\beta \notin \mathbb{Z}$ is satisfied then the general solutions to the equation (2.7) can be written as:

$$X(\tau) = C_1 e^{\mu\tau} \sum_{n=-\infty}^{\infty} c_n e^{2ni\tau} + C_2 e^{-\mu\tau} \sum_{n=-\infty}^{\infty} c_n e^{-2ni\tau}, \tag{2.9}$$

where the constants C must be determined from initial conditions. Substitution of the solution (2.9) back into the differential equation (2.7) gives the following recurrence relation for the coefficients c_n:

$$\gamma_n(\mu)c_{n-2} + c_n + \gamma_n(\mu)c_{n+2} = 0, \tag{2.10}$$

with

$$\gamma_n(\mu) = \frac{q}{(2n - \mathrm{i}\mu)^2 - a}. \tag{2.11}$$

The characteristic exponent μ is determined from the equation:

$$\Delta(\mu) = 0, \tag{2.12}$$

where $\Delta(\mu)$ is the determinant of the system of equations (2.10). Equation (2.12) can be reduced to a simpler form:

$$\cosh(\pi\mu) = 1 - 2\Delta(0)\sin^2\left(\frac{1}{2}\pi\sqrt{a}\right). \tag{2.13}$$

In the stable domain μ is purely imaginary and the solution (2.9) can be written as a real Fourier series:

$$X(\tau) = C_1 \sum_{n=-\infty}^{\infty} c_n \cos[(2n + \beta)\tau] + C_2 \sum_{n=-\infty}^{\infty} c_n \sin[(2n + \beta)\tau]. \tag{2.14}$$

For the case in which the variation of the applied fields is negligible over the particle motion amplitude the adiabatic approximation can be used to determine the charged particle trajectory. In this case it is assumed that the particle motion consists in a small amplitude oscillation at the frequency Ω of the applied RF field superimposed over a smooth secular motion driven by the DC field. Thus, we expect that the solution has the form:

$$X(t) = u(t) + \xi_\Omega(t), \tag{2.15}$$

where $\xi_\Omega(t)$ oscillates at frequency Ω, and where the average of $X(t)$ over one period of the RF field is equal to $u(t)$. Plugging this approximation in the equation of motion (2.5) and expanding up to the first order in ξ_Ω, we obtain:

$$\frac{d^2u}{dt^2} + \frac{d^2\xi_\Omega}{dt^2} \simeq \frac{Q}{m}\left[E^{\mathrm{DC}} + \xi_\Omega \frac{dE^{\mathrm{DC}}}{dX} + E^{\mathrm{RF}}\cos(\Omega \mathrm{t}) + \xi_\Omega \frac{dE^{\mathrm{RF}}}{dX}\cos(\Omega \mathrm{t})\right], \tag{2.16}$$

where the electrical potentials where replaced by their corresponding fields. The next step of the approximation is to require the oscillating terms and smooth varying terms to separately satisfy the equation of motion (2.16). So for the oscillating term we obtain:

$$\frac{d^2\xi_\Omega}{dt^2} \simeq \frac{Q}{m}E^{\mathrm{RF}}\cos(\Omega \mathrm{t}), \tag{2.17}$$

with the solution:

$$\xi_\Omega(t) = -\frac{Q}{m\Omega^2}E^{\mathrm{RF}}(u)\cos(\Omega \mathrm{t}). \tag{2.18}$$

Substituting the above result back into the equation of motion (2.16) and averaging over the oscillating period, the equation of motion for the smooth varying part $u(t)$ becomes:

$$\frac{d^2u}{dt^2} \simeq \frac{Q}{m}E^{\mathrm{DC}} - \frac{Q^2}{m^2\Omega^2}\overline{\left(E^{\mathrm{RF}}\frac{dE^{\mathrm{RF}}}{dX}\cos^2(\Omega \mathrm{t})\right)}, \tag{2.19}$$

from which it follows that the secular motion is determined by the an effective (pseudo) potential:

$$\Phi_{\mathrm{eff}}(X) = \Phi_{\mathrm{DC}}(X) + \frac{Q}{4m\Omega^2}F^2_{\mathrm{RF}}(X). \tag{2.20}$$

The advantage of using the adiabatic approximation is that the quantitative behavior

of the particle confinement can be obtain without solving the exact equation equations of motion (2.14) or knowing the particle's initial conditions (Fig. 2-7). By replacing the definitions of a and q into Eq. (2.20) and solving the equation of motion in the secular approximation, we obtain the solution:

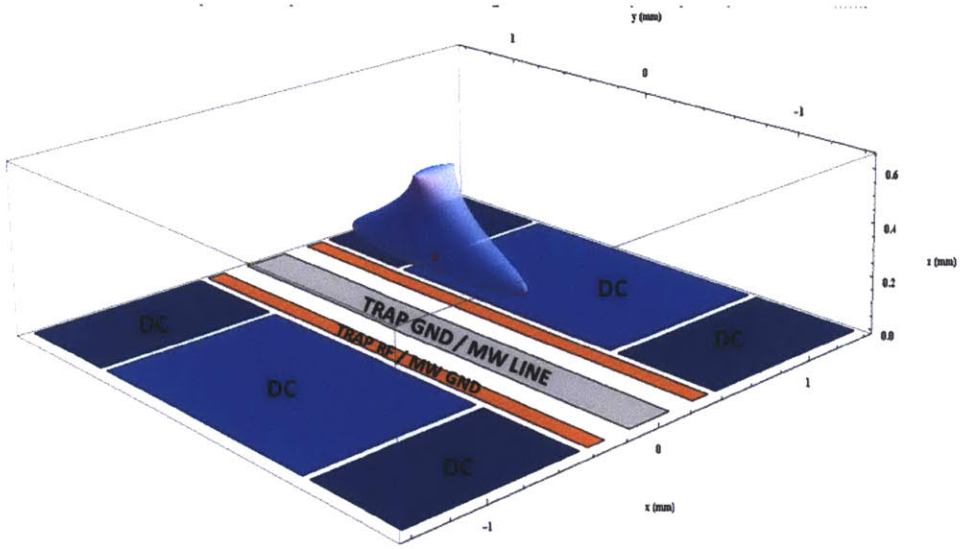

Figure 2-7: Example of a pseudopotential for a surface electrode trap obtain by numerical modeling.

$$u(t) = A\cos\left(\sqrt{\left(a+\frac{q^2}{2}\right)}\frac{\Omega}{2}t\right) + B\sin\left(\sqrt{\left(a+\frac{q^2}{2}\right)}\frac{\Omega}{2}t\right), \tag{2.21}$$

where A and B are two integration constants. By comparing the solution (2.21) with the exact solution (2.14), we recognize that the adiabatic approximation is equivalent with expanding the exact solution up to $n = \pm 1$ terms, which is true if the imaginary part of the characteristic exponent satisfies the condition:

$$\beta^2 \simeq a + \frac{q^2}{2} \ll 1. \tag{2.22}$$

2.2.2 Boundary element method for numerical simulation

In practice any quadrupole ion trap is a set of metallic electrodes held at fixed positions with respect to each other, on which either DC or RF voltages are applied. But

in order to analyze their trapping properties it is necessary to know the potentials created outside of the trap electrodes. Except for highly symmetric trap geometries most often it is impossible to derive an analytic solution for the trapping potentials. The recourse is to either numerically solve the trapping potentials or to experimentally characterize the trap, although the latter case becomes unfeasible when the search space for the applied voltages is high. Essentially, the numerical modeling of the trapping potentials reduces to solving the Laplace equation for the potentials for a given set of boundary conditions. The main numerical methods for solving partial differential equations (PDE) are boundary element method (BEM) and finite element method (FEM) [Jin02], with the former method being particulary suitable for modeling surface electrode ion traps (although BEM has few other advantages over FEM: only surfaces need to be discretized, the solution is more accurate since BEM solves the equivalent integral equation, there is no need for unphysical bounding boxes, etc.). The boundary element method starts with the observation that the applied electrode voltages are equivalent with a set of (surface) electric sources and related to them by the Poisson equation (only the electrostatic case is considered here; the retardation effects for the RF potentials can be safely neglected for the frequencies and distances involved in the ion traps):

$$\nabla^2 \Phi\left(\vec{x}\right) = -\frac{\rho\left(\vec{x}\right)}{\epsilon_0}, \tag{2.23}$$

which in integral form and specifically for the electrode surface only becomes:

$$\Phi_{\text{electrode}}\left(\vec{x}\right) = \frac{1}{4\pi\epsilon_0} \int_{S_{\text{electrode}}} \frac{\sigma\left(\vec{x}'\right)}{\left|\vec{x} - \vec{x}'\right|} d^2x'. \tag{2.24}$$

In principle, the integral equation (2.24) can be solved analytically for the equivalent surface charge density, but in practice except for very simple trap geometries the method becomes very cumbersome (the problem is equivalent with finding a complete set of orthogonal functions over the surface of all electrodes). This is the point where the surface discretization comes into play. The electrode surfaces are commonly tessellated with variable shaped triangles and/or fixed size squares. For both

tessellation shapes the integrals appearing in Eq. (2.27) have analytical solutions, which helps in speeding up the numerical computations. The choice between tiling with triangles or squares depends on the geometry of the problem. Triangles can approximate curved boundaries or surfaces very well, but their description requires nine real numbers (three for each vertex). On the other hand, squares are suitable for tiling flat rectangular surfaces (which is often the case for surface electrode ion traps), and their position and orientation can be described with only five real numbers. Let us assume that all the trap electrodes were divided in a set of finite size elements; then equation (2.24) takes the form:

$$\Phi_i = \Phi_{\text{electrode}}\left(\overrightarrow{x_i}\right) = \frac{1}{4\pi\epsilon_0} \sum_{j\in \text{ all surface elements}} \int_{S_j} \frac{\sigma\left(\vec{x}'\right)}{|\overrightarrow{x_i} - \vec{x}'|} d^2x'. \tag{2.25}$$

There is leeway in where exactly the potentials are evaluated and in what position dependence for the charges we assume. The most common choice is to evaluate the discrete set of surface potentials at the corresponding geometric center of each surface element (i.e. collocation method) and to assume constant surface charge densities over each surface element. Under these conditions equation (2.25) can be written further as:

$$\Phi_i = \frac{1}{4\pi\epsilon_0} \sum_{j\in \text{ all surface elements}} \sigma_j \int_{S_j} \frac{1}{|\overrightarrow{x_i} - \overrightarrow{x_j}|} d^2x_j, \tag{2.26}$$

or

$$\Phi_i = \sum_j M_{\text{ij}}\sigma_j,\ M_{\text{ij}} = \frac{1}{4\pi\epsilon_0} \int_{S_j} \frac{1}{|\overrightarrow{x_i} - \overrightarrow{x_j}|} d^2x_j. \tag{2.27}$$

Since the surface voltages are given, finding the discrete set of surface charges σ_j is just a matter of inverting the matrix formed from the elements M_{ij}:

$$|\sigma\rangle = M^{-1}\big|\,\Phi\big\rangle, \tag{2.28}$$

where we used Dirac notation. With the equivalent electric charges known, the electrical potentials can be easily determined anywhere in space:

$$\Phi(\vec{x}) = \frac{1}{4\pi\epsilon_0}\sum_j \sigma_j \int_{S_j} \frac{1}{|\vec{x} - \vec{x_j}|} d^2x_j. \tag{2.29}$$

Since the electrical potentials satisfy the superposition principle Eqs. (2.28) and (2.29) can be solved only once for any arbitrary set of applied voltages:

$$\sigma_j(k) = \sum_i M_{ji}^{-1}\Phi_i(k), \Phi_i(k) = \begin{cases} 1, & i \in \text{electrode with voltage } V_k \\ 0, & \text{otherwise} \end{cases}, \tag{2.30a}$$

$$\Phi(\vec{x}) = \frac{1}{4\pi\epsilon_0} \sum_{k \in \text{ all independent voltages}} V_k \sum_{j \in \text{ all surface elements}} \sigma_j(k) \int_{S_j} \frac{1}{|\vec{x} - \vec{x_j}|} d^2x_j. \tag{2.30b}$$

Equation (2.28) can be solved numerically by some simple method such as Gaussian elimination, but equation (2.30a) requires applying the method for every independent applied voltage, which becomes time consuming. The alternative is to invert the matrix M before proceeding with solving the set of equations (2.30). There are various ways to numerically invert matrices, but considering the capabilities of a desktop computer and the programming language used, few aspects must be kept in mind when choosing the matrix inversion algorithm. In most cases the matrix to be inverted would not fit in the computer RAM memory in which case it is necessary to break it in sub-matrices of lower dimensionality (the alternative is to just use the programming language linear algebra pack inversion algorithm and to let the computer utilize the virtual memory, but the computation becomes exceedingly slow). One such matrix inversion algorithm which satisfies the above requirements is based on block LDU decomposition [Ste98]. Suppose that the matrix M is partitioned in sub-matrices of various dimensionalities with the only restriction that the main diagonal blocks must be square (i.e. be invertible):

$$M = \begin{pmatrix} M_{1,1} & \vdots & \vdots & \vdots & \vdots & M_{1,N} \\ \cdots & \ddots & \vdots & \vdots & \iddots & \cdots \\ \cdots & \cdots & M_{i,i} & M_{i,i+1} & \cdots & \cdots \\ \cdots & \cdots & M_{i+1,i} & M_{i+1,i+1} & \cdots & \cdots \\ \cdots & \iddots & \vdots & \vdots & \ddots & \cdots \\ M_{N,1} & \vdots & \vdots & \vdots & \vdots & M_{N,N} \end{pmatrix}, \tag{2.31}$$

then the following pseudocode implements the in place inversion of matrix M:

```
! LDU decomposition
for i=1 to N-1
 M[i+1:N;i]=M[i+1:N;i]*M$_i,i^-1$
 M[i+1:N;i+1:N]=M[i+1:N;i+1:N]-M[i+1:N;i]*M[i;i+1:N]
end for i
! M inversion
for j=1 to N
 M_j,j=M_j,j^-1
  for i=1 to j-1
   M_j,j=-M_j,j*M[i;i:j-1]*M[i:j-1;j]
  end for i
end for j
for i=N-1 to 1 step -1
 a=M[i+1:N;i]
 M[i+1:N,i]=0
 M[1:N;i]=M[1:N;i]-M[1:N;i+1:N]*a
end for i
```

where the notation $M[i+1:N;i]$, for example, stands for all blocks from row $i+1$ to row N on ith column of matrix M. In Appendix A I present an example of this algorithm implemented in Mathematica 7.

2.3 CPW microwave resonator

The use of microwave resonators based on transmission lines was proposed before as a method to realize cavity quantum electrodynamics with superconducting electrical circuits [BHW+04], which was subsequently demonstrated experimentally [WSB+04]. The same microwave resonators based on transmission lines can be also used to realize cavity quantum electrodynamics with molecular ions. Here, I give a short classical description of the CPW microwave resonators integrated in surface electrode ion traps.

2.3.1 Classical description of CPW microwave resonators

Let us consider a lossless microwave resonator formed from a CPW transmission line of length L embedded between two semi-infinite CPW transmission lines but separated from them by two small gaps. We model the transmission lines as a distributed set of capacitances c and inductances l (and as such both the resonator itself and the semi-infinite transmission lines have the same characteristic impedances Z), while for simplicity the coupling gaps are modeled as two capacitor of capacitance C_0 [Wad91, Sim01, MYJ80]. Assuming that the system is fed from the left with a sinusoidal signal of amplitude V_+^L at frequency ω, the left semi-infinite line will contain a positive propagating current wave and a reflected negative propagating wave, and the right semi-infinite line will contain only a positive propagating current wave, while the resonator will contain both types of current waves (see Fig. 2-8). Since the system is driven at a single frequency ω in the following all the appearing quantities will implicitly contain a term of the form $exp(i\omega t)$. In order to determine the resonator properties, we make use of the charge conservation law at the two coupling gaps:

$$I_L = \frac{V_+^L - V_-^L}{Z} = \frac{V_+ e^{-\mathrm{i}k\frac{L}{2}} - V_- e^{+\mathrm{i}k\frac{L}{2}}}{Z} = \frac{dQ_L}{dt} = i\omega Q_L, \tag{2.32a}$$

$$I_R = \frac{V_+^R}{Z} = \frac{V_+ e^{+\mathrm{i}k\frac{L}{2}} - V_- e^{-\mathrm{i}k\frac{L}{2}}}{Z} = \frac{dQ_R}{dt} = i\omega Q_R, \tag{2.32b}$$

where the currents were written in terms of their associated voltage amplitudes, and where the subscripts $+/-$ show the direction of propagation of the respective waves.

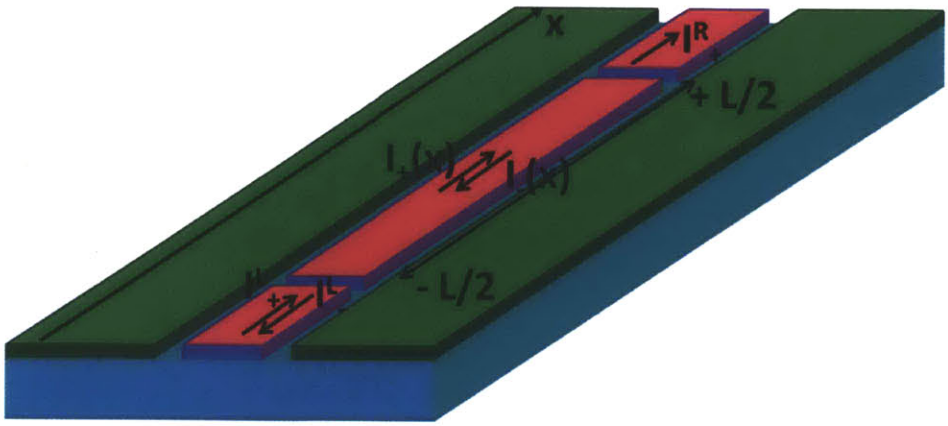

Figure 2-8: CPW based microwave resonator.

The charges on two coupling capacitor $Q_{L,R}$ are related to voltage drops across the two gaps by the relations:

$$\Delta \mathrm{V}_L = \left(V_+^L + V_-^L\right) - \left(V_+ e^{-\mathrm{ik}\frac{L}{2}} + V_- e^{+\mathrm{ik}\frac{L}{2}}\right) = \frac{Q_L}{C_0}, \tag{2.33a}$$

$$\Delta \mathrm{V}_R = \left(V_+ e^{+\mathrm{ik}\frac{L}{2}} + V_- e^{-\mathrm{ik}\frac{L}{2}}\right) - V_+^R = \frac{Q_R}{C_0}. \tag{2.33b}$$

The set of linear equations (2.32) and (2.32) can be solved for the unknown voltages as function of the applied voltage V_+^L. Making the notations $\beta = 2\omega C_0 Z = 2k\frac{C_0}{c}$ and $\gamma = e^{-2ikL}$, the results are:

$$V_-^L = \frac{(\beta+i)+\gamma(\beta-i)}{i\left[1+\gamma(\beta-i)^2\right]} V_+^L, \tag{2.34a}$$

$$V_+ = \gamma^{3/4} \frac{(1+\beta^2)(\beta-i)}{\beta\left[1+\gamma(\beta-i)^2\right]} V_+^L, \tag{2.34b}$$

$$V_- = -\gamma^{1/4} \frac{(1+\beta^2)\, i}{\beta\left[1+\gamma(\beta-i)^2\right]} V_+^L, \tag{2.34c}$$

$$V_+^R = \gamma^{1/2} \frac{(1+\beta^2)}{\left[1+\gamma(\beta-i)^2\right]} V_+^L. \tag{2.34d}$$

If the feeding line is to be electrically matched to the resonator, there should by no reflected wave inside the feeding line. This is equivalent to setting the Eq. (2.34a) equal to zero, from which we obtain a condition for the length L of the resonator has

to satisfy:

$$\tan(kL) = 2k\frac{C_0}{c}. \tag{2.35}$$

The quality factor of the resonator can be calculated from the definition of the quality factor $Q = \omega \times \frac{\text{Stored Energy}}{\text{Power Loss}}$:

$$Q = \frac{\omega}{2}\frac{C_0\left(|\Delta \mathrm{V}_L|^2 + |\Delta \mathrm{V}_R|^2\right) + \int_{-L/2}^{+L/2}\left[c\,|V_+(x) + V_-(x)|^2 + l|\,I_+(x) + I_-(x)|^2\right]\,dx}{V_-^L I_-^{L*} + V_+^R I_+^{R*}}, \tag{2.36}$$

which after performing the integral becomes:

$$Q = \omega Z\frac{4C_0\left\{(1+\beta^2)^2 - [\beta^3\sin(2kL) + \beta^2\cos(2\mathrm{kL}) + 0.5]\right\} + cL\,(1+\beta^2)^2\,(2+\beta^2)}{\beta^2\left\{\beta^4 + 4[\beta\cos(kL) - \sin(kL)]^2\right\}}. \tag{2.37}$$

2.3.2 Numerical estimates

As an example, I analyze a CPW microwave resonator compatible with a surface electrode ion trap. Consider a superconducting resonator built from a Nb layer deposited on top of a sapphire substrate with following characteristics: specific impedance $Z = 50\ \Omega$, specific capacitance $c = 153$ pF/m, specific inductance $l = 383$ nH/m, central electrode width 400 μm, and coupling capacitances C_0=1.53 $\times 10^{-14}$ F. Figure 2-9 shows the quality factor of the microwave resonator versus the resonator length L, for an incoming radiation of angular frequency $\omega = 2\ \pi\ 6.52 \times 10^9$ Hz.

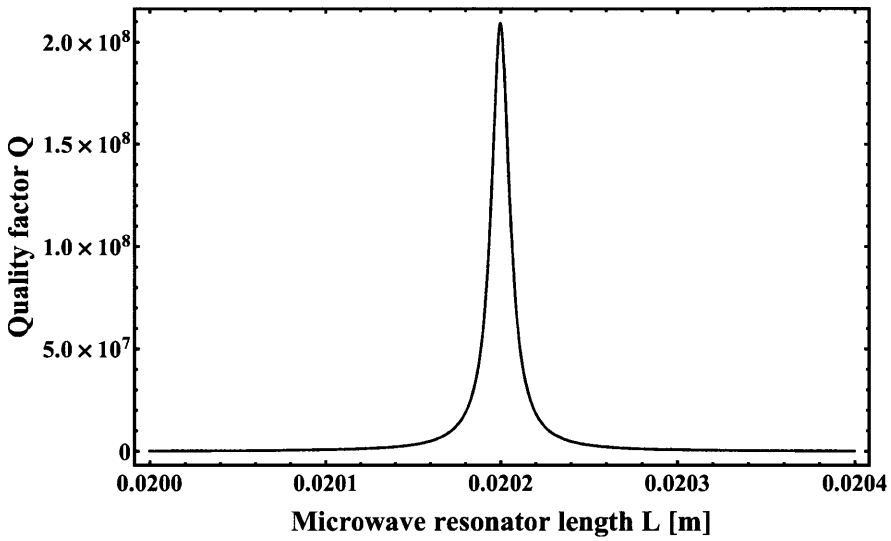

Figure 2-9: CPW microwave resonator quality factor versus its length for a radiation of angular frequency $\omega = 2\ \pi\ 6.52 \times 10^9$ Hz. Resonator characteristics: specific impedance $Z = 50\ \Omega$, specific capacitance $c = 153$ pF/m, specific inductance $l = 383$ nH/m, central electrode width 400 μm, and coupling capacitances C_0=1.53 $\times 10^{-14}$ F.

Chapter 3

Dynamics of co-trapped atomic and polar molecular ions in the presence of electromagnetic fields

This chapter presents two methods for the detection of microwave field coupling to the rotational transitions of a polar molecular ion. Preliminarily, I present the atomic ion interacting with a laser field, and the structure of the molecular ion. The rest of the chapter presents a theoretical analysis of the molecular rotational states evolution coupled to a microwave filed in two cases: in the presence of atomic - molecular ions collisions and in the presence of a microwave cavity.

3.1 Laser cooling of systems with Λ level structure

In atoms or atomic ions with one valence electron more than a closed shell like Sr^+, the excited states usually display a Λ-like structure as shown in Fig. 3-1. For such atoms the excited state $|e\rangle$ can decay either to the ground state $|g\rangle$ or to the metastable level $|m\rangle$. Once the atom reaches the metastable level, it cannot be addressed any longer by the cooling laser tuned to the $g \leftrightarrow e$ transition [KP09]. Consequently, a second laser tuned to the $m \leftrightarrow e$ transition is necessary in order to repump the metastable level $|m\rangle$ back to the active level $|e\rangle$.

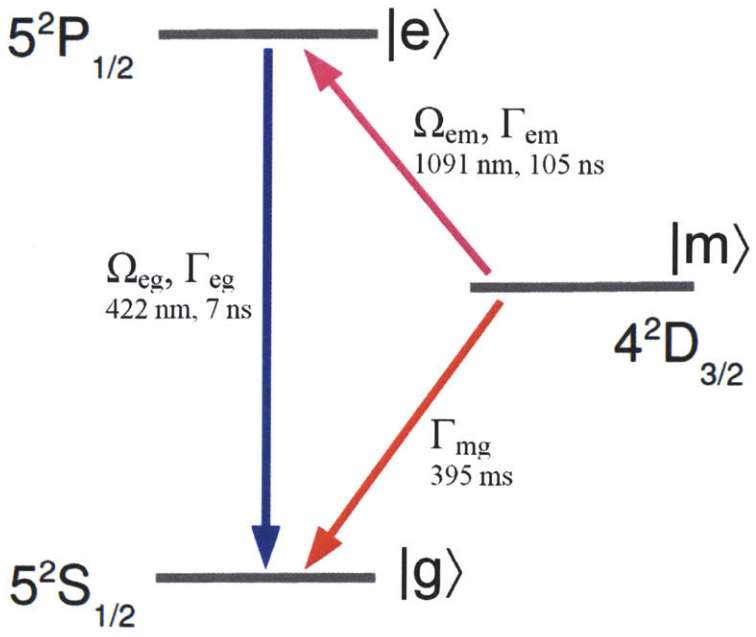

Figure 3-1: Λ level structure in $^{88}Sr^{+}$ ion.

The evolution of the system under the influence of the two coherent radiation fields is described by the following set of optical Bloch equations [CTDRG92, LS84]:

$$\dot{\rho}_{gg} = -i\Omega_{eg}\cos\left(\omega_{L,eg}t\right)\left(\rho_{eg}-\rho_{ge}\right)+\rho_{ee}\Gamma_{eg}+\rho_{mm}\Gamma_{mg}\ , \tag{3.1a}$$

$$\dot{\rho}_{mm} = -i\Omega_{em}\cos\left(\omega_{L,em}t\right)\left(\rho_{em}-\rho_{me}\right)+\rho_{ee}\Gamma_{em}-\rho_{mm}\Gamma_{mg}\ , \tag{3.1b}$$

$$\dot{\rho}_{ee} = i\Omega_{em}\cos\left(\omega_{L,em}t\right)\left(\rho_{em}-\rho_{me}\right)+i\Omega_{eg}\cos\left(\omega_{L,eg}t\right)\left(\rho_{eg}-\rho_{ge}\right)-\rho_{ee}\Gamma_{em}-\rho_{ee}\Gamma_{eg}\ , \tag{3.1c}$$

$$\dot{\rho}_{ge} = i\omega_{eg}\rho_{ge}-i\Omega_{eg}\cos\left(\omega_{L,eg}t\right)\left(\rho_{ee}-\rho_{gg}\right)+i\Omega_{em}\cos\left(\omega_{L,em}t\right)\rho_{gm}-\frac{1}{2}\rho_{ge}\left(\Gamma_{eg}+\Gamma_{em}\right)\ , \tag{3.1d}$$

$$\begin{aligned}\dot{\rho}_{me} &= i\omega_{em}\rho_{me}-i\Omega_{em}\cos\left(\omega_{L,em}t\right)\left(\rho_{ee}-\rho_{mm}\right)+i\Omega_{eg}\cos\left(\omega_{L,eg}t\right)\rho_{mg}\\ &\quad -\frac{1}{2}\rho_{me}\left(\Gamma_{eg}+\Gamma_{em}+\Gamma_{mg}\right)\ ,\end{aligned} \tag{3.1e}$$

$$\dot{\rho}_{gm} = i\omega_{mg}\rho_{gm}+i\Omega_{eg}\cos\left(\omega_{L,eg}t\right)\rho_{me}-i\Omega_{em}\cos\left(\omega_{L,em}t\right)\rho_{eg}-\frac{1}{2}\rho_{gm}\Gamma_{mg}\ , \tag{3.1f}$$

$$\rho_{eg}=\rho_{ge}{}^{\dagger},\ \rho_{em}=\rho_{me}{}^{\dagger},\ \rho_{mg}=\rho_{gm}{}^{\dagger}\ , \tag{3.1g}$$

where the various symbols appearing in the above equations have the typical meanings, i.e.: ρ's are the populations and coherences, ω's are the transition frequencies, Γ's are the decay rates, ω_L's are the frequencies of the applied lasers, and Ω's are the Rabi frequencies. In the laser frame ($\rho_{ge} \to \rho_{ge}e^{i\omega_{L,eg}t}$, $\rho_{me} \to \rho_{me}e^{i\omega_{L,em}t}$, $\rho_{gm} \to \rho_{gm}e^{i(\omega_{L,eg}-\omega_{L,em})t}$) and with the rotating wave approximation the optical Bloch equations become:

$$\dot{\rho}_{gg} = -i\frac{\Omega_{eg}}{2}(\rho_{eg} - \rho_{ge}) + \rho_{ee}\Gamma_{eg} + \rho_{mm}\Gamma_{mg} \ , \tag{3.2a}$$

$$\dot{\rho}_{mm} = -i\frac{\Omega_{em}}{2}(\rho_{em} - \rho_{me}) + \rho_{ee}\Gamma_{em} - \rho_{mm}\Gamma_{mg} \ , \tag{3.2b}$$

$$\dot{\rho}_{ee} = i\frac{\Omega_{em}}{2}(\rho_{em} - \rho_{me}) + i\frac{\Omega_{eg}}{2}(\rho_{eg} - \rho_{ge}) - \rho_{ee}\Gamma_{em} - \rho_{ee}\Gamma_{eg} \ , \tag{3.2c}$$

$$\dot{\rho}_{ge} = -i\delta_{eg}\rho_{ge} - i\frac{\Omega_{eg}}{2}(\rho_{ee} - \rho_{gg}) + i\frac{\Omega_{em}}{2}\rho_{gm} - \frac{1}{2}\rho_{ge}(\Gamma_{eg} + \Gamma_{em}) \ , \tag{3.2d}$$

$$\dot{\rho}_{me} = -i\delta_{em}\rho_{me} - i\frac{\Omega_{em}}{2}(\rho_{ee} - \rho_{mm}) + i\frac{\Omega_{eg}}{2}\rho_{mg} - \frac{1}{2}\rho_{me}(\Gamma_{eg} + \Gamma_{em} + \Gamma_{mg}) \ , \tag{3.2e}$$

$$\dot{\rho}_{gm} = -i(\delta_{eg} - \delta_{em})\rho_{gm} - i\frac{\Omega_{eg}}{2}\rho_{em} + i\frac{\Omega_{em}}{2}\rho_{ge} - \frac{1}{2}\rho_{gm}\Gamma_{mg} \ , \tag{3.2f}$$

$$\rho_{eg} = \rho_{ge}^{\dagger}, \ \rho_{em} = \rho_{me}^{\dagger}, \ \rho_{mg} = \rho_{gm}^{\dagger} \ , \tag{3.2g}$$

where $\delta = \omega_L - \omega$ are the detunings between the applied fields frequencies and the atomic transition frequencies. For numerical calculations is preferable to replace the complex coherences with their real and imaginary parts:

$$\rho_{ge} = x_{ge} - iy_{ge}, \ \rho_{me} = x_{me} - iy_{me}, \ \rho_{gm} = x_{gm} - iy_{gm} \ . \tag{3.3}$$

Also note that because of the normalization condition $\rho_{ee} + \rho_{mm} + \rho_{gg} = 1$ the system of equations is over-determined, we can eliminate one of the populations (for example ρ_{mm}), and then the Eqs. (3.2) take the form:

$$\frac{d}{dt}|\rho(t)\rangle = M|\rho(t)\rangle + |c\rangle, \tag{3.4a}$$

$$\langle\rho(t)| = \begin{pmatrix} \rho_{ee} & \rho_{gg} & x_{ge} & y_{ge} & x_{me} & y_{me} & x_{gm} & y_{gm} \end{pmatrix}, \tag{3.4b}$$

$$M = \begin{pmatrix}
-\Gamma_{em}-\Gamma_{eg} & 0 & 0 & -\Omega_{eg} & 0 & -\Omega_{em} & 0 & 0 \\
\Gamma_{eg}-\Gamma_{mg} & -\Gamma_{mg} & 0 & \Omega_{eg} & 0 & 0 & 0 & 0 \\
0 & 0 & -\frac{\Gamma_{eg}+\Gamma_{em}}{2} & -\delta_{eg} & 0 & 0 & 0 & \frac{\Omega_{em}}{2} \\
\frac{\Omega_{eg}}{2} & -\frac{\Omega_{eg}}{2} & \delta_{eg} & -\frac{\Gamma_{eg}+\Gamma_{em}}{2} & 0 & 0 & -\frac{\Omega_{em}}{2} & 0 \\
0 & 0 & 0 & 0 & -\frac{\Gamma_{eg}+\Gamma_{em}+\Gamma_{mg}}{2} & -\delta_{em} & 0 & -\frac{\Omega_{eg}}{2} \\
\Omega_{em} & \frac{\Omega_{em}}{2} & 0 & 0 & \delta_{em} & -\frac{\Gamma_{eg}+\Gamma_{em}+\Gamma_{mg}}{2} & -\frac{\Omega_{eg}}{2} & 0 \\
0 & 0 & 0 & \frac{\Omega_{em}}{2} & 0 & \frac{\Omega_{eg}}{2} & -\frac{\Gamma_{mg}}{2} & \delta_{em}-\delta_{eg} \\
0 & 0 & -\frac{\Omega_{em}}{2} & 0 & \frac{\Omega_{eg}}{2} & 0 & \delta_{eg}-\delta_{em} & -\frac{\Gamma_{mg}}{2}
\end{pmatrix} \tag{3.4c}$$

$$\langle c| = \begin{pmatrix} 0 & \Gamma_{mg} & 0 & 0 & 0 & -\frac{\Omega_{em}}{2} & 0 & 0 \end{pmatrix}, \tag{3.4d}$$

The steady state solution can be obtained analytically by setting the left-hand side of Eq. (3.4a) to zero. For the case in which $\Gamma_{mg} \to 0$ (a very good approximation given that $|m\rangle$ is metastable) the excited state population ρ_{ee} becomes proportional with $(\delta_{eg} - \delta_{em})^2$:

$$\begin{aligned}
\rho_{ee} &= 4\left(\Gamma_{eg}+\Gamma_{em}\right)\left(\delta_{eg}-\delta_{em}\right)^2\Omega_{eg}^2\Omega_{em}^2 \\
&\times\left[\Gamma_{em}\Omega_{eg}^2\left(\left(4\left(\delta_{eg}-\delta_{em}\right)\delta_{em}+\Omega_{eg}^2\right)^2+4\left(\delta_{eg}-\delta_{em}\right)^2\left(\Gamma_{eg}+\Gamma_{em}\right)^2\right)\right. \\
&+\Gamma_{eg}\Omega_{em}^2\left(\left(4\left(\delta_{eg}-\delta_{em}\right)\delta_{eg}-\Omega_{em}^2\right)^2+4\left(\delta_{eg}-\delta_{em}\right)^2\left(\Gamma_{eg}+\Gamma_{em}\right)^2\right) \\
&\left.+\Omega_{eg}^2\Omega_{em}^2\left(\Omega_{em}^2\left(2\Gamma_{eg}+\Gamma_{em}\right)+\Omega_{eg}^2\left(\Gamma_{eg}+2\Gamma_{em}\right)+8\left(\delta_{eg}-\delta_{em}\right)^2\left(\Gamma_{eg}+\Gamma_{em}\right)\right)\right]^{-1}
\end{aligned} \tag{3.5}$$

This shows that when the two laser detunings are equal the atom gets trapped in a dark state and no longer can scatter light. The absorbtion and emission of photons by the atom generates a force on the atom proportional with the momentum exchanged between the radiation filed and the atom. If the spontaneous emission is isotropic then the scattering force averages to zero and the only force felt by the atom is due to the photon absorbtion (one dimension and one laser color) [MS99]:

$$F = \hbar k_{eg}\Gamma_{eg}\rho_{ee}, \tag{3.6}$$

since at steady state the number of absorbed and emitted photons is the same. If the atom is in motion the radiation absorbed is Doppler shifted by $\delta_{\rm eg} \simeq \omega_{L,\rm eg} - \omega_{\rm eg} - \omega_{L,\rm eg}\frac{v}{c}$ for small atomic velocities. To the first order in the atomic velocity the light force becomes:

$$F = \hbar k_{L,\rm eg}\Gamma_{\rm eg}\left(\rho_{\rm ee}|_{v=0} - k_{L,\rm eg}\frac{\partial\rho_{\rm ee}}{\partial\omega_{L,\rm eg}}|_{v=0}v\right). \tag{3.7}$$

So the motion of the atom is damped at the rate (Fig. 3-2):

$$\alpha = \hbar {k_{L,\rm eg}}^2\Gamma_{\rm eg}\frac{\partial\rho_{\rm ee}}{\partial\omega_{L,\rm eg}}|_{v=0}, \tag{3.8}$$

while the constant zeroth order force just shifts the equilibrium position of a trapped atom.

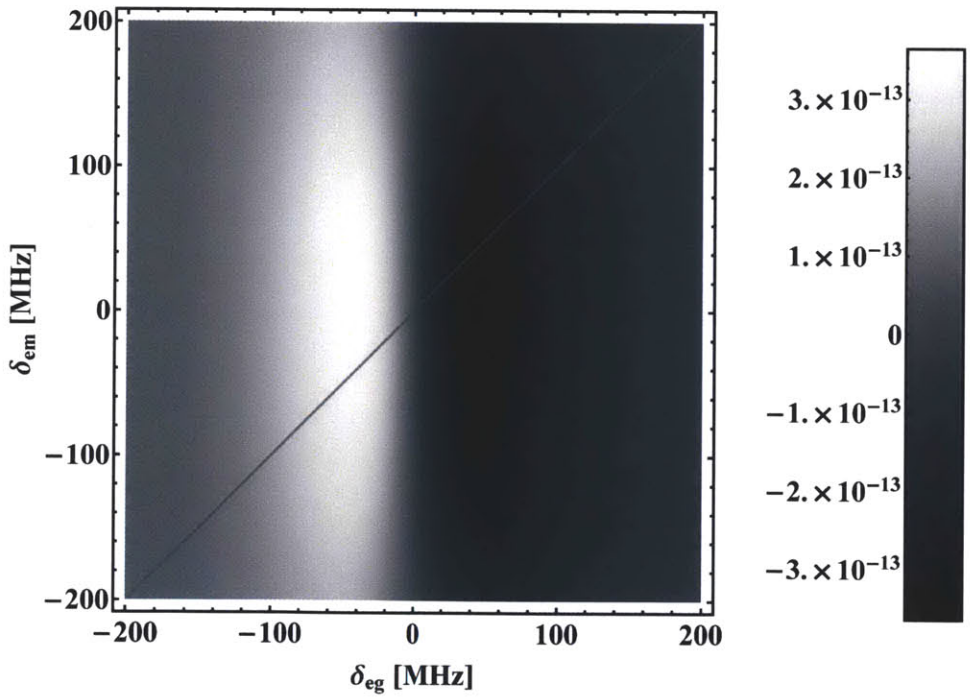

Figure 3-2: Damping coefficient α vs. laser detunings for $^{88}Sr^{+}$ ion cooled on 422 nm transition with $\Omega_{\rm eg} = \Omega_{\rm em} = 1$MHz. For $\delta_{\rm eg} = \delta_{\rm em}$ the damping coefficient and excited population ρ_{ee} become zero.

Equation (3.7) implies that the atom would come to a rest, which however is not true. Due to the time randomness of the photon absorbtion and space randomness

of the photon emission the atom's momentum variance increases in time with the momentum diffusion coefficient:

$$\frac{d\langle p^2\rangle}{dt} = 2D_p = \frac{1}{2}\left(\hbar k_{L,\mathrm{eg}}\right)^2 \Gamma_{\mathrm{eg}} \rho_{\mathrm{ee}}|_{v=0}. \tag{3.9}$$

At steady state the heating and cooling rates become equal and the atom reaches a final temperature:

$$k_B T_D = \frac{\hbar \rho_{\mathrm{ee}}|_{v=0}}{4\frac{\partial \rho_{\mathrm{ee}}}{\partial \omega_{L,\mathrm{eg}}}|_{v=0}}. \tag{3.10}$$

The temperature (or velocity) of a single atom can be determined by monitoring the photon scattering rate, which according to equation (3.5) is:

$$\Phi_{\mathrm{eg}} = \Gamma_{\mathrm{eg}} \rho_{\mathrm{ee}} \left[\delta_{\mathrm{eg}}(v), \delta_{\mathrm{em}}(v)\right]. \tag{3.11}$$

For an ensemble of trapped atoms in thermal equilibrium the above expression must be integrated over their Maxwell-Boltzmann velocity distribution (obtaining a Voigt profile).

3.2 Rotational levels of diatomic heteronuclear molecules in $^1\Sigma$ electronic ground state

Most diatomic molecules have a $^1\Sigma$ electronic ground state [BC03, GC84]. When the nuclear coupling and the interaction between molecular rotation and vibration are neglected, the molecule can be approximated by a rigid rotor. For diatomic molecules in $^1\Sigma$ states, the principal moment of inertia about the molecular axis is zero, and the other two moments corresponding to rotations perpendicular to the molecular bond are equal. Therefore, the Hamiltonian is:

$$H = \frac{1}{2I}\left(J_x^2 + J_y^2\right) = \frac{J^2}{2I}, \tag{3.12}$$

where its energy eigenfunctions are the usual spherical harmonics $\langle \vec{r}|\mathrm{jm}\rangle = Y_{\mathrm{jm}}(\theta,\phi)$ with the corresponding eigenvalues given by $E_{\mathrm{jm}} = \frac{\hbar^2}{2I} j(j+1)$. During the molecular rotation, as a result of the centrifugal force, the internuclear distance increases and hence the moment of inertia increases too. A better model which accounts for the centrifugal distortion is that of a non-rigid rotor. During the molecular rotation the new internuclear equilibrium position R_c is determined by the balance of the centrifugal force F_c and the the electronic restoring force $k(R_c - R_e)$, where R_e is the bond length in the absolute molecular ground state ($j = 0$). If m is the reduced mass of the molecule, and ω is its angular velocity, the classical angular momentum becomes:

$$J = \omega I_c = \omega m R_c^2, \tag{3.13}$$

and the centrifugal force is given by:

$$F_c = \omega m^2 R_c = \frac{J^2}{m R_c^3}, \tag{3.14}$$

But at equilibrium $F_c = k(R_c - R_e)$, and we have:

$$R_c - R_e = \frac{J^2}{k m R_c^3} \simeq \frac{J^2}{k m R_e^3}. \tag{3.15}$$

The total Hamiltonian is now the sum of the kinetic and potential energy:

$$H = \frac{J^2}{2I_c} + \frac{1}{2} k \left(R_c - R_e\right)^2. \tag{3.16}$$

Using the expression of R_c from (3.15) in the Hamiltonian (3.16), and keeping terms to the second order in $R_c - R_e$, the Hamiltonian becomes:

$$H = \frac{J^2}{2mR_e^2} - \frac{J^4}{2km^2 R_e^6} + \ldots . \tag{3.17}$$

The eigenfunctions of the Hamiltonian (3.17) corrected for the centrifugal distortion remain the same spherical harmonics, but the corresponding eigenvalues become:

$$E_{\mathrm{jm}} = \frac{\hbar^2}{2mR_e^2} j(j+1) - \frac{\hbar^4}{2km^2R_e^6} j^2(j+1)^2 + \ldots \,. \tag{3.18}$$

3.3 Collisional assisted microwave heating

Here I present the theory of collisional assisted microwave heating (Figure 3-3). The section begins with a derivation of the cross section for the angular momentum transfer between an atomic ion and molecular ion during Coulomb collisions. From the collisional cross section I determine the rotational de-/excitation rates for the molecular ions in motional thermal equilibrium with the co-trapped atomic ions. Both the cross section for the angular momentum transfer in ion - ion collisions and the rotational de-/excitation rates for the molecular ions were studied before in connection with electrical excitation of nuclei [MG51, ABH+56] and collisional excitation of interstellar molecular ions [CD74, Chu75, Jac72, PM79, FT01]. In the last part, I present an original derivation of the rate at which energy from an applied microwave field is transferred to the translational motion of the molecular ions.

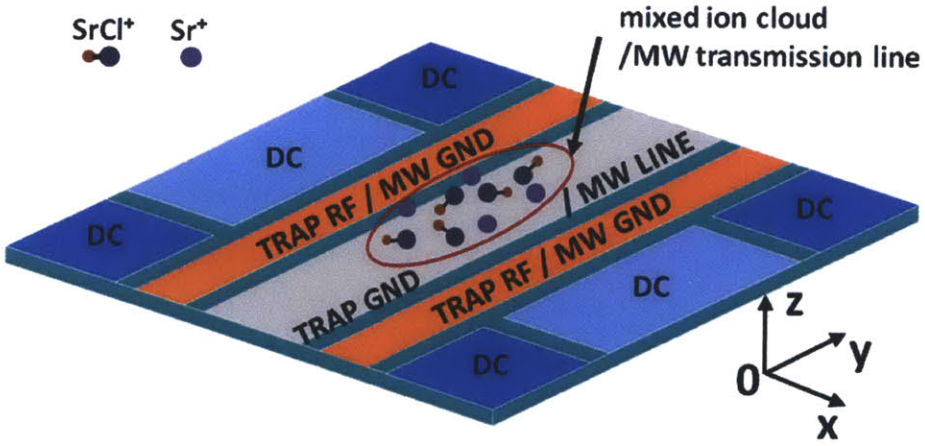

Figure 3-3: Schematic of the collisional assisted microwave heating experiment. A mixed ion cloud of Sr^+ and $SrCl^+$ is trapped in a surface electrode ion trap above a CPW microwave transmission line.

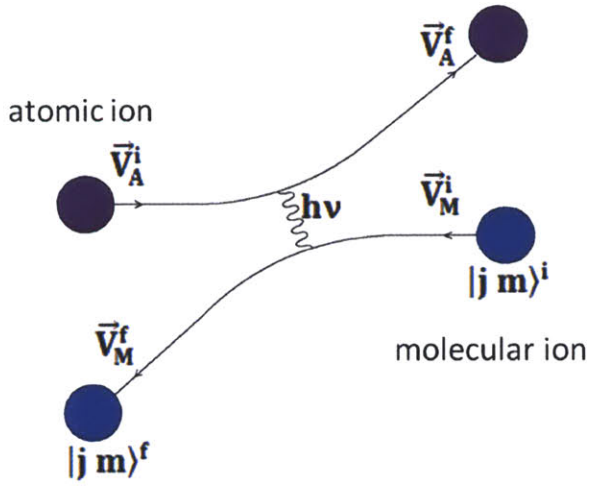

Figure 3-4: Schematic of the angular momentum transfer between an atomic ion and molecular ion during a Coulomb collision. Internal angular momentum of the molecular ion can be transferred from or to the relative motion of the two ions.

3.3.1 Collisional excitation cross section

Consider the following reaction (Figure 3-4):

$$A^+ + M^+(jm) \rightarrow A^+ + M^+(j'm'), \tag{3.19}$$

where j and m are the angular and magnetic quantum numbers of the molecular ion M^+. The internal structure of the molecular ion is modeled as a rigid rotator having an permanent electric dipole μ, while the the atomic ion is taken to be a point charge.

The Hamiltonian which describes the above system (in CM coordinates) is:

$$H = H_{\text{rigidrotator}} - \frac{\hbar^2}{2m_0}\nabla_r^2 + \frac{1}{4\pi\epsilon_0}\frac{e^2}{r} + V_{\text{monopole-multipole}}, \tag{3.20}$$

where m_0 is the reduced mass of the atomic-molecular ions, and r is the distance between their centers of mass [CD74, Chu75, ABH$^+$56, CBK82]. Choosing the unperturbed Hamiltonian to be:

$$H_0 = H_{\text{rigidrotator}} - \frac{\hbar^2}{2m_0}\nabla_r^2 + \frac{1}{4\pi\epsilon_0}\frac{e^2}{r}, \tag{3.21}$$

then the unperturbed wave function ψ separates into a product of a Coulomb wave

function $\phi(\vec{k}, \vec{r}) \equiv |\vec{k}\rangle$, and a spherical harmonic function $Y_{\rm jm}(\hat{n})$ representing the molecular rigid rotator ($\hat{n}$ is the molecular internuclear unit vector).

The higher order molecular electric multipole - atomic ion interaction $V_{\rm monopole\text{-}multipole}$, can be written quite generally as [Jac99, Joa75]:

$$V_{\rm monopole-multipole} = \sum_{\lambda=1}^{\infty} \frac{1}{4\pi\epsilon_0} \frac{P_\lambda(\hat{r}\cdot\hat{n})\,{\rm eQ}_\lambda}{r^{\lambda+1}}, \tag{3.22}$$

where P_λ is the Legendre polynomial of λth order, and Q_λ is the λth permanent electric moment of the molecular ion.

The first order transition probability per unit time dw corresponding to particle scattered from $\vec{k}_i$ to $\vec{k}_f$ within an element of solid angle $d\Omega_f$, while the molecular ion undergoes a transition from $j \to j'$ is given by:

$$dw = \frac{2\pi}{\hbar} \sum_{m,m'} \frac{1}{2j+1} |\langle\psi_f|V|\psi_i\rangle|^2 \frac{m_0 k_f}{(2\pi)^3\hbar^2} d\Omega_f, \tag{3.23}$$

where the matrix elements of the transition were averaged over the magnetic number m of the initial states, and summed over m' that of the final states. Since the total energy is conserved during the transition the wave vector of the final state $\vec{k}_f$ satisfies the relation:

$$\frac{\hbar^2 {k_i}^2}{2m_0} + \frac{\hbar^2 j(j+1)}{2I_{M^+}} = \frac{\hbar^2 {k_f}^2}{2m_0} + \frac{\hbar^2 j'(j'+1)}{2I_{M^+}}, \tag{3.24}$$

In order to determine the total cross section for $j \to j'$ rotational transition, we divide the transition rate dw to the incident particle flux and integrate over the direction of the final state wave vector $\vec{k}_f$:

$$\sigma(j \to j') = \frac{1}{4\pi^2} \frac{{m_0}^2}{\hbar^4} \frac{k_f}{k_i} \sum_{m,m'} \frac{1}{2j+1} \int |\langle\psi_f|V|\psi_i\rangle|^2 d\Omega_f, \tag{3.25}$$

To proceed further, we need to calculate the value of the matrix element:

$$B_{fi} = \langle\psi_f|V|\psi_i\rangle = \langle Y_{j'm'}(\hat{n})|{\rm I}(\hat{n})|Y_{jm}(\hat{n})\rangle, \tag{3.26}$$

where

$$\mathrm{I}(\hat{n})=\frac{e}{4\pi\epsilon_0}\,\langle\vec{k}_f|\,\sum_{\lambda=1}^{\infty}\frac{P_\lambda\,(\hat{r}\cdot\hat{n})\,Q_\lambda}{r^{\lambda+1}}\,|\,\vec{k}_i\rangle, \tag{3.27}$$

The expressions for the Coulomb wave functions are:

$$\langle\vec{r}\,|\,\vec{k}_i\rangle=\exp(-\pi\eta_i/2)\Gamma(1+\mathrm{i}\eta_i)\exp(\mathrm{i}\vec{k}_i\cdot\vec{r})\;{}_1F_1(-\mathrm{i}\eta_i,1;\mathrm{i}(k_ir-\vec{k}_i\cdot\vec{r})), \tag{3.28}$$

and

$$\langle\vec{k}_f\,|\,\vec{r}\rangle=\exp(-\pi\eta_f/2)\Gamma(1-\mathrm{i}\eta_f)\exp(\mathrm{i}\vec{k}_f\cdot\vec{r})\;{}_1F_1(\mathrm{i}\eta_f,1;-\mathrm{i}(k_fr+\vec{k}_f\cdot\vec{r})), \tag{3.29}$$

where the $\eta_{i,f}$ represent the Sommerfeld parameters:

$$\eta_{i,f}=\frac{e^2}{4\pi\epsilon_0}\frac{m_0}{\hbar k_{i,f}}, \tag{3.30}$$

and ${}_1F_1()$ is the confluent hypergeometric function. To calculate the integral in Eq. (3.25), we expand the Coulomb wave function into partial waves [BJ03, AC04, Joa75]:

$$\langle\vec{r}\,|\,\vec{k}_i\rangle=\sum_{l,m}4\pi(-1)^m i^l\exp(\mathrm{i}\sigma_l(\eta_i))Y_{l,-m}(\hat{k}_i)Y_{\mathrm{lm}}(\hat{r})\frac{F_l\,(k_ir)}{k_ir}, \tag{3.31}$$

and

$$\langle\vec{k}_f\,|\,\vec{r}\rangle=\sum_{l,m}4\pi(-1)^m i^l\exp(-\mathrm{i}\sigma_l(\eta_f))Y_{l,-m}(\hat{k}_f)Y_{\mathrm{lm}}(\hat{r})\frac{F_l\,(k_fr)}{k_fr}, \tag{3.32}$$

where $\sigma_l(\eta)=\arg\Gamma(\mathrm{l}+1+\mathrm{i}\eta)$ is the Coulomb phase shift, and where $F_l(kr)$ is the regular solution to the radial wave equation for the orbital angular momentum l.

Using the addition theorem for the spherical harmonics [AW95]:

$$P_\lambda(\hat{r}\cdot\hat{n})=\frac{4\pi}{2\lambda+1}\sum_{\mu=-\lambda}^{\lambda}Y^*_{\lambda\mu}(\hat{n})Y_{\lambda\mu}(\hat{r}), \tag{3.33}$$

and the relation:

$$\langle Y_{j'm'}(\hat{n})|Y^*_{\lambda\mu}(\hat{n})|Y_{\mathrm{jm}}(\hat{n})\rangle = \sqrt{\frac{(2j'+1)(2\lambda+1)(2j+1)}{4\pi}} \begin{pmatrix} j' & \lambda & j \\ 0 & 0 & 0 \end{pmatrix} \begin{pmatrix} j' & \lambda & j \\ m' & \mu & m \end{pmatrix} \tag{3.34}$$

the angular integration over $\hat{n}$ can be performed, yielding [Sak81, DM77, MG51]:

$$\begin{aligned} \langle \overrightarrow{k}_f | \frac{Y_{\lambda\mu}(\hat{r})}{r^{\lambda+1}} | \overrightarrow{k}_i \rangle = & \\ & 4\pi^{3/2} \sum_{l_i,l_f} \sum_{m_i,m_f} i^{l_i-l_f} (-1)^{\mu} \exp(\mathrm{i}(\sigma_i+\sigma_f)) \sqrt{(2l_i+1)(2\lambda+1)(2l_f+1)} \\ & \times Y_{l_i,-m_i}(\hat{k_i}) Y_{l_f,m_f}(\hat{k_f}) \begin{pmatrix} l_i & l_f & \lambda \\ 0 & 0 & 0 \end{pmatrix} \begin{pmatrix} l_i & l_f & \lambda \\ m_i & -m_f & \mu \end{pmatrix} M^{-\lambda-1}_{l_i,l_f}, \end{aligned} \tag{3.35}$$

where the radial matrix element M is defined by:

$$M^{-\lambda-1}_{l_i,l_f} = \frac{1}{k_i k_f} \int_0^{\infty} \frac{F_{l_f}(k_f r) F_{l_i}(k_i r)}{r^{\lambda+1}} dr. \tag{3.36}$$

Hence Eq. (3.27) becomes:

$$I(\hat{n}) = \frac{e}{4\pi\epsilon_0} \sum_{\lambda,\mu} \sum_{l_i,l_f} \sum_{m_i,m_f} Q_\lambda T^{\lambda\mu}_{l_i m_i l_f m_f} Y^*_{\lambda\mu}(\hat{n}) Y_{l_i,-m_i}(\hat{k_i}) Y_{l_f,m_f}(\hat{k_f}) M^{-\lambda-1}_{l_i,l_f}, \tag{3.37}$$

where

$$\begin{aligned} T^{\lambda\mu}_{l_i m_i l_f m_f} = \quad & (4\pi)^{5/2} i^{l_i-l_f} (-1)^{\mu} \exp(\mathrm{i}(\sigma_i+\sigma_f)) \\ & \times \sqrt{\frac{(2l_i+1)(2l_f+1)}{(2\lambda+1)}} \begin{pmatrix} l_i & l_f & \lambda \\ 0 & 0 & 0 \end{pmatrix} \begin{pmatrix} l_i & l_f & \lambda \\ m_i & -m_f & \mu \end{pmatrix}. \end{aligned} \tag{3.38}$$

The transition matrix element B_{fi} can be evaluated [AG92, RST98, OKKN01]:

$$B_{fi} = \sum_{\lambda,\mu} \sum_{l_i,l_f} G^{\lambda\mu}_{l_i l_f j j' m m'} Y_{l_f,\mu}(\hat{k_f}) M^{-\lambda-1}_{l_i,l_f}, \tag{3.39}$$

where

$$\begin{aligned} G^{\lambda\mu}_{l_i l_f j j' m m'} = \quad & \frac{\mathrm{eQ}_\lambda}{16\pi^2\epsilon_0} T^{\lambda\mu}_{l_i 0 l_f \mu} \sqrt{(2l_i+1)\,(2j+1)(2j'+1)(2\lambda+1)} \\ & \times \begin{pmatrix} j & j' & \lambda \\ 0 & 0 & 0 \end{pmatrix} \begin{pmatrix} j & j' & \lambda \\ m & m' & -\mu \end{pmatrix}. \end{aligned} \tag{3.40}$$

Substituting the expression for B_{fi} in Eq. (3.25), we obtain:

$$\sigma(j \to j') = \sum_{\lambda=1}^{\infty} \sigma_\lambda, \tag{3.41}$$

where σ_λ is defined as:

$$\begin{aligned} \sigma_\lambda(j \to j') = \quad & \frac{e^2}{\pi\epsilon_0} \frac{{m_0}^2}{\hbar^4} \frac{k_f}{k_i} {Q_\lambda}^2 \frac{2j'+1}{2\lambda+1} \begin{pmatrix} j & j' & \lambda \\ 0 & 0 & 0 \end{pmatrix}^2 \\ & \times \sum_{l_i,l_f} (2l_i{+}1)(2l_f{+}1) \begin{pmatrix} l_i & l_f & \lambda \\ 0 & 0 & 0 \end{pmatrix} |M^{-\lambda-1}_{l_i,l_f}|^2 \end{aligned} \tag{3.42}$$

For the special case of electric dipole excitation $\lambda = 1$ the radial matrix elements $M^{-2}_{l_i,l_f}$ are related to the well known electric dipole bremsstrahlung radial matrix elements $M^{+1}_{l_i,l_f}$ [ABH+56]. The connection is given through the equation of motion (Ehrenfest theorem):

$$m_0 \frac{d\vec{r}}{\mathrm{dt}} = \frac{1}{4\pi\epsilon_0} \frac{e^2}{r^2} \vec{r}, \tag{3.43}$$

which leads to

$$-m_0\omega^2 \langle \vec{k}_f | \mathrm{r} Y_{1\mu}(\hat{r}) | \vec{k}_i \rangle = \frac{e^2}{4\pi\epsilon_0} \langle \vec{k}_f | \frac{Y_{1\mu}(\hat{r})}{r^2} | \vec{k}_i \rangle, \tag{3.44}$$

or

$$-m_0\omega^2 M^{+1}_{l_i,l_f} = \frac{e^2}{4\pi\epsilon_0} M^{-2}_{l_i,l_f}, \tag{3.45}$$

where

$$\omega = \frac{\hbar\,({k_i}^2 - {k_f}^2)}{2m_0}. \tag{3.46}$$

The $M^{+1}_{l_i,l_f}$ can be evaluated analytically by expressing the Coulomb wave function in parabolically coordinates [Som53] and the righthand sum in the Eq. (3.42) can be written in closed form as:

$$\sum_{l_i,l_f} (2l_i{+}1)(2l_f{+}1) \begin{pmatrix} l_i & l_f & 1 \\ 0 & 0 & 0 \end{pmatrix} |M^{-2}_{l_i,l_f}|^2 = \frac{9}{64\pi^2}\frac{1}{k_i k_f} f_{\mathrm{E1}}\,(\eta_i,\zeta)\,, \tag{3.47}$$

where

$$f_{\mathrm{E1}}(\eta_i,\zeta) = -\frac{32\pi^4}{9}\frac{\exp(2\pi\eta_i)}{(\exp(2\pi\eta_i)-1)\,(\exp(2\pi\eta_f)-1)}\,(-\chi_0)\frac{d}{d\chi_0}\,|\,{}_2F_1(\text{-i }\eta_i,\text{-i }\eta_i,1;\chi_0)|^2, \tag{3.48}$$

with $\zeta = \eta_f - \eta_i$ and $\chi_0 = -\frac{4\eta_i\eta_f}{\zeta^2}$. Hence

$$\sigma_1(j, j' = j \pm 1) = \frac{12\pi{\epsilon_0}^2\hbar^4}{e^4{m_0}^2}(1+2j')\,(Q_1\eta_i)^2 \begin{pmatrix} j & j' & 1 \\ 0 & 0 & 0 \end{pmatrix}^2 f_{\mathrm{E1}}(\eta_i,\zeta) \tag{3.49}$$

For the case in which $|\chi_0| > 1$ the Gauss hypergeometric function ${}_2F_1$ does not converge [AW95, TC01]. In order to evaluate f_{E1} it is necessary to use the analytic continuity of ${}_2F_1$:

$$
\begin{aligned}
{}_2F_1(a,b;c;z) = \quad & \frac{(\Gamma(c)\Gamma(b-a))\,{}_2F_1\left(a,a-c+1;a-b+1;\frac{1}{z}\right)}{(-z)^a(\Gamma(b)\Gamma(c-a))} \\
& + \frac{(\Gamma(c)\Gamma(a-b))\,{}_2F_1\left(b,b-c+1;-a+b+1;\frac{1}{z}\right)}{(-z)^b(\Gamma(a)\Gamma(c-b))},
\end{aligned} \tag{3.50}
$$

With the help of the following relations:

$$
\frac{\partial\,{}_2F_1(a,b;c;z)}{\partial z} = \frac{(ab)\,{}_2F_1(a+1,b+1;c+1;z)}{c}, \tag{3.51}
$$

and

$$
{}_2F_1(a,b;c;z)=(1\text{-}z)^{-a-b+c}\,{}_2F_1(c-a,c-b;c;z), \tag{3.52}
$$

f_{E1} becomes:

$$
\begin{aligned}
f_{\mathrm{E1}}(\eta_i,\zeta) = & -\frac{32\pi^3}{9}\frac{\eta_f\eta_i}{\zeta}\frac{1}{\exp(2\pi\zeta)-1}\,\mathrm{Im}\{\frac{1}{\eta_i}\,{}_2F_1\left(i\eta_i,i\eta_i;1-\mathrm{i}\zeta;\frac{1}{\chi_0}\right) \\
& \times\,{}_2F_1\left(1-i\eta_i,-i\eta_i;1+\mathrm{i}\zeta;\frac{1}{\chi_0}\right) + \exp(\mathrm{i}\,\phi)\;{}_2F_1\left(1-i\eta_f,-i\eta_f;1-\mathrm{i}\zeta;\frac{1}{\chi_0}\right) \\
& + \eta_i \rightleftarrows \eta_f\},
\end{aligned} \tag{3.53}
$$

where

$$
\phi = 2\mathrm{arg}[\Gamma(i\zeta)\Gamma(i\eta_i)/\Gamma(i\eta_f)] + \zeta ln|\chi_0|. \tag{3.54}
$$

3.3.2 Collisional excitation reaction rate

Consider a two component non-neutral plasma mixture of atomic ions and molecular ions with the densities n_A and $n_M(j,T_R)$, respectively. Assuming that both species are in translational thermal equilibrium described by a Maxwell-Boltzmann distribution with a translational temperature T_T, the reaction rate per unit volume $k(j \to j', T_T, T_R)$ for the collisional transition $j \to j'$ is given by [TF79, SB73, DF81]:

$$k(j \to j', T_T, T_R) = n_A n_M(j, T_R) \left(\frac{m_0}{2\pi k_B T_T}\right)^{3/2} \int \sigma(v, j \to j') v \exp\left(-\frac{m_0 v^2}{2k_B T_T}\right) d^3\vec{v}, \tag{3.55}$$

where $\vec{v}$ is the relative speed of the atomic ions to the molecular ions. The molecular ion internal (rotational) and external (translational) degrees of freedom are not necessarily in thermal equilibrium, hence their characteristic temperatures are taken to be different. Since the reaction cross section is independent of the absolute orientation of the relative speed, the transition rate *per molecular ion* $\gamma(j \to j', T_T)$ initially in the rotational state j becomes [Jac72, PM79, FT01]:

$$\gamma(j \to j', T_T) = 4\pi n_A \left(\frac{m_0}{2\pi k_B T_T}\right)^{3/2} \int \sigma(v, j \to j') v^3 \exp\left(-\frac{m_0 v^2}{2k_B T_T}\right) dv, \tag{3.56}$$

where the velocity integration interval still must be defined. A typical surface electrode ion trap has a trap depth of $\sim$ 6000 K ($\sim$ 0.5 eV), while a Doppler cooled trapped ion cloud has a temperature of $\sim$ 1 K. Thus the velocity upper limit of integration can be extended to the infinity. The lower velocity limit depends on which direction the energy is transferred during the collision: for $j < j'$ there is a threshold velocity

$$v_0 = \sqrt{\frac{\hbar^2[j'(j'+1) - j(j+1)]}{m_0 I_{M^+}}} \tag{3.57}$$

below which the reaction cannot proceed, and for the case $j > j'$ the system gains translational energy so the initial relative velocity can be zero. The de-excitation transition rate can be readily calculated from the excitation transition rate, as they are related by the detailed-balance equation [DF81]:

$$(2j+1)\gamma(j \to j+1, T_T) = (2j+3)\gamma(j+1 \to j, T_T) \exp\left(-\frac{2B(j+1)}{k_B T_T}\right), \tag{3.58}$$

where B is the rotational constant of the molecular ion.

Consider a mixed ion cloud of $^{88}Sr^{+}$ and $^{88}Sr^{35}Cl^{+}$ with a translational temperature $T_T = 1\ K$ and with an atomic ion density $n_A = 1.25 \times 10^{14}\ m^{-3}$ (a 20 μm separation between ions). The collisional transition rates per molecular ion are: $\gamma_{coll}(0 \rightarrow 1) = 1.73 \times 10^{7}\ Hz$ and $\gamma_{coll}(1 \rightarrow 0) = 7.92 \times 10^{6}\ Hz$. For comparison in a 10 K cryogenic environment the black body radiation induced transitions rates are: $\gamma_{BB}(0 \rightarrow 1) = 9.75 \times 10^{-6}\ Hz$ and $\gamma_{BB}(1 \rightarrow 0) = 3.25 \times 10^{-6}\ Hz$, while the spontaneous transition rate is $\gamma_{sp}(1 \rightarrow 0) = 1.03 \times 10^{-7}\ Hz$. With these results, I estimate the internal and external molecular ion temperature equilibration time to be of the order of $\sim 1/\gamma_{coll} \simeq 100\ ns$, which means the two temperatures can be taken to be equal.

3.3.3 Collisional enhanced heating rate

Here I examine the effect of an applied microwave field on the rotational population distribution of the molecular ions. We take the microwave radiation to be liner polarized along $\hat{z}$ direction with an angular frequency ω_M comparable with the $j = 0 \leftrightarrow j = 1$ rotational transition frequency of $^{88}Sr^{35}Cl^{+}$, and to have an electric field amplitude E_M. To model the microwave field - molecular ions - atomic ions system, we make the following simplifying assumptions: 1.) only electric dipole transitions are allowed, i.e. $j \rightarrow j \pm 1$, 2.) the magnetic sublevels of the same rotational level are degenerated, 3.) the atomic ions are considered to be an infinite heat reservoir with a constant temperature T_T , and 3.) neglect the black body and vacuum radiation induced transitions compared with the collisional transition rates. In order to write the optical Bloch equations, we remark that the $\hat{z}$ linear polarized microwave field links only the $m = 0 \leftrightarrow m' = 0$ rotational sublevels, and the collisional transition rates between rotational sublevels are given by Eq. (3.56) multiplied with their transition probabilities computed from Eq. (3.34) (Fig. 3-5). Since the evolution of all coherences except for $n^0_{01'}$ are neither influenced by the microwave field nor connected to the evolution of the populations, we do not write them explicitly. With the observation that the populations of the degenerated

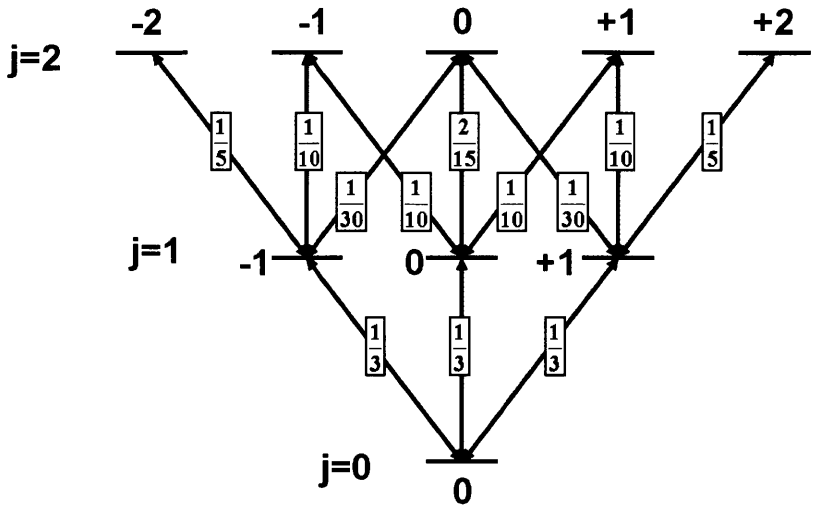

Figure 3-5: Transition probabilities between the magnetic sublevels of the rotational levels j=0, 1, and 2.

magnetic sublevels for each rotational level $j \geq 2$ can be summed in one population per level, the optical Bloch equations are [CTDRG92, CKK08]:

$$\frac{dn_{00}}{dt} = -\,\mathrm{i}\,\Omega\cos(\omega_M\,\mathrm{t})\,(n^0_{10} - n^0_{01}) + \gamma^{\mathrm{coll}}_{10}\,(n^+_{11} + n^0_{11} + n^-_{11}) - \gamma^{\mathrm{coll}}_{01} n_{00} \tag{3.59a}$$

$$\frac{dn^+_{11}}{dt} = -\,(\gamma^{\mathrm{coll}}_{10} + \gamma^{\mathrm{coll}}_{12})\,n^+_{11} + \frac{\gamma^{\mathrm{coll}}_{01}}{3} n_{00} + \frac{\gamma^{\mathrm{coll}}_{21}}{3} n_{22} \tag{3.59b}$$

$$\frac{dn^0_{11}}{dt} = \mathrm{i}\,\Omega\cos(\omega_M\,\mathrm{t})\,(n^0_{10} - n^0_{01}) - (\gamma^{\mathrm{coll}}_{10} + \gamma^{\mathrm{coll}}_{12})\,n^0_{11} + \frac{\gamma^{\mathrm{coll}}_{01}}{3} n_{00} + \frac{\gamma^{\mathrm{coll}}_{21}}{3} n_{22} \tag{3.59c}$$

$$\frac{dn^-_{11}}{dt} = -\,(\gamma^{\mathrm{coll}}_{10} + \gamma^{\mathrm{coll}}_{12})\,n^-_{11} + \frac{\gamma^{\mathrm{coll}}_{01}}{3} n_{00} + \frac{\gamma^{\mathrm{coll}}_{21}}{3} n_{22} \tag{3.59d}$$

$$\frac{dn^0_{01}}{dt} = -\,\mathrm{i}\,\Omega\cos(\omega_M\,\mathrm{t})\,(n^0_{11} - n_{00}) + \mathrm{i}\,\omega_{01} n^0_{01} - \frac{\gamma^{\mathrm{coll}}_{10} + \gamma^{\mathrm{coll}}_{01}}{2} n^0_{01} \tag{3.59e}$$

$$\frac{dn^0_{10}}{dt} = \mathrm{i}\,\Omega\cos(\omega_M\,\mathrm{t})\,(n^0_{11} - n_{00}) - \mathrm{i}\,\omega_{01} n^0_{10} - \frac{\gamma^{\mathrm{coll}}_{10} + \gamma^{\mathrm{coll}}_{01}}{2} n^0_{10} \tag{3.59f}$$

$$\frac{dn_{\mathrm{jj}}}{dt} = -\,(\gamma^{\mathrm{coll}}_{j,j-1} + \gamma^{\mathrm{coll}}_{j,j+1})\,n_{\mathrm{jj}} + \gamma^{\mathrm{coll}}_{j-1,j} n_{j-1,j-1} + \gamma^{\mathrm{coll}}_{j+1,j} n_{j+1,j+1},\ j \geq 2 \tag{3.59g}$$

where $\Omega = \mu\,\langle Y_{00}\,|\hat{n}\cdot\hat{z}|\,Y_{10}\rangle\,E_M/\hbar$ is the Rabi frequency, ω_{01} is the $j = 1 \leftrightarrow j = 0$ angular transition frequency, and $n^m_{jj'}$ are the populations and coherences of the rota-

tional sublevels/levels (the magnetic number for $j = 0$ level is not shown). Introducing a new set of variables by switching to a rotating frame:

$$\begin{aligned} \bar{n}_{11}^{m} &= n_{11}^{m} \\ \bar{n}_{jj} &= n_{jj} \\ \bar{n}_{01}^{m} &= n_{01}^{m} exp\left(-i\omega_M t\right) \\ \bar{n}_{10}^{m} &= n_{10}^{m} exp\left(i\omega_M t\right), \end{aligned} \tag{3.60}$$

and making use of the rotating wave approximation, Eqs. (3.59) become:

$$\frac{d\bar{n}_{00}}{dt} = \text{- i } \frac{\Omega}{2} \left(\bar{n}_{10}^{0} - \bar{n}_{01}^{0}\right) + \gamma_{10}^{\text{coll}} \left(\bar{n}_{11}^{+} + \bar{n}_{11}^{0} + \bar{n}_{11}^{-}\right) \text{ - } \gamma_{01}^{\text{coll}} \bar{n}_{00} \tag{3.61a}$$

$$\frac{d\bar{n}_{11}^{+}}{dt} = \text{- } \left(\gamma_{10}^{\text{coll}} + \gamma_{12}^{\text{coll}}\right) \bar{n}_{11}^{+} + \frac{\gamma_{01}^{\text{coll}}}{3} \bar{n}_{00} + \frac{\gamma_{21}^{\text{coll}}}{3} \bar{n}_{22} \tag{3.61b}$$

$$\frac{d\bar{n}_{11}^{0}}{dt} = \text{i } \frac{\Omega}{2} \left(\bar{n}_{10}^{0} - \bar{n}_{01}^{0}\right) \text{ - } \left(\gamma_{10}^{\text{coll}} + \gamma_{12}^{\text{coll}}\right) \bar{n}_{11}^{0} + \frac{\gamma_{01}^{\text{coll}}}{3} \bar{n}_{00} + \frac{\gamma_{21}^{\text{coll}}}{3} \bar{n}_{22} \tag{3.61c}$$

$$\frac{d\bar{n}_{11}^{-}}{dt} = \text{- } \left(\gamma_{10}^{\text{coll}} + \gamma_{12}^{\text{coll}}\right) \bar{n}_{11}^{-} + \frac{\gamma_{01}^{\text{coll}}}{3} \bar{n}_{00} + \frac{\gamma_{21}^{\text{coll}}}{3} \bar{n}_{22} \tag{3.61d}$$

$$\frac{d\bar{n}_{01}^{0}}{dt} = \text{- i } \frac{\Omega}{2} \left(\bar{n}_{11}^{0} \text{ - } \bar{n}_{00}\right) \text{ - i } \Delta_M \bar{n}_{01}^{0} \text{ - } \frac{\gamma_{10}^{\text{coll}} + \gamma_{01}^{\text{coll}}}{2} \bar{n}_{01}^{0} \tag{3.61e}$$

$$\frac{d\bar{n}_{10}^{0}}{dt} = \text{i } \frac{\Omega}{2} \left(\bar{n}_{11}^{0} \text{ - } \bar{n}_{00}\right) + \text{i } \Delta_M \bar{n}_{10}^{0} \text{ - } \frac{\gamma_{10}^{\text{coll}} + \gamma_{01}^{\text{coll}}}{2} \bar{n}_{10}^{0} \tag{3.61f}$$

$$\frac{d\bar{n}_{\text{jj}}}{dt} = \text{- } \left(\gamma_{j,j-1}^{\text{coll}} + \gamma_{j,j+1}^{\text{coll}}\right) \bar{n}_{\text{jj}} + \gamma_{j-1,j}^{\text{coll}} \bar{n}_{j-1,j-1} + \gamma_{j+1,j}^{\text{coll}} \bar{n}_{j+1,j+1}, \; j \geq 2 \tag{3.61g}$$

where $\Delta_M = \omega_M$ - ω_{01} is the detuning between the microwave radiation frequency and rotational transition frequency. Since we are interested in the steady state populations of the rotational states, we set the time derivatives in Eqs. (3.61) to zero, and solve the remaining system of linear equations. In order to reduce the infinite set of equations to a finite set, we proceed as follows. From Eq. (3.59g) and the detailed balance relation Eq. (3.58), we note that at steady state, the populations for rotational levels with $j \geq 1$ remain in thermal equilibrium:

$$\frac{n_{jj}}{n_{11}} = \frac{2j+1}{3} \frac{\exp\left(-\frac{\mathrm{Bj}(j+1)}{k_B T_T}\right)}{\exp\left(-\frac{2B}{k_B T_T}\right)}, \tag{3.62}$$

and making use of the definition of the partition function for the rigid rotator at temperature T_T, we obtain:

$$\begin{aligned} Z(T_T) &= \sum_{j=0}^{\infty} (2j+1) \exp\left(-\frac{\mathrm{Bj}(j+1)}{k_B T_T}\right) \\ &= 1 + 3\exp\left(-\frac{2B}{k_B T_T}\right) + \frac{1}{n_{11}} 3\exp\left(-\frac{2B}{k_B T_T}\right) \sum_{j=2}^{\infty} n_{jj}, \end{aligned} \tag{3.63}$$

or

$$\sum_{j=1}^{\infty} n_{jj} = \frac{\gamma_{10}^{coll}}{\gamma_{01}^{coll}} \left(Z(T_T) - 1\right) n_{11}. \tag{3.64}$$

But since

$$\sum_{j=1}^{\infty} n_{jj} = 1\text{-}n_{00}, \tag{3.65}$$

Eq. (46) becomes:

$$n_{00} = 1 - \frac{\gamma_{10}^{coll}}{\gamma_{01}^{coll}} \left(Z(T_T) - 1\right) n_{11}, \tag{3.66}$$

Thus the infinite set of equations Eqs. (3.61g) are replaced by one equation Eq. (3.66). Solving for n_{00} and n_{11} yields:

$$n_{00} = \frac{1}{1 + \frac{\gamma_{10}^{coll}}{\gamma_{01}^{coll}} \left(Z(T_T) - 1\right) P_{10}}, \tag{3.67a}$$

$$n_{11} = \frac{P_{10}}{1 + \frac{\gamma_{10}^{coll}}{\gamma_{01}^{coll}} \left(Z(T_T) - 1\right) P_{10}}, \tag{3.67b}$$

with

$$P_{10} = \frac{3}{\kappa}\frac{\kappa S + \gamma_{01}^{coll}}{\kappa S + 3\gamma_{10}^{coll}} + \frac{2}{\kappa}\frac{\gamma_{01}^{coll}}{\gamma_{10}^{coll} + \gamma_{12}^{coll}}, \tag{3.68a}$$

$$\kappa = \frac{3\gamma_{10}^{coll} + \gamma_{12}^{coll}}{\gamma_{10}^{coll} + \gamma_{12}^{coll}}, \tag{3.68b}$$

$$S = \frac{\left(\gamma_{01}^{coll} + \gamma_{10}^{coll} + \gamma_{12}^{coll}\right)\Omega^2}{4\Delta_M{}^2 + \left(\gamma_{01}^{coll} + \gamma_{10}^{coll} + \gamma_{12}^{coll}\right)^2}. \tag{3.68c}$$

Since the populations of rotational levels with $j \geq 1$ remain in thermal equilibrium with the ion cloud, the rate per molecular ion at which the microwave radiation energy is transferred to the atomic - molecular ion plasma as translational energy is given by:

$$R_H = \hbar\omega_{01}\left(n_{11}\gamma_{10}^{coll} - n_{00}\gamma_{01}^{coll}\right), \tag{3.69}$$

or using Eqs. (3.67):

$$R_H = \hbar\omega_{01}\frac{P_{10}\gamma_{10}^{coll} - \gamma_{01}^{coll}}{1 + \frac{\gamma_{10}^{coll}}{\gamma_{01}^{coll}}\left(Z\left(T_T\right) - 1\right)P_{10}}. \tag{3.70}$$

The direction of energy transfer is determined by the sign of $P_{10}\gamma_{10}^{coll}/\gamma_{01}^{coll} - 1$, where $P_{10}\gamma_{10}^{coll}/\gamma_{01}^{coll}$ is the population inversion between $j = 0$ and $j = 1$ rotational levels in the presence of the microwave field.

3.3.4 Numerical evaluation of collisional enhanced heating rates

As an example, consider a plasma of $^{88}Sr^+$ and $^{88}Sr^{35}Cl^+$ with an atomic ion density $n_A = 1.25 \times 10^{14}\ m^{-3}$ (a 20 μm separation between ions). We take the microwave radiation to have an angular frequency ω_M equal with the $j = 0 \leftrightarrow j = 1$ rotational transition frequency of $^{88}Sr^{35}Cl^+$, and to have an electric field amplitude $E_M = 1500\ V/m$ (which is easily attainable in a surface electrode ion trap with integrated CPW microwave transmission line). With this field amplitude the Rabi frequency becomes $\Omega = \mu\left\langle Y_{00}\left|\hat{n}\cdot\hat{z}\right|Y_{10}\right\rangle E_M/\hbar = 2.68 \times 10^8\ Hz$. Under these assumptions the popu-

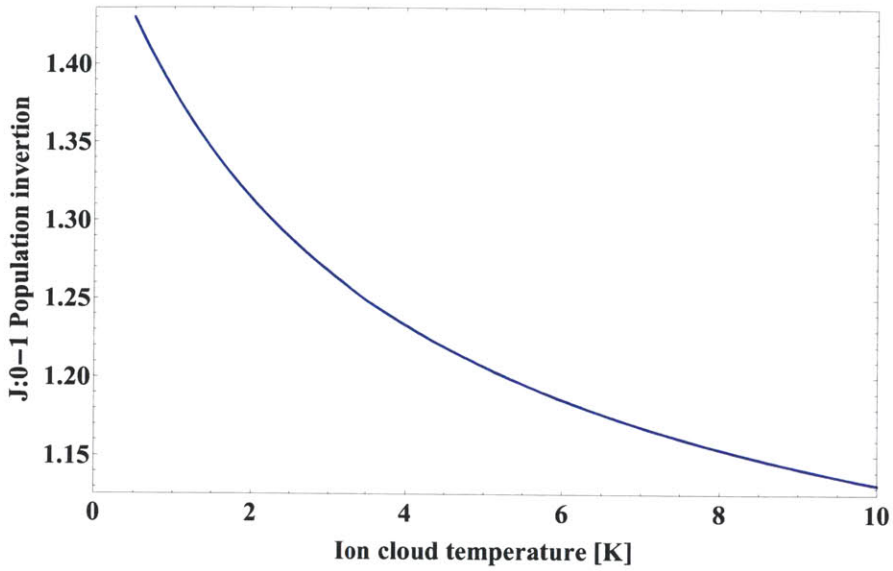

Figure 3-6: Population inversion as function of the ion cloud temperature, in the presence of microwave radiation tuned to resonance with the $j = 0 \leftrightarrow j = 1$ transition ($\Delta_M = 0$). The other parameters are as in text: $E_M = 1500\ V/m$, $n_A = 1.25 \times 10^{14}\ m^{-3}$.

lation inversion between $j = 0$ and $j = 1$ rotational levels in the presence of the microwave field is presented in Figure 3-6, while the rate per molecular ion at which the microwave radiation energy is transferred to the atomic - molecular ion plasma as translational energy is shown in Figure 3-7 (see Appendix B for details).

For the actual experiment, it is required to know the maximum microwave frequency step at which the microwave - rotational transition resonance needs to be scanned with. Since the rotational transition frequency is not known exactly, it is necessary to set the scan step to be less or equal to half of the full width at half maximum (FWHM) of the rotational transition frequency. For the case in which the $SrCl^+$ is trapped in an ion cloud the transition FWHM has three components: the natural width, the collisional width, and the Doppler width. The natural width was shown previously to have a value of $\gamma_{sp}(1 \rightarrow 0) = 1.03 \times 10^{-7}\ Hz$. The other two widths are temperature dependent, and for an ion cloud temperature $T_T = 1\ K$ the collisional width becomes $\gamma_{coll}(1 \rightarrow 0) = 7.92 \times 10^6\ Hz$, while the Doppler width has a value of $\gamma_{Doppler} = 2.8 \times 10^3\ Hz$. Thus, the microwave frequency scan step should be set to $\Delta\nu_{\mathrm{MW,step}} \lesssim 4 \times 10^6\ Hz$.

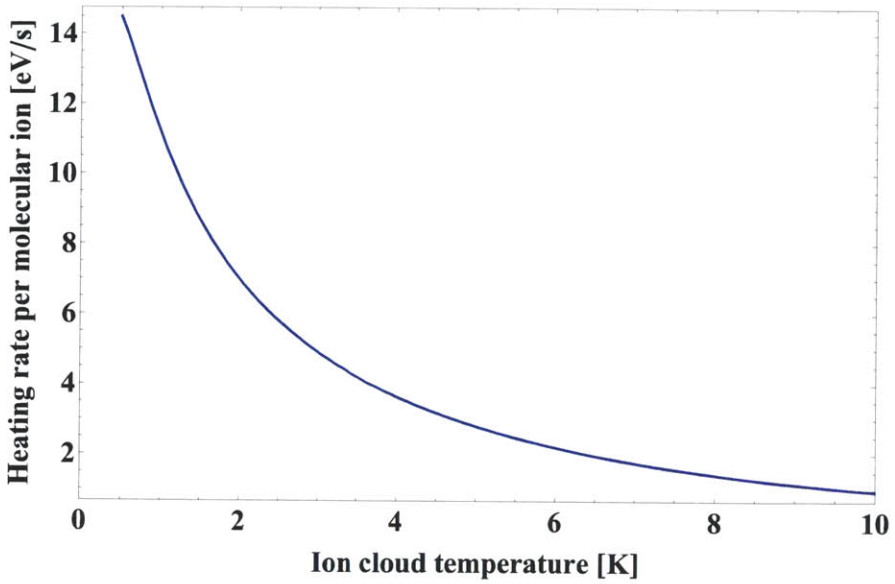

Figure 3-7: Heating rate per molecular ion as function of the ion cloud temperature, in the presence of microwave radiation tuned to resonance with the $j = 0 \leftrightarrow j = 1$ transition ($\Delta_M = 0$). The other parameters are as in text: $E_M = 1500\ V/m$, $n_A = 1.25 \times 10^{14}\ m^{-3}$.

3.4 Cavity assisted microwave heating

In this section, I derive the side band microwave cavity assisted heating rates for a system of one molecular ion and one atomic ion (Figure 3-8). The heating or cooling mechanisms are similar with those involved in assisted laser cooling techniques for atoms trapped in optical cavities [CLZ95, HHG+97, VCB01]. The molecular and atomic ions are co-trapped in a RF ion trap in the presence of a microwave cavity. The first rotational transition of the molecular ion is pumped on the first red motional sideband, while the microwave cavity is tuned to the natural rotational transition frequency (Figure 3-9). This section is divided in three main parts. The first two parts present preliminary result necessary for the actual derivation of the heating rates: in the first part, I review the quantized motion of the two co-trapped ions [Jam98, MECZ99], while in the second part, I compute the quantized electromagnetic normal modes for a CPW microwave cavity [BHW+04, RGRS09] necessary in the determination of the molecular vacuum Rabi frequency. In the final part, I derive the side band microwave cavity assisted heating rates based on a density matrix

approach [ADD+06, WRLZ08].

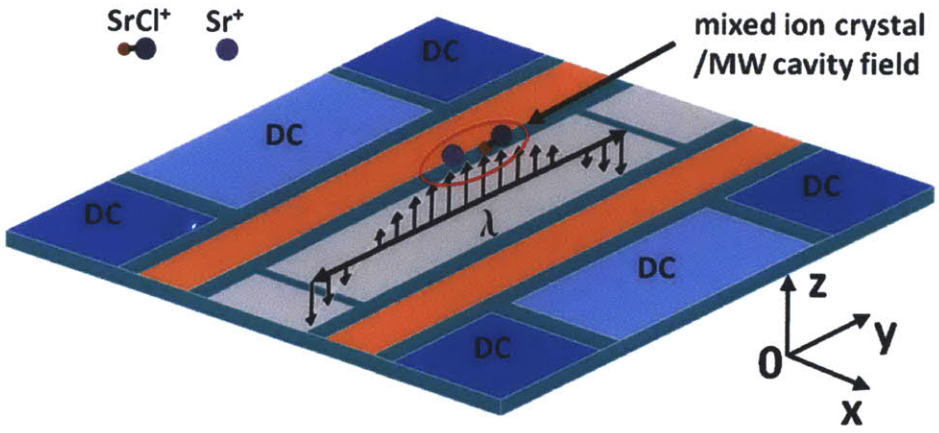

Figure 3-8: Schematic of the cavity assisted microwave heating experiment. An ion crystal composed of one Sr^+ ion and one $SrCl^+$ ion is trapped in a surface electrode ion trap above a CPW microwave cavity.

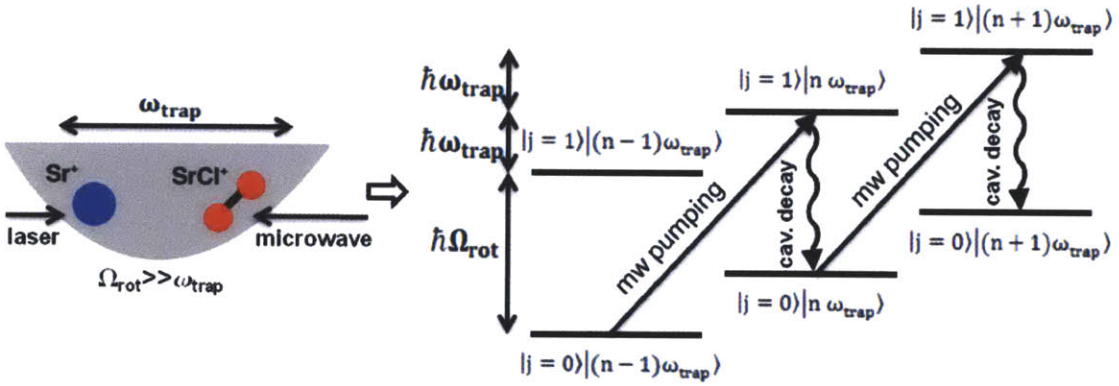

Figure 3-9: Overview of side band microwave cavity assisted heating for a system of one molecular ion and one atomic ion. The molecular and atomic ions are co-trapped in a RF ion trap in Lamb-Dicke regime and in the presence of a microwave cavity. The first rotational transition of the molecular ion is pumped on the first red motional sideband, while the microwave cavity is tuned to the natural rotational transition frequency. In the presence of the microwave cavity the spontaneous decay rate of the molecular excited rotational state is enhanced by the Purcell effect.

3.4.1 Normal modes of a one dimensional harmonic ion trap

Let us consider a system of one atomic ion and one molecular ion confined together by a one dimensional harmonic (parabolic) electric potential. We define a system of

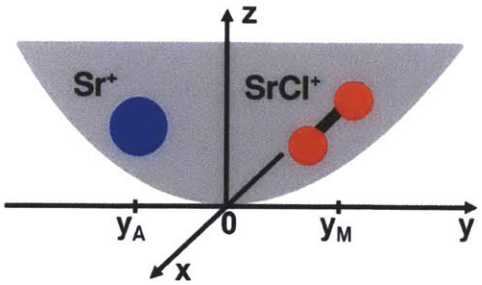

Figure 3-10: System of right-handed cartesian coordinates for analyzing the normal modes of a one dimensional harmonic ion trap. The ion motion is confined to y axis only, and the microwave field is directed along the z axis.

right-handed cartesian coordinates such that the axis of the planar trap lies along the y direction and the normal to the trap surface lies along the z direction (the x direction is automatically defined by the rule $\hat{x} = \hat{y} \times \hat{z}$) (see Figure 3-10). Assuming that the confining potential has a minimum at $y = 0$, without loss of generality it can be written as:

$$\Phi(y) = \frac{a}{2} y^2. \tag{3.71}$$

With this definition for the confining electric potential, the Lagrangian of the ion trap and ions is [GPS01]:

$$\mathcal{L} = \frac{m_A \dot{y_A}^2}{2} + \frac{m_M \dot{y_M}^2}{2} - e\frac{a}{2} {y_A}^2 - e\frac{a}{2} {y_M}^2 - \frac{e^2}{4\pi\epsilon_0} \frac{1}{|y_M - y_A|}, \tag{3.72}$$

where the subscripts A and M stand for the atomic ion coordinates and molecular ion coordinates, respectively. Since we are interested in the small amplitude motion of the ions around their equilibrium positions, we need to determine these equilibrium positions by minimizing the potential energy in the Lagrangian $\mathcal{L}$ with respect to y_A and y_M:

$$\frac{\partial}{\partial y_A} V(y_A, y_M) = e a y_A + \frac{e^2}{4\pi\epsilon_0} \frac{1}{(y_M - y_A)^2} = 0, \tag{3.73a}$$

$$\frac{\partial}{\partial y_M} V(y_A, y_M) = e a y_M - \frac{e^2}{4\pi\epsilon_0} \frac{1}{(y_M - y_A)^2} = 0, \tag{3.73b}$$

where we assumed that $y_M > y_A$. Solving the system of equations (3.73), we obtain:

$$y_{\mathrm{Meq}} = -y_{\mathrm{Aeq}} = y_0 = \left(\frac{e}{16\pi\epsilon_0 a}\right)^{1/3}. \tag{3.74}$$

Let us define a new set of coordinates for the ions (small amplitude motion):

$$y_A = -y_0 + \xi_A, |\xi_A| \ll y_0, \tag{3.75a}$$

$$y_M = y_0 + \xi_M, |\xi_M| \ll y_0. \tag{3.75b}$$

Expanding the potential energy to the second order in $\xi_{A,M}$ (by the definition of equilibrium the first order expansion is zero), the Lagrangian (3.72) becomes:

$$\mathcal{L} = \frac{m_A \dot{\xi_A}^2}{2} + \frac{m_M \dot{\xi_M}^2}{2} - ea\left({\xi_A}^2 + {\xi_M}^2 - \xi_A \xi_M\right), \tag{3.76}$$

where the constant energy terms were neglected. The Lagrangian (3.76) can be written in a matriceal form by defining a displacement vector:

$$|\xi\rangle = \begin{pmatrix} \xi_A \\ \xi_M \end{pmatrix}, \tag{3.77}$$

a mass matrix:

$$M = \begin{pmatrix} m_A & 0 \\ 0 & m_M \end{pmatrix}, \tag{3.78}$$

and an elastic constant matrix:

$$K = \begin{pmatrix} 2\mathrm{ea} & -\mathrm{ea} \\ -\mathrm{ea} & 2\mathrm{ea} \end{pmatrix}, \tag{3.79}$$

yielding:

$$\mathcal{L} = \frac{1}{2}\left\langle \dot{\xi} | M | \dot{\xi} \right\rangle - \frac{1}{2}\langle \xi | K | \xi \rangle. \tag{3.80}$$

In order to determine the normal modes $|\zeta\rangle$, it is necessary to find a time independent

matrix T

$$|\xi\rangle = T|\zeta\rangle, \tag{3.81}$$

such that $T^\dagger MT = I$ and $T^\dagger KT$ is diagonal [GPS01]. The matrix T can be formed from the eigenvectors $|v\rangle$ of the following eigensystem:

$$K|v\rangle = \omega^2 M|v\rangle\,, \tag{3.82}$$

where the eigenvectors are normalized such that:

$$\langle v_i|M|v_j\rangle = \delta_{\mathrm{ij}}. \tag{3.83}$$

Solving the eigensystem (3.82), we obtain the following eigenvalues:

$$\omega_{\mathrm{BM,CM}}{}^2 = \frac{ea}{\mu}\left(1 \pm \sqrt{1 - 3\frac{\mu}{M}}\right), \tag{3.84}$$

where M is the total mass of the ions, μ is the reduced mass of the ions, and where the subscripts BM and CM stand for the breathing mode and center of mass mode, respectively. The corresponding eigenvectors are:

$$|v_{\mathrm{BM}}\rangle = \frac{1}{\sqrt{M}}\sqrt{\frac{1+\alpha}{\alpha + \left(1 - \alpha - \sqrt{\alpha^2 - \alpha + 1}\right)^2}}\begin{pmatrix} 1 \\ 1 - \alpha - \sqrt{\alpha^2 - \alpha + 1} \end{pmatrix}, \tag{3.85a}$$

$$|v_{\mathrm{CM}}\rangle = \frac{1}{\sqrt{M}}\sqrt{\frac{1+\alpha}{\alpha + \left(1 - \alpha + \sqrt{\alpha^2 - \alpha + 1}\right)^2}}\begin{pmatrix} 1 \\ 1 - \alpha + \sqrt{\alpha^2 - \alpha + 1} \end{pmatrix}, \tag{3.85b}$$

with $\alpha = m_A/m_M$. With

$$T = \left(|v_{\mathrm{BM}}\rangle\,, |v_{\mathrm{CM}}\rangle\right), \tag{3.86}$$

and

$$|\zeta\rangle = \begin{pmatrix} \zeta_{\mathrm{BM}} \\ \zeta_{\mathrm{CM}} \end{pmatrix}, \tag{3.87}$$

the Lagrangian (3.76) becomes:

$$\mathcal{L} = \frac{\dot{\zeta}_{\mathrm{BM}}{}^2}{2} + \frac{\dot{\zeta}_{\mathrm{CM}}{}^2}{2} - \frac{\omega_{\mathrm{BM}}{}^2\zeta_{\mathrm{BM}}{}^2}{2} - \frac{\omega_{\mathrm{CM}}{}^2\zeta_{\mathrm{CM}}{}^2}{2}. \tag{3.88}$$

The Hamiltonian associated with the Lagrangian (3.88) is:

$$\mathcal{H} = \frac{\pi_{\mathrm{BM}}{}^2}{2} + \frac{\pi_{\mathrm{CM}}{}^2}{2} + \frac{\omega_{\mathrm{BM}}{}^2\zeta_{\mathrm{BM}}{}^2}{2} + \frac{\omega_{\mathrm{CM}}{}^2\zeta_{\mathrm{CM}}{}^2}{2}, \tag{3.89}$$

where π_i are the canonical conjugate momenta to ζ_i. Using the canonical quantization the quantum Hamiltonian of the ion trap - ions system becomes [MECZ99, VMD06, Jam98, ICZ10]:

$$\mathcal{H} = \sum_{i=\mathrm{BM,CM}} \hbar\omega_i \left(a_i^\dagger a_i + \frac{1}{2}\right), \tag{3.90}$$

where $a_i^\dagger$ and a_i are the usual rising and lowering operators:

$$a_i^\dagger = \sqrt{\frac{\omega_i}{2\hbar}}\zeta_i - i\sqrt{\frac{1}{2\hbar\omega_i}}\pi_i, \tag{3.91a}$$

$$a_i = \sqrt{\frac{\omega_i}{2\hbar}}\zeta_i + i\sqrt{\frac{1}{2\hbar\omega_i}}\pi_i, \tag{3.91b}$$

satisfying the commutation relation $\left[a_i, a_i^\dagger\right] = 1$. In terms of quantized normal modes the absolute displacements of the atomic and molecular ions are:

$$y_A = -y_0 + \sum_{i=\mathrm{BM,CM}} (v_i)_1 \sqrt{\frac{\hbar}{2\omega_i}} \left(a_i^\dagger + a_i\right), \tag{3.92a}$$

$$y_M = y_0 + \sum_{i=\mathrm{BM,CM}} (v_i)_2 \sqrt{\frac{\hbar}{2\omega_i}} \left(a_i^\dagger + a_i\right). \tag{3.92b}$$

As an example let us consider a Sr^+ ion and a $SrCl^+$ ion trapped at a motional temperature of 500 mK. The ions are assumed to have a center of mass mode secular

frequency of $\omega_{CM} = 2\pi$ MHz, and a breathing mode secular frequency of $\omega_{BM} = 2\pi \times 1.78$ MHz. Under these assumptions the maximal displacements for the atomic ion and molecular ion are $\xi_{A,max} = 2.6\ \mu m$ and $\xi_{M,max} = 1.8\ \mu m$, respectively.

3.4.2 Circuit QED description of CPW microwave resonator

A lossless microwave resonator formed from a CPW transmission line of finite length L much larger than its transversal dimensions, can be modeled as a one dimensional circuit described by the following classical Hamiltonian [SvdWCL04, DGS07]:

$$H = \int_{-L/2}^{L/2} \left[\frac{l}{2} j(x,t)^2 + \frac{c}{2} v(x,t)^2 \right] dx, \tag{3.93}$$

where l and c are the CPW inductance and capacitance, respectively, per unit length, and where $j(x,t)$ and $v(x,t)$ are the local current and voltage, respectively. From the charge conservation law and Faraday's law equations [Jac99]:

$$\frac{\partial v(x,t)}{\partial t} = -\frac{1}{c}\frac{\partial j(x,t)}{\partial x}, \tag{3.94a}$$

$$\frac{\partial v(x,t)}{\partial x} = -l\frac{\partial j(x,t)}{\partial t}, \tag{3.94b}$$

we obtain a set of wave equations which describe the current $j(x,t)$ and voltage $v(x,t)$ behavior in the microwave resonator:

$$\frac{\partial^2 j(x,t)}{\partial x^2} - \frac{1}{u^2}\frac{\partial^2 j(x,t)}{\partial t^2} = 0, \tag{3.95a}$$

$$\frac{\partial^2 v(x,t)}{\partial x^2} - \frac{1}{u^2}\frac{\partial^2 v(x,t)}{\partial t^2} = 0, \tag{3.95b}$$

with $u = 1 \Big/ \sqrt{lc}$ being the phase velocity. Since the boundary conditions are expressed in terms of the current it is preferably to solve first the current equation (3a) and then use the set of equations (3.94) to determine the microwave resonator voltage. Using the separation of variables method on the current equation (3.95a):

$$\frac{\partial^2 R(x)}{R(x)\partial x^2} = \frac{1}{u^2}\frac{\partial^2 T(t)}{T(t)\partial t^2} = -k^2,\ j(x,t) = R(x)T(t), \tag{3.96}$$

and the relation (3.94b)the solutions for the current and voltage become:

$$j_k(x,t) = T_k(t)\left[A_k e^{\mathrm{ikx}} + B_k e^{-\mathrm{ikx}}\right], \tag{3.97a}$$

$$v_k(x,t) = i\frac{l}{k}\dot{T}_k(t)\left[A_k e^{\mathrm{ikx}} - B_k e^{-\mathrm{ikx}}\right], \tag{3.97b}$$

The time dependence was not explicitly displayed as it is not necessary in the following calculations. The wavevector k and the integration constants A and B are determined from the boundary conditions, which require that there be no current flow at the microwave resonator ends:

$$j_k\left(x = \pm\frac{L}{2}, t\right) \equiv 0. \tag{3.98}$$

Applying the condition (3.98) on the current solution, we obtain:

$$k = n\frac{\pi}{L}, n \in \mathbb{Z}, \tag{3.99a}$$

$$B_n = -(-1)^n A_n, \tag{3.99b}$$

and the general solutions:

$$j(x,t) = \sum_{n\geq 2,\ \text{even}} T_n(t)\sin\left(n\frac{\pi}{L}x\right) + \sum_{n\geq 1,\ \text{odd}} T_n(t)\cos\left(n\frac{\pi}{L}x\right), \tag{3.100a}$$

$$v(x,t) = -\sum_{n\geq 2,\ \text{even}} \frac{l}{k_n}\dot{T}_n(t)\cos\left(n\frac{\pi}{L}x\right) + \sum_{n\geq 1,\ \text{odd}} \frac{l}{k_n}\dot{T}_n(t)\sin\left(n\frac{\pi}{L}x\right), \tag{3.100b}$$

where the constants A_n were absorbed in the definition of T_n. With the solutions as in Eqs. (3.100) the classical Hamiltonian becomes:

$$H = \frac{Ll}{4}\sum_{n\geq 1} T_n(t)^2 + \frac{Ll}{4}\sum_{n\geq 1}\frac{\dot{T}_n(t)^2}{(uk_n)^2}. \tag{3.101}$$

By defining the canonical conjugate variables:

$$q_n = \sqrt{\frac{Ll}{2}} \frac{T_n(t)}{\omega_n}, \tag{3.102a}$$

$$p_n = \sqrt{\frac{Ll}{2}} \frac{\dot{T}_n(t)}{\omega_n}, \ \omega_n = uk_n = n\frac{\pi}{L}u, \tag{3.102b}$$

the Hamiltonian (3.101) takes the form of a set of harmonic oscillators:

$$H = \sum_{n\geq 1} \left(\frac{{p_n}^2}{2} + \frac{{\omega_n}^2 {q_n}^2}{2} \right). \tag{3.103}$$

The Hamiltonian (3.103) can be easily quantized by introducing the bosonic creation and annihilation operators [BHW+04, SBC+11, RGRS09]:

$$a_n^\dagger = \sqrt{\frac{\omega_n}{2\hbar}} q_n - i\sqrt{\frac{1}{2\hbar\omega_n}} p_n, \tag{3.104a}$$

$$a_n = \sqrt{\frac{\omega_n}{2\hbar}} q_n + i\sqrt{\frac{1}{2\hbar\omega_n}} p_n, \tag{3.104b}$$

with $\left[a_n, a_m^\dagger\right] = \delta_{\mathrm{nm}}$. With the help of relations (3.102) and (3.104) the quantized voltage becomes:

$$v(x,t) = i \sum_{n\geq 2,\mathrm{even}} \sqrt{\frac{\hbar\omega_n}{Lc}} \cos\left(n\frac{\pi}{L}x\right)\left(a_n - a_n^\dagger\right) - i \sum_{n\geq 1,\mathrm{odd}} \sqrt{\frac{\hbar\omega_n}{Lc}} \sin\left(n\frac{\pi}{L}x\right)\left(a_n - a_n^\dagger\right). \tag{3.105}$$

In the case in which the microwave resonator is embedded between two semi-infinite CPW transmission lines, where the couplings can be modeled as two capacitors of capacitance C_0, it was shown (Ch. 2) that the discrete wavevectors are given by the following non-linear equations:

$$\frac{C_0}{c}k = \operatorname{cotan}\left(k\frac{L}{2}\right), \text{ odd modes,} \tag{3.106a}$$

$$\frac{C_0}{c}k = -\tan\left(k\frac{L}{2}\right), \text{ even modes.} \tag{3.106b}$$

Although the algebraic expression for the current and voltage remain the same as in

Eqs. (3.100) (with the new set of wavevectors), the trigonometric functions appearing in Eqs. (3.100) no longer form a complete set over the length of the microwave resonator, and as such the Hamiltonian cannot be diagonalized exactly anymore.

3.4.3 Quantum Hamiltonian for a system of one molecular ion and one atomic ion co-trapped in the presence of a microwave cavity

In the presence of a microwave cavity and an applied microwave field the Hamiltonian describing the evolution of the trapped atomic and molecular ions is [ADD+06, WRLZ08, RZ07]:

$$\mathcal{H} = \mathcal{H}_{\text{trap}} + \mathcal{H}_{\text{rotational}} + \mathcal{H}_{\text{cavity}} + \mathcal{H}_{\text{trap-dipole}} + \mathcal{H}_{\text{cavity-dipole}} + \mathcal{H}_{\text{microwave-dipole}}. \quad (3.107)$$

In the following, we will show that the $\mathcal{H}_{\text{trap-dipole}}$ interaction term can be neglected due to the ion trap and microwave cavity geometry. $\mathcal{H}_{\text{trap-dipole}}$ is produced by the interaction of the electric field at the molecular ion location due to the small displacements of the ions from their equilibrium positions and the permanent electric dipole of the molecular ion. The last two interaction terms $\mathcal{H}_{\text{cavity-dipole}}$ and $\mathcal{H}_{\text{microwave-dipole}}$ are due to the coupling of the vacuum cavity field and applied microwave field to the molecular electric dipole. With our particular choice of coordinates the trap electric field is oriented along y axis and the cavity/microwave fields are aligned along the z (although the exact orientation is irrelevant, only the relative orientation of the fields is important). Choosing the quantization axis along the z direction and assuming that the $j = 1$ magnetic sublevels are degenerated the relevant rotational levels are:

$$|g\rangle = |Y_{00}\rangle\,, \quad (3.108a)$$

$$|e\rangle = e_{-1}\,|Y_{1,-1}\rangle + e_0\,|Y_{1,0}\rangle + e_{+1}\,|Y_{1,+1}\rangle\,. \quad (3.108b)$$

From Eq. (3.22) the matrix elements for the electric dipole electric - field interaction are proportional to:

$$\mu_{\text{trap}} \propto \langle e| P_1 (\hat{n} \cdot \hat{y}) |g\rangle , \tag{3.109a}$$

$$\mu_{\text{cavity/MW}} \propto \langle e| P_1 (\hat{n} \cdot \hat{z}) |g\rangle , \tag{3.109b}$$

where $\hat{n}$ is the direction of the molecular permanent electric dipole. Making use of the spherical harmonics addition theorem the transition matrix elements become:

$$\begin{aligned} \mu_{\text{trap}} \quad &\propto \langle e| \left(\sum_{m=-1}^{1} Y^*_{1,m} Y_{1,m} (\hat{y}) \right) |g\rangle \propto \langle e| \left(\sum_{m=-1}^{1} Y^*_{1,m} Y_{1,m} (\theta = \pi/2, \phi = \pi/2) \right) |g\rangle \\ &\propto \langle e \left| \left(Y^*_{1,-1} + Y^*_{1,+1} \right) \right. |g\rangle \propto e_{-1} \langle Y_{1,-1} | Y^*_{1,-1} | g\rangle + e_{+1} \langle Y_{1,+1} | Y^*_{1,+1} | g\rangle , \end{aligned} \tag{3.110a}$$

$$\begin{aligned} \mu_{\text{cavity/MW}} \quad &\propto \langle e| \left(\sum_{m=-1}^{1} Y^*_{1,m} Y_{1,m} (\hat{z}) \right) |g\rangle \propto \langle e| \left(\sum_{m=-1}^{1} Y^*_{1,m} Y_{1,m} (\theta = 0, \phi) \right) |g\rangle \\ &\propto \langle e \left| \left(Y^*_{1,0} \right) \right. |g \rangle \propto e_0 \langle Y_{1,0} | Y^*_{1,0} | g\rangle , \end{aligned} \tag{3.110b}$$

which shows that the two orthogonal electric fields couple the ground state to two orthogonal subspaces of the excited state. Thus transitions between $j = 0$ and $j = 1, m = \pm 1$ can be mediated only by transitions in the ion trap phonon number. But given that the discrepancy between the phonon frequency and microwave frequency is 4 orders of magnitude such transitions are energy forbidden, which was also experimentally confirmed [BJD06, KRS07]. Based on these observation the Hilbert space of the molecular internal degrees of freedom becomes a two dimensional space composed from the $|j = 0, m = 0\rangle$ and $|j = 1, m = 0\rangle$ states. With the applied microwave field described as a classical field with the frequency ω_{MW} and with rotating wave approximation the Hamiltonian (3.107) becomes:

$$\mathcal{H} = \sum_{i=\mathrm{BM,CM}} \hbar\omega_i a_i^\dagger a_i - \frac{\hbar\Delta}{2}\sigma_z + \hbar\left(\Delta_C - \Delta\right) c^\dagger c + \hbar g\left(y_M\right)\left(\sigma_+ c + \sigma_- c^\dagger\right) + \frac{\hbar\Omega\left(y_M\right)}{2}\sigma_x, \tag{3.111}$$

where $\Omega\left(y_M\right)$ is the Rabi frequency of the applied microwave field, $g\left(y_M\right)$ is the coupling of the cavity vacuum field to the molecular electric dipole, $c^\dagger$ and c are the rising and lowering operators of the cavity field, $\Delta = \omega_{\mathrm{MW}} - \omega_0$ is the detuning between the applied microwave field and microwave transition frequency, and $\Delta_C = \omega_C - \omega_0$ is the detuning between cavity and molecular transition frequency. Since the displacement of the molecular ion from the equilibrium position is in hundreds of nanometers range, while the wavelengths of the standing applied microwave field and vacuum cavity field are in the centimeter range (Lamb-Dicke regime), both the Rabi frequency and the cavity coupling constant can be expanded to the first order in the molecular ion position [Jam98, MECZ99]:

$$\Omega\left(y_M\right) = \Omega_0 \cos\left(k_{\mathrm{MW}} y_M + \phi\right) \simeq \Omega_0 \cos(\phi) - \Omega_0 \sin(\phi) k_{\mathrm{MW}} y_M, \tag{3.112a}$$

$$g\left(y_M\right) = g_0 \cos\left(k_C y_M + \phi\right) \simeq g_0 \cos(\phi) - g_0 \sin(\phi) k_C y_M. \tag{3.112b}$$

Since both the zeroth and the first order terms are important in the cavity assisted heating (or cooling) a suitable choice for the wave phase is $\phi = \pi/4$.

3.4.4 Microwave cavity assisted side band heating rates

The evolution of the trapped atomic ion and molecular ion coupled to the microwave cavity field system is given by the density matrix $\rho(t)$, described by the following master equation [CBZP92]:

$$\dot{\rho} = \mathcal{L}(\rho) = -\frac{i}{\hbar}[\mathcal{H}, \rho] + \mathcal{L}_{\mathrm{th}}(\rho), \tag{3.113}$$

where $\mathcal{L}_{\mathrm{th}}(\rho)$ describes the coupling of the microwave cavity to the black body radi-

ation of the environment [Car93, Sac84, CRZ91]:

$$\mathcal{L}_{\text{th}}(\rho) = \frac{\kappa}{2}\left(n_{\text{th}}+1\right)\mathcal{L}[c](\rho) + \frac{\kappa}{2} n_{\text{th}} \mathcal{L}\left[c^{\dagger}\right](\rho), \tag{3.114}$$

with $\mathcal{L}[c](\rho) = 2c\rho c^{\dagger} - \rho c^{\dagger}c - c^{\dagger}c\rho$, and where κ is the microwave cavity decay rate and where n_{th} is the mean number of photons at the cavity frequency and temperature T, $n_{\text{th}} = 1 \Big/ \left[\exp\left(\frac{\hbar\omega_C}{k_B T}\right) - 1\right]$. The couplings of the molecular levels to other modes than cavity modes were neglected as the natural life time of the excited levels is of the order of 10^7 s. The subsequent analysis follows the one presented in reference [WRLZ08], with the difference that here two ionic external degrees of freedom are present. To proceed further, we separate the Liouville operator (3.113) in three components [CBZP92, MNP+06, WRLZ08]:

$$\mathcal{L} = \mathcal{L}_M + \mathcal{L}_C + \mathcal{L}_g, \tag{3.115}$$

where the first term $\mathcal{L}_M$ describes the uncoupled dynamics of the molecular ion:

$$\mathcal{L}_M(\rho) = -\frac{i}{\hbar}\left[\mathcal{H}_M, \rho\right], \ \mathcal{H}_M = \sum_{i=\text{BM,CM}} \hbar\omega_i a_i^{\dagger} a_i - \frac{\hbar\Delta}{2}\sigma_z + \frac{\hbar\Omega\left(y_M\right)}{2}\sigma_x, \tag{3.116}$$

where the second term $\mathcal{L}_C$ describes the dynamics of the cavity coupled to the black body radiation:

$$\mathcal{L}_C(\rho) = -\frac{i}{\hbar}\left[\hbar\left(\Delta_C - \Delta\right)c^{\dagger}c, \rho\right] + \mathcal{L}_{\text{th}}(\rho), \tag{3.117}$$

and where the last term $\mathcal{L}_g$ describes the coupling between cavity mode and molecule:

$$\mathcal{L}_g(\rho) = -\frac{i}{\hbar}\left[\hbar g\left(y_M\right)\left(\sigma_+ c + \sigma_- c^{\dagger}\right), \rho\right]. \tag{3.118}$$

In the weak coupling regime $\kappa \gg g$ the system relaxes into the state $\rho(t) \approx \rho_M(t) \otimes \rho_C^0$, where ρ_C^0 is the cavity equilibrium density operator defined as:

$$\mathcal{L}_C\left(\rho_C^0\right) = 0. \tag{3.119}$$

Following references [Zwa64, CBZP92], we introduce the projection operators:

$$\mathcal{P}\rho = \mathrm{Tr}_C\{\rho\} \otimes \rho_C^0, \tag{3.120a}$$

$$\mathcal{Q} = 1 - \mathcal{P}, \tag{3.120b}$$

with the following properties:

$$\mathcal{P}\mathcal{L}_M = \mathcal{L}_M\mathcal{P}, \tag{3.121a}$$

$$\mathcal{P}\mathcal{L}_C = \mathcal{L}_C\mathcal{P} = 0, \tag{3.121b}$$

$$\mathcal{P}\mathcal{L}_g\mathcal{P} = 0, \tag{3.121c}$$

$$\mathcal{P}^2 = \mathcal{P},\ \mathcal{Q}^2 = \mathcal{Q}. \tag{3.121d}$$

Making the notations:

$$\mathcal{P}\rho(t) = v(t),\ \mathcal{Q}\rho(t) = w(t), \tag{3.122}$$

and applying the Laplace transform to the equation of motion (3.113), we obtain the following set of equations:

$$s\tilde{v}(s) - v(0) = \mathcal{L}_M\tilde{v}(s) + \mathcal{P}\mathcal{L}_g\tilde{w}(s), \tag{3.123a}$$

$$s\tilde{w}(s) - w(0) = \left(\mathcal{L}_M + \mathcal{L}_C + \mathcal{Q}\mathcal{L}_g\right)\tilde{w}(s) + \mathcal{Q}\mathcal{L}_g\tilde{w}(s), \tag{3.123b}$$

where $\tilde{f}(s) = \int_0^\infty f(t)e^{-st}dt$. Solving the system of equations (3.123) for $\tilde{v}(s)$, and inverting back to time domain with the help of the convolution theorem, we obtain an equation of motion which involves only the molecular degrees of freedom:

$$\dot{\rho}_M(t) = -\frac{i}{\hbar}\left[\mathcal{H}_M, \rho_M(t)\right] + \mathrm{Tr}_C\left\{\mathcal{L}_g \int_0^\infty e^{\langle \mathcal{L}_M + \mathcal{L}_C \rangle \tau} \mathcal{Q}\mathcal{L}_g e^{-\mathcal{L}_M \tau}\left[\rho_M(t) \otimes \rho_C^0\right] d\tau\right\}, \tag{3.124}$$

with $\rho_M(t) = \mathrm{Tr}_C\{\mathcal{P}\rho(t)\}$. Inserting the definitions of $\mathcal{L}_M$, $\mathcal{L}_C$ and $\mathcal{L}_g$ in (3.124) and using the quantum regression theorem [Swa81, GZ04], we obtain the following effective molecular master equation [WRLZ08]:

$$\dot{\rho}_M = -\frac{i}{\hbar}\left[\mathcal{H}_M, \rho_M\right] + \left[(n_{\mathrm{th}}+1)\left(\mathrm{T}\rho_M S^\dagger - S^\dagger \mathrm{T}\rho_M\right) + n_{\mathrm{th}}\left(T^\dagger \rho_M S^\dagger - \mathrm{S}\mathrm{T}^\dagger \rho_M\right) + h.c.\right], \tag{3.125}$$

where we made the notations:

$$S = g\left(y_M\right)\sigma_-,\ S(t) = e^{\mathrm{i}\mathcal{H}_M t}\mathrm{S}e^{-\mathrm{i}\mathcal{H}_M t},\ T = \int_0^\infty e^{-i(\Delta_C - \Delta)\tau} e^{-\kappa\tau/2} S(-\tau) d\tau. \tag{3.126}$$

In the Lamb-Dicke regime the internal and external molecular degrees of freedom interact weakly, which allows to use the same procedure as for the cavity mode to adiabatically eliminate the molecular internal degrees of freedom. Expanding $\Omega\left(y_M\right)$ and $g\left(y_M\right)$ to the first order in Lamb-Dicke parameters yields:

$$\Omega\left(y_M\right) \simeq \Omega\left[1 + \sum_{i=\mathrm{BM,CM}} \eta_{\mathrm{MW},i}\left(a_i^\dagger + a_i\right)\right], \tag{3.127a}$$

$$g\left(y_M\right) \simeq g\left[1 + \sum_{i=\mathrm{BM,CM}} \eta_{C,i}\left(a_i^\dagger + a_i\right)\right], \tag{3.127b}$$

with

$$\Omega = \Omega_0\cos(\phi) - \Omega_0\sin(\phi)k_{\mathrm{MW}}y_0,\ \eta_{\mathrm{MW},i} = -\Omega_0\sin(\phi)k_{\mathrm{MW}}\left(\upsilon_i\right)_2\sqrt{\frac{\hbar}{2\omega_i}}\Big/\Omega, \tag{3.128a}$$

$$g = g_0 \cos(\phi) - g_0 \sin(\phi) k_C y_0,\ \eta_{C,i} = -g_0 \sin(\phi) k_C \left(v_i\right)_2 \sqrt{\frac{\hbar}{2\omega_i}} \Big/ g. \tag{3.128b}$$

To the same order approximation the operator T defined in Eq. (3.126) becomes:

$$T \simeq g \left[\Sigma_- + \sum_{i=\mathrm{BM,CM}} \eta_{C,i} \left(\Sigma_- \left(\omega_i\right) a_i + \Sigma_+ \left(-\omega_i\right) a_i^\dagger \right) \right], \tag{3.129}$$

where

$$\Sigma_\pm(\omega) = \int_0^\infty e^{i[\omega \pm (\Delta_C - \Delta)]\tau} e^{-\kappa\tau/2} \sigma_\pm(-\tau) d\tau,\ \Sigma_\pm = \Sigma_\pm(0), \tag{3.130}$$

and

$$\sigma_\pm(t) = e^{\mathrm{i}\mathcal{H}_I t} \sigma_\pm e^{-\mathrm{i}\mathcal{H}_I t},\ \mathcal{H}_I = -\frac{\hbar\Delta}{2}\sigma_z + \frac{\hbar\Omega}{2}\sigma_x. \tag{3.131}$$

Using the properties of Pauli matrices the exponentials appearing in Eq. (3.131) can be expanded as:

$$e^{-\mathrm{i}\mathcal{H}_I t} = \cos\left(\frac{\Omega_1 t}{2}\right) I + i \sin\left(\frac{\Omega_1 t}{2}\right) \left[\frac{\Delta}{\Omega_1}\sigma_z - \frac{\Omega}{\Omega_1}\sigma_x \right],\ \Omega_1 = \sqrt{\Omega^2 + \Delta^2} \tag{3.132}$$

Using the above relation the integral in Eq. (3.130) can be evaluated yielding:

$$\Sigma_-(\omega) = C_-(\omega)\sigma_- + C_+(\omega)\sigma_+ + C_z(\omega)\sigma_z,\ \Sigma_+(\omega) = \Sigma_-^\dagger(-\omega), \tag{3.133}$$

where the coefficients $C(\omega)$ are defined as:

$$C_-(\omega) = \frac{1}{4{\Omega_1}^2} \left[\frac{2\Omega^2}{\kappa/2 - i\left(\omega - \Delta_g\right)} + \sum_{p=\pm} \frac{\left(\Delta + \mathrm{p}\Omega_1\right)^2}{\kappa/2 - i\left(\omega - \left(\Delta_g + \mathrm{p}\Omega_1\right)\right)} \right], \tag{3.134a}$$

$$C_+(\omega) = \frac{1}{4{\Omega_1}^2} \left[\frac{2\Omega^2}{\kappa/2 - i\left(\omega - \Delta_g\right)} - \sum_{p=\pm} \frac{\Omega^2}{\kappa/2 - i\left(\omega - \left(\Delta_g + \mathrm{p}\Omega_1\right)\right)} \right], \tag{3.134b}$$

$$C_z(\omega) = \frac{1}{4{\Omega_1}^2}\left[\frac{-2\Omega\Delta}{\kappa/2 - i\left(\omega - \Delta_g\right)} + \sum_{p=\pm}\frac{\Omega\left(\Delta + \mathrm{p}\Omega_1\right)}{\kappa/2 - i\left(\omega - \left(\Delta_g + \mathrm{p}\Omega_1\right)\right)}\right], \tag{3.134c}$$

where $\Delta_g = \Delta_C - \Delta$. The molecular master equation (3.125) expanded up to second order in Lamb-Dicke parameters becomes:

$$\dot{\rho}_M(t) \simeq \left(\mathcal{L}_0 + \mathcal{L}_1 + \mathcal{L}_2\right)\rho_M(t). \tag{3.135}$$

The zeroth order term $\mathcal{L}_0$ is:

$$\mathcal{L}_0 = \mathcal{L}_E + \mathcal{L}_I, \tag{3.136}$$

where $\mathcal{L}_E$ represents the uncoupled dynamics of the molecular external degrees of freedom:

$$\mathcal{L}_E\rho_M = -\frac{i}{\hbar}\left[\sum_{i=\mathrm{BM,CM}}\hbar\omega_i a_i^\dagger a_i, \rho_M\right], \tag{3.137}$$

and where $\mathcal{L}_I$ represents the uncoupled effective dynamics of the molecular internal degrees of freedom:

$$\begin{aligned}\mathcal{L}_I\rho_M = \quad & -\frac{i}{\hbar}\left[\mathcal{H}_I, \rho_M\right] + g^2\left(n_{\mathrm{th}} + 1\right)\left[\Sigma_-\rho_M\sigma_+ - \sigma_+\Sigma_-\rho_M + h.c.\right] \\ & + g^2 n_{\mathrm{th}}\left[\Sigma_+\rho_M\sigma_- - \sigma_-\Sigma_+\rho_M + h.c.\right].\end{aligned} \tag{3.138}$$

The first order $\mathcal{L}_1$ and second order $\mathcal{L}_2$ terms are given by:

$$\begin{aligned}\mathcal{L}_1\rho_M = \quad & -i\frac{\Omega}{2}\sum_{i=\mathrm{BM,CM}}\eta_{\mathrm{MW},i}\left[\sigma_x\left(a_i^\dagger + a_i\right),\rho_M\right] \\ & +g^2\left(n_{\mathrm{th}}+1\right)\sum_{i=\mathrm{BM,CM}}\eta_{C,i}\left\{\left[\left(\Sigma_-\left(\omega_i\right)a_i+\Sigma_-\left(-\omega_i\right)a_i^\dagger\right)\rho_M,\sigma_+\right]\right. \\ & \left.+\left[\Sigma_-\rho_M,\sigma_+\left(a_i^\dagger+a_i\right)\right]+h.c.\right\} \\ & +g^2 n_{\mathrm{th}}\sum_{i=\mathrm{BM,CM}}\eta_{C,i}\left\{\left[\left(\Sigma_+\left(\omega_i\right)a_i+\Sigma_+\left(-\omega_i\right)a_i^\dagger\right)\rho_M,\sigma_-\right]\right. \\ & \left.+\left[\Sigma_+\rho_M,\sigma_-\left(a_i^\dagger+a_i\right)\right]+h.c.\right\} \end{aligned} \tag{3.139}$$

and

$$\begin{aligned}\mathcal{L}_2\rho_M = & \\ & g^2\left(n_{\mathrm{th}}+1\right)\sum_{i=\mathrm{BM,CM}}\eta_{C,i}\left\{\left[\left(\Sigma_-\left(\omega_i\right)a_i+\Sigma_-\left(-\omega_i\right)a_i^\dagger\right)\rho_M,\sigma_+\left(a_i^\dagger+a_i\right)\right]+h.c.\right\} \\ & +g^2 n_{\mathrm{th}}\sum_{i=\mathrm{BM,CM}}\eta_{C,i}\left\{\left[\left(\Sigma_+\left(\omega_i\right)a_i+\Sigma_+\left(-\omega_i\right)a_i^\dagger\right)\rho_M,\sigma_-\left(a_i^\dagger+a_i\right)\right]+h.c.\right\}. \end{aligned} \tag{3.140}$$

Proceeding as before, we define the projection operator:

$$\mathcal{P}_\mu\left(\rho_M\right) = \mathrm{Tr}_I\left\{\rho_M\right\}\otimes\rho_I^0, \tag{3.141}$$

where $\mathcal{L}_0\left(\rho_I^0\right)=0$, and obtain the following effective master equation for the molecular external degrees of freedom $\mu(t)=\mathrm{Tr}_I\left\{\mathcal{P}_\mu\rho_M(t)\right\}$:

$$\dot{\mu}(t) = \mathrm{Tr}_I\left\{\mathcal{P}_\mu\mathcal{L}_1\int_0^\infty e^{\mathcal{L}_0\tau}\mathcal{Q}_\mu\mathcal{L}_1\left[\mu(t)\otimes\rho_I^0\right]d\tau\right\}+\mathrm{Tr}_I\left\{\mathcal{P}_\mu\mathcal{L}_2\left[\mu(t)\otimes\rho_I^0\right]\right\}, \tag{3.142}$$

Using the definitions of $\mathcal{L}_{1,2}$ the master equation (3.142) takes the form:

$$\dot{\mu}(t) = \sum_{i=\mathrm{BM,CM}} \left\{ A_{-}(\omega_i)\, \mathcal{L}[a_i](\mu(t)) + A_{+}(\omega_i)\, \mathcal{L}\left[a_i^{\dagger}\right](\mu(t)) \right\} \tag{3.143}$$

The coefficients $A_{\pm}(\omega_i)$ are defined as:

$$A_{\pm}(\omega_i) = S_{\Omega}(\mp\omega_i) + S_g(\mp\omega_i) + S_I(\mp\omega_i), \tag{3.144}$$

where

$$S_{\Omega}(\omega_i) = \frac{(\eta_{\mathrm{MW},i}\Omega)^2}{2} \mathrm{Re} \int_0^{\infty} \mathrm{Tr}_I \left\{ \sigma_x e^{\mathcal{L}_0 \tau} \left(\sigma_x \rho_I^0 \right) \right\} e^{\mathrm{i}\omega_i \tau} d\tau, \tag{3.145}$$

$$S_g(\omega_i) = 2(\eta_{C,i} g)^2 \mathrm{Re} \left\{ (n_{\mathrm{th}} + 1) \langle \sigma_{+} \Sigma_{-}(\omega_i) \rangle_I + n_{\mathrm{th}} \langle \sigma_{-} \Sigma_{+}(\omega_i) \rangle_I \right\}, \tag{3.146}$$

$$S_I(\pm\omega_i) = 2\mathrm{Re} \int_0^{\infty} \mathrm{Tr}_I \left\{ \mathcal{K}_{\pm}^{\dagger} \left(e^{\mathcal{L}_0 \tau} \mathcal{K}_{\pm} \left(\rho_I^0 \right) \right) \right\} e^{\pm \mathrm{i}\omega_i \tau} d\tau - S_{\Omega}(\pm\omega_i), \tag{3.147}$$

with the superoperator $\mathcal{K}$ defined as:

$$\begin{aligned} \mathcal{K}_{\pm}(\rho) = \quad & -i\frac{\Omega}{2}\eta_{\mathrm{MW},i}\sigma_x\rho + \eta_{C,i} g^2 (n_{\mathrm{th}} + 1) \left[\sigma_{-}\rho\Sigma_{+} + \Sigma_{-}(\pm\omega_i)\rho\sigma_{+} \right. \\ & \left. -\sigma_{+}\Sigma_{-}(\pm\omega_i)\rho - \sigma_{+}\Sigma_{-}\rho \right] \\ & +\eta_{C,i} g^2 n_{\mathrm{th}} \left[\sigma_{+}\rho\Sigma_{-} + \Sigma_{+}(\pm\omega_i)\rho\sigma_{-} \right. \\ & \left. -\sigma_{-}\Sigma_{+}(\pm\omega_i)\rho - \sigma_{-}\Sigma_{+}\rho \right]. \end{aligned} \tag{3.148}$$

In order to solve the three terms appearing in the expansion (3.144) it is necessary to determine the time evolution of the molecular internal degrees of freedom ρ_I^0 as described by Eq. (3.138). In order to simplify the notation in the following, we introduce a set of new constants. First, we define:

$$C_- = C_-(0),\ C_+ = C_+(0),\ C_z = C_z(0). \tag{3.149}$$

With the above notations, we introduce a set of energy shifts:

$$\delta = -g^2 \left(2n_{\text{th}} + 1\right) \text{Im}\left[C_-\right], \tag{3.150a}$$

$$\delta_x = \delta_x = g^2 \left(2n_{\text{th}} + 1\right) \text{Im}\left[C_+\right], \tag{3.150b}$$

a set of decay rates:

$$\gamma = 2g^2 \text{Re}\left[C_-\right], \tag{3.151a}$$

$$\gamma_n = 2g^2 \left(2n_{\text{th}} + 1\right) \text{Re}\left[C_-\right], \tag{3.151b}$$

$$\gamma_x = \gamma_y = 2g^2 \left(2n_{\text{th}} + 1\right) \text{Re}\left[C_+\right], \tag{3.151c}$$

$$\Gamma_x = -2g^2 \text{Re}\left[C_z\right], \tag{3.151d}$$

$$\Gamma_y = 2g^2 \text{Im}\left[C_z\right], \tag{3.151e}$$

and a set of effective Rabi frequencies:

$$\Omega_x = 2g^2 \left(2n_{\text{th}} + 1\right) \text{Re}\left[C_z\right], \tag{3.152a}$$

$$\Omega_y = 2g^2 \left(2n_{\text{th}} + 1\right) \text{Im}\left[C_z\right]. \tag{3.152b}$$

With the constants introduced in Eqs. (3.149-3.152) the Bloch equations describing the effective dynamics of the molecular internal degrees of freedom take the form:

$$\left\langle \dot{\vec{\sigma}} \right\rangle = A \left\langle \vec{\sigma} \right\rangle + \vec{\Gamma}, \tag{3.153}$$

where

$$\vec{\sigma} = \begin{pmatrix} \sigma_x \\ \sigma_y \\ \sigma_z \end{pmatrix}, \; A = \begin{pmatrix} -\frac{(\gamma_n - \gamma_x)}{2} & \Delta + \delta - \delta_x & 0 \\ -(\Delta + \delta + \delta_y) & -\frac{(\gamma_n + \gamma_y)}{2} & -\Omega \\ \Omega_x & \Omega + \Omega_y & -\gamma_n \end{pmatrix}, \; \vec{\Gamma} = \begin{pmatrix} \Gamma_x \\ \Gamma_y \\ \gamma \end{pmatrix}. \quad (3.154)$$

Expression (3.145) can be evaluated with the help of quantum regression theorem, which after integration becomes:

$$S_\Omega(\omega_i) = \frac{(\eta_{\mathrm{MW},i}\Omega)^2}{2} \mathrm{Re}\left[\frac{i}{\omega_i}(1,0,0)\cdot(i\omega_i + A)^{-1}\cdot\left(i\omega_i \langle\vec{\sigma}\sigma_x\rangle_0 + \vec{\Gamma}\langle\sigma_x\rangle_0\right)\right]. \quad (3.155)$$

Using Eq. (3.154), in the resolved side band limit the expressions (3.155) and (3.146) become:

$$S_\Omega(\omega_i) = \frac{(\eta_{\mathrm{MW},i}\Omega)^2}{4} \sum_{p=+1,\,0,-1} \frac{\alpha_p \gamma_p}{(\omega_i - p\Omega_1)^2 + {\gamma_p}^2/4}, \quad (3.156)$$

$$\begin{aligned} S_g(\omega_i) = {} & \frac{(\eta_{C,i}g)^2}{4}\sin^2\varphi\left[\frac{\kappa(n_{\mathrm{th}}+1)}{\kappa^2/4 + (\omega_i - \Delta_g)^2} + \frac{\kappa n_{\mathrm{th}}}{\kappa^2/4 + (\omega_i + \Delta_g)^2}\right] \\ & + \frac{(\eta_{C,i}g)^2}{4{\Omega_1}^2}\sum_{p=\pm1}\left[(\Delta + \mathrm{p}\Omega_1)^2\rho^0_{\mathrm{ee}} + \Omega^2\bar{\rho}_{\mathrm{ee}}\right]\frac{\kappa(n_{\mathrm{th}}+1)}{\kappa^2/4 + (\omega_i - (\Delta_g + \mathrm{p}\Omega_1))^2} \\ & + \frac{(\eta_{C,i}g)^2}{4{\Omega_1}^2}\sum_{p=\pm1}\left[(\Delta + \mathrm{p}\Omega_1)^2\rho^0_{\mathrm{gg}} - \Omega^2\bar{\rho}_{\mathrm{ee}}\right]\frac{\kappa n_{\mathrm{th}}}{\kappa^2/4 + (\omega_i + (\Delta_g + \mathrm{p}\Omega_1))^2}, \end{aligned} \quad (3.157)$$

where we introduced further simplifying notations defined below:

$$\rho^0_{\mathrm{gg}} = \frac{n_{\mathrm{th}}+1}{2n_{\mathrm{th}}+1}, \; \rho^0_{\mathrm{ee}} = \frac{n_{\mathrm{th}}}{2n_{\mathrm{th}}+1}, \; \bar{\rho}_{\mathrm{ee}} = \frac{\Omega^2}{2(2n_{\mathrm{th}}+1)(\Delta^2 + {\Omega_1}^2)}, \quad (3.158a)$$

$$\sin\varphi = \Omega/\Omega_1\,, \quad (3.158b)$$

$$\gamma_{\pm} = \gamma_n \left(2 + \sin^2\varphi\right)/2,\ \gamma_0 = \gamma_n \left(2 - \sin^2\varphi\right)/2, \tag{3.158c}$$

$$\alpha_p = \cos^2\varphi \left[\rho_{ee}^0 + \frac{(1 + p|\cos\varphi|)^2}{2\left(2n_{th} + 1\right)\left(1 + \cos^2\varphi\right)}\right]. \tag{3.158d}$$

The evolution of the phonon number in the mode $i = CM, BM$ is determined from the master equation (3.143), and it takes the form [CBZP92, Ste86, ZM05]:

$$\langle \dot{n}_i \rangle = \left[A_+\left(\omega_i\right) - A_-\left(\omega_i\right)\right]\langle n_i \rangle + A_+\left(\omega_i\right). \tag{3.159}$$

3.4.5 Numerical evaluation of cavity assisted side band heating rates

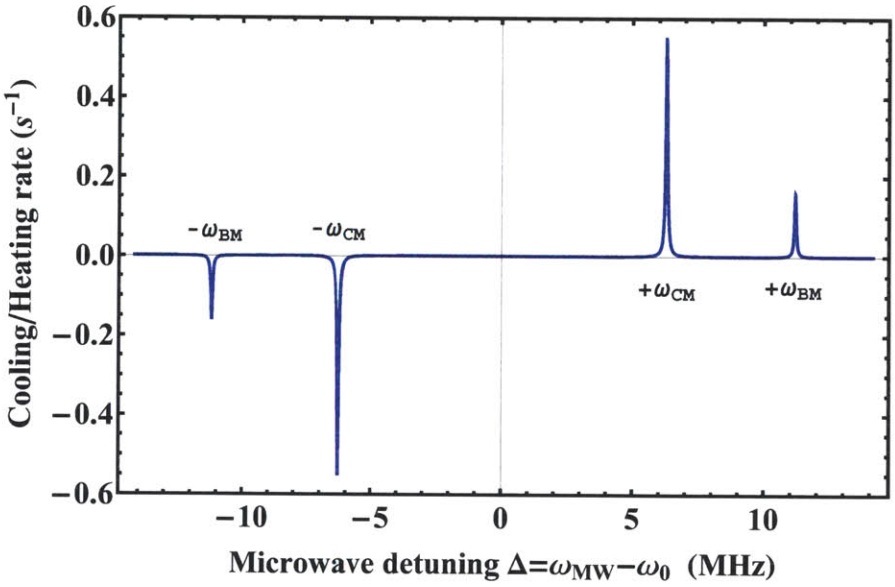

Figure 3-11: Center of mass mode and breathing mode phonon numbers time evolution constant $[A_+(\omega_i) - A_-(\omega_i)]$ as function of the applied microwave field frequency. Negative values signify cooling, while positive values indicate heating. Physical parameters of the trap are provided in text.

Here I analyze a possible scenario for the realization of the microwave cavity assisted side band heating experiment. As an example let us consider a Sr^+ ion and a $SrCl^+$ ion trapped 10 μm above a 50 Ω microwave resonator with a quality factor of $Q = 10^6$. We assume an environment temperature of 500 mK, which sets the ground and excited state initial populations to $n_{j=0,m=0} = 0.28$ and $n_{j=1,m=0} = 0.15$.

The first rotational transition of the molecular ion is driven by a microwave field of 1500 V/m, while the cavity is tuned at resonance with the transition frequency $\Delta_C = 0$. The ions are assumed to have a separation of 4 μm and a center of mass mode secular frequency of $\omega_{CM} = 2\pi$ MHz, and a breathing mode secular frequency of $\omega_{BM} = 2\pi \times 1.78$ MHz. In figure 3-11 I show the value of the proportionality constant $[A_+(\omega_i) - A_-(\omega_i)]$ which determines the cooling or heating rate, as a function of the applied microwave field frequency (see Appendix C for details). As in the case of the collisional assisted heating, it is of experimental importance to know the FWHM of the resonances for the center of mass and breathing modes. For the physical parameters considered here, the two resonance widths are $\Delta\nu_{\mathrm{CM}} = 13.6$ kHz and $\Delta\nu_{\mathrm{BM}} = 14.7$ kHz.

Chapter 4

Experimental Apparatus

Two of the main elements required for the experiments presented here are the superconducting microwave resonator and a source of molecular ions. And since invariably the superconducting regime involves cryogenic temperatures, I have to develop an ion trapping system compatible with the cryogenic environment. The components and the particular requirements necessary to build a cryogenic ion trapping system are presented in first part of this chapter, while in the second I describe a cryogenic compatible atomic and molecular ion source based on a laser ablation method.

There are a number of cryostat designs such as bath, closed cycle and flow cryostats. The simplest design is the bath cryostat, consisting of a vacuum enclosure and thermally insulated reservoirs of liquid cryogens. Several other cryogenic ion traps based on bath cryostats were successfully operated in previous experiments. A cryogenic linear RF ion trap for trapping $^{199}Hg^{+}$ was built by the NIST ion storage group and used as a frequency standard [PBIW96]. A similar system was employed by Okada *et al.* for studying the Bohr-Weisskopf effect in unstable Be^{+} isotopes [OWN+01].

The cryogenic system I present here is based on a closed cycle cryostat, in which the cryogenic refrigerant is continuously cooled in an external heat exchanger. To my knowledge this is the first cryogenic ion trap system built around a closed cycle cryostat.

4.1 Experimental Setup

A good cryogenic ion trapping system must present some of the same characteristics as a room temperature system such as high vacuum and an easy method for ion loading. A low temperature system also brings new benefits like the suppression of electrical noise and a faster turnaround time. On the other hand, the cryogenic systems present few challenges which are not present in the room temperature systems. The cryogenic systems have a limited thermal load capacity, thus special attention must be paid to reduce the heat loads from radiation, conduction and internal heat sources. Specifically, for the cryogenic ion traps, connection wires with low thermal conductivity are required and they have to be heat-sunk at each temperature stage of the cryostat. In the case of the surface-electrode ion trap due to the dielectric RF dissipation in the trap substrate the trap must be carefully thermally anchored to the 4.2 K substrate. Another problem that must be addressed with the closed cycle cryostats due to their principle of operation, is the damping of vibration.

4.1.1 The closed cycle cryostat

The closed cycle cryostat system (Figure 4-1) is constructed around a low vibration cryostat produced by Advanced Research Systems (Model GMX-20B). The cryocooler is based on a two-stage Gifford-McMahon thermal cycle, where typically the first stage can reach a temperature of 40 K at 35 W heat load, and the second stage can reach a temperature of 4.2 K at 0.8 W load. The cryocooler expander head of the cryostat is mechanically decoupled from sample holder tip and vacuum chamber around it. The cavity formed between the expander and sample holder (and a rubber bellow) is filled with ultra high purity helium (99.999 %) at 1.5 atm pressure through which the heat exchange takes place. The cryostat interface comes with an 8 inch conflat (CF) flange and the UHV chamber is built by attaching a full CF nipple, a spherical octagon (Kimball Physics, Model MCF800-SO2000800-A) and an 4 inch glass viewport. The experiment chamber is made from an OFHC cooper tube attached to the 4.2 K cold tip. The cold tip and the experiment chamber are surrounded by a custom made

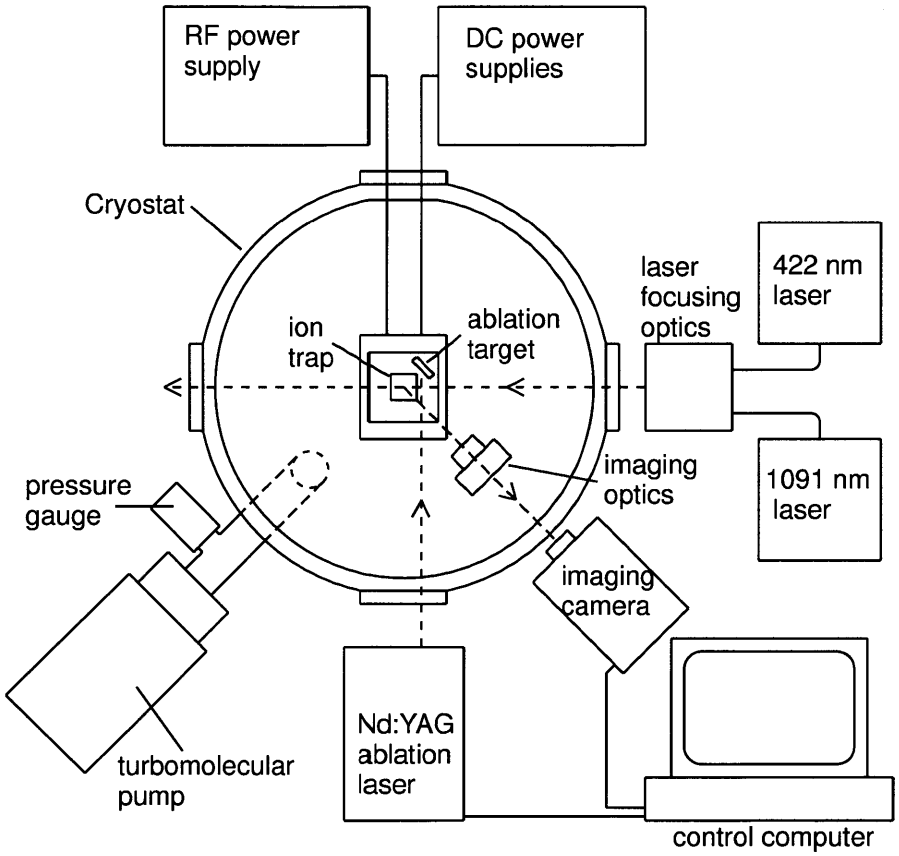

Figure 4-1: Principal components used in the design of the cryostat system. The fluorescence light is collected through the bottom viewport.

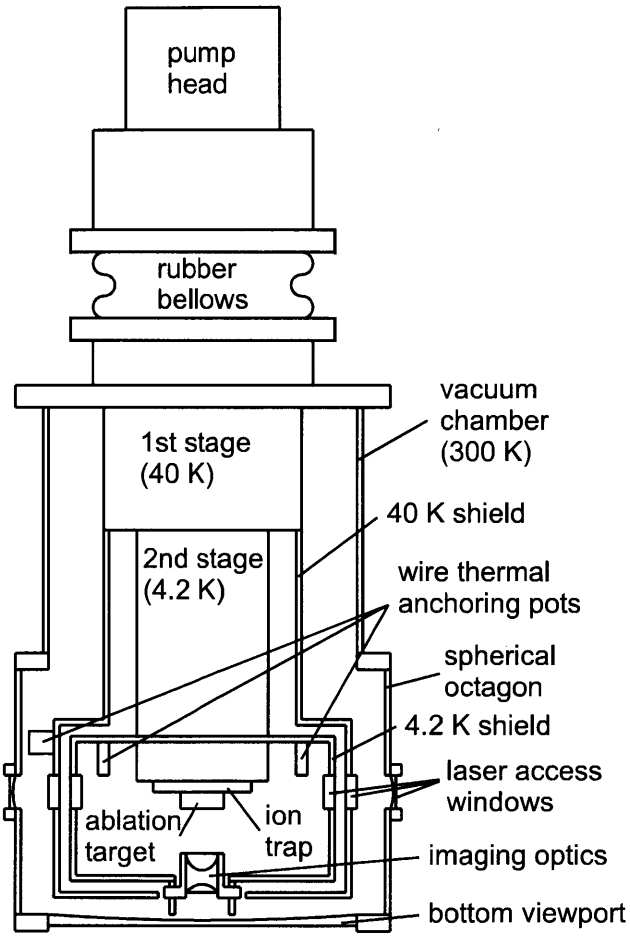

Figure 4-2: Schematic cross section through the closed cycle cryostat. The imaging optics anchored onto 4 K radiation shield is exposed directly to the 300 K radiation from the bottom viewport. (Not to scale)

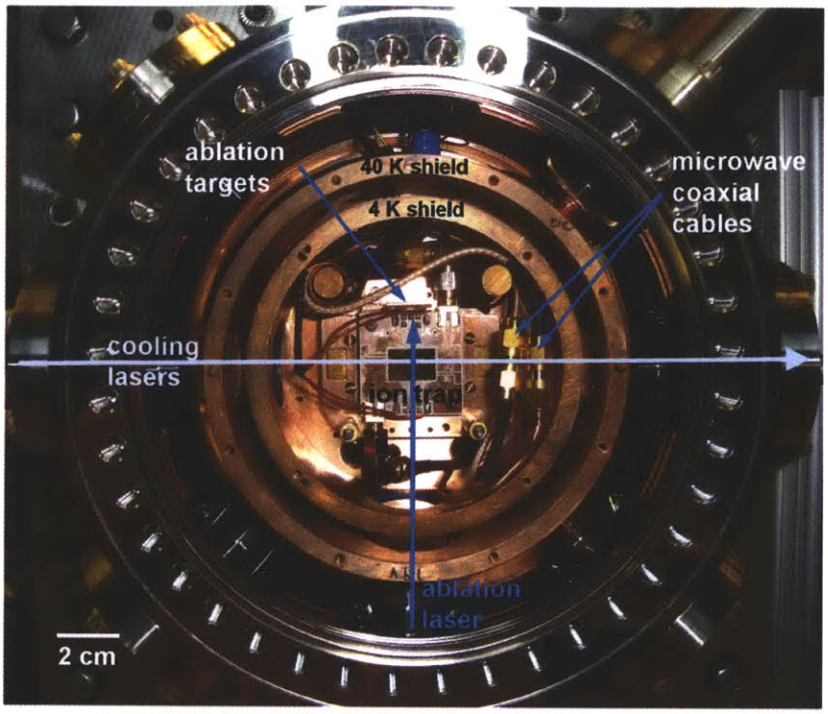

Figure 4-3: View of the closed cycle cryostat working chamber. The rest of visible components are described in Figure 4-2.

radiation shield attached to the 40 K stage of the cryostat (Figure 4-2). Only the room temperature outer chamber is vacuum sealed, with the inner chambers non-hermetically closed. The temperatures of the 4.2 K and 40 K stages are monitored with two silicon diodes (LakeShore, DT-670A-SD).

The cryocooler expander head contains a valve that is actuated by the signal sent from a helium compressor, and which allows the high pressure helium to expand at a rate of about 2 Hz. Since the cryocooler expander head is mechanically decoupled from the cryostat sample interface, it must be supported such that the vibration transfer to the cryostat interface is minimized. In our setup, we chose to place the cryostat on an optical table with the cryocooler expander head supported independently by a holder anchored to the ceiling. But even with this setup, some amount of vibration energy produced by the vertical movement of the expansion valve is transferred between the expander and sample holder through the helium used as heat exchanger between them. In order to measure vertical vibration amplitude of the sample tip, we built a

Michelson interferometer by placing a mirror on the sample tip and a beam splitter and the second mirror on the supporting optical table, and used the light provided by the 422 nm laser. During the operation of the cryocooler compressor, we found that the maximum vertical displacement of the cold tip was below 106 nm (one quarter of an interference fringe). A typical vibration power spectrum of the cold tip is shown in Figure 4-4. The 2 Hz repetition rate of the expansion cycle can be observed in Figure 4-4 inset.

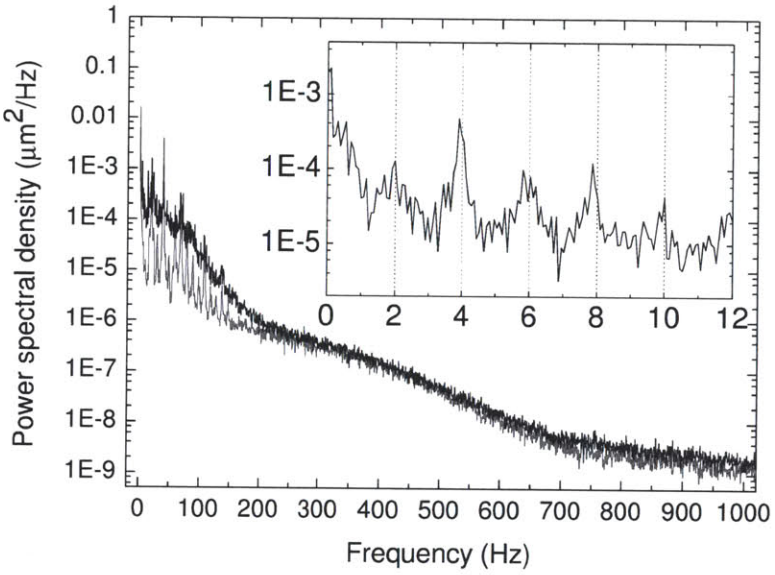

Figure 4-4: Vibration power spectrum of the closed cycle cryostat sample holder. The vibration power spectrum was measured with the cryostat compressor turned off (gray curve) and on (black curve). The inset shows the lower part of the spectrum where the fundamental and higher harmonics of the cryocooler expander head vibration can be distinguished. The spectrum has 2.5 kHz bandwidth and 0.17 Hz resolution.

4.1.2 Trapping potentials delivery components

The ion trap and its pcb carrier are inserted into a socket that is thermally anchored to the 4.2 K cold tip through an OFHC copper pedestal (Figure 4-5), and through which electrical connections are made to the socket. In order to limit the heat conduc-

tion DC bias potentials are applied to the trap through 36AWG phosphorus-bronze wires (Lakeshore, WSL-36-500). The RF voltage generated by a function generator and amplified by a quarter-wavelength helical resonator [Der86, DWC96, Fis76] is delivered to the trap through a 20 AWG silver coated copper wire. To heatsink the heat conducted by the wires between the three temperature stages, the wires are wrapped around copper posts mounted on the 40 K cooling stage heatshield and on the 4.2 K baseplate.

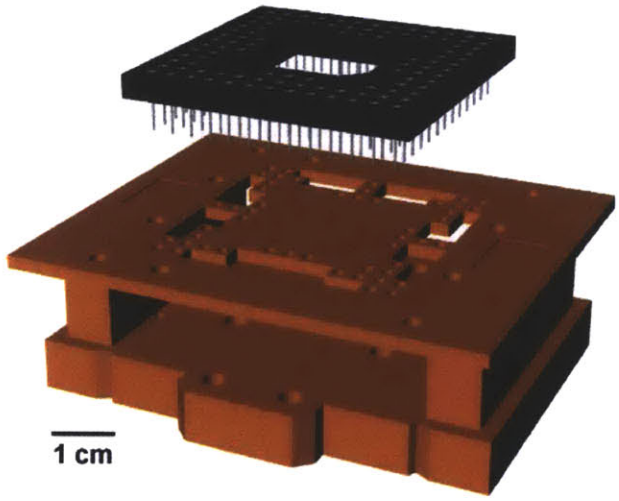

Figure 4-5: Ion trap carrier ensemble. To insure good thermal contact the unused pins of the socket are soldered to the copper plate base. The pedestal is mounted directly on to 4.2 K baseplate.

4.1.3 Microwave source

The microwave source and delivery components are shown schematically in Figure 4-6. The microwave signal produced by an analog signal generator (Agilent N5183A, 100 kHz - 40 GHz, 1 W max. output) is passed though a broad band microwave amplifier (Quinstar QPJ-06183630, 6 GHz - 18 GHz, 32 dB gain, 4 W max. output) and then fed through a DC block (Minicircuits BLK-18-S+) into the cryostat microwave coaxial cables. In order to protect the signal generator from any reflected signal a broad band isolator (Raditek RADI-2-18, 2 GHz- 18 GHz, 15 dB isolation) is inserted between it and the microwave amplifier.

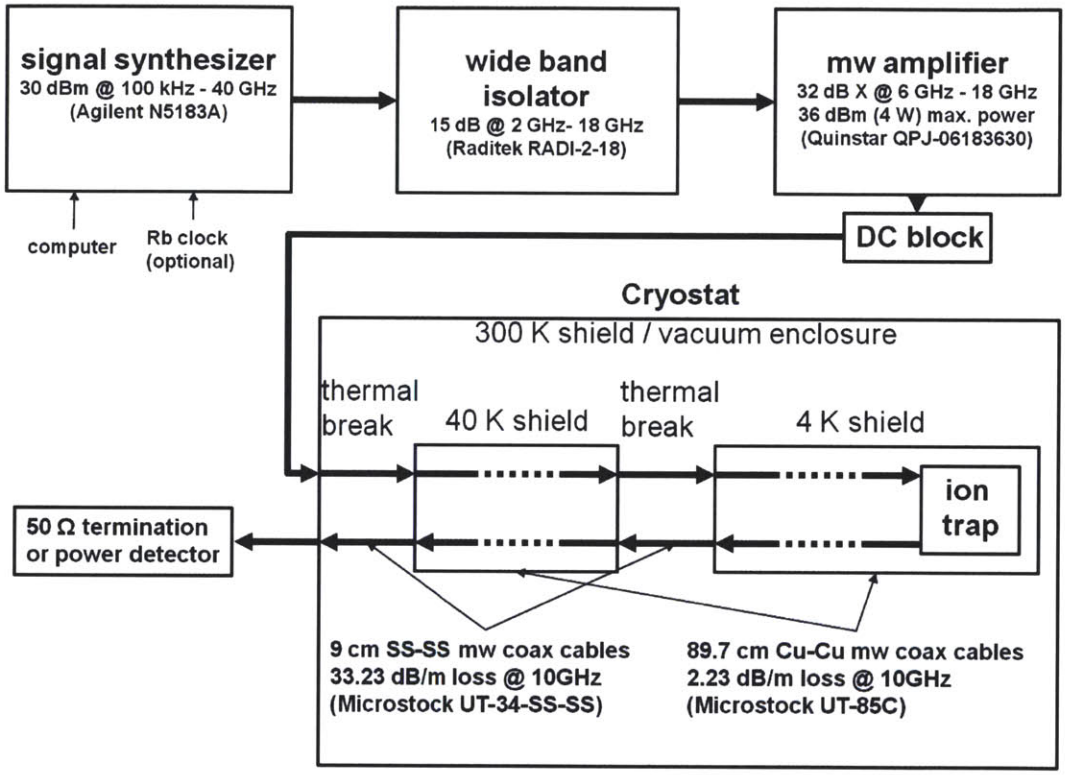

Figure 4-6: Diagram of the main components involved in the production and delivery of the microwave signal to the ion trap. All the elements present in the setup have 50 Ω characteristic impedances.

Because of the cryogenic environment the delivery of the microwave signal from the 300 K shield to the 4 K stage of the cryostat becomes a complex problem. On the one hand, the microwave transmission lines should have low electrical losses so that little microwave radiation is converted into heat and on the other hand they should have very low thermal conductivity in order not to overload the cryostat with the conducted heat. These two requirements are difficult to satisfy in general since for the most materials the electrical and thermal conductivities are proportional. For this setup, I selected to build the input and output microwave transmission lines from a set of coaxial cables with properties alternating between the previous mentioned requirements. Between the three temperature stages of the cryostat, I chose to use as thermal breaks two 9 cm coaxial cables of low thermal/electrical conductivity with both core and shield made out of stainless steel (Microstock UT-34-SS-SS, 33.23 dB/m loss @ 10GHz, 70 $\mu W/K$ thermal conductance). In order to heatsink the heat conducted through the short coaxial cables and also to insure good thermal contact between the inner conductor of the microwave cables to the cooling stages, another two 89.7 cm long coaxial cables with high thermal/electrical conductivity (Microstock UT-85C, copper core - copper shield, 2.23 dB/m loss @ 10GHz) were tightly wrapped around the 40 K and 4 K shields (Figure 4-7).

4.1.4 Imaging optics

To allow for laser access to the trap, a set of three 2.75 inch viewports are attached on the side of the spherical octagon. The access through the 40 K and 4.2 K heat shields is provided by six 1 inch BK7 windows (Thorlabs, WG11050), with three windows mounted on each shield. The imaging of the ions is done through the bottom 4 inch viewport. The light scattered by the trapped ions is collected and collimated by an aspheric lens (Edmund Optics, NT49-100, 22.50 mm EFL, f/1.50). The aspheric lens was chosen such that it had a good light collection and it can be positioned far enough from the trap so that the electrostatic charges on it do not affect the ions. The collimated light is focused outside the cryostat by a 75 mm plano-convex lens. Both lenses are mounted in 1 inch Thorlabs cage mount which can slide on four

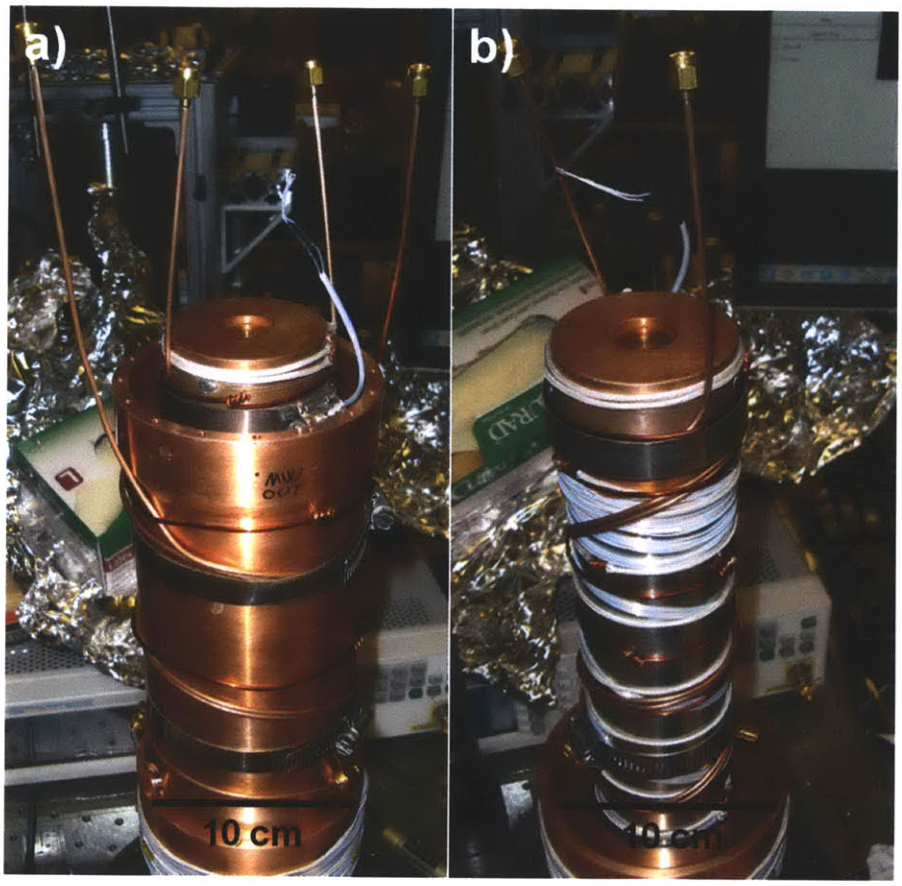

Figure 4-7: For good thermal contact the copper-copper microwave coaxial cables are tightly wrapped around a) 40 K shield and b) 4 K stage of the cryostat.

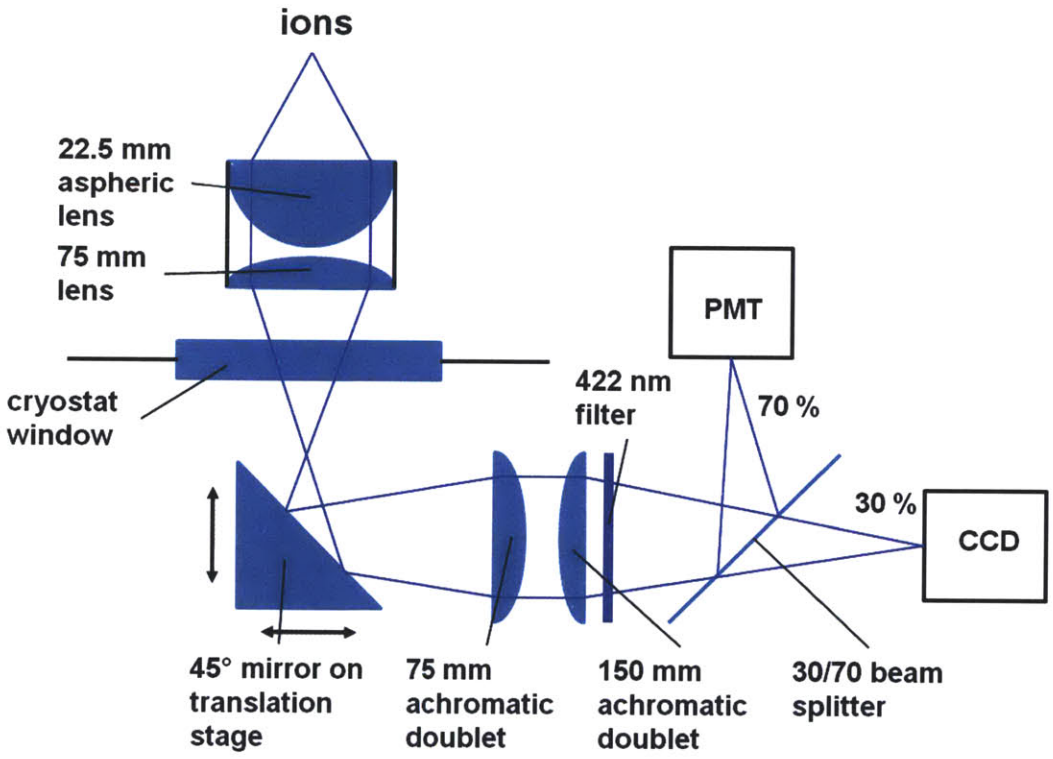

Figure 4-8: Imaging setup schematic. The fluorescence signal is collected by an aspheric lens placed at 22.5 mm from the ions. The focused light is dived by a 30/70 beam splitter and collected by a CCD camera and a photon counting PMT.

posts attached to the bottom plate of the cryostat second stage chamber (Figure 4-2). Although there is a mismatch in the thermal expansion coefficients between the lenses and cage mount, the lenses have survived hundreds of cool down cycles. The light outside the cryostat is collimated by two lenses, a 75 mm and a 150 mm achromatic doublet, and then passed thought a notch filter (Semrock, FF01-427/10-25, > 98 % transmission at 422 nm) in order to reduce the stray light scatter. The focused light is divided by 30/70 beam splitter with 30 % of the light being directed to a CCD camera (SBIG, ST-402ME), while the other 70 % of the light being directed to photon counting PMT (Hamamatsu H7360-02) (Figure 4-8). The expected photon counter efficiency at 400 nm is 20 %, resulting in overall theoretical photon detection efficiency of 1 %. The entire imaging system has a 7.5× magnification and provides a theoretical resolution of 1.2 μm.

4.1.5 Laser systems

The energy levels of $^{88}Sr^{+}$ and the transitions used to conduct the experiments reported here were shown in Chapter 2 (Fig. 3-1). The $S_{1/2} \leftrightarrow P_{1/2}$ transition is used for Doppler cooling the trapped ions and is driven by a 422 nm laser with 20 μW power focused to a 33 μm spot size. The $P_{1/2}$ state has a probability of 1 in 13 to decay to the metastable $D_{3/2}$ level. To avoid the depopulation of the Doppler cooling transition, we use a 1091 nm repumping laser with 50 μW power focused to a 100 μm spot size. The light necessary to drive these transitions is produced from two external cavity diode lasers [LRB+07, RWE+95]. The laser diode is mounted on a temperature stabilized baseplate, and current (50 - 100 mA) is passed through it to produce laser radiation. An external cavity is formed by using a diffraction grating to reflect a portion of the radiation back into the diode and provide optical feedback. The grating also allows for additional tuning of the laser frequency. After leaving the grating, the laser beam passes through an optical isolator, which prevents the light reflected from various optical elements to provide unintended optical feedback to the laser diode. The output laser beam is coupled into a single-mode optical fiber through mode-matching lenses and delivered at the experimental setup.

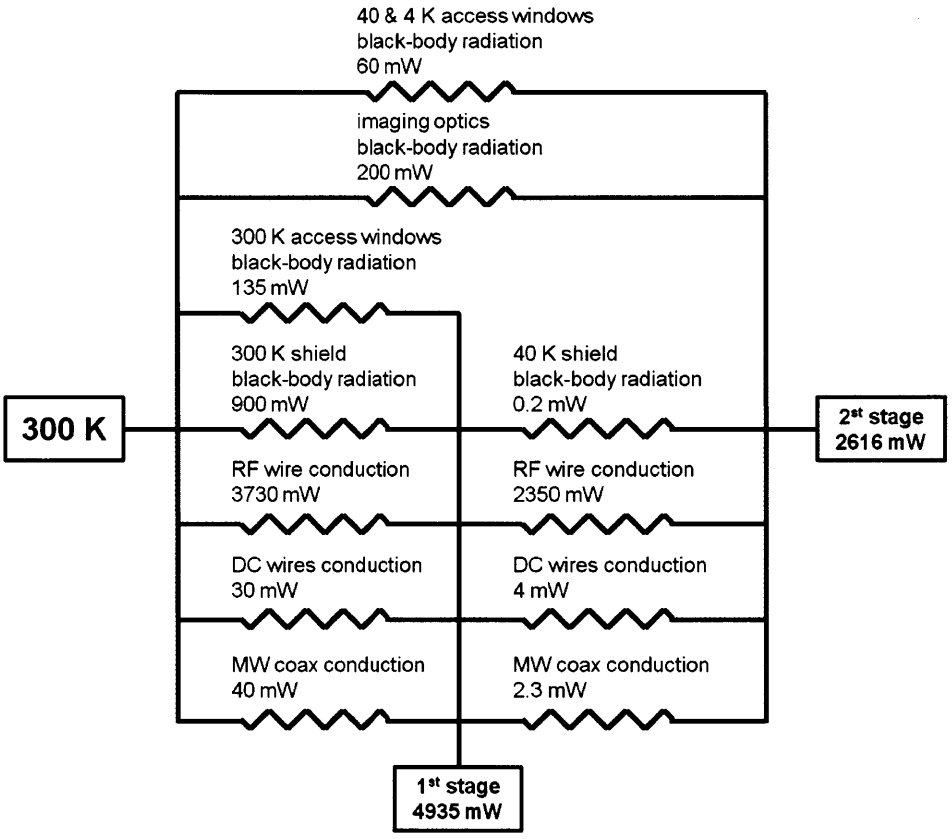

Figure 4-9: Detailed chart with the heat loads on the two cooling stages of the closed cycle cryostat.

4.1.6 Vacuum system and heat load

The ultra high vacuum in cryogenic systems can be obtained because of the cryosorption of residual gas molecules on the cold surfaces, even in the presence of materials not compatible with room temperature UHV systems. To attain the UHV environment the cryostat is first pumped with a turbomolecular pump to 5×10^{-7} torr measured by an inverted magnetron pressure gauge attached at the pump inlet. In the second stage the cryostat vacuum chamber is isolated from the turbomolecular pump and the cool down process is started, while the pumping is continued by a small ion pump attached directly to the spherical octagon. The cooling of the cryostat takes 4 hours, with the cold stage reaching a final temperature of 13 K and the pressure at the ion pump getting to 3×10^{-9} torr, although the pressure at the ion trap location is expected to be much lower due to the cryosorption and cryotrapping [GPQ+95]. The computed heat load from radiation and conduction to the second stage cold tip is about 2.6 W (see Figure 4-9 for the various sources of heat). The calculated heat load and measured temperature agrees well with cryostat heat load map supplied by the manufacturer (Figures 4-10 and 4-9). The highest heat loads on the 4.2 K stage come from the 300 K radiation absorbed by the exposed lenses assembly and from heat conduction through the RF wire (total combined power of $\sim$ 2.5 W). For comparison, the thermally unloaded cold tip reaches 4.2 K after 2 hours of cooling.

4.2 Atomic and molecular ion production through laser ablation

In our system, we successfully tested few of the ion loading methods available in room temperature systems. For atomic ion production, we tested the following methods: neutral atoms obtained from a resistively heated oven were ionized by impact with electrons emitted by an e-gun or through laser photoionization [BLW+07, KP09], and the ions were directly produced by laser ablation of a solid target [HMO+06, LCL+07] or indirectly by photoionization of the neutrals inside the ablation plume [HGH+07];

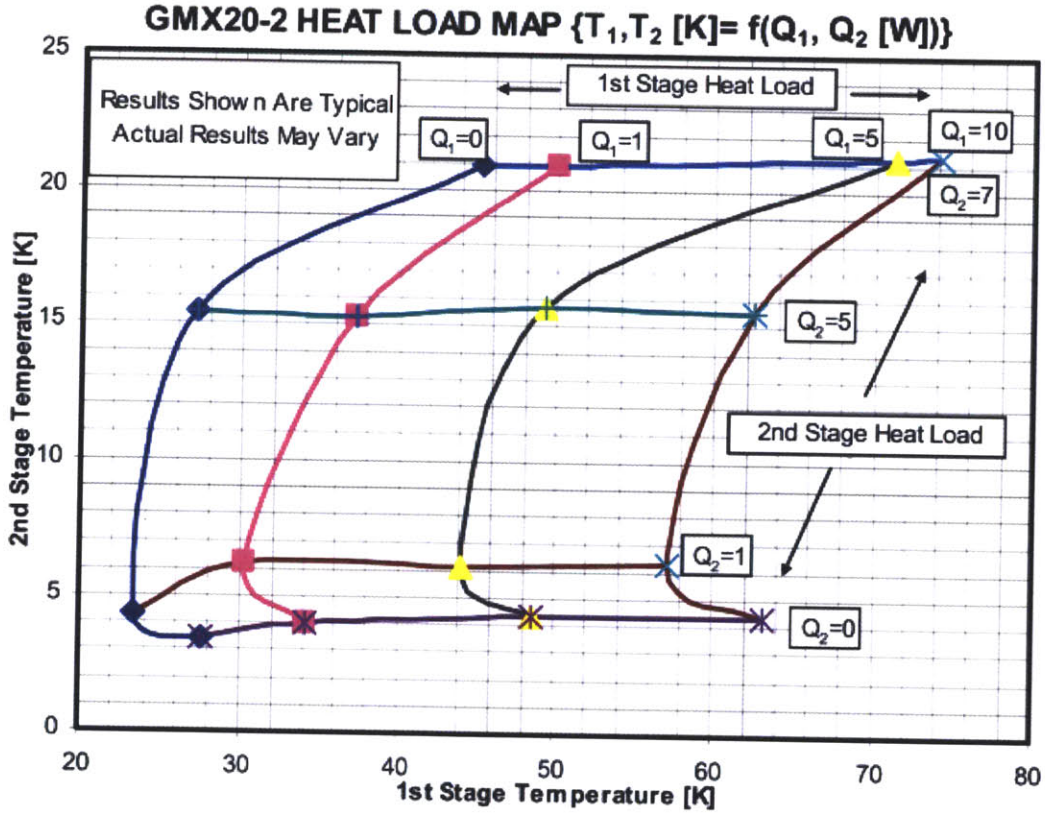

Figure 4-10: Temperature vs. heat load for the two stages of ARS GMX-20B cryocooler (provided by the manufacturer).

while for molecular ion production, we tried the following methods: ions were again directly produced by laser ablation, or trapped Sr ions were reacted with chlorinated organic compounds leaked into the experimental chamber [ROZS08, WBG+08, DG99]. For our experiments, we chose the laser ablation loading method as it has some advantages compared with the other loading methods. During the ion loading from an oven, the heat production is of the order of hundreds of Joules, but in comparison a single ablation pulse of 1.5 mJ can load our trap. If the ion trap were operated in a cryostat which could reach temperatures in the milikelvin range, the system would likely not be able to handle the dissipated heat from an oven. We also found that the in situ chemical reaction method has a major drawback as the reacting compound leaked into the cryogenic environment condenses on all optical surfaces making them opaque. But the main benefit of laser ablation is that it can produce atomic and molecular ions from materials with very high melting temperature.

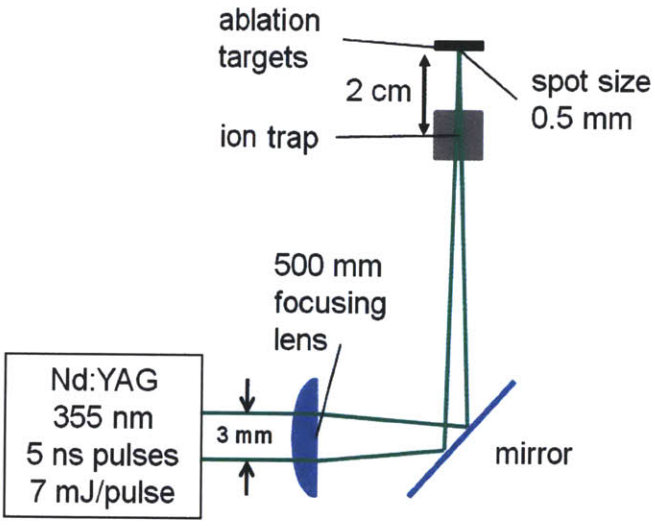

Figure 4-11: The light produced by a frequency tripled Nd:YAG laser is focused to a 0.5 mm spot size onto the ablation targets.

The mechanism of ion trapping from the ablation plume was described by Hashimoto *et al.* [HMO+06]. The fast electrons from the ablation plume arrive first to the trap and cancel the RF voltage applied to the trap, thus allowing the slower moving ions to enter the trapping region even if their kinetic energy is lower than the trap well depth. To produce the ablation plume, we use a Q-switched Nd:YAG laser (Con-

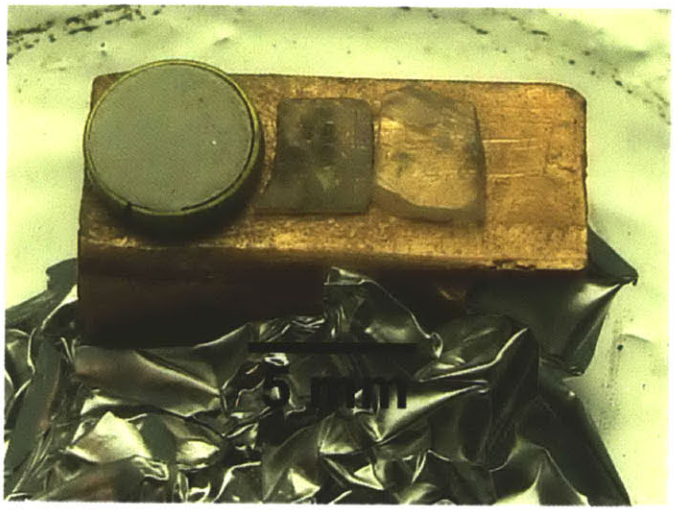

Figure 4-12: Example of a set of three ablation targets: (from left to right) $SrCl_2$ compressed powder, 0.5 mm thick $SrTiO_3$ crystal, 1 mm thick $SrTiO_3$ crystal. The ablation targets are bonded to the copper carrier with cyanoacrylate based adhesive.

tinuum Electro-Optics, Minilite II), which produces a maximum energy in its third harmonic (355 nm) of 8 mJ per pulse. The pulse duration is around 5 ns. The YAG beam is steered by a high-energy mirror (CVI Laser, Y3-1025-45-P). The energy loss in optics is around 1 mJ, thus the maximum energy delivered to the target is 7 mJ as measured with a pyroelectric meter. The beam is focused onto the ablation target to spot size of 0.5 mm. Because metallic ^{88}Sr easily oxidizes in open atmosphere a single crystal of $SrTiO_3$ (MTI Crystal, STOa100505S1) placed 20 mm from the center of the trap (Figures 4-11 and 4-12) is used as source for atomic ions. Molecular ions together with atomic ions are produced by ablating a small $SrCl_2$ target. The $SrCl_2$ pellet (Figure 4-12) used for ablation is made in house by sinterization of compressed anhydrous $SrCl_2$ powder (Alfa Aesar 12202, 95 % purity) at 300 °C under open atmosphere for one hour. $SrCl_2$ is a hygroscopic substance and it reacts with the atmospheric moisture to form a hexahydrate $SrCl_2 \cdot 6H_2O$ below 61 °C ambient temperature [MPG+00]. Experimentally, I found that the laser ablation of hydrated $SrCl_2$ does not produce ions, thus making the drying process an essential step for the target preparation. Although the $SrCl_2$ target is capable of producing both the atomic and molecular ions, the $SrTiO_3$ target is a more reliable source of ions [LCL+07] and

we still utilize it for characterization of new trap designs.

Chapter 5

The ion traps

The previous chapter described the infrastructure necessary for ion trapping, while this chapter aims to present the main component of the ion trapping: the surface electrode ion trap with integrated coplanar microwave waveguide. The development of the experimentally suitable trap geometry was an iterative process in which various trap designs were tested and abandoned as functional flaws were discovered. The beginning of the chapter is a review of the trap designs, I evaluated prior deciding on the final trap geometry. The surface electrode ion trap with integrated coplanar microwave waveguide is presented in detailed in the remaining part of the chapter.

5.1 3D ion traps

The purpose of the traps described in this section was to investigate the feasibility of integrating slot and strip line microwave waveguides with planar ion traps. Because of the geometry of these two types of microwave waveguides, the resulting ion traps became three dimensional structures. The ion traps were built by patterning the copper electrodes on printed circuit boards. As substrate, we chose to use 20 mil thick Rogers RO4350B laminate given its low loss tangent at microwave frequencies.

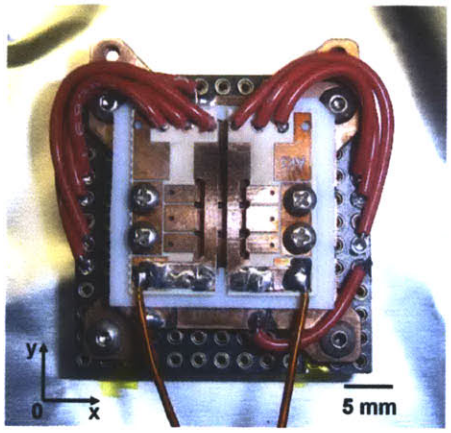

Figure 5-1: Example of a two layer ion trap with integrated microwave slot line. The copper electrodes are patterned on a 20 mil thick Rogers RO4350B laminate. The distance between the RF/MW electrodes is 0.8 mm, and the two electrode layers are separated by a 0.127 mm thick PTFE spacer.

5.1.1 Slot line ion trap (Azkaban traps)

The slot line ion trap (Figure 5-1) has a two layer structure. The top layer contains the 0.8 mm wide microwave slot line and the main ion trap electrodes. In the example presented here, the bottom layer is separated from the top one by a 0.127 mm thick PTFE spacer and contains another set of three DC electrodes which aid in ion confinement. The spacing between the two layers determines the ion position along the normal to the ion trap plane and, as such, the ion position can be adjusted at will. The microwave slot lines supports two modes of operation: the even mode where both halves of the line are driven in phase and which requires a ground plane electrode as return path for the current, and the odd mode where only a half of the line is driven with the other half acting as current return and making a third ground electrode redundant (but not forbidden). In the even operation mode the two RF electrodes act as microwave electrodes, so the RF and MW fields have an identical space distribution. Given the fact that the ions are trapped at the point where the RF field vanish, in the even mode the microwave field necessarily vanish too at the ion location. This leaves only the odd mode as the suitable mode operation for the microwave slot line. For this trap geometry the ions are trapped at 70 μm above the top layer surface. With the following voltages applied on the trap electrodes (as identified in Figure 5-

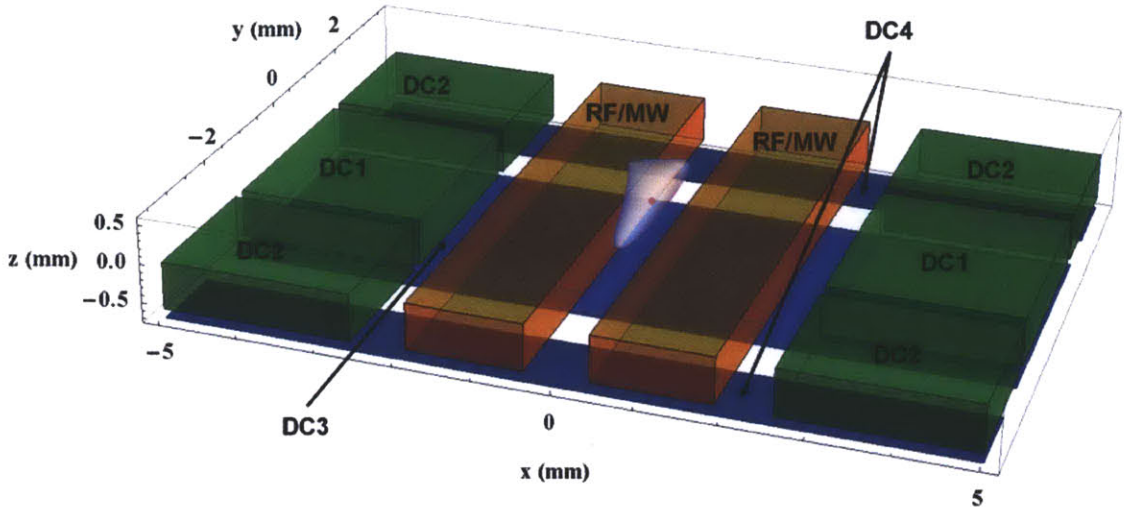

Figure 5-2: Slot line ion trap geometry and the numerically simulated trapping pseudopotential. The red dot marks the trapped ions location.

2): $DC1 = -79\ V,\ DC2 = 0\ V,\ DC3 = 0\ V,\ DC4 = 92\ V,\ RF = 400\ V\ @\ 10\ MHz$, the ion trap has a trap depth of 0.75 eV (see Figure 5-3). Although this ion trap geometry was successful in confining atomic and molecular ions (Figure 5-4), the main difficulty I encountered was the delivery of the radio frequency and microwave fields on the same electrodes. The filter used in order to prevent the cross talk between the two signal sources, presented an additional load for the step up RF helical resonator which limited the maximum RF field delivered at the ion trap below the required value.

5.1.2 Strip line ion trap (plate and wire)

The strip line ion trap is another two layer ion trap design. This geometry eliminates the problem encounter in the slot line ion trap by keeping the ion trap electrodes separated from the microwave transmission line.

The top layer contains only a rectangular shaped microwave electrode, while the bottom layer contains the ion trap (Figure 5-5). In order to allow for the trapped ions imaging the microwave electrode includes a pinhole, which size (0.8×1.2 mm) is matched to the numerical aperture of the imaging system. The microwave electrode width and the separation between layers are determined by the wanted characteristic

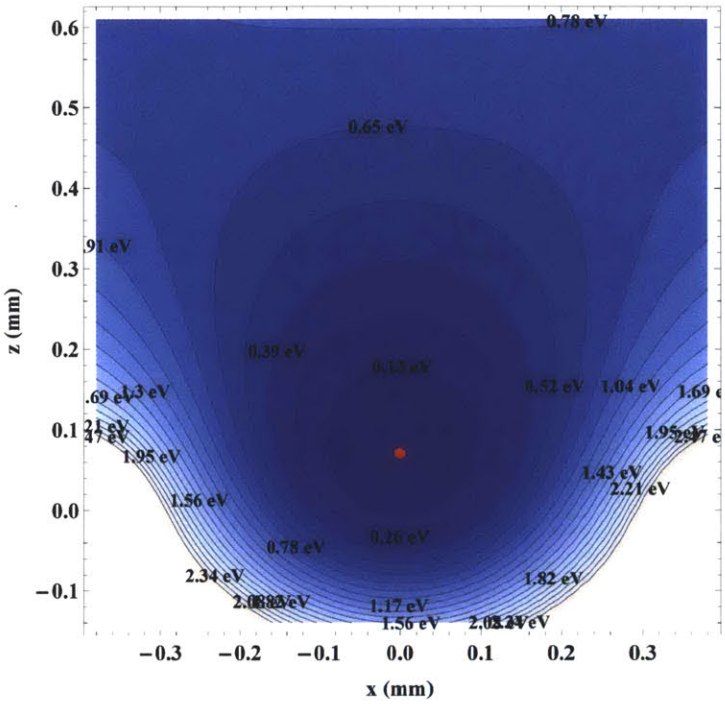

Figure 5-3: Cross section through the trapping pseudopotential for the slot line ion trap. The contours represent equipotential surfaces with their values indicated in units of eV. The red dot marks the trapped ions location.

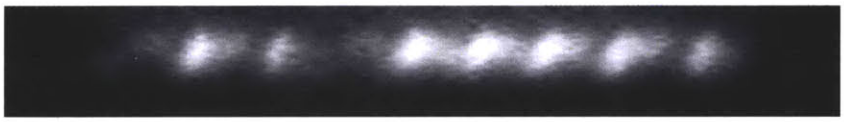

Figure 5-4: Example of a $^{88}Sr^{+}$ ion chain trapped in the slot line ion trap. The third ion from the left is non-fluorescent (dark ion). The mean separation between ions is $\sim 10\ \mu m$.

impedance of the transmission line (in this case 50 Ω for 1.58 mm separation and 7 mm line width). The numerical modeling (Figure 5-6) of the ion trap predicts that the ions are trapped at 0.65 mm above the trap surface (bottom layer) at a trap depth of 0.92 eV (for $DC1 = -150\ V$, $DC2 = 150\ V$, $DC3 = 0\ V$, $DC4 = 0\ V$, $DC5 = 90\ V, MW(DC) = 0\ V$, $RF = 500\ V$ @ $10\ MHz$). With this trap design, we found it quite difficult to align the imaging pinhole to the trapped ions location, which determined us to employ a modified type of microwave strip line. In the new design, we replaced the rectangular microwave electrode with a 1 mm diameter silver rod placed at 1 mm from the ion trap layer (Figure 5-7). To insure maximum light

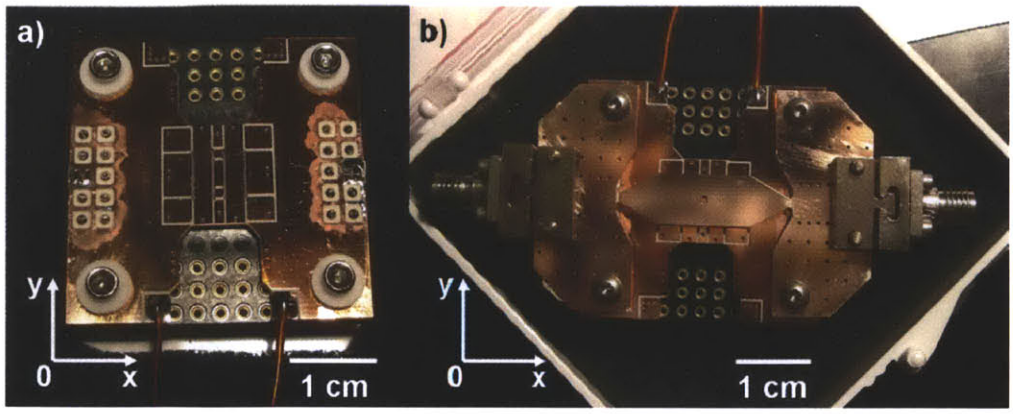

Figure 5-5: Ion trap with integrated rectangular microwave strip line: a) the bottom layer containing the ion trap electrodes, and b) the ion trap with the transmission line installed.

collection the ion trap plane was tilted at 30° from the imaging axis (Figure 5-8). From the numerical modeling of the the ion trap with integrated cylindrical microwave transmission line the ions were expected to be trapped at 0.49 mm above the ion trap surface at a trap depth of 3.52 eV (for $DC1 = -11\ V$, $DC2 = 15\ V$, $DC3 = 0\ V$, $DC4 = 15\ V$, $DC5 = 15\ V, MW(DC) = 0\ V$, $RF = 400\ V$ @ $8\ MHz$). But even with the modified microwave electrode geometry, we could not confirm that our strip line ion trap design can successfully confine atomic or molecular ions.

5.2 Nb surface electrode ion traps with superconducting CPW resonator (Giants traps)

One prerequisite for the success of the experiments presented here is the presence of a superconducting microwave resonator integrated into the ion trap geometry. The 3D traps described in the previous section have, beside the issues already presented, one more limitation regarding the thermal transfer efficiency which can be achieved between the microwave line and cryostat cooling stage. By design, in all the two layer ion traps the microwave transmission lines cannot make direct contact with the cooling substrate, restricting the accessible thermal contact points to the outside of the trap area. Thus, it becomes apparent that a new design is necessary, in which

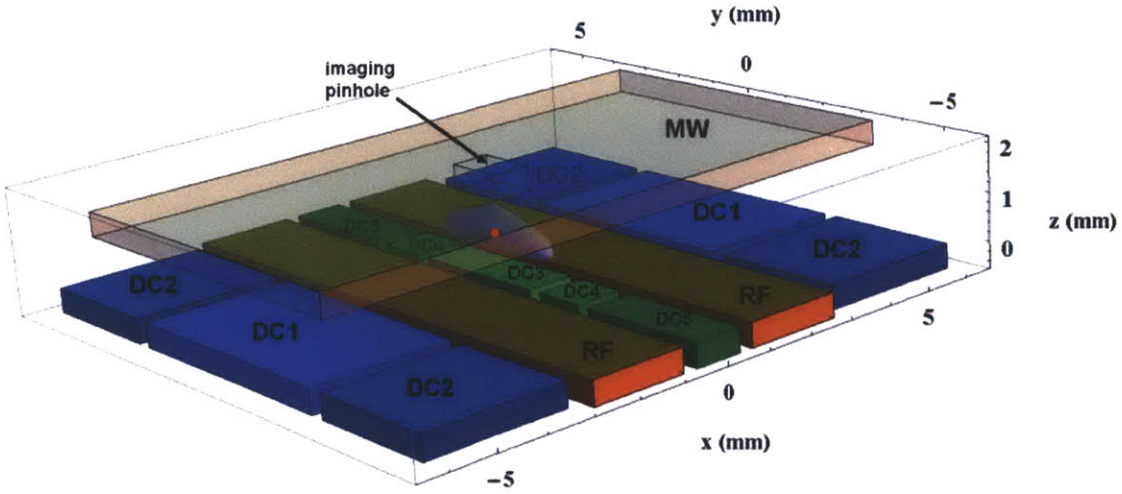

Figure 5-6: Ion trap with integrated rectangular microwave strip line geometry and the numerically modeled trapping pseudopotential. The red dot marks the trapped ions location.

the ion trap and the microwave line share the same substrate.

5.2.1 Trap geometry

The new design is based on the "standard" surface electrode ion trap [SHO+06, LGA+08, SCR+06], where all the trap electrodes lay in one single plane as shown in Figure 5-9. In this geometry, the central DC electrode together with the two lateral RF electrodes naturally form a coplanar waveguide structure (CPW), which can be used for microwave radiation delivery. As discussed in Chapter 2, the CPW line can be easily transformed into a resonator by placing two capacitor gaps in the transmission line at the appropriate locations for a given radiation frequency [FWS+05, BGW+07, WHW+09]. (The capacitor gaps are the easiest structures to implement, but any other type of impedance discontinuity in the transmission line will act as radiation mirrors.) With just capacitor gaps the CPW resonator presents to the ions a floating DC potential, but the situation can be fixed by placing a DC source at one of the cavity standing wave nodes.

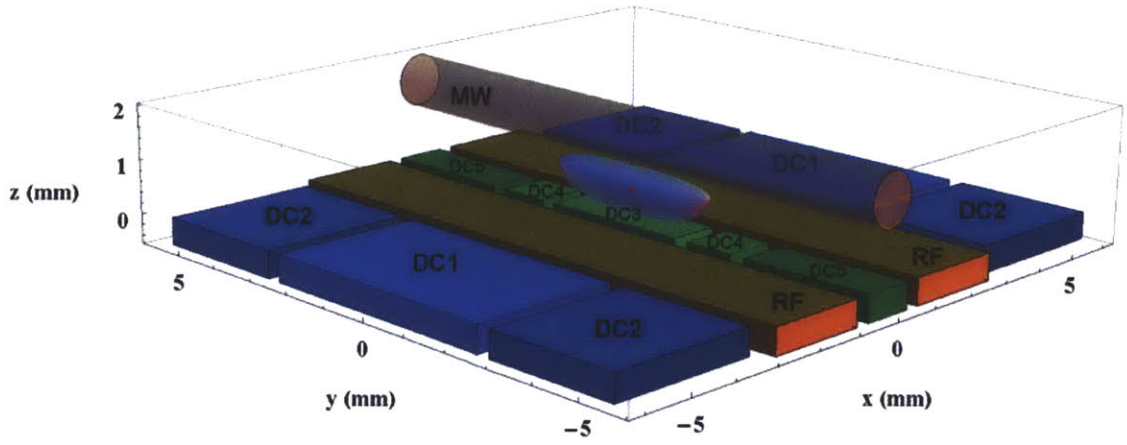

Figure 5-7: Geometry of the ion trap with integrated cylindrical microwave transmission line and the numerically modeled trapping pseudopotential. The red dot marks the trapped ions location.

5.2.2 Trap design and trapping properties

There are five parameters which determine the characteristic impedance of a microwave CPW: substrate thickness and its electric permittivity, metallization thickness, central CPW electrode width and its spacing to the the two ground planes (or RF electrodes) between which is embedded. In practice, as discussed in the next section, the first three parameters are set by the chosen fabrication method. If an ion trap is built with a transmission line its characteristic impedance must be matched to the delivery coaxial cables impedance (50 Ω in this case) [HWR$^+$09], in which case the last two parameters become dependent. Alternatively, if a microwave cavity is used the last two parameters remain independent as the cavity impedance can be chosen at will. The next step of the trap design is to optimize the RF and DC electrodes geometry within the constraints imposed by the microwave CPW, such that the ion trap meets a certain set of performance goals: maximum trapping potential depth, maximum trap stability (have trap $q \sim 0.2 \div 0.3$ and trap $a \sim 0$), and maximum microwave electric field at the trapped ions location. Once the entire ion trap geometry is establish, its trapping properties can be modeled numerically. A full three-dimensional numerical simulation is a time consuming process, but fortunately the problem has a mathematical approximation in which the optimal ion trap geome-

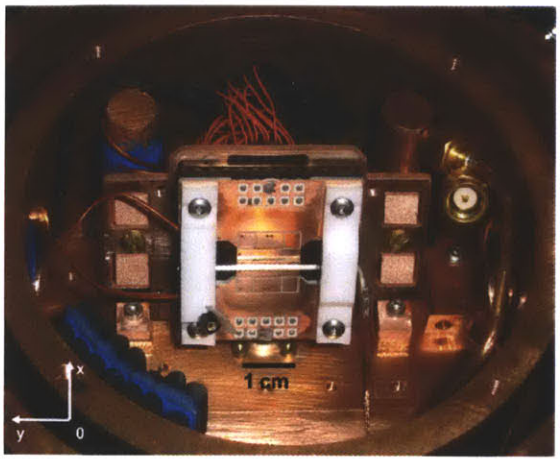

Figure 5-8: Ion trap with integrated cylindrical microwave transmission line. A 1 mm diameter silver rod placed 1 mm above the ion trap acts as microwave electrode. The ion trap is mounted such that the plane of the trap makes a 30° angle with the imaging axis.

try can be estimated in few minutes. The approximation is based on the observation that a finite area conductor kept at potential V_0 embedded in a infinite grounded flat plane in otherwise empty space, produces a potential $\Phi(\vec{r})$ proportional with the solid angle subtended at the observation point $\vec{r}$ by the electrode area a, i.e.:

$$\Phi(\vec{r}) = \frac{V_0}{2\pi}\Omega_a(\vec{r}). \tag{5.1}$$

The proof of relation (5.1) is based on the Green's second identity applied to Laplace equation with Dirichlet boundary conditions, and it can be found in a number of publications [OM01, Wes08]. Equation (5.1) is an exact result. The approximation comes into play when the ion trap electrodes are assumed to be embedded in a infinite grounded flat plane, so that equation (5.1) can be applied to them. From relation (5.1), we also see that the approximation becomes excellent when the height at which the ions are trapped is small compared with the entire trap linear dimension, and when the gaps between electrodes are small compared with the electrodes lateral extent. Usually, the surface electrode ion traps satisfy the first condition adequately. Our ion traps fulfill the second condition well, but generally it depends on the specific ion trap design. The main trapping properties are set by the RF electrodes and the central

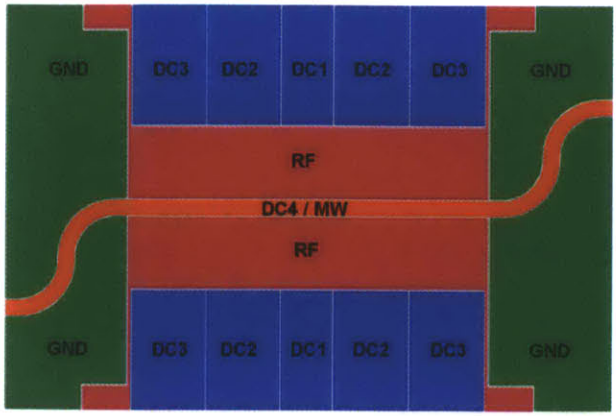

Figure 5-9: A surface electrode ion trap with integrated microwave coplanar waveguide. In this example the ion trap contains eleven DC control electrodes and two RF trapping electrodes. In order to allow for cooling lasers access the ends of the microwave transmission line are displaced from the ion trap longitudinal axis.

CPW electrode, which allows us to neglect the presence of the DC electrodes in our approximation. We can make one more simplification by considering the remaining electrodes infinitely long (compared with the trapped ions height), with the final trap geometry shown in Figure 5-10. Under these assumptions the main trapping parameters can be expressed in close analytical form:

$$z_{\text{ion}} = \sqrt{bc}, \tag{5.2a}$$

$$D_{\text{iontrap}} = \frac{e{V_{\text{RF}}}^2}{4M_{\text{ion}}{\omega_{\text{RF}}}^2} \frac{4bc(c-b)^2}{\pi^2(b+c)^2\left(2bc+\sqrt{bc(b+c)^2}\right)^2}, \tag{5.2b}$$

$$q_{\text{trap}} = \frac{8\ eV_{\text{RF}}}{\pi M_{\text{ion}}\omega_{\text{RF}}^2} \frac{(c-b)}{(b+c)^2\sqrt{bc}}, \tag{5.2c}$$

$$E_{\text{MW/ion}} = V_{\text{MW}} \frac{4a}{\pi\left(a^2+4bc\right)}. \tag{5.2d}$$

In Figure 5-11 I show a Nb surface electrode ion trap with integrated microwave CPW transmission line which was successfully operated (Figure 5-12). The trap geometry was optimized with the approximate method previously described, and its trapping properties obtained from the numerical modeling are presented in Figure 5-13 and Figure 5-14 (for $DC1 = -6\ V,\ DC2 = 0\ V,\ DC3 = 5\ V,\ DC4 = 0\ V, MW =$

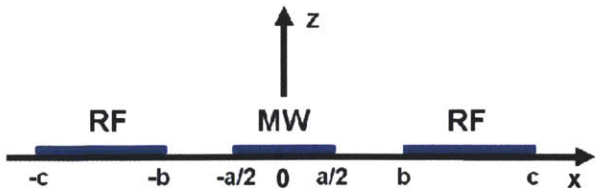

Figure 5-10: Simplified geometry for the surface electrode ion trap. The letters indicate the dimensions used in computing the approximate solution.

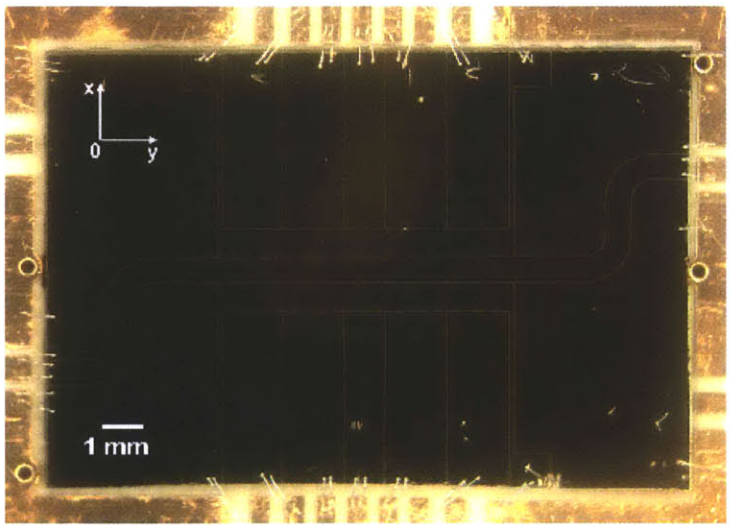

Figure 5-11: Example of Nb surface electrode ion trap with integrated microwave CPW transmission line. The ion trap electrodes are identified in Figure 5-9. The gaps between electrodes are 25 μm wide, the RF electrodes are 0.7 mm wide, and the central CPW electrode is 0.6 mm wide.

$1\ V,\ RF = 250\ V\ @\ 7.22\ MHz$).

Also in Table 5.1, I compare the results obtained from the numerical modeling with those obtained from the approximation method. Except for the trap depth which the approximation method underestimates by 25 %, all the other results are in an excellent agreement.

5.2.3 Trap fabrication and packaging

All our niobium based surface electrode ion traps are fabricated in house through standard photolithographic methods. As electrode substrate, we use 0.5 mm thick c-cut single crystal sapphire (ALC50D05C2, MTI Corporation) given its low dielec-

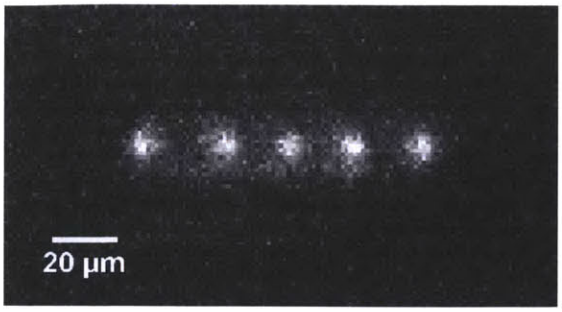

Figure 5-12: Chain of five $^{88}Sr^{+}$ ions trapped in the Nb surface electrode ion trap with integrated microwave CPW transmission line. The mean separation between ions is μm.

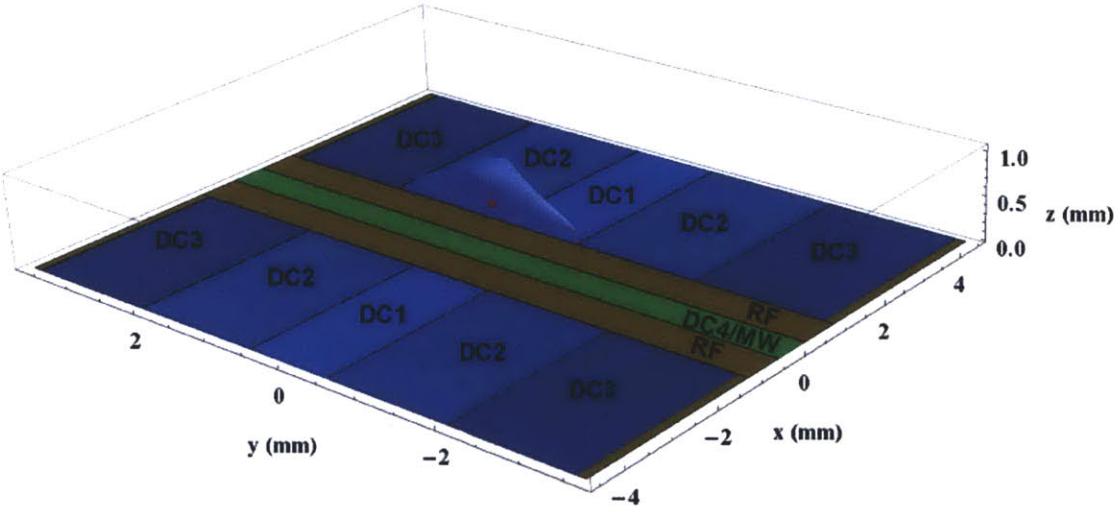

Figure 5-13: Geometry and trapping pseudopotential for the Nb surface electrode ion trap with integrated microwave CPW transmission line. The red dot marks the trapped ions location.

Table 5.1: Comparison between the trapping parameters obtained from full the numerical modeling and from the approximate method.

Trap parameter	Numerical modeling	Approximate method
Ion height (mm)	0.58	0.57
Trap depth (eV)	0.20	0.15
Trap q parameter	0.22	0.23
Microwave electric field (kV/m)[1]	460	466

[1]At 1 V amplitude microwave signal applied on the CPW electrode.

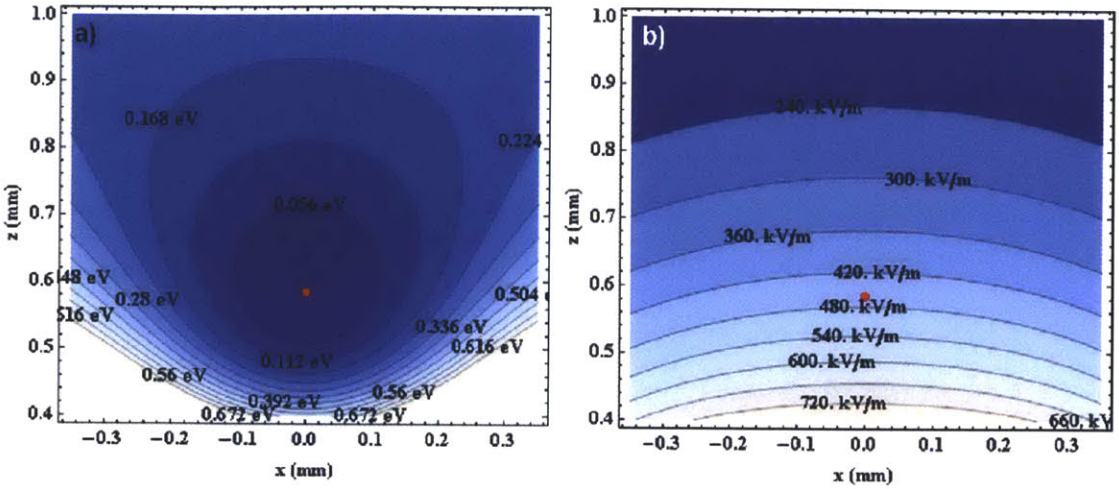

Figure 5-14: Nb surface electrode ion trap x0z cross sections for: a) pseudopotential, and b) microwave electric field absolute value. The microwave electric field is orthogonal to the lines of constant value. The red dot marks the trapped ions location.

tric loss tangent and high thermal conductivity at low temperatures. The niobium layer is deposited on the sapphire substrate by DC sputtering. The metallic layer is limited at 200 nm thickness in order to prevent the sputtering target from getting shorted to ground. The ion trap electrodes are patterned with a Heidelberg μPG 101 micro pattern generator, and exposed by a final etch. The ion trap is glued with a cyanoacrylate based adhesive on a custom made carrier (Figure 5-15). The carrier acts as breakout box for the various electrical signals necessary to drive the ion trap. It is necessary to use a trap carrier since the microwave SMA end launchers (142-0761-871, Emerson/Johnson) cannot be mounted directly to the trap. The connections between the trap electrodes and the trap carrier are made with aluminium wirebonds (Figure 5-15)(the more common gold wire does not bond to niobium). The trap carrier is fabricated from the same materials (2 oz copper on 20 mil thick Rogers RO4350B laminate) as the 3D ion traps described earlier.

5.2.4 Trap issues: ablation charging and electrode arcing

There are two main issues which affect the surface electrode ion traps operations: one is due to the ion loading method I employ, and the second one is due to the ion

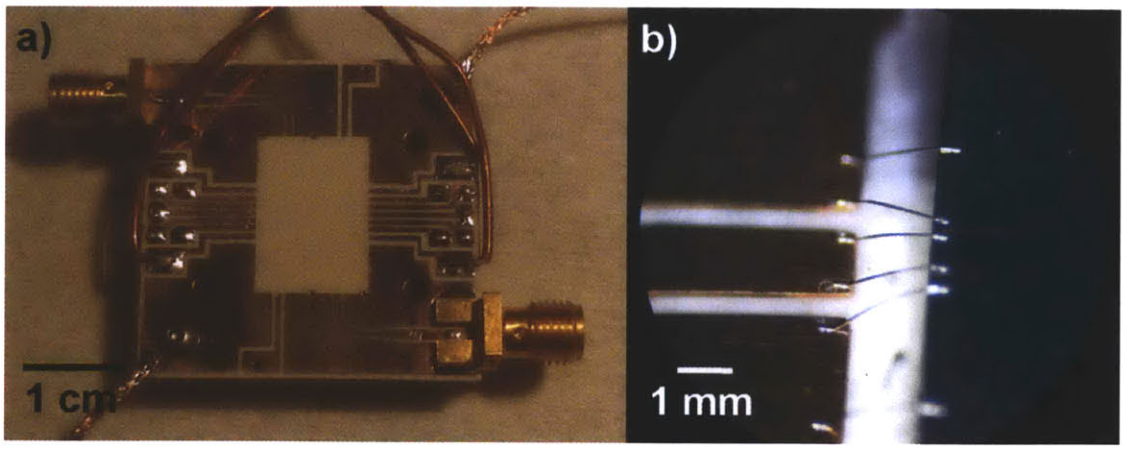

Figure 5-15: a) Ion trap carrier with the microwave end launchers installed. The ion trap chip is glued to the central white area of the carrier. b) Detail of the wirebond connections between the ion trap and carrier CPW transmission lines.

trap fabrication. The charges produced during laser ablation strike the surface of the exposed dielectric between electrodes, where they remain trapped for long periods of time (and more so at cryogenic temperatures). The electric field produced by these dielectric charges disrupts the trapping potential leaving the ion trap non operational. I measured (Figure 5-16) that one 7 mJ ablation pulse directed at a $SrTiO_3$ target placed 2 cm away from the ion trap center delivers at the trap location a charge density of 4.38×10^{-10} C/mm^2. At this charge density an exposed dielectric area of 1 mm^2 can produce a maximum electric field of about 16 MV/m; for comparison the maximum RF electric field in a typical surface electrode ion trap is around 1 MV/m. There are two methods to mitigate the dielectric charging problem: decrease the number of charges produced during the laser ablation by reducing the laser energy used, and decrease the exposed dielectric area by narrowing the electrode gaps. But as we will see, the second method exacerbates the issue due to the trap fabrication.

The etching process used for trap fabrication leaves rough edges on the niobium electrodes. Depending on the electrical field intensity present and on the radius of curvature of these sharp points they can become electron emission sources (Figure 5-17). The arcing between the trap electrodes negatively impacts the ion trap operation in two aspects: it physically damages the ion trap (Figure 5-18), and it disrupts the trapping potential.

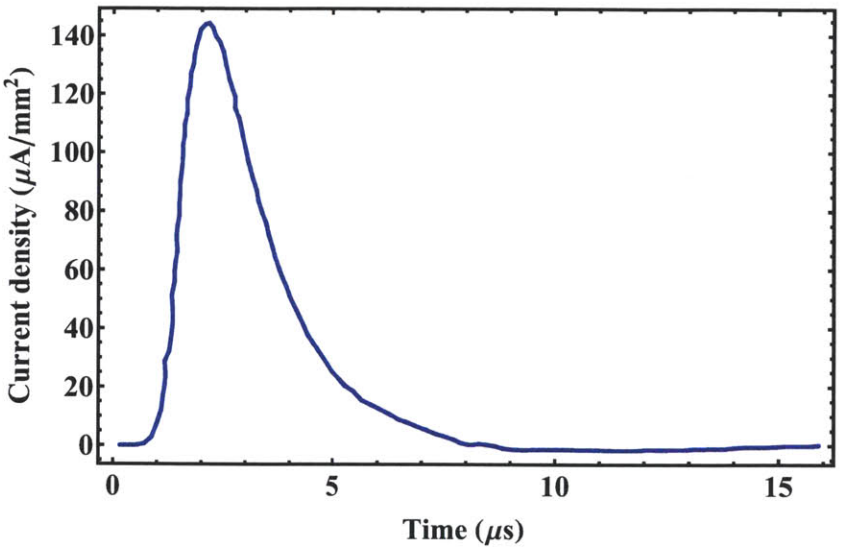

Figure 5-16: Current density delivered at the trap location by a 7 mJ ablation pulse directed at a $SrTiO_3$ target placed 2 cm away from the ion trap center.

In general the roughness of the electrodes edges can be improved by annealing, but because of the high melting temperature of the niobium (2750 K) the method is impractical in this case. The other option is to reduce the electrical field intensity between the trap electrodes by increasing the dividing gaps span. Initially, in order to reduce the dielectric charging, the ion traps were fabricated with 10 μm gaps, but because of electrode arcing they were impossible to operate. By trial and error, I found that 25 μm wide gaps and rounded electrode corners (Figure 5-19) gave us the least problems with the electrode arcing and dielectric charging issues.

5.3 Trapping and detection of molecular ions

The ion confinement in an RF ion trap involves two distinct processes: the initial ion trapping itself, and the subsequent ion cooling. When the ions are produced outside the trapping region, depending on their initial kinetic energy, the ions are either reflected from the trapping barrier or pass through the conservative trapping potential. Therefore, it is necessary to have a mechanism through which the ions with lower kinetic energy than the trap depth are able to penetrate the into the

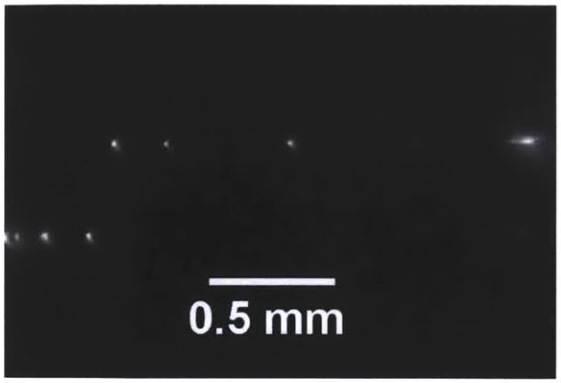

Figure 5-17: Arcing between the niobium electrodes of the ion trap. The gaps between the electrodes are 10 μm wide, and they are kept at a potential difference of 250 V.

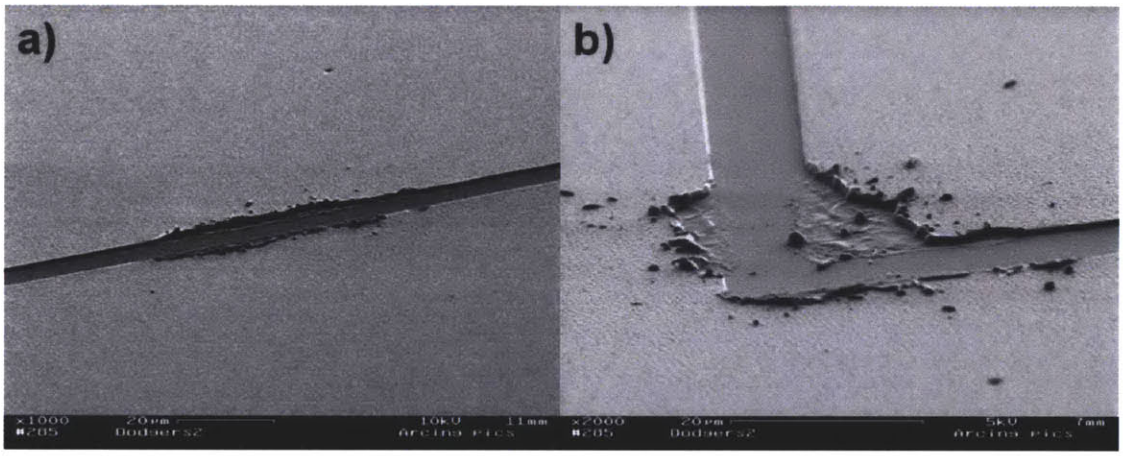

Figure 5-18: Electron microscope images of the electrodes damaged by arcing in the 10 μm gap ion traps: a) on the straight edges of the electrodes, b) at the electrodes, corners.

trapping region. In the case of laser ablation method such a mechanism is provided by the electrons generated together with the ions as it was described in more detail in Section 4.2. The trapped ions through the process called RF heating can absorb energy from field during multibody Coulomb collisions [PWM$^+$91, RZS05], and they need to be actively cooled in order to maintain their temperature below the trapping potential. Since the atomic ions $^{88}Sr^+$ have closed electronic transitions they can be laser cooled as shown in Section 3.1. On the other hand, the molecular ions $SrCl^+$ are cooled indirectly through the Coulomb interactions with the atomic ions (sympathetic cooling) [OZW$^+$06, BW02, RBD$^+$06]. From the standard plasma theory

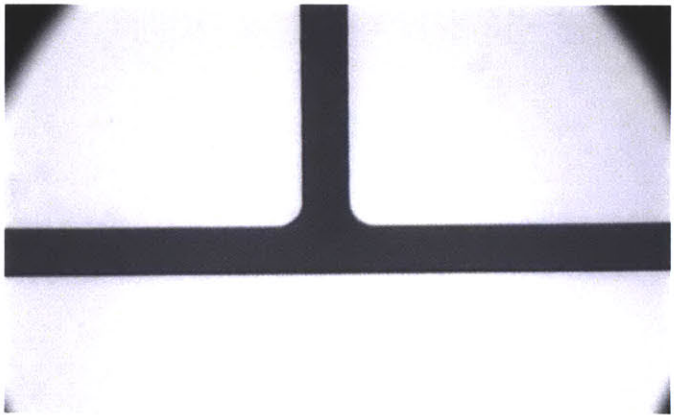

Figure 5-19: New ion trap design with 25 μm electrode gaps and rounded electrode corners with 5 μm radius of curvature.

of non-neutral plasmas, the thermalization time between the two species of ions is given by [GR95]:

$$\tau = (4\pi\epsilon_0)^2 \frac{m_A m_M}{10 n_A e^4} \left(\frac{k_B T_A}{m_A} + \frac{k_B T_M}{m_M} \right)^{3/2}, \tag{5.3}$$

where the subscripts A and M stand for atomic ions and molecular ions, respectively, and where the temperatures represent the initial temperatures of the two species of ions. For example, in the case of our surface electrode ion traps this thermalization time is of the order of few milliseconds. The trapped ion species can be identified using resonant secular excitation. As shown in Chapter 2, the trapped ions execute secular oscillatory motions along the three principal axes of the trapping pseudopotential. In the case of axial motion (along the RF electrodes), since the confinement is provided mainly by the applied DC potentials, the axial secular frequency is related to the ion charge to mass ratio in a particularly simple way $\nu_{\text{axial}} \propto \sqrt{\frac{Q}{m}}$. The expressions for the other two radial secular motions are bit more involved, since the radial pseudopotential itself depends on the ion charge to mass ratio. By applying a small exterior AC "tickle" voltage to one of the trap DC electrodes, any of the ion secular motions can be selectively excited and thus heating up the ion cloud or crystal [ZRS02, BW02, CGD+10]. The change in temperature of the trapped ions is determined by monitoring the laser induced fluorescence rate, which in Chapter 3

was shown to be related to the ions temperature by (Voigt profile):

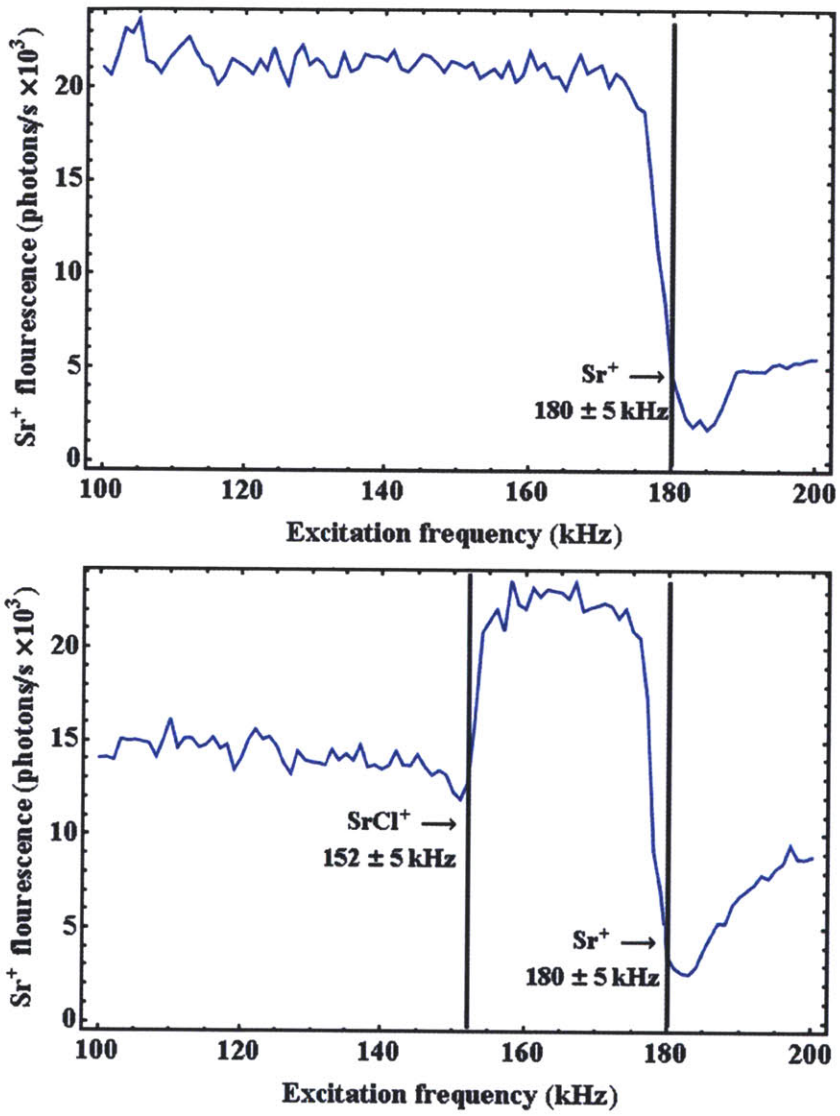

Figure 5-20: Mass spectroscopy spectra obtained from axial secular excitation of ion clouds trapped in the Nb surface electrode ion traps. Top: spectrum is obtained from a cloud which contains only Sr^+ atomic ions; Bottom: spectrum is acquired from an ion cloud containing a mixture of Sr^+ atomic ions and $SrCl^+$ molecular ions. The experimental ratio of the two axial frequencies is $(\nu_{Sr^+}/\nu_{SrCl^+})_{exp} = 1.18 \pm 0.07$, which is in very good agreement with the theoretical ratio $(\nu_{Sr^+}/\nu_{SrCl^+})_{th} = 1.18$. Both scans were done from low to high frequencies. The fluorescence signal increases after the ejection of the $SrCl^+$ molecular ions because the temperature of the remaining Sr^+ atomic ions falls bellow the temperature of the initial mixed ion cloud.

$$\Phi_{\mathrm{eg}} \propto \int_{-\infty}^{\infty} \frac{e^{-x^2}}{\left(\frac{\nu_{L,\mathrm{eg}}-\nu_{\mathrm{eg}}}{\Gamma_D} - x\right)^2 + \left(\frac{\Gamma_{\mathrm{eg}}}{2\Gamma_D}\right)^2} dx, \tag{5.4}$$

where $\Gamma_D = \frac{\nu_{\mathrm{eg}}}{c}\sqrt{\frac{2k_B T_A}{m_A}}$ is the Doppler width of the atomic ions. Although the temperature of the molecular ions cannot be monitored directly during the secular excitation, due to the fast thermalization (Eq. (5.3)) with the co-trapped atomic ions, the same atomic fluorescence can be used to determine the molecular ions secular frequency. In Figure 5-20, I show two typical mass spectroscopy spectra obtained from axial secular excitation of ion clouds trapped in the Nb surface electrode ion traps. The top spectrum is obtained from a cloud which contains only Sr^+ atomic ions, while the bottom one is acquired from an ion cloud containing a mixture of Sr^+ atomic ions and $SrCl^+$ molecular ions. The ratio of the two axial frequencies as obtained experimentally is $(\nu_{Sr^+}/\nu_{SrCl^+})_{\mathrm{exp}} = 1.18 \pm 0.07$, which is in very good agreement with the theoretical ratio $(\nu_{Sr^+}/\nu_{SrCl^+})_{\mathrm{th}} = 1.18$. For both species of ions the excitation voltage amplitude (1 V) was high enough to rise the ions temperature above the trap depth and eject them outside the trap. The rise in fluorescence signal after the ejection of the $SrCl^+$ molecular ions is due to the decrease in the temperature of the remaining Sr^+ atomic ions.

If the cooling laser frequency is swept around the atomic transition frequency, the florescence profile as modified by the Doppler effect (Eq. (5.4)) allows one to extract the ion cloud temperature [JHB04, MD00]. Once the laser frequency moves above the atomic transition frequency, the laser action switches from cooling to heating the atomic ions. As such, only the lower frequency part of the laser scan provides information about the ion cloud temperature. Figure 5-21 shows the fluorescence signal of an ion cloud containing a mixture of Sr^+ atomic ions and $SrCl^+$ molecular ions, as the cooling laser frequency is swept across the atomic ion transition frequency. By fitting a Voigt profile (Eq. (5.4)) through the experimentally obtained data points, the temperature of the mixed species ion cloud is determined to be approximately 5.8 K.

With the laser ablation method, we were able to trap other molecular ion species

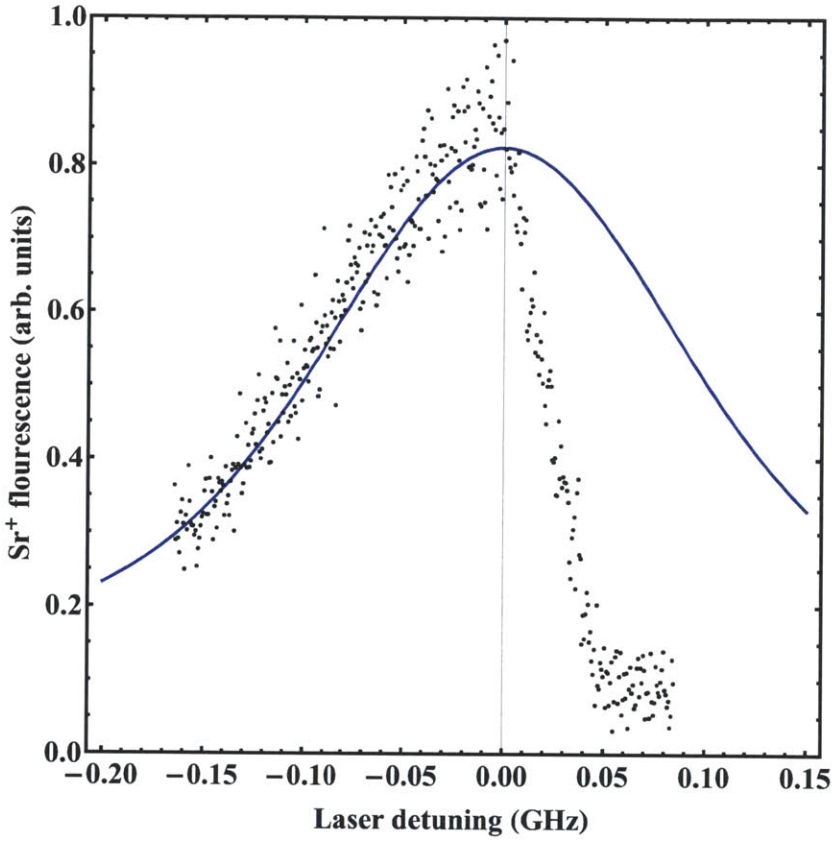

Figure 5-21: Fluorescence signal versus cooling laser frequency acquired from an ion cloud containing a mixture of Sr^+ atomic ions and $SrCl^+$ molecular ions. Black dots: experimental data points; Blue curve: fitted Voigt profile (Eq. (5.4)). The temperature of the ion cloud is approximately 5.8 K.

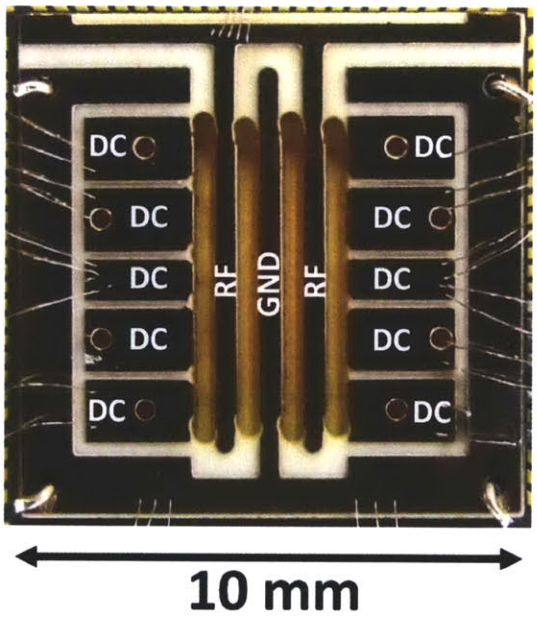

Figure 5-22: Example of Bastille surface electrode ion trap built by patterning the copper electrodes on 20 mil thick Rogers RO4350B laminate.

beside $SrCl^+$. From the $SrClO_3$ crystal ablation target, we produced TiO_2^+, TiO_3^+, and SrO^+ molecular ions, which were subsequently successfully trapped them in a simple cryogenic surface electrode RF ion trap design containing no integrated microwave transmission line (Bastille trap series). Similarly to the slot line and strip line ion traps, the Bastille ion trap was built by patterning its copper electrodes on 20 mil thick Rogers RO4350B laminate (Figure 5-22). Its characteristics are described in more detail in reference [LCL+07]. The Bastille ion trap is capable of reaching trap depths of 1.5 eV, although for the molecular ion loading test it was operated at 0.75 eV only.

The axial secular oscillatory motion of the trapped ions is characterized by the secular frequency:

$$\nu = \frac{1}{2\pi}\sqrt{\kappa\frac{QU_0}{m{y_0}^2}}, \tag{5.5}$$

where Q and m represent the ion charge and mass, U_0 is the DC axial confining potential, y_0 is the distance from the axial confining DC electrodes to the trap center,

and where κ is a geometric factor which depends on the trap geometry and it can be determined either from numerical modeling or experimentally. In the case of Bastille ion trap $y_0 = 3.05$ mm, while the geometric factor was determined numerically to be $\kappa = 0.031$. In Figure 5-23, I present the fluorescence signal from mixed ion clouds versus "tickle" frequency obtained at three different axial confining voltages U_0. The ablation targets were prepared similarly with those described in Section 4.2, except that instead of $SrCl_2$ I used $CaCl_2$. Although only the $SrTiO_3$ crystal ablation target was used to load the mixed species ion clouds, the surface of the crystal got contaminated with $CaCl_2$ during the ablation targets preparation and, as such, some ion clouds contained $CaCl^+$ molecular ions. Figure 5-24 shows a comparison between the theoretical and experimentally obtain secular frequencies for the Bastille ion trap in the case of four different ion species.

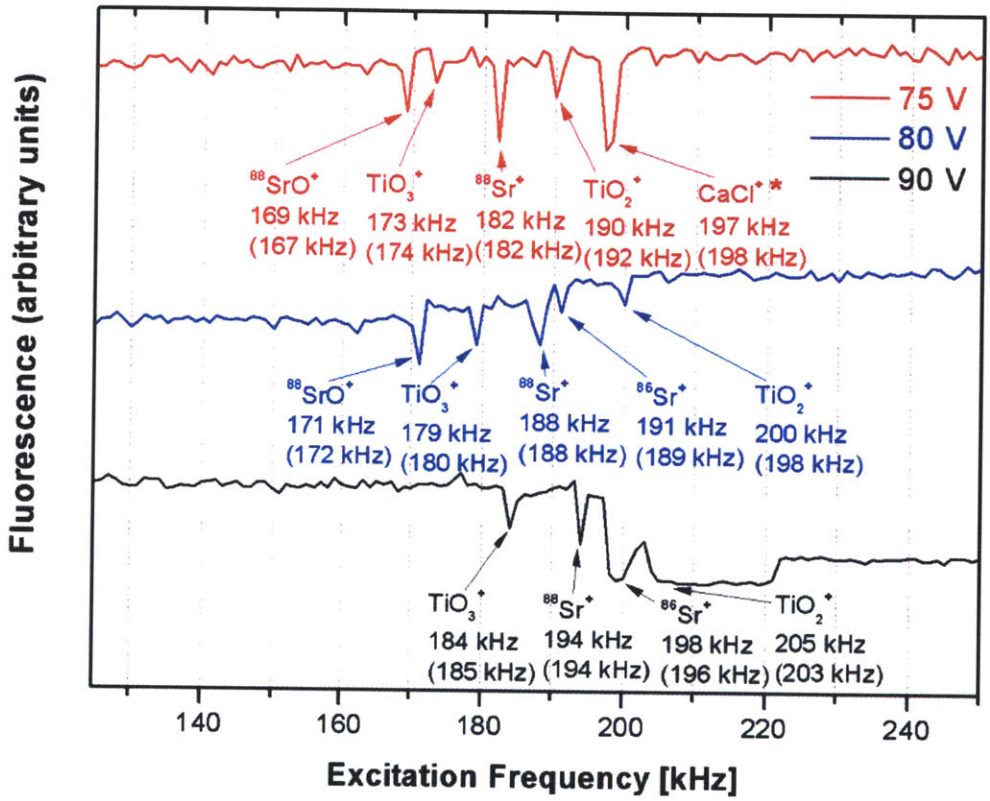

Figure 5-23: Fluorescence signal of mixed ion clouds versus "tickle" frequency obtained at three different axial confining voltages U_0 as shown on figure. For all three scans the amplitude of the excitation voltage was kept at 0.2 V. The numbers under the fluorescence dips mark their positions, while the numbers in parentheses indicate the theoretical axial secular frequencies for the corresponding ionic species. All the ion clouds were produced from the $SrTiO_3$ crystal ablation target, although during the preparation its surface got contaminated with $CaCl_2$.

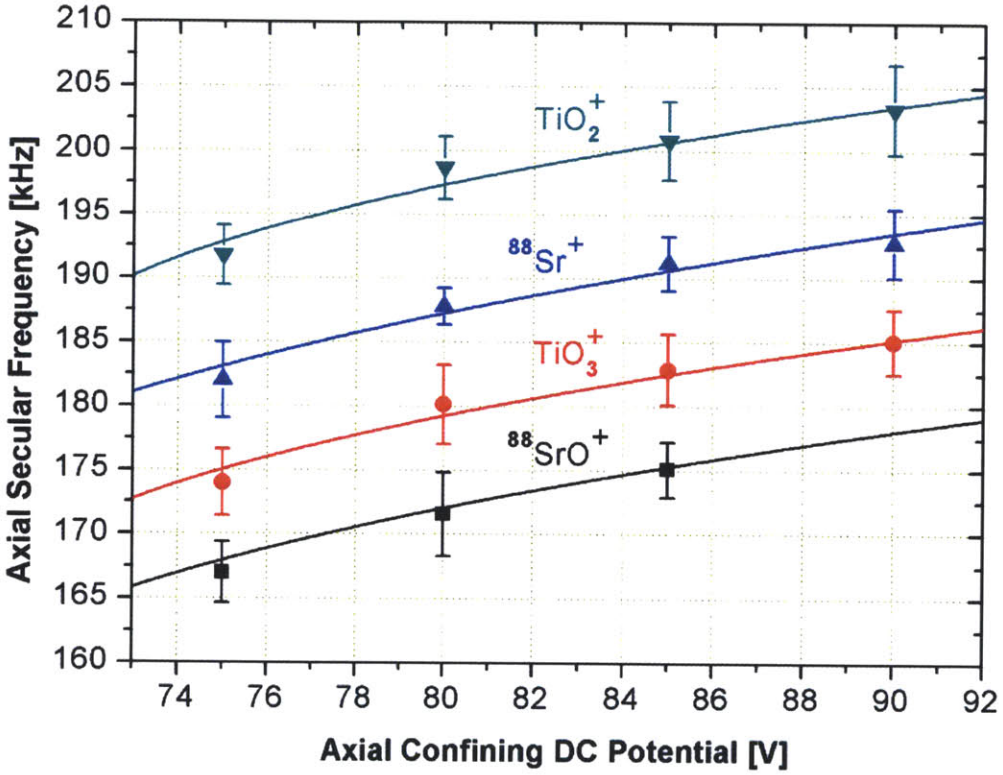

Figure 5-24: Comparison between the theoretical (curves) secular frequencies based on Eq. (5.5) and experimentally (points) obtain secular frequencies for the Bastille ion trap in the case of four different ion species. Every displayed point is an average of 20 experimentally measured data points.

Chapter 6

Conclusions and outlook

In this thesis I investigated some of the challenges associated with performing microwave spectroscopy of rotational the levels of polar molecular ions trapped in RF ion traps with integrated superconducting microwave cavities. I have looked at both the theoretical and experimental aspects of this project, and the main results are summarized here.

One difficulty in observing the coupling of the microwave radiation to the rotational levels of a molecule is posed by the very long lifetime of the excited rotational levels. As a consequence, a first step of the experiment was to identify a mechanism capable of reducing the effective lifetime of the excited rotational levels. I proposed and analyzed two such schemes. The first method is based on the fact that in a mixed ion cloud containing both atomic and molecular ions, during the Coulomb collisions, the molecular internal angular momentum can be transferred from or to the atomic ions. I showed that the collisional enhanced rotational de-excitation rate can be observed in a cryogenic environment with moderate temperatures of 4-10 K. The second method I proposed starts with the observation that when the molecular rotational transition is strongly coupled to a microwave cavity, the effective rotational decay rate becomes proportional to $\propto \ g^2/\kappa$, where g is the vacuum Rabi frequency and κ is the microwave cavity decay rate [ADD$^+$06]. To enhance g requires that the molecular ion be trapped very closed ($1 - 10\ \mu$m) to the microwave cavity electrode, while in order to reduce cavity κ necessitates a very high microwave cavity quality

factor ($\sim 10^6$). Both of these requirements demand that the RF ion traps be operated in cryostats capable of reaching temperatures of $\sim$ 100 mK, on one hand to suppress the molecular ion motional heating rates [LGA+08] and on the other hand to enhance the microwave cavity quality factor.

The second part of the thesis describes the experimental components necessary to implement this project. One immediate implication of the presence of superconducting microwave resonators is that the entire experiment must be carried out in a cryogenic environment. So, the initial task was to build a cryogenic ion trapping system based on a closed cycle cryostat and to show that RF ion traps can be successfully operated in such system. The second challenge I met was to find a suitable RF ion trap geometry capable of supporting a microwave transmission line or resonator. The nature of the experiment requires both a high trap depth and a high microwave field at the trapped ion location. I found experimentally and theoretically that these two ion trap requirements are conflicting with each other. I tested four ion trap designs one based on slot line, two based on strip line (plate and wire), and one based on a coplanar waveguide (CPW), which I deemed to have the best characteristics. Another experimental requirement was to find a source of molecular ions compatible with the cryogenic environment. I demonstrated that molecular ion source based on a laser ablation method can reliable load an RF ion trap without adversely affecting the trapping system.

Bibliography

[ABH+56] K. Alder, A. Bohr, T. Huus, B. Mottelson, and A. Winther. Study of Nuclear Structure by Electromagnetic Excitation with Accelerated Ions. *Reviews of Modern Physics*, **28**(4), 432–542, 1956.

[AC04] L. U. Ancarani and M. C. Chidichimo. Partial Wave Completion Technique for Scattering Amplitudes in Coulomb Dipole Excitation. *Journal of Physics B: Atomic, Molecular and Optical Physics*, **37**(21), 4339, 2004.

[ADD+06] A. Andre, D. DeMille, J. M. Doyle, M. D. Lukin, S. E. Maxwell, P. Rabl, R. J. Schoelkopf, and P. Zoller. A Coherent All-Electrical Interface between Polar Molecules and Mesoscopic Superconducting Resonators. *Nature Physics*, **2**(9), 636–642, 2006.

[AG92] H. F. Arnoldus and T. F. George. Analytical Evaluation of Elastic Coulomb Integrals. *Journal of Mathematical Physics*, **33**(2), 578–583, 1992.

[ASA+09] P. B. Antohi, D. Schuster, G. M. Akselrod, J. Labaziewicz, Y. Ge, Z. Lin, W. S. Bakr, and I. L. Chuang. Cryogenic Ion Trapping Systems with Surface-Electrode Traps. *Review of Scientific Instruments*, **80**(1), 013103, 2009.

[AW95] George B. Arfken and Hans J. Weber. *Mathematical Methods for Physicists*. Academic Press, Inc., San Diego, CA, 4th edition, 1995.

[BBM99] H. L. Bethlem, G. Berden, and G. Meijer. Decelerating Neutral Dipolar Molecules. *Physical Review Letters*, **83**(8), 1558–1561, 1999.

[BC03] John M. Brown and Alan Carrington. *Rotational Spectroscopy of Diatomic Molecules.* Cambridge University Press, Cambridge, 2003.

[BGW+07] A. Blais, J. Gambetta, A. Wallraff, D. I. Schuster, S. M. Girvin, M. H. Devoret, and R. J. Schoelkopf. Quantum-Information Processing with Circuit Quantum Electrodynamics. *Physical Review A: Atomic, Molecular and Optical Physics*, **75**(3), 032329, 2007.

[BHW+04] A. Blais, R. Huang, A. Wallraff, S. M. Girvin, and R. J. Schoelkopf. Cavity Quantum Electrodynamics for Superconducting Electrical Circuits: An Architecture for Quantum Computation. *Physical Review A: Atomic, Molecular and Optical Physics*, **69**(6), 062320, 2004.

[BJ03] B. H. Bransden and C. J. Joachain. *Physics of Atoms and Molecules.* Benjamin Cummings, Harlow, England, 2nd edition, 2003.

[BJD06] A. Bertelsen, S. Jorgensen, and M. Drewsen. The Rotational Temperature of Polar Molecular Ions in Coulomb Crystals. *Journal of Physics B: Atomic, Molecular and Optical Physics*, **39**(5), L83, 2006.

[BLW+07] M. Brownnutt, V. Letchumanan, G. Wilpers, R.C. Thompson, P. Gill, and A.G. Sinclair. Controlled Photoionization Loading of $^{8}8Sr^{+}$ for Precision Ion-Trap Experiments. *Applied Physics B: Lasers and Optics*, **87**, 411–415, 2007.

[BRF+05] P. Blythe, B. Roth, U. Fröhlich, H. Wenz, and S. Schiller. Production of Ultracold Trapped Molecular Hydrogen Ions. *Physical Review Letters*, **95**(18), 183002, 2005.

[BW02] T. Baba and I. Waki. Spectral Shape of In Situ Mass Spectra of Sympathetically Cooled Molecular Ions. *Journal of Applied Physics*, **92**(7), 4109–4116, 2002.

[Car93] Howard Carmichael. *An Open Systems Approach to Quantum Optics.* Springer-Verlag, Berlin, 1993.

[CBB+05] J. Chiaverini, R. B. Blakestad, J. Britton, J. D. Jost, C. Langer, D. Leibfried, R. Ozeri, and D. J. Wineland. Surface-Electrode Architecture for Ion-Trap Quantum Information Processing. *Quantum Information & Computation*, **5**, 419, 2005.

[CBK82] A. Carrington, J. Buttenshaw, and R. A. Kennedy. Vibration-Rotation Spectroscopy of the HD^+ Ion. *Journal of Molecular Structure*, **80**, 47–69, 1982.

[CBZP92] J. I. Cirac, R. Blatt, P. Zoller, and W. D. Phillips. Laser Cooling of Trapped Ions in a Standing Wave. *Physical Review A: Atomic, Molecular and Optical Physics*, **46**(5), 2668–2681, 1992.

[CD74] Shih-I. Chu and A. Dalgarno. Rotational Excitation of CH^+ by Electron Impact. *Physical Review A: Atomic, Molecular and Optical Physics*, **10**(3), 788–792, 1974.

[CDKY09] L. D. Carr, D. DeMille, R. V. Krems, and J. Ye. Cold and Ultracold Molecules: Science, Technology and Applications. *New Journal of Physics*, **11**(5), 055049, 2009.

[CGD+10] C. R. Clark, J. E. Goeders, Y. K. Dodia, C. R. Viteri, and K. R. Brown. Detection of Single-Ion Spectra by Coulomb-Crystal Heating. *Physical Review A: Atomic, Molecular and Optical Physics*, **81**(4), 043428, 2010.

[Chu75] Shih-I. Chu. Rotational Excitation of Symmetric-Top Molecular Ions by Electron Impact. *Physical Review A: Atomic, Molecular and Optical Physics*, **12**(2), 396–405, 1975.

[CKK08] J. Czechowska-Kryszk and S. Kryszewski. Positivity of Bloch-Boltzmann Equations: Degenerate case. *Physical Review A: Atomic, Molecular and Optical Physics*, **77**(3), 032715, 2008.

[CLZ95] J. I. Cirac, M. Lewenstein, and P. Zoller. Laser Cooling of a Trapped Atom in a Cavity: Bad-Cavity Limit. *Physical Review A: Atomic, Molecular and Optical Physics*, **51**(2), 1650–1655, 1995.

[CRZ91] J. I. Cirac, H. Ritsch, and P. Zoller. Two-Level System Interacting with a Finite-Bandwidth Thermal Cavity Mode. *Physical Review A: Atomic, Molecular and Optical Physics*, **44**(7), 4541–4551, 1991.

[CTDRG92] Claude Cohen-Tannoudji, Jacques DuPont-Roc, and Gilbert Grynberg. *Atom-Photon Interactions: Basic Processes and Applications.* John Wiley & Sons, Inc., New York, NY, 1992.

[DCM+08] D. DeMille, S. B. Cahn, D. Murphree, D. A. Rahmlow, and M. G. Kozlov. Using Molecules to Measure Nuclear Spin-Dependent Parity Violation. *Physical Review Letters*, **100**(2), 023003, 2008.

[DeM02] D. DeMille. Quantum Computation with Trapped Polar Molecules. *Physical Review Letters*, **88**(6), 067901, 2002.

[Der86] R. J. Deri. Dielectric Measurements with Helical Resonators. *Review Of Scientific Instruments*, **57**(1), 82–86, 1986.

[DF81] A. S. Dickinson and D. R. Flower. Electron Collisional Excitation of Interstellar Molecular Ions. *Monthly Notices of the Royal Astronomical Society*, **196**, 297–+, 1981.

[DFKP95] J. M. Doyle, B. Friedrich, J. Kim, and D. Patterson. Buffer-Gas Loading of Atoms and Molecules into a Magnetic Trap. *Physical Review A: Atomic, Molecular and Optical Physics*, **52**(4), R2515–R2518, 1995.

[DG99] T. C. Devore and J. L. Gole. Energetics, Molecular Electronic Structure, and Spectroscopy Of Forming Group IIA Dihalide Complexes. *Chemical Physics*, **241**(2), 221 – 238, 1999.

[DGS07] M. H. Devoret, S. Girvin, and R. Schoelkopf. Circuit-QED: How Strong Can the Coupling between a Josephson Junction Atom and a Transmission Line Resonator Be? *Annalen der Physik*, **16**(10-11), 767–779, 2007.

[DM77] A. S. Dickinson and J. M. Munoz. Rotational Excitation of Polar Molecular Ions by Slow Electrons. *Journal of Physics B: Atomic and Molecular Physics*, **10**(15), 3151, 1977.

[DMM+04] M. Drewsen, A. Mortensen, R. Martinussen, P. Staanum, and J. L. Sørensen. Nondestructive Identification of Cold and Extremely Localized Single Molecular Ions. *Physical Review Letters*, **93**(24), 243201, 2004.

[DWC96] R. Diehl, D. M. Wheatley, and T. G. Castner. The Electromagnetic Modes of a Helical Resonator. *Review Of Scientific Instruments*, **67**(11), 3904–3913, 1996.

[Fis76] J. R. Fisk. Helical Resonator Design Techniques. *QST*, p. 11, 1976.

[FT01] A. Faure and J. Tennyson. Electron-Impact Rotational Excitation of Linear Molecular Ions. *Monthly Notices of the Royal Astronomical Society*, **325**(1), 443–448, 2001.

[FWS+05] L. Frunzio, A. Wallraff, D. Schuster, J. Majer, and R. Schoelkopf. Fabrication and Characterization of Superconducting Circuit QED Devices for Quantum Computation. *Applied Superconductivity, IEEE Transactions on*, **15**(2), 860 – 863, 2005.

[Gau] Gaussian 03W. Computational chemistry electronic structure software.

[GC84] Walter Gordy and Robert L. Cook. *Microwave Molecular Spectra.* Wiley-Interscience, New York, NY, 1984.

[Ger95] D. Gerlich. Ion-Neutral Collisions in a 22-Pole Trap at Very Low Energies. *Physica Scripta*, **1995**(T59), 256, 1995.

[Gho96] P. K. Ghosh. *Ion Traps.* Oxford University Press, Clarendon, Oxford, 1996.

[GPQ+95] G. Gabrielse, D. Phillips, W. Quint, H. Kalinowsky, G. Rouleau, and W. Jhe. Special Relativity and the Single Antiproton: Fortyfold Improved Comparison of $\bar{p}$ and p Charge-to-Mass Ratios. *Physical Review Letters*, **74**(18), 3544–3547, 1995.

[GPS01] Herbert Goldstein, Charles P. Poole, and John L. Safko. *Classical Mechanics.* Addison Wesley Longman, San Francisco, 3rd edition, 2001.

[GR95] R. J. Goldston and P. H. Rutherford. *Introduction to Plasma Physics.* Taylor & Francis Group, Bristol, UK, 1995.

[GZ04] C. W. Gardiner and P. Zoller. *Quantum Noise: A Handbook of Markovian and Non-Markovian Quantum Stochastic Methods with Applications to Quantum Optics.* Springer, Berlin, 3rd edition, 2004.

[HBL+04] E. R. Hudson, J. R. Bochinski, H. J. Lewandowski, B. C. Sawyer, and J. Ye. Efficient Stark Deceleration of Cold Polar Molecules. *European Physical Journal D: Atomic, Molecular, Optical and Plasma Physics*, **31**(2), 351–358, 2004.

[HGH+07] R. J. Hendricks, D. M. Grant, P. F. Herskind, A. Dantan, J. L. Sørensen, and M. Drewsen. An All-Optical Ion-Loading Technique for Scalable Microtrap Architectures. In *CLEO/Europe and IQEC 2007 Conference Digest*, pp. IC3–3. Optical Society of America, 2007.

[HHG+97] P. Horak, G. Hechenblaikner, K. M. Gheri, H. Stecher, and H. Ritsch. Cavity-Induced Atom Cooling in the Strong Coupling Regime. *Physical Review Letters*, **79**(25), 4974–4977, 1997.

[HMO+06] Y. Hashimoto, L. Matsuoka, H. Osaki, Y. Fukushima, and S. Hasegawa. Trapping Laser Ablated Ca^+ Ions in Linear Paul Trap. *Japanese Journal Of Applied Physics Part 1: Regular Papers, Brief Communications and Review Papers*, **45**(9A), 7108–7113, 2006.

[HTS+06] E. R. Hudson, C. Ticknor, B. C. Sawyer, C. A. Taatjes, H. J. Lewandowski, J. R. Bochinski, J. L. Bohn, and J. Ye. Production of Cold Formaldehyde Molecules for Study and Control of Chemical Reaction Dynamics with Hydroxyl Radicals. *Physical Review A: Atomic, Molecular and Optical Physics*, **73**(6), 063404, 2006.

[HWR+09] G. Hammer, S. Wuensch, M. Roesch, K. Ilin, E. Crocoll, and M. Siegel. Coupling of Microwave Resonators to Feed Lines. *Applied Superconductivity, IEEE Transactions on*, **19**(3), 565 –569, 2009.

[ICZ10] Z. Idziaszek, T. Calarco, and P. Zoller. Ion-Assisted Ground-State Cooling of a Trapped Polar Molecule. *ArXiv e-prints*, 2010.

[Jac72] A. Jacobs. Analytical Expressions for Excitation and Ionization Cross-Sections and Rate Coefficients of Hydrogen-Like Ions by Electron and Proton Impact. *Journal of Quantitative Spectroscopy and Radiative Transfer*, **12**(2), 243 - 257, 1972.

[Jac99] John David Jackson. *Classical Electrodynamics*. John Wiley & Sons, New York, 3rd edition, 1999.

[Jam98] D. F. V. James. Quantum Dynamics of Cold Trapped Ions with Application to Quantum Computation. *Applied Physics B: Lasers and Optics*, **66**, 181–190, 1998.

[JHB04] M. J. Jensen, T. Hasegawa, and J. J. Bollinger. Temperature and Heating Rate of Ion Crystals in Penning Traps. *Physical Review A: Atomic, Molecular and Optical Physics*, **70**(3), 033401, 2004.

[Jin02] Jianming Jin. *The Finite Element Method in Electromagnetics.* Wiley-IEEE Press, New York, NY, 2002.

[Joa75] C. J. Joachain. *Quantum Collision Theory.* North-Holland Publishing Company, Amsterdam, 1975.

[KP09] E. Kirilov and S. Putterman. 2-Photon Ionization for Efficient Seeding and Trapping of Strontium Ions. *European Physical Journal D: Atomic, Molecular, Optical and Plasma Physics*, **54**, 683–691, 2009.

[KRS07] J. C. J. Koelemeij, B. Roth, and S. Schiller. Blackbody Thermometry with Cold Molecular Ions and Application to Ion-Based Frequency Standards. *Physical Review A: Atomic, Molecular and Optical Physics*, **76**(2), 023413, 2007.

[LCL+07] D. R. Leibrandt, R. J. Clark, J. Labaziewicz, P. B. Antohi, W. Bakr, K. R. Brown, and I. L. Chuang. Laser Ablation Loading of a Surface-Electrode Ion Trap. *Physical Review A: Atomic, Molecular and Optical Physics*, **76**(5), 055403, 2007.

[LGA+08] J. Labaziewicz, Y. Ge, P. B. Antohi, D. Leibrandt, K. R. Brown, and I. L. Chuang. Suppression of Heating Rates in Cryogenic Surface-Electrode Ion Traps. *Physical Review Letters*, **100**(1), 013001, 2008.

[LHP+93] P. D. Lett, K. Helmerson, W. D. Phillips, L. P. Ratliff, S. L. Rolston, and M. E. Wagshul. Spectroscopy of Na_2 by Photoassociation of Laser-Cooled Na. *Physical Review Letters*, **71**(14), 2200–2203, 1993.

[LRB+07] J. Labaziewicz, P. Richerme, K. R. Brown, I. L. Chuang, and K. Hayasaka. Compact, Filtered Diode Laser System for Precision Spectroscopy. *Optics Letters*, **32**(5), 572–574, 2007.

[LS84] M. Lindberg and S. Stenholm. The Master Equation for Laser Cooling of Trapped Particles. *Journal of Physics B: Atomic and Molecular Physics*, **17**(16), 3375, 1984.

[MCH93] J. D. Miller, R. A. Cline, and D. J. Heinzen. Photoassociation Spectrum of Ultracold Rb Atoms. *Physical Review Letters*, **71**(14), 2204–2207, 1993.

[MD00] K. Molhave and M. Drewsen. Formation of Translationally Cold MgH^+ and MgD^+ Molecules in an Ion Trap. *Physical Review A: Atomic, Molecular and Optical Physics*, **62**(1), 011401, 2000.

[MECZ99] G. Morigi, J. Eschner, J. I. Cirac, and P. Zoller. Laser Cooling of Two Trapped Ions: Sideband Cooling Beyond the Lamb-Dicke Limit. *Physical Review A: Atomic, Molecular and Optical Physics*, **59**(5), 3797–3808, 1999.

[MG51] C. J. Mullin and E. Guth. Electric Excitation and Disintegration of Nuclei. I. Excitation and Disintegration of Nuclei by the Coulomb Field of Positive Particles. *Physical Review*, **82**(2), 141–155, 1951.

[MGW05] F. G. Major, V. N. Gheorghe, and G. Werth. *Charged Particle Traps: Physics and Techniques of Charged Particle Field Confinement.* Springer, Berlin, 1st edition, 2005.

[MNP+06] K. Murr, S. Nußmann, T. Puppe, M. Hijlkema, B. Weber, S. C. Webster, A. Kuhn, and G. Rempe. Three-Dimensional Cavity Cooling and Trapping in an Optical Lattice. *Physical Review A: Atomic, Molecular and Optical Physics*, **73**(6), 063415, 2006.

[MPG+00] J. Paul MacMillan, Jai Won Park, Rolf Gerstenberg, Heinz Wagner, Karl Kohler, and Peter Wallbrecht. *Strontium and Strontium Compounds.* Wiley-VCH Verlag GmbH & Co. KGaA, 2000.

[MS99] Harold J. Metcalf and Peter Van Der Straten. *Laser Cooling and Trapping.* Springer-Verlag, New York, NY, 1999.

[MYJ80] G. Matthaei, L. Young, and E. M. T. Jones. *Microwave Filters, Impedance-Matching Networks, and Coupling Structures.* Artech House Publishers, Norwood, MA, 1980.

[OKKN01] A. Ohsaki, T. Kai, E. Kimura, and S. Nakazaki. Analytic Expressions of Radial Integral on Multiple Transitions for Coulomb-Born Approximation. *Journal of Physics A: Mathematical and General*, **34**(9), 1935, 2001.

[OM01] M. H. Oliveira and J. A. Miranda. Biot-Savart-Like Law in Electrostatics. *European Journal of Physics*, **22**(1), 31, 2001.

[OWN+01] K. Okada, M. Wada, T. Nakamura, I. Katayama, L. Boesten, and S. Ohtani. Cryogenic Ion Trap for Minimization of Trapped Ion Loss. *Japanese Journal Of Applied Physics Part 1: Regular Papers, Short Notes and Review Papers*, **40**(6A), 4221–4222, 2001.

[OZW+06] A. Ostendorf, C. B. Zhang, M. A. Wilson, D. Offenberg, B. Roth, and S. Schiller. Sympathetic Cooling of Complex Molecular Ions to Millikelvin Temperatures. *Physical Review Letters*, **97**(24), 243005, 2006.

[PBIW96] M. E. Poitzsch, J. C. Bergquist, W. M. Itano, and D. J. Wineland. Cryogenic Linear Ion Trap for Accurate Spectroscopy. *Review Of Scientific Instruments*, **67**(1), 129–134, 1996.

[PLB+06] C. E. Pearson, D. R. Leibrandt, W. S. Bakr, W. J. Mallard, K. R. Brown, and I. L. Chuang. Experimental Investigation of Planar Ion Traps. *Physical Review A: Atomic, Molecular and Optical Physics*, **73**(3), 032307, 2006.

[PM79] J. E. Potter and J. Macek. Low-Energy Proton-Hydrogenlike-Ion Scattering in The Coulomb-Born Approximation. *Physical Review A: Atomic, Molecular and Optical Physics*, **20**(6), 2302–2309, 1979.

[POHDL95] J. C. Pearson, L. C. Oesterling, Eric Herbst, and F. C. De Lucia. Pressure Broadening of Gas Phase Molecular Ions at Very Low Temperature. *Physical Review Letters*, **75**(16), 2940–2943, 1995.

[PWM+91] J. D. Prestage, A. Williams, L. Maleki, M. J. Djomehri, and E. Harabetian. Dynamics of Charged-Particles in a Paul Radiofrequency Quadrupole Trap. *Physical Review Letters*, **66**(23), 2964–2967, 1991.

[RBD+06] B. Roth, P. Blythe, H. Daerr, L. Patacchini, and S. Schiller. Production of Ultracold Diatomic and Triatomic Molecular Ions of Spectroscopic and Astrophysical Interest. *Journal of Physics B: Atomic, Molecular and Optical Physics*, **39**(19), S1241, 2006.

[RDD+06] P. Rabl, D. DeMille, J. M. Doyle, M. D. Lukin, R. J. Schoelkopf, and P. Zoller. Hybrid Quantum Processors: Molecular Ensembles as Quantum Memory for Solid State Circuits. *Physical Review Letters*, **97**(3), 033003, 2006.

[RGRS09] G. Romero, J. J. García-Ripoll, and E. Solano. Microwave Photon Detector in Circuit QED. *Physical Review Letters*, **102**(17), 173602, 2009.

[ROZS08] B. Roth, D. Offenberg, C. B. Zhang, and S. Schiller. Chemical Reactions between Cold Trapped Ba^+ Ions and Neutral Molecules in the Gas Phase. *Physical Review A: Atomic, Molecular and Optical Physics*, **78**(4), 042709, 2008.

[RST98] I. Rabadan, B. K. Sarpal, and J. Tennyson. On the Calculation of Electron-Impact Rotational Excitation Cross Sections for Molecular Ions. *Journal of Physics B: Atomic, Molecular and Optical Physics*, **31**(9), 2077, 1998.

[RWE+95] L. Ricci, M. Weidemller, T. Esslinger, A. Hemmerich, C. Zimmermann, V. Vuletic, W. Knig, and T. W. Hnsch. A Compact Grating-Stabilized

Diode Laser System for Atomic Physics. *Optics Communications*, **117**(5-6), 541 – 549, 1995.

[RZ07] P. Rabl and P. Zoller. Molecular Dipolar Crystals as High-Fidelity Quantum Memory for Hybrid Quantum Computing. *Physical Review A: Atomic, Molecular and Optical Physics*, **76**(4), 042308, 2007.

[RZS05] V. L. Ryjkov, X. Z. Zhao, and H. A. Schuessler. Simulations of the RF Heating Rates in a Linear Quadrupole Ion Trap. *Physical Review A: Atomic, Molecular and Optical Physics*, **71**(3, Part B), 2005.

[Sac84] S. Sachdev. Atom in a Damped Cavity. *Physical Review A: Atomic, Molecular and Optical Physics*, **29**(5), 2627–2633, 1984.

[Sak81] K. Sakimoto. Rotational Excitation of Symmetric-Top Molecules by Low-Energy Ion Impact. *Journal of the Physical Society of Japan*, **50**(5), 1668–1675, 1981.

[SB73] T. Su and M. T. Bowers. Theory of Ion-Polar Molecule Collisions. Comparison with Experimental Charge Transfer Reactions of Rare Gas Ions to Geometric Isomers of Difluorobenzene and Dichloroethylene. *The Journal of Chemical Physics*, **58**(7), 3027–3037, 1973.

[SBC+11] D. I. Schuster, Lev S. Bishop, I. L. Chuang, D. DeMille, and R. J. Schoelkopf. Cavity QED in a Molecular Ion Trap. *Physical Review A: Atomic, Molecular and Optical Physics*, **83**(1), 012311, 2011.

[SBD10] E. S. Shuman, J. F. Barry, and D. DeMille. Laser Cooling of a Diatomic Molecule. *Nature*, **467**(7317), 820–823, 2010.

[SCR+06] S. Seidelin, J. Chiaverini, R. Reichle, J. J. Bollinger, D. Leibfried, J. Britton, J. H. Wesenberg, R. B. Blakestad, R. J. Epstein, D. B. Hume, W. M. Itano, J. D. Jost, C. Langer, R. Ozeri, N. Shiga, and D. J. Wineland. Microfabricated Surface-Electrode Ion Trap for Scalable

Quantum Information Processing. *Physical Review Letters*, **96**(25), 253003, 2006.

[SHMvdM09] L. Scharfenberg, H. Haak, G. Meijer, and S. Y. T. van de Meerakker. Operation of a Stark Decelerator with Optimum Acceptance. *Physical Review A: Atomic, Molecular and Optical Physics*, **79**(2), 023410, 2009.

[SHO+06] D. Stick, W. K. Hensinger, S. Olmschenk, M. J. Madsen, K. Schwab, and C. Monroe. Ion Trap in a Semiconductor Chip. *Nature Physics*, **2**(1), 36–39, 2006.

[SHS+10] P. F. Staanum, K. Hojbjerre, P. S. Skyt, A. K. Hansen, and M. Drewsen. Rotational Laser Cooling of Vibrationally and Translationally Cold Molecular Ions. *Nature Physics*, **6**(4), 271–274, 2010.

[Sim01] Rainee N. Simons. *Coplanar Waveguide Circuits, Components, and Systems*. Wiley-IEEE Press, New York, NY, 1st edition, 2001.

[Som53] Arnold Sommerfeld. *Atombau und Spektrallinien*, Volume II. Band. Frederick Ungar Publishing Co., New York, NY, 1953.

[SRD+10] T. Schneider, B. Roth, H. Duncker, I. Ernsting, and S. Schiller. All-Optical Preparation of Molecular Ions in the Rovibrational Ground State. *Nature Physics*, **6**(4), 275–278, 2010.

[SSBD05] J. M. Sage, S. Sainis, T. Bergeman, and D. DeMille. Optical Production of Ultracold Polar Molecules. *Physical Review Letters*, **94**(20), 203001, 2005.

[Ste86] S. Stenholm. The Semiclassical Theory of Laser Cooling. *Reviews of Modern Physics*, **58**(3), 699–739, 1986.

[Ste98] G. W. Stewart. *Matrix Algorithms*, Volume 1. Society for Industrial and Applied Mathematics, Philadelphia, PA, 1st edition, 1998.

[SvdWCL04] A. S. Sørensen, C. H. van der Wal, L. I. Childress, and M. D. Lukin. Capacitive Coupling of Atomic Systems to Mesoscopic Conductors. *Physical Review Letters*, **92**(6), 063601, 2004.

[Swa81] S. Swain. Master Equation Derivation of Quantum Regression Theorem. *Journal of Physics A: Mathematical and General*, **14**(10), 2577, 1981.

[TC01] M. D. Thorsley and M. C. Chidichimo. An Asymptotic Expansion for the Hypergeometric Function $_2F_1$(a,b;c;x). *Journal of Mathematical Physics*, **42**(4), 1921–1930, 2001.

[TF79] J. Turulski and M. Forys. Ion-Polar Molecule Collision Frequency. A Thermodynamic Treatment. *The Journal of Physical Chemistry*, **83**(22), 2815–2817, 1979.

[VCB01] V. Vuletic, H. W. Chan, and A. T. Black. Three-Dimensional Cavity Doppler Cooling and Cavity Sideband Cooling by Coherent Scattering. *Physical Review A: Atomic, Molecular and Optical Physics*, **64**(3), 033405, 2001.

[VMD02] I. S. Vogelius, L. B. Madsen, and M. Drewsen. Blackbody-Radiation–Assisted Laser Cooling of Molecular Ions. *Physical Review Letters*, **89**(17), 173003, 2002.

[VMD04a] I. S. Vogelius, L. B. Madsen, and M. Drewsen. Rotational Cooling of Heteronuclear Molecular Ions with $^1\Sigma$, $^2\Sigma$, $^3\Sigma$, and $^2\Pi$ Electronic Ground States. *Physical Review A: Atomic, Molecular and Optical Physics*, **70**(5), 053412, 2004.

[VMD04b] I. S. Vogelius, L. B. Madsen, and M. Drewsen. Rotational Cooling of Molecules Using Lamps. *Journal of Physics B: Atomic, Molecular and Optical Physics*, **37**(22), 4571, 2004.

[VMD06] I. S. Vogelius, L. B. Madsen, and M. Drewsen. Rotational Cooling of Molecular Ions through Laser-Induced Coupling to the Collective Modes of a Two-Ion Coulomb Crystal. *Journal of Physics B: Atomic, Molecular and Optical Physics*, **39**(19), S1267, 2006.

[Wad91] Brian C. Wadell. *Transmission Line Design Handbook.* Artech House Publishers, Norwood, MA, 1991.

[WBG+08] S. Willitsch, M. T. Bell, A. D. Gingell, S. R. Procter, and T. P. Softley. Cold Reactive Collisions between Laser-Cooled Ions and Velocity-Selected Neutral Molecules. *Physical Review Letters*, **100**(4), 043203, 2008.

[WdG+98] J. D. Weinstein, R. deCarvalho, T. Guillet, B. Friedrich, and J. M. Doyle. Magnetic Trapping of Calcium Monohydride Molecules at Millikelvin Temperatures. *Nature*, **395**(6698), 148–150, 1998.

[Wes08] J. H. Wesenberg. Electrostatics of Surface-Electrode Ion Traps. *Physical Review A: Atomic, Molecular and Optical Physics*, **78**(6), 063410, 2008.

[WHW+09] H. Wang, M. Hofheinz, J. Wenner, M. Ansmann, R. C. Bialczak, M. Lenander, Erik Lucero, M. Neeley, A. D. O'Connell, D. Sank, M. Weides, A. N. Cleland, and John M. Martinis. Improving the Coherence Time of Superconducting Coplanar Resonators. *Applied Physics Letters*, **95**(23), 233508, 2009.

[WRLZ08] M. Wallquist, P. Rabl, M. D. Lukin, and P. Zoller. Theory of Cavity-Assisted Microwave Cooling of Polar Molecules. *New Journal of Physics*, **10**(6), 063005, 2008.

[WSB+04] A. Wallraff, D. I. Schuster, A. Blais, L. Frunzio, R.-S. Huang, J. Majer, S. Kumar, S. M. Girvin, and R. J. Schoelkopf. Strong Coupling of a

Single Photon to a Superconducting Qubit Using Circuit Quantum Electrodynamics. *Nature*, **431**(7005), 162–167, 2004.

[ZKY08] T. Zelevinsky, S. Kotochigova, and Jun Ye. Precision Test of Mass-Ratio Variations with Lattice-Confined Ultracold Molecules. *Physical Review Letters*, **100**(4), 043201, 2008.

[ZM05] S. Zippilli and G. Morigi. Mechanical Effects of Optical Resonators on Driven Trapped Atoms: Ground-State Cooling in a High-Finesse Cavity. *Physical Review A: Atomic, Molecular and Optical Physics*, **72**(5), 053408, 2005.

[ZRS02] X. Zhao, V. L. Ryjkov, and H. A. Schuessler. Parametric Excitations of Trapped Ions in a Linear RF Ion Trap. *Physical Review A: Atomic, Molecular and Optical Physics*, **66**(6), 063414, 2002.

[Zwa64] R. Zwanzig. On the Identity of Three Generalized Master Equations. *Physica*, **30**(6), 1109 – 1123, 1964.

Appendix A

Boundary element method code for rf ion traps numerical modeling

The entire code was written in Mathematica 7, and it is intended to be run on any 64-bit OS which Mathematica supports. The code can be copied in a Mathematica notebook and be run as it is. The code has four main components: in the first two the user inputs the ion rf trap geometry and specifies the grid on which the dc potentials and rf electric field are to be calculated; the third part does the actual computations based on the boundary element method (BEM); and the last component computes the rf ion trap characteristics.

A.1 Trap geometry

The axes orientation is specified in Figure 5-13. The possible trap geometries are limited to traps with rectangular electrodes parallel to either x0y plane or y0z plane, and which possess reflection symmetries to x0z and y0z planes. As such the trap geometry needs to be specified only in the first octant of the axes system. The electrodes parallel to y0z plane are specified in ez table, and the electrodes parallel to x0y are specified in ex table. The position of the electrode is determined by specifying two of its opposite corners coordinates, i.e. $\{\{x_1, x_2\}, \{y_1, y_2\}, \{z_1, z_2\}, \text{axis } \#, V + \text{electrode name}\}$, where axis # represents the number of the axis which the electrode is perpendicular

to. Vrf electrode is a mandatory entry. None of the ez and ex tables can be empty; in case that all the electrodes are parallel only to one of the planes, one very small and far away electrode can be introduced in the empty table. All the electrodes are tesselated with squares, which side sizes (in millimeters) are specified by *segmentsize*; the *segmentsize* must be chosen such that is a common divisor of all the electrodes. *memorysize* specifies the maximum dimension ($memorysize \times memorysize$) the matrices entering the programm can have. The *memorysize* as the name suggests is related to the available ram memory, and the code execution speed gets faster as *memorysize* is increased. For example for 8 GB a suitable value for *memorysize* is 4500, while for 48 GB it is 7500.

```
(*specifies the trap electrodes coordinates*)
$HistoryLength = 0
ClearAll[ez, ex, d, pardir, electrodename, voltagename, segments, segmentsz,
segmentsx, Vgnd, Vmid, Vend, Vrf, Vquad, segmentsize, memorysize]
ez = {{{0, 0.32}, {0, 3.68}, {0, 0}, 3, Vgnd},
{{0.32, 1.04}, {0, 3.64}, {0, 0}, 3, Vrf},
{{1.04, 5.04}, {0, 0.52}, {0, 0}, 3, Vmid},
{{1.04, 5.04}, {0.52, 2.04}, {0, 0}, 3, Vquad},
{{1.04, 5.04}, {2.04, 3.56}, {0, 0}, 3, Vend},
{{1.04, 5.04}, {3.56, 3.64}, {0, 0}, 3, Vrf}};
ex = {{{20, 20}, {20, 20.04}, {20, 20.04}, 1, Vgnd}};
segmentsize = 0.04/3;
memorysize = 4500;

(*creates the directories*)
pardir = SetDirectory[NotebookDirectory[]]
CreateDirectory["Positions"]
CreateDirectory["Segments"]
CreateDirectory["TransferMatrix"]
```

```
CreateDirectory["Results"]
voltagename = Map[ToString, Union[ez[[All, 5]], ex[[All, 5]]]]
electrodename = StringDrop[voltagename, 1]
CreateDirectory["Charges"]
SetDirectory["Charges"]
For[i = 1, i ≤ Length[electrodename], CreateDirectory[electrodename[[i]]]; i++]
SetDirectory[pardir]
CreateDirectory["Potentials"]
SetDirectory["Potentials"]
CreateDirectory["Positions"]
For[i = 1, i ≤ Length[electrodename], CreateDirectory[electrodename[[i]]]; i++]
SetDirectory[pardir <> "\Segments"]
DumpSave["voltagename.mx", voltagename];
DumpSave["electrodename.mx", electrodename];
ClearAll[electrodename, voltagename, pardir]

(*divides the electrodes*)
d = segmentsize;
segmentsz = {}
For[j = 1, j<=Length[ez], j++,
f = Which[ez[[j, 4]] == 1,
Table[{ez[[j, 1, 1]], ez[[j, 2, 1]] + d * (n - 0.5) * Sign[ez[[j, 2, 2]] - ez[[j, 2, 1]]]],
ez[[j, 3, 1]] + d * (m - 0.5) * Sign[ez[[j, 3, 2]] - ez[[j, 3, 1]]], ez[[j, 5]]},
{n, Round[Abs[ez[[j,2,2]]-ez[[j,2,1]]]/d]},
{m, Round[Abs[ez[[j,3,2]]-ez[[j,3,1]]]/d]}],
ez[[j, 4]] == 2,
Table[{ez[[j, 1, 1]] + d * (n - 0.5) * Sign[ez[[j, 1, 2]] - ez[[j, 1, 1]]]],
ez[[j, 2, 1]], ez[[j, 3, 1]] + d * (m - 0.5) * Sign[ez[[j, 3, 2]] - ez[[j, 3, 1]]]],
ez[[j, 5]]}, {n, Round[Abs[ez[[j,1,2]]-ez[[j,1,1]]]/d]},
{m, Round[Abs[ez[[j,3,2]]-ez[[j,3,1]]]/d]}], ez[[j, 4]] == 3,
```

```
Table[{ez[[j, 1, 1]] + d * (n - 0.5) * Sign[ez[[j, 1, 2]] - ez[[j, 1, 1]]],
ez[[j, 2, 1]] + d * (m - 0.5) * Sign[ez[[j, 2, 2]] - ez[[j, 2, 1]]], ez[[j, 3, 1]],
ez[[j, 5]]}, {n, Round[(Abs[ez[[j, 1, 2]] - ez[[j, 1, 1]]])/d]},
{m, Round[(Abs[ez[[j, 2, 2]] - ez[[j, 2, 1]]])/d]}];
segmentsz = Join[segmentsz, Flatten[f, 1]]; ClearAll[f]; ClearSystemCache[]; ];
Dimensions[segmentsz]
DumpSave["segmentsz.mx", segmentsz];
ClearAll[segmentsz]
ClearSystemCache[]
segmentsx = {}
For[j = 1, j<=Length[ex], j++,
f = Which[ex[[j, 4]] == 1,
Table[{ex[[j, 1, 1]], ex[[j, 2, 1]] + d * (n - 0.5) * Sign[ex[[j, 2, 2]] - ex[[j, 2, 1]]],
ex[[j, 3, 1]] + d * (m - 0.5) * Sign[ex[[j, 3, 2]] - ex[[j, 3, 1]]], ex[[j, 5]]},
{n, Round[(Abs[ex[[j, 2, 2]] - ex[[j, 2, 1]]])/d]},
{m, Round[(Abs[ex[[j, 3, 2]] - ex[[j, 3, 1]]])/d]},
ex[[j, 4]] == 2,
Table[{ex[[j, 1, 1]] + d * (n - 0.5) * Sign[ex[[j, 1, 2]] - ex[[j, 1, 1]]],
ex[[j, 2, 1]], ex[[j, 3, 1]] + d * (m - 0.5) * Sign[ex[[j, 3, 2]] - ex[[j, 3, 1]]],
ex[[j, 5]]}, {n, Round[(Abs[ex[[j, 1, 2]] - ex[[j, 1, 1]]])/d]},
{m, Round[(Abs[ex[[j, 3, 2]] - ex[[j, 3, 1]]])/d]}, ex[[j, 4]] == 3,
Table[{ex[[j, 1, 1]] + d * (n - 0.5) * Sign[ex[[j, 1, 2]] - ex[[j, 1, 1]]],
ex[[j, 2, 1]] + d * (m - 0.5) * Sign[ex[[j, 2, 2]] - ex[[j, 2, 1]]], ex[[j, 3, 1]],
ex[[j, 5]]}, {n, Round[(Abs[ex[[j, 1, 2]] - ex[[j, 1, 1]]])/d]},
{m, Round[(Abs[ex[[j, 2, 2]] - ex[[j, 2, 1]]])/d]}];
segmentsx = Join[segmentsx, Flatten[f, 1]]; ClearAll[f]; ClearSystemCache[]; ];
Dimensions[segmentsx]
DumpSave["segmentsx.mx", segmentsx];
DumpSave["segmentsize.mx", segmentsize];
DumpSave["memorysize.mx", memorysize];
```

```
ClearAll[segmentsx, segmentsize, d, memorysize, ex, ey]
ClearSystemCache[]
```

A.2 Dc potentials and rf electric field grid

The grid is specified (in millimeters) in the M table:
$M = \text{Table}\left[\{i, j, k\}, \{i, x_1, x_2, \text{x\_step}\}, \{j, y_1, y_2, \text{y\_step}\}, \{k, z_1, z_2, \text{z\_step}\}\right]$.
None of the grid points can be in the same planes containing the trap electrodes. For example if all the electrodes are perpendicular to z axis and located at z=0 (in x0y plane) there cannot be grid points with the z coordinate equal to zero.

```
(*Specifies the grid on which the dc potentials and the rf
electric field are computed*)
Needs["UtilitiesCleanSlate"]
CleanSlate["Global"]
$HistoryLength = 0
ClearSystemCache[]
SetDirectory[NotebookDirectory[] <> "\\Segments"]
Get["memorysize.mx"];
SetDirectory[NotebookDirectory[] <> "\\Potentials\\Positions"];
M = Table[{i, j, k}, {i, 0, 0.714, 0.017}, {j, 0, 3.604, 0.068},
{k, 0.001, 1.361, 0.034}];
M = Flatten[M, 2];
Dimensions[M]
DumpSave["M.mx", M];
For[i = 1, i<=Quotient[Length[M], memorysize] + 1, i++,
nl = (i - 1) * memorysize + 1; nh = Min[memorysize * i, Length[M]];
px = M[[nl;;nh, 1]];
py = M[[nl;;nh, 2]];
pz = M[[nl;;nh, 3]];
DumpSave["px" <> ToString[i] <> ".mx", px];
DumpSave["py" <> ToString[i] <> ".mx", py];
DumpSave["pz" <> ToString[i] <> ".mx", pz];
];
ClearAll[M, nl, px, py, pz, memorysize]
ClearSystemCache[]
```

A.3 BEM

This part of the program is entirely automated and requires no user input (except for starting it). Also this is the most time consuming part of the code; as an example on a 8 GB machine, for about 80000 electrode segments and about 80000 grid points it takes around 8 hours to run. The last segment of the code *Potentials* can be run independently from the rest of the code (by commenting out the rest of the code). This is useful if the initial chosen grid did not capture the entire pseudopotential.

```
ClearAll[timestart, timeend];
timestart = AbsoluteTime[];


(*SegmentsSmall  -  computes the distances between all possible pairs of segments *)
Print[SegmentsSmall]

Needs["UtilitiesCleanSlate"]
CleanSlate["Global", Verbose->False]
$HistoryLength = 0
SetDirectory[NotebookDirectory[] <> "\\Segments"];
Get["segmentsz.mx"];
Get["memorysize.mx"];
x = segmentsz[[All, 1;;3]];
ClearAll[segmentsz]
ClearSystemCache[]
Needs["UtilitiesCleanSlate"]
CleanSlate["Global", Verbose->False]
f = Compile[{{x, _Real, 2}},
Module[{s}, s = x; Do[nl = (i - 1) * memorysize + 1; nh = Min[memorysize * i, Length[s]];
Do[ml = (j - 1) * memorysize + 1; mh = Min[memorysize * j, Length[s]];
Dmx = Outer[Plus, s[[nl;;nh, 1]], -s[[ml;;mh, 1]]];
DumpSave["Dm" <> ToString[i] <> x <> ToString[j] <> ".mx", Dmx];
ClearSystemCache[]; ClearAll[Dmx, Dpx, Dmy, Dpy, Dz];
Needs["UtilitiesCleanSlate"]; CleanSlate["Global", Verbose->False];
Dpx = Outer[Plus, s[[nl;;nh, 1]], s[[ml;;mh, 1]]];
DumpSave["Dp" <> ToString[i] <> x <> ToString[j] <> ".mx", Dpx];
ClearSystemCache[]; ClearAll[Dmx, Dpx, Dmy, Dpy, Dz];
```

```
Needs["Utilities`CleanSlate`"]; CleanSlate["Global`", Verbose->False];
Dmy = Outer[Plus, s[[nl;;nh, 2]], -s[[ml;;mh, 2]]];
DumpSave["Dm" <> ToString[i] <> y <> ToString[j] <> ".mx", Dmy];
ClearSystemCache[]; ClearAll[Dmx, Dpx, Dmy, Dpy, Dz];
Needs["Utilities`CleanSlate`"]; CleanSlate["Global`", Verbose->False];
Dpy = Outer[Plus, s[[nl;;nh, 2]], s[[ml;;mh, 2]]];
DumpSave["Dp" <> ToString[i] <> y <> ToString[j] <> ".mx", Dpy];
ClearSystemCache[]; ClearAll[Dmx, Dpx, Dmy, Dpy, Dz];
Needs["Utilities`CleanSlate`"]; CleanSlate["Global`", Verbose->False];
Dz = Outer[Plus, s[[nl;;nh, 3]], -s[[ml;;mh, 3]]];
DumpSave[D <> ToString[i] <> z <> ToString[j] <> ".mx", Dz];
ClearSystemCache[]; ClearAll[Dmx, Dpx, Dmy, Dpy, Dz, ml, mh];
Needs["Utilities`CleanSlate`"]; CleanSlate["Global`", Verbose->False],
{j, i, Quotient[Length[s], memorysize] + 1}];
ClearSystemCache[]; ClearAll[nl, nh]; Needs["Utilities`CleanSlate`"];
CleanSlate["Global`", Verbose->False],
{i, 1, Quotient[Length[s], memorysize] + 1}]; ]];
f[x]
Get["segmentsx.mx"];
y = segmentsx[[All, 1;;3]];
ClearAll[segmentsx]
ClearSystemCache[]
Needs["Utilities`CleanSlate`"]
CleanSlate["Global`", Verbose->False]
g = Compile[{{x, _Real, 2}, {y, _Real, 2}},
Module[{s, p}, s = x; p = y; Do[nl = (i - 1) * memorysize + 1;
nh = Min[memorysize * i, Length[s]];
Do[ml = (j - Quotient[Length[s], memorysize] - 2) * memorysize + 1;
mh = Min[memorysize * (j - Quotient[Length[s], memorysize] - 1), Length[p]];
Dmx = Outer[Plus, s[[nl;;nh, 1]], -p[[ml;;mh, 1]]];
DumpSave["Dm" <> ToString[i] <> x <> ToString[j] <> ".mx", Dmx];
ClearSystemCache[]; ClearAll[Dmx, Dpx, Dmy, Dpy, Dz];
Needs["Utilities`CleanSlate`"]; CleanSlate["Global`", Verbose->False];
Dpx = Outer[Plus, s[[nl;;nh, 1]], p[[ml;;mh, 1]]];
DumpSave["Dp" <> ToString[i] <> x <> ToString[j] <> ".mx", Dpx];
ClearSystemCache[]; ClearAll[Dmx, Dpx, Dmy, Dpy, Dz];
Needs["Utilities`CleanSlate`"]; CleanSlate["Global`", Verbose->False];
Dmy = Outer[Plus, s[[nl;;nh, 2]], -p[[ml;;mh, 2]]];
```

```
DumpSave["Dm" <> ToString[i] <> y <> ToString[j] <> ".mx", Dmy];
ClearSystemCache[]; ClearAll[Dmx, Dpx, Dmy, Dpy, Dz];
Needs["Utilities`CleanSlate`"]; CleanSlate["Global`", Verbose->False];
Dpy = Outer[Plus, s[[nl;;nh, 2]], p[[ml;;mh, 2]]];
DumpSave["Dp" <> ToString[i] <> y <> ToString[j] <> ".mx", Dpy];
ClearSystemCache[]; ClearAll[Dmx, Dpx, Dmy, Dpy, Dz];
Needs["Utilities`CleanSlate`"]; CleanSlate["Global`", Verbose->False];
Dz = Outer[Plus, s[[nl;;nh, 3]], -p[[ml;;mh, 3]]];
DumpSave[D <> ToString[i] <> z <> ToString[j] <> ".mx", Dz];
ClearSystemCache[]; ClearAll[Dmx, Dpx, Dmy, Dpy, Dz, ml, mh];
Needs["Utilities`CleanSlate`"]; CleanSlate["Global`", Verbose->False],
{j, Quotient[Length[s], memorysize] + 2,
Quotient[Length[s], memorysize] + Quotient[Length[p], memorysize] + 2}];
ClearSystemCache[]; ClearAll[nl, nh]; Needs["Utilities`CleanSlate`"];
CleanSlate["Global`", Verbose->False],
{i, 1, Quotient[Length[s], memorysize] + 1}]; ]];
g[x, y]
Needs["Utilities`CleanSlate`"]
CleanSlate["Global`", Verbose->False]
h = Compile[{{y, _Real, 2}},
Module[{p}, p = y; Do[nl = (i - Quotient[Length[x], memorysize] - 2) * memorysize + 1;
nh = Min[memorysize * (i - Quotient[Length[x], memorysize] - 1), Length[p]];
Do[ml = (j - Quotient[Length[x], memorysize] - 2) * memorysize + 1;
mh = Min[memorysize * (j - Quotient[Length[x], memorysize] - 1), Length[p]];
Dmx = Outer[Plus, p[[nl;;nh, 1]], -p[[ml;;mh, 1]]];
DumpSave["Dm" <> ToString[i] <> x <> ToString[j] <> ".mx", Dmx];
ClearSystemCache[]; ClearAll[Dmx, Dpx, Dmy, Dpy, Dz];
Needs["Utilities`CleanSlate`"]; CleanSlate["Global`", Verbose->False];
Dpx = Outer[Plus, p[[nl;;nh, 1]], p[[ml;;mh, 1]]];
DumpSave["Dp" <> ToString[i] <> x <> ToString[j] <> ".mx", Dpx];
ClearSystemCache[]; ClearAll[Dmx, Dpx, Dmy, Dpy, Dz];
Needs["Utilities`CleanSlate`"]; CleanSlate["Global`", Verbose->False];
Dmy = Outer[Plus, p[[nl;;nh, 2]], -p[[ml;;mh, 2]]];
DumpSave["Dm" <> ToString[i] <> y <> ToString[j] <> ".mx", Dmy];
ClearSystemCache[]; ClearAll[Dmx, Dpx, Dmy, Dpy, Dz];
Needs["Utilities`CleanSlate`"]; CleanSlate["Global`", Verbose->False];
Dpy = Outer[Plus, p[[nl;;nh, 2]], p[[ml;;mh, 2]]];
DumpSave["Dp" <> ToString[i] <> y <> ToString[j] <> ".mx", Dpy];
```

```
ClearSystemCache[]; ClearAll[Dmx, Dpx, Dmy, Dpy, Dz];
Needs["Utilities`CleanSlate`"]; CleanSlate["Global`", Verbose->False];
Dz = Outer[Plus, p[[nl;;nh, 3]], -p[[ml;;mh, 3]]];
DumpSave[D <> ToString[i] <> z <> ToString[j] <> ".mx", Dz];
ClearSystemCache[]; ClearAll[Dmx, Dpx, Dmy, Dpy, Dz, ml, mh];
Needs["Utilities`CleanSlate`"]; CleanSlate["Global`", Verbose->False],
{j, i, Quotient[Length[x], memorysize] + Quotient[Length[p], memorysize] + 2}];
ClearSystemCache[]; ClearAll[nl, nh]; Needs["Utilities`CleanSlate`"];
CleanSlate["Global`", Verbose->False],
{i, Quotient[Length[x], memorysize] + 2,
Quotient[Length[x], memorysize] + Quotient[Length[p], memorysize] + 2}]; ]];
h[y]
ClearAll[x, y, Dmx, Dpx, Dmy, Dpy, Dz, ml, mh, nl, nh, segmentsz, segmentsx, f, g, h]
Needs["Utilities`CleanSlate`"]
CleanSlate["Global`", Verbose->False]
ClearSystemCache[]


(*Charges&Positions  -  sets one electrode at 1 V with the others at 0 V*)
Print[Charges&Positions]

Needs["Utilities`CleanSlate`"]
CleanSlate["Global`", Verbose->False]
$HistoryLength = 0
SetDirectory[NotebookDirectory[] <> "\\Segments"];
ClearAll[voltagename, electrodename, x, y];
Get["voltagename.mx"];
Get["electrodename.mx"];
For[i = 1, i<=Length[voltagename],
For[j = 1, j<=Length[voltagename],
ToExpression[voltagename[[j]] <> "=" <> ToString[If[i == j, 1, 0]]];
j++];
Get["segmentsz.mx"];
ToExpression[x <> electrodename[[i]] <> "=" <> ToString[segmentsz]];
ClearAll[segmentsz];
For[k = 1, k<=Length[voltagename],
ToExpression["ClearAll[" <> voltagename[[k]] <> "]"];
k++];
```

```
i++];
Get["segmentsz.mx"];
Get["memorysize.mx"];
x = segmentsz;
ClearAll[segmentsz]
ClearSystemCache[]
Needs["Utilities`CleanSlate`"]
CleanSlate["Global`", Verbose->False]
Do[nl = (i - 1) * memorysize + 1; nh = Min[memorysize * i, Length[x]];
SetDirectory[NotebookDirectory[] <> "\\Positions"];
Rx = x[[nl;;nh, 1]];
DumpSave["Rx" <> ToString[i] <> ".mx", Rx];
Ry = x[[nl;;nh, 2]];
DumpSave["Ry" <> ToString[i] <> ".mx", Ry];
Rz = x[[nl;;nh, 3]];
DumpSave["Rz" <> ToString[i] <> ".mx", Rz];
For[k = 1, k<=Length[electrodename],
SetDirectory[NotebookDirectory[] <> "\\Charges\\" <> electrodename[[k]]];
ToExpression[electrodename[[k]] <> "=" <> x <> electrodename[[k]] <>
"[[nl;;nh,4]]"];
DumpSave[electrodename[[k]] <> ToString[i] <> ".mx", Evaluate[electrodename[[k]]]];
k++];
ClearSystemCache[]; ClearAll[nl, nh, Rx, Ry, Rz];
For[k = 1, k<=Length[electrodename],
ToExpression["ClearAll[" <> electrodename[[k]] <> "]"];
k++];
Needs["Utilities`CleanSlate`"]; CleanSlate["Global`", Verbose->False],
{i, 1, Quotient[Length[x], memorysize] + 1}];
For[k = 1, k<=Length[electrodename],
ToExpression["ClearAll[" <> x <> electrodename[[k]] <> "]"];
k++];
ClearSystemCache[]
Needs["Utilities`CleanSlate`"]
CleanSlate["Global`", Verbose->False]
SetDirectory[NotebookDirectory[] <> "\\Segments"]
For[i = 1, i<=Length[voltagename],
For[j = 1, j<=Length[voltagename],
ToExpression[voltagename[[j]] <> "=" <> ToString[If[i == j, 1, 0]]];
```

```
j++];
Get["segmentsx.mx"];
ToExpression[y <> electrodename[[i]] <> "=" <> ToString[segmentsx]];
ClearAll[segmentsx];
For[k = 1, k<=Length[voltagename],
ToExpression["ClearAll[" <> voltagename[[k]] <> "]"];
k++];
i++];
Get["segmentsx.mx"];
y = segmentsx;
ClearAll[segmentsx]
ClearSystemCache[]
Needs["Utilities`CleanSlate`"]
CleanSlate["Global`", Verbose->False]
Do[nl = (i - Quotient[Length[x], memorysize] - 2) * memorysize + 1;
nh = Min[memorysize * (i - Quotient[Length[x], memorysize] - 1), Length[y]];
SetDirectory[NotebookDirectory[] <> "\\Positions"];
Rx = y[[nl;;nh, 1]];
DumpSave["Rx" <> ToString[i] <> ".mx", Rx];
Ry = y[[nl;;nh, 2]];
DumpSave["Ry" <> ToString[i] <> ".mx", Ry];
Rz = y[[nl;;nh, 3]];
DumpSave["Rz" <> ToString[i] <> ".mx", Rz];
For[k = 1, k<=Length[electrodename],
SetDirectory[NotebookDirectory[] <> "\\Charges\\" <> electrodename[[k]]];
ToExpression[electrodename[[k]] <> "=" <> y <> electrodename[[k]] <>
"[[nl;;nh,4]]"];
DumpSave[electrodename[[k]] <> ToString[i] <> ".mx", Evaluate[electrodename[[k]]]];
k++];
ClearSystemCache[]; ClearAll[nl, nh, Rx, Ry, Rz];
For[k = 1, k<=Length[electrodename],
ToExpression["ClearAll[" <> electrodename[[k]] <> "]"];
k++];
Needs["Utilities`CleanSlate`"]; CleanSlate["Global`", Verbose->False],
{i, Quotient[Length[x], memorysize] + 2,
Quotient[Length[x], memorysize] + Quotient[Length[y], memorysize] + 2}];
For[k = 1, k<=Length[electrodename],
ToExpression["ClearAll[" <> y <> electrodename[[k]] <> "]"];
```

k++];

ClearSystemCache[];

ClearAll[i, j, k, nl, nh, x, y, electrodename, voltagename, Rx, Ry, Rz];

Needs["Utilities`CleanSlate`"]; CleanSlate["Global", Verbose->False];

(*TransferMatrix − computes $\int \frac{1}{r} da$ between all possible pairs of segments,
i.e. the potential produced by the the total charge of one segment at the
location of another/same segment; used colocation method*)

Print[TransferMatrix]

Needs["Utilities`CleanSlate`"]

CleanSlate["Global"]

$HistoryLength = 0

ClearSystemCache[]

ClearAll[int, a, b, c, segments, seg, x, z, lz, lx, TM, A, d]

SetDirectory[NotebookDirectory[] <> "\\Segments"];

Get["memorysize.mx"];

Get["segmentsize.mx"];

int = Compile[{{a, _Real, 2}, {b, _Real, 2}, {c, _Real, 2}},

$-c$

ArcTan[

$(c(-(\text{segmentsize}/2 + a)(-\text{segmentsize}/2 + b)$

$\sqrt{(-\text{segmentsize}/2 + a)^2 + (-\text{segmentsize}/2 + b)^2 + c^2}+$

$(-\text{segmentsize}/2 + a)(-\text{segmentsize}/2 + b)$

$\sqrt{(\text{segmentsize}/2 + a)^2 + (-\text{segmentsize}/2 + b)^2 + c^2}\Big)\Big)\Big/$

$\big((-\text{segmentsize}/2 + a)(\text{segmentsize}/2 + a)(-\text{segmentsize}/2 + b)^2+$

$c^2\sqrt{(-\text{segmentsize}/2 + a)^2 + (-\text{segmentsize}/2 + b)^2 + c^2}$

$\sqrt{(\text{segmentsize}/2 + a)^2 + (-\text{segmentsize}/2 + b)^2 + c^2}\Big)\Big] +$

c

ArcTan[

$(c(-(\text{segmentsize}/2 + a)(\text{segmentsize}/2 + b)$

$\sqrt{(-\text{segmentsize}/2 + a)^2 + (\text{segmentsize}/2 + b)^2 + c^2}+$

$(-\text{segmentsize}/2 + a)(\text{segmentsize}/2 + b)$

$\sqrt{(\text{segmentsize}/2 + a)^2 + (\text{segmentsize}/2 + b)^2 + c^2}\Big)\Big)\Big/$

$\big((-\text{segmentsize}/2 + a)(\text{segmentsize}/2 + a)(\text{segmentsize}/2 + b)^2+$

$c^2\sqrt{(-\text{segmentsize}/2 + a)^2 + (\text{segmentsize}/2 + b)^2 + c^2}$

$\sqrt{(\text{segmentsize}/2 + a)^2 + (\text{segmentsize}/2 + b)^2 + c^2}\Big)\Big] +$

$$(-\text{segmentsize}/2 + b)$$
$$\text{Log}\left[\frac{-\text{segmentsize}/2+a+\sqrt{(-\text{segmentsize}/2+a)^2+(-\text{segmentsize}/2+b)^2+c^2}}{\text{segmentsize}/2+a+\sqrt{(\text{segmentsize}/2+a)^2+(-\text{segmentsize}/2+b)^2+c^2}}\right] +$$
$$(-\text{segmentsize}/2 + a)$$
$$\text{Log}\left[\frac{-\text{segmentsize}/2+b+\sqrt{(-\text{segmentsize}/2+a)^2+(-\text{segmentsize}/2+b)^2+c^2}}{\text{segmentsize}/2+b+\sqrt{(-\text{segmentsize}/2+a)^2+(\text{segmentsize}/2+b)^2+c^2}}\right] +$$
$$(\text{segmentsize}/2 + b)$$
$$\text{Log}\left[\frac{\text{segmentsize}/2+a+\sqrt{(\text{segmentsize}/2+a)^2+(\text{segmentsize}/2+b)^2+c^2}}{-\text{segmentsize}/2+a+\sqrt{(-\text{segmentsize}/2+a)^2+(\text{segmentsize}/2+b)^2+c^2}}\right] +$$
$$(\text{segmentsize}/2 + a)$$
$$\text{Log}\left[\frac{\text{segmentsize}/2+b+\sqrt{(\text{segmentsize}/2+a)^2+(\text{segmentsize}/2+b)^2+c^2}}{-\text{segmentsize}/2+b+\sqrt{(\text{segmentsize}/2+a)^2+(-\text{segmentsize}/2+b)^2+c^2}}\right]];$$

SetDirectory[NotebookDirectory[] <> "\\Segments"]

Get["segmentsz.mx"];

lz = Quotient[Length[segmentsz], memorysize] + 1;

ClearAll[segmentsz]

ClearSystemCache[]

Get["segmentsx.mx"];

lx = Quotient[Length[segmentsx], memorysize] + 1;

ClearAll[segmentsz]

ClearSystemCache[]

TM = Compile[{{z, _Integer}, {x, _Integer}, {w, _Real, 2}}, Module[{s, p}, $s = z; p = x$;

Dmx = Dpx = Dmy = Dpy = Dz = w;

Do[

Do[

SetDirectory[NotebookDirectory[] <> "\\Segments"];

Get["Dm" <> ToString[i] <> x <> ToString[j] <> ".mx"];

Get["Dp" <> ToString[i] <> x <> ToString[j] <> ".mx"];

Get["Dm" <> ToString[i] <> y <> ToString[j] <> ".mx"];

Get["Dp" <> ToString[i] <> y <> ToString[j] <> ".mx"];

Get[D <> ToString[i] <> z <> ToString[j] <> ".mx"];

Print["first_" <> ToString[i] <> "_" <> ToString[j]];

SetDirectory[NotebookDirectory[] <> "\\TransferMatrix"];

A = int[Dmx, Dmy, Dz] + int[Dmx, Dpy, Dz] + int[Dpx, Dpy, Dz]+

int[Dpx, Dmy, Dz];

DumpSave[A <> ToString[i] <> "_" <> ToString[j] <> ".mx", A];

ClearAll[A, Dmx, Dpx, Dmy, Dpy, Dz]; ClearSystemCache[];

Needs["Utilities`CleanSlate`"]; CleanSlate["Global`", Verbose → False],

{j, i, s}],

{i, 1, s}];

Needs["Utilities`CleanSlate`"]; CleanSlate["Global`", Verbose → False];

Do[

```
Do[
SetDirectory[NotebookDirectory[] <> "\\Segments"];
Get["Dm" <> ToString[j] <> x <> ToString[i] <> ".mx"];
Get["Dp" <> ToString[j] <> x <> ToString[i] <> ".mx"];
Get["Dm" <> ToString[j] <> y <> ToString[i] <> ".mx"];
Get["Dp" <> ToString[j] <> y <> ToString[i] <> ".mx"];
Get[D <> ToString[j] <> z <> ToString[i] <> ".mx"];
Dmx = Transpose[Dmx];
Dpx = Transpose[Dpx];
Dmy = Transpose[Dmy];
Dpy = Transpose[Dpy];
Dz = Transpose[Dz];
Print["second_" <> ToString[i] <> "_" <> ToString[j]];
SetDirectory[NotebookDirectory[] <> "\\TransferMatrix"];
A = int[Dmx, Dmy, Dz] + int[Dmx, Dpy, Dz] + int[Dpx, Dpy, Dz]+
int[Dpx, Dmy, Dz];
DumpSave[A <> ToString[i] <> "_" <> ToString[j] <> ".mx", A];
ClearAll[A, Dmx, Dpx, Dmy, Dpy, Dz]; ClearSystemCache[];
Needs["Utilities`CleanSlate`"]; CleanSlate["Global`", Verbose → False],
{j, 1, s}],
{i, s + 1, s + p}];
Needs["Utilities`CleanSlate`"]; CleanSlate["Global`", Verbose → False];
Do[
Do[
SetDirectory[NotebookDirectory[] <> "\\Segments"];
Get["Dm" <> ToString[i] <> x <> ToString[j] <> ".mx"];
Get["Dp" <> ToString[i] <> x <> ToString[j] <> ".mx"];
Get["Dm" <> ToString[i] <> y <> ToString[j] <> ".mx"];
Get["Dp" <> ToString[i] <> y <> ToString[j] <> ".mx"];
Get[D <> ToString[i] <> z <> ToString[j] <> ".mx"];
Print["third_" <> ToString[i] <> "_" <> ToString[j]];
SetDirectory[NotebookDirectory[] <> "\\TransferMatrix"];
A = int[Dz, Dmy, Dmx] + int[Dz, Dpy, Dmx] + int[Dz, Dpy, Dpx]+
int[Dz, Dmy, Dpx];
DumpSave[A <> ToString[i] <> "_" <> ToString[j] <> ".mx", A];
ClearAll[A, Dmx, Dpx, Dmy, Dpy, Dz]; ClearSystemCache[];
Needs["Utilities`CleanSlate`"]; CleanSlate["Global`", Verbose → False],
{j, s + 1, s + p}],
```

```
{i, 1, s}];
Needs["Utilities`CleanSlate`"]; CleanSlate["Global`", Verbose → False];
Do[
Do[
SetDirectory[NotebookDirectory[] <> "\\Segments"];
Get["Dm" <> ToString[i] <> x <> ToString[j] <> ".mx"];
Get["Dp" <> ToString[i] <> x <> ToString[j] <> ".mx"];
Get["Dm" <> ToString[i] <> y <> ToString[j] <> ".mx"];
Get["Dp" <> ToString[i] <> y <> ToString[j] <> ".mx"];
Get[D <> ToString[i] <> z <> ToString[j] <> ".mx"];
Print["fourth_" <> ToString[i] <> "_" <> ToString[j]];
SetDirectory[NotebookDirectory[] <> "\\TransferMatrix"];
A = int[Dz, Dmy, Dmx] + int[Dz, Dpy, Dmx] + int[Dz, Dpy, Dpx]+
int[Dz, Dmy, Dpx];
DumpSave[A <> ToString[i] <> "_" <> ToString[j] <> ".mx", A];
ClearAll[A, Dmx, Dpx, Dmy, Dpy, Dz]; ClearSystemCache[];
Needs["Utilities`CleanSlate`"]; CleanSlate["Global`", Verbose → False],
{j, i, s + p}],
{i, s + 1, s + p}];
Needs["Utilities`CleanSlate`"]; CleanSlate["Global`", Verbose → False];
];
];
TimeUsed[]
TM[lz, lx, ConstantArray[0, {2, 2}]]; //AbsoluteTiming
TimeUsed[]
ClearSystemCache[]
ClearAll[int, a, b, c, segments, seg, x, z, lz, lx, TM, A]
Needs["Utilities`CleanSlate`"]
CleanSlate["Global`"]


(*LDU decomposition  −  prepares the transfer matrix for inversion by doing
first a LDU block decomposition*)
Print[LDUdecomposition]

ClearAll[A, lz, lx, x, y, z, w, i, j, k, a, b, c, d, s, p, LDU, tran, prod, fun]
Needs["Utilities`CleanSlate`"]
CleanSlate["Global`"]
```

```
$HistoryLength = 0
ClearSystemCache[]
SetDirectory[NotebookDirectory[] <> "\\Segments"];
Get["memorysize.mx"];
Get["segmentsize.mx"];
Get["segmentsz.mx"];
lz = Quotient[Length[segmentsz], memorysize] + 1;
ClearAll[segmentsz]
ClearSystemCache[]
Get["segmentsx.mx"];
lx = Quotient[Length[segmentsx], memorysize] + 1;
ClearAll[segmentsz]
ClearSystemCache[]
tran = Compile[{{x, _Real, 2}}, Transpose[x]];
Do[
Do[
SetDirectory[NotebookDirectory[] <> "\\TransferMatrix"];
Get[A <> ToString[j] <> "_" <> ToString[i] <> ".mx"];
A = tran[A];
DumpSave[A <> ToString[i] <> "_" <> ToString[j] <> ".mx", A];
ClearAll[A]; ClearSystemCache[];
Needs["Utilities`CleanSlate`"]; CleanSlate["Global", Verbose → False],
{j, 1, i - 1}],
{i, 2, lz}];
Do[
Do[
SetDirectory[NotebookDirectory[] <> "\\TransferMatrix"];
Get[A <> ToString[j] <> "_" <> ToString[i] <> ".mx"];
A = tran[A];
DumpSave[A <> ToString[i] <> "_" <> ToString[j] <> ".mx", A];
ClearAll[A]; ClearSystemCache[];
Needs["Utilities`CleanSlate`"]; CleanSlate["Global", Verbose → False],
{j, lz + 1, i - 1}],
{i, lz + 2, lz + lx}];
Needs["Utilities`CleanSlate`"]
CleanSlate["Global"]
prod = Compile[{{b, _Real, 2}, {c, _Real, 2}}, b.c];
fun = Compile[{{a, _Real, 2}, {b, _Real, 2}, {c, _Real, 2}}, a - b.c];
```

```
LDU = Compile[{{z, _Integer}, {x, _Integer}, {w, _Real, 2}},
Module[{s, p}, s = z; p = x;
A = d = b = c = w;
Do[
SetDirectory[NotebookDirectory[] <> "\\TransferMatrix"];
Get[A <> ToString[k] <> "_" <> ToString[k] <> ".mx"];
A = d = Inverse[A];
DumpSave[A <> ToString[k] <> "_" <> ToString[k] <> ".mx", A];
ClearAll[A]; ClearSystemCache[];
Needs["Utilities`CleanSlate`"];
CleanSlate["Global`", Verbose → False];
Do[
Get[A <> ToString[i] <> "_" <> ToString[k] <> ".mx"];
A = prod[A, d];
DumpSave[A <> ToString[i] <> "_" <> ToString[k] <> ".mx", A];
ClearAll[A]; ClearSystemCache[];
Needs["Utilities`CleanSlate`"];
CleanSlate["Global`", Verbose → False],
{i, k + 1, s + p}];
Do[
Get[A <> ToString[i] <> "_" <> ToString[k] <> ".mx"];
b = A;
Do[
Get[A <> ToString[k] <> "_" <> ToString[j] <> ".mx"];
c = A;
Get[A <> ToString[i] <> "_" <> ToString[j] <> ".mx"];
A = fun[A, b, c];
DumpSave[A <> ToString[i] <> "_" <> ToString[j] <> ".mx", A];
ClearAll[A, c]; ClearSystemCache[];
Needs["Utilities`CleanSlate`"];
CleanSlate["Global`", Verbose → False],
{j, k + 1, s + p}];
ClearAll[A, b, c]; ClearSystemCache[];
Needs["Utilities`CleanSlate`"];
CleanSlate["Global`", Verbose → False],
{i, k + 1, s + p}];
Do[
Get[A <> ToString[k] <> "_" <> ToString[j] <> ".mx"];
```

```
A = prod[d, A];
DumpSave[A <> ToString[k] <> "_" <> ToString[j] <> ".mx", A];
ClearAll[A]; ClearSystemCache[];
Needs["Utilities`CleanSlate`"];
CleanSlate["Global`", Verbose → False],
{j, k + 1, s + p}];
ClearAll[A, d]; ClearSystemCache[];
Needs["Utilities`CleanSlate`"];
CleanSlate["Global`", Verbose → False],
{k, 1, s + p − 1}];
Get[A <> ToString[s + p] <> "_" <> ToString[s + p] <> ".mx"];
A = Inverse[A];
DumpSave[A <> ToString[s + p] <> "_" <> ToString[s + p] <> ".mx", A];
ClearAll[A]; ClearSystemCache[];
Needs["Utilities`CleanSlate`"];
CleanSlate["Global`", Verbose → False];];];
TimeUsed[]
LDU[lz, lx, ConstantArray[0, {2, 2}]]; //AbsoluteTiming
TimeUsed[]
ClearAll[A, lz, lx, x, y, z, w, i, j, k, a, b, c, d, s, p, LDU, tran, prod, fun]
ClearSystemCache[]
Needs["Utilities`CleanSlate`"]
CleanSlate["Global`"]


(*ChargesFinder  −  the transfer matrix gets inverted*)
Print[ChargesFinder]

Needs["Utilities`CleanSlate`"]
CleanSlate["Global`"]
$HistoryLength = 0
ClearSystemCache[]
ClearAll[voltagename, electrodename, lx, lz, prod, fun, k, q, i, A, a, b, c];
SetDirectory[NotebookDirectory[] <> "\\Segments"];
Get["memorysize.mx"];
Get["segmentsize.mx"];
Get["segmentsz.mx"];
lz = Quotient[Length[segmentsz], memorysize] + 1;
```

```
ClearAll[segmentsz]
ClearSystemCache[]
Get["segmentsx.mx"];
lx = Quotient[Length[segmentsx], memorysize] + 1;
ClearAll[segmentsz, a, b, c]
ClearSystemCache[];
prod = Compile[{{b, _Real, 2}, {c, _Real, 1}}, b.c];
fun = Compile[{{a, _Real, 1}, {b, _Real, 2}, {c, _Real, 1}}, a - b.c];
SetDirectory[NotebookDirectory[] <> "\\Segments"]
Get["voltagename.mx"];
Get["electrodename.mx"];
For[k = 1, k ≤ lz + lx - 1, k++,
For[q = 1, q<=Length[electrodename],
SetDirectory[NotebookDirectory[] <> "\\Charges\\" <> electrodename[[q]]];
Get[electrodename[[q]] <> ToString[k] <> ".mx"];
ToExpression[s <> electrodename[[q]] <> "=" <> electrodename[[q]]];
q++];
For[i = k + 1, i ≤ lz + lx, i++,
SetDirectory[NotebookDirectory[] <> "\\TransferMatrix"];
Get[A <> ToString[i] <> "_" <> ToString[k] <> ".mx"];
For[q = 1, q<=Length[electrodename],
SetDirectory[NotebookDirectory[] <> "\\Charges\\" <> electrodename[[q]]];
Get[electrodename[[q]] <> ToString[i] <> ".mx"];
ToExpression[electrodename[[q]] <> "=fun[" <> electrodename[[q]] <>
",A,s" <> electrodename[[q]] <> "]"];
DumpSave[electrodename[[q]] <> ToString[i] <> ".mx",
Evaluate[electrodename[[q]]]];
q++];
];
ClearAll[A];
For[q = 1, q<=Length[electrodename],
ToExpression["ClearAll[" <> electrodename[[q]] <> "]"];
ToExpression["ClearAll[s" <> electrodename[[q]] <> "]"];
q++];
ClearSystemCache[];
Needs["Utilities`CleanSlate`"];
CleanSlate["Global`", Verbose → False];
]; //AbsoluteTiming
```

```
Needs["Utilities`CleanSlate`"];
CleanSlate["Global`", Verbose → False];
For[i = 1, i ≤ lz + lx, i++,
SetDirectory[NotebookDirectory[] <> "\\TransferMatrix"];
Get[A <> ToString[i] <> "_" <> ToString[i] <> ".mx"];
For[q = 1, q<=Length[electrodename],
SetDirectory[NotebookDirectory[] <> "\\Charges\\" <> electrodename[[q]]];
Get[electrodename[[q]] <> ToString[i] <> ".mx"];
ToExpression[electrodename[[q]] <> "=prod[A," <> electrodename[[q]] <> "]"];
DumpSave[electrodename[[q]] <> ToString[i] <> ".mx",
Evaluate[electrodename[[q]]]];
q++];
]; //AbsoluteTiming
ClearAll[A];
For[q = 1, q<=Length[electrodename],
ToExpression["ClearAll[" <> electrodename[[q]] <> "]"];
ToExpression["ClearAll[s" <> electrodename[[q]] <> "]"];
q++];
ClearSystemCache[];
Needs["Utilities`CleanSlate`"];
CleanSlate["Global`", Verbose → False];
For[k = lz + lx, k ≥ 2, k--,
For[q = 1, q<=Length[electrodename],
SetDirectory[NotebookDirectory[] <> "\\Charges\\" <> electrodename[[q]]];
Get[electrodename[[q]] <> ToString[k] <> ".mx"];
ToExpression[s <> electrodename[[q]] <> "=" <> electrodename[[q]]];
q++];
For[i = k - 1, i ≥ 1, i--,
SetDirectory[NotebookDirectory[] <> "\\TransferMatrix"];
Get[A <> ToString[i] <> "_" <> ToString[k] <> ".mx"];
For[q = 1, q<=Length[electrodename],
SetDirectory[NotebookDirectory[] <> "\\Charges\\" <> electrodename[[q]]];
Get[electrodename[[q]] <> ToString[i] <> ".mx"];
ToExpression[electrodename[[q]] <> "=fun[" <> electrodename[[q]] <>
",A,s" <> electrodename[[q]] <> "]"];
DumpSave[electrodename[[q]] <> ToString[i] <> ".mx",
Evaluate[electrodename[[q]]]];
q++];
```

```
];
For[q = 1, q<=Length[electrodename],
ToExpression["ClearAll[" <> electrodename[[q]] <> "]"];
ToExpression["ClearAll[s" <> electrodename[[q]] <> "]"];
q++];
ClearAll[A];
ClearSystemCache[];
Needs["UtilitiesCleanSlate"];
CleanSlate["Global", Verbose → False];
]; //AbsoluteTiming
ClearAll[A, prod, fun, electrodename, voltagename, lx, lz];
ClearSystemCache[];
Needs["UtilitiesCleanSlate"];
CleanSlate["Global", Verbose → False];


(*Potentials − computes the dc potentials and rf electric fields on the
specified grid*)
Print[Potentials]
Print["Memorybegin = ", MemoryInUse[]]

Needs["UtilitiesCleanSlate"]
CleanSlate["Global"]
$HistoryLength = 0
ClearSystemCache[]
ClearAll[int, a, b, c, segments, seg, x, pot, lp, exy, ez, prod, sum, f, fx, fy,
fz, lp, lz, lx, electrodenamedc, d]
SetDirectory[NotebookDirectory[] <> "\\Segments"];
Get["memorysize.mx"];
Get["segmentsize.mx"];
int = Compile[{{a, _Real, 2}, {b, _Real, 2}, {c, _Real, 2}},
−c
ArcTan[
(c(−(segmentsize/2 + a)(−segmentsize/2 + b)
√((−segmentsize/2 + a)^2 + (−segmentsize/2 + b)^2 + c^2)+
(−segmentsize/2 + a)(−segmentsize/2 + b)
√((segmentsize/2 + a)^2 + (−segmentsize/2 + b)^2 + c^2)))/
((−segmentsize/2 + a)(segmentsize/2 + a)(−segmentsize/2 + b)^2+
```

```
c^2 Sqrt[(-segmentsize/2 + a)^2 + (-segmentsize/2 + b)^2 + c^2]
 Sqrt[(segmentsize/2 + a)^2 + (-segmentsize/2 + b)^2 + c^2]]) +
c
ArcTan[
(c(-(segmentsize/2 + a)(segmentsize/2 + b)
Sqrt[(-segmentsize/2 + a)^2 + (segmentsize/2 + b)^2 + c^2]+
(-segmentsize/2 + a)(segmentsize/2 + b)
 Sqrt[(segmentsize/2 + a)^2 + (segmentsize/2 + b)^2 + c^2])) /
((-segmentsize/2 + a)(segmentsize/2 + a)(segmentsize/2 + b)^2+
c^2 Sqrt[(-segmentsize/2 + a)^2 + (segmentsize/2 + b)^2 + c^2]
 Sqrt[(segmentsize/2 + a)^2 + (segmentsize/2 + b)^2 + c^2]]) +
(-segmentsize/2 + b)
Log[(-segmentsize/2+a+Sqrt[(-segmentsize/2+a)^2+(-segmentsize/2+b)^2+c^2])/
(segmentsize/2+a+Sqrt[(segmentsize/2+a)^2+(-segmentsize/2+b)^2+c^2])] +
(-segmentsize/2 + a)
Log[(-segmentsize/2+b+Sqrt[(-segmentsize/2+a)^2+(-segmentsize/2+b)^2+c^2])/
(segmentsize/2+b+Sqrt[(-segmentsize/2+a)^2+(segmentsize/2+b)^2+c^2])] +
(segmentsize/2 + b)
Log[(segmentsize/2+a+Sqrt[(segmentsize/2+a)^2+(segmentsize/2+b)^2+c^2])/
(-segmentsize/2+a+Sqrt[(-segmentsize/2+a)^2+(segmentsize/2+b)^2+c^2])] +
(segmentsize/2 + a)
 Log[(segmentsize/2+b+Sqrt[(segmentsize/2+a)^2+(segmentsize/2+b)^2+c^2])/
(-segmentsize/2+b+Sqrt[(segmentsize/2+a)^2+(-segmentsize/2+b)^2+c^2])]];
exy = Compile[{{a, _Real, 2}, {b, _Real, 2}, {c, _Real, 2}},
Log[
((segmentsize/2 - b + Sqrt[(-segmentsize/2 + a)^2 + (-segmentsize/2 + b)^2 + c^2])
 (-segmentsize/2 - b + Sqrt[(segmentsize/2 + a)^2 + (segmentsize/2 + b)^2 + c^2])) /
((segmentsize/2 - b + Sqrt[(segmentsize/2 + a)^2 + (-segmentsize/2 + b)^2 + c^2])
 (-segmentsize/2 - b + Sqrt[(-segmentsize/2 + a)^2 + (segmentsize/2 + b)^2 + c^2]))]];
ez = Compile[{{a, _Real, 2}, {b, _Real, 2}, {c, _Real, 2}},
ArcTan[
(c(-(segmentsize/2 + a)(-segmentsize/2 + b)
Sqrt[(-segmentsize/2 + a)^2 + (-segmentsize/2 + b)^2 + c^2]+
(-segmentsize/2 + a)(-segmentsize/2 + b)
 Sqrt[(segmentsize/2 + a)^2 + (-segmentsize/2 + b)^2 + c^2])) /
((-segmentsize/2 + a)(segmentsize/2 + a)(-segmentsize/2 + b)^2+
c^2 Sqrt[(-segmentsize/2 + a)^2 + (-segmentsize/2 + b)^2 + c^2]
 Sqrt[(segmentsize/2 + a)^2 + (-segmentsize/2 + b)^2 + c^2]]) -
ArcTan[
(c(-(segmentsize/2 + a)(segmentsize/2 + b)
Sqrt[(-segmentsize/2 + a)^2 + (segmentsize/2 + b)^2 + c^2]+
(-segmentsize/2 + a)(segmentsize/2 + b)
```

```
 √((segmentsize/2 + a)^2 + (segmentsize/2 + b)^2 + c^2))) /
((-segmentsize/2 + a)(segmentsize/2 + a)(segmentsize/2 + b)^2 +
c^2 √((-segmentsize/2 + a)^2 + (segmentsize/2 + b)^2 + c^2)
 √((segmentsize/2 + a)^2 + (segmentsize/2 + b)^2 + c^2))]];
prod = Compile[{{b, _Real, 2}, {c, _Real, 1}}, b.c];
sum = Compile[{{a, _Real, 2}, {b, _Real, 2}, {c, _Real, 2}, {d, _Real, 2}},
a + b + c + d];
SetDirectory[NotebookDirectory[] <> "\\Segments"];
Get["electrodename.mx"];
electrodenamedc = Complement[electrodename, {"rf"}];
Get["segmentsz.mx"];
lz = Quotient[Length[segmentsz], memorysize] + 1;
ClearAll[segmentsz]
ClearSystemCache[]
Get["segmentsx.mx"];
lx = Quotient[Length[segmentsx], memorysize] + 1;
ClearAll[segmentsz]
ClearSystemCache[]
SetDirectory[NotebookDirectory[] <> "\\Potentials\\Positions"];
Get["M.mx"];
lp = Quotient[Length[M], memorysize] + 1;
ClearAll[M]
ClearSystemCache[]
pot = Function[{p, z, x, w, v},
Module[{lp, lz, lx},
lp = p;
lz = z;
lx = x;
px = py = pz = Rx = Ry = Rz = rf = v;
For[q = 1, q<=Length[electrodenamedc],
ToExpression[electrodenamedc[[q]] <> "=" <> v];
q++];
am = ap = bm = bp = c = f = fx = fy = fz = w;
For[i = 1, i ≤ lp, i++,
Print["Memory1 = ", MemoryInUse[]];
SetDirectory[NotebookDirectory[] <> "\\Potentials\\Positions"];
Get["px" <> ToString[i] <> ".mx"];
Get["py" <> ToString[i] <> ".mx"];
```

```
Get["pz" <> ToString[i] <> ".mx"];
For[q = 1, q<=Length[electrodenamedc],
ToExpression[p <> electrodenamedc[[q]] <> "=" <> "0"];
q++];
xrf = 0; yrf = 0; zrf = 0;
For[j = 1, j ≤ lz, j++,
Print["Memory2 = ", MemoryInUse[]];
SetDirectory[NotebookDirectory[] <> "\\Positions"];
Get["Rx" <> ToString[j] <> ".mx"];
Get["Ry" <> ToString[j] <> ".mx"];
Get["Rz" <> ToString[j] <> ".mx"];
am = Outer[Plus, px, -Rx];
ap = Outer[Plus, px, Rx];
bm = Outer[Plus, py, -Ry];
bp = Outer[Plus, py, Ry];
c = Outer[Plus, pz, -Rz];
ClearAll[Rx, Ry, Rz];
ClearSystemCache[];
Needs["Utilities`CleanSlate`"];
CleanSlate["Global`", Verbose->False];
f = int[am, bm, c];
f = f + int[am, bp, c];
f = f + int[ap, bm, c];
f = f + int[ap, bp, c];
ClearSystemCache[];
Needs["Utilities`CleanSlate`"];
CleanSlate["Global`", Verbose->False];
For[q = 1, q<=Length[electrodenamedc],
SetDirectory[NotebookDirectory[] <> "\\Charges\\" <> electrodenamedc[[q]]];
Get[electrodenamedc[[q]] <> ToString[j] <> ".mx"];
ToExpression[p <> electrodenamedc[[q]] <> "=p" <> electrodenamedc[[q]] <>
"+prod[f," <> electrodenamedc[[q]] <> "]"];
q++];
ClearAll[f];
For[q = 1, q<=Length[electrodenamedc],
ToExpression["ClearAll[" <> electrodenamedc[[q]] <> "]"];
q++];
ClearSystemCache[];
```

```
Needs["Utilities`CleanSlate`"];
CleanSlate["Global`", Verbose->False];
Print["Memory3 = ", MemoryInUse[]];
SetDirectory[NotebookDirectory[] <> "\\Charges\\rf"];
Get["rf" <> ToString[j] <> ".mx"];
fx = exy[am, bm, c] + exy[am, bp, c] + exy[ap, bm, c] + exy[ap, bp, c];
xrf = xrf + prod[fx, rf];
ClearAll[fx];
ClearSystemCache[];
Needs["Utilities`CleanSlate`"];
CleanSlate["Global`", Verbose->False];
fy = exy[bm, am, c] + exy[bm, ap, c] + exy[bp, am, c] + exy[bp, ap, c];
yrf = yrf + prod[fy, rf];
ClearAll[fy];
ClearSystemCache[];
Needs["Utilities`CleanSlate`"];
CleanSlate["Global`", Verbose->False];
fz = ez[am, bm, c] + ez[am, bp, c] + ez[ap, bm, c] + ez[ap, bp, c];
zrf = zrf + prod[fz, rf];
ClearAll[fz, rf, am, ap, bm, bp, c];
ClearSystemCache[];
Needs["Utilities`CleanSlate`"];
CleanSlate["Global`", Verbose->False];
Print["Memory4 = ", MemoryInUse[]];
];
For[j = lz + 1, j ≤ lz + lx, j++,
Print["Memory5 = ", MemoryInUse[]];
SetDirectory[NotebookDirectory[] <> "\\Positions"];
Get["Rx" <> ToString[j] <> ".mx"];
Get["Ry" <> ToString[j] <> ".mx"];
Get["Rz" <> ToString[j] <> ".mx"];
am = Outer[Plus, px, -Rx];
ap = Outer[Plus, px, Rx];
bm = Outer[Plus, py, -Ry];
bp = Outer[Plus, py, Ry];
c = Outer[Plus, pz, -Rz];
ClearAll[Rx, Ry, Rz];
ClearSystemCache[];
```

```
Needs["Utilities`CleanSlate`"];
CleanSlate["Global`", Verbose->False];
f = int[c, bm, am];
f = f + int[c, bp, am];
f = f + int[c, bm, ap];
f = f + int[c, bp, ap];
ClearSystemCache[];
Needs["Utilities`CleanSlate`"];
CleanSlate["Global`", Verbose->False];
For[q = 1, q<=Length[electrodenamedc],
SetDirectory[NotebookDirectory[] <> "\\Charges\\" <> electrodenamedc[[q]]];
Get[electrodenamedc[[q]] <> ToString[j] <> ".mx"];
ToExpression[p <> electrodenamedc[[q]] <> "=p" <> electrodenamedc[[q]] <>
"+prod[f," <> electrodenamedc[[q]] <> "]"];
q++];
ClearAll[f];
For[q = 1, q<=Length[electrodenamedc],
ToExpression["ClearAll[" <> electrodenamedc[[q]] <> "]"];
q++];
ClearSystemCache[];
Needs["Utilities`CleanSlate`"];
CleanSlate["Global`", Verbose->False];
Print["Memory6 = ", MemoryInUse[]];
SetDirectory[NotebookDirectory[] <> "\Charges\\rf"];
Get["rf" <> ToString[j] <> ".mx"];
fx = ez[c, bm, am] + ez[c, bp, am] + ez[c, bm, ap] + ez[c, bp, ap];
xrf = xrf + prod[fx, rf];
ClearAll[fx];
ClearSystemCache[];
Needs["Utilities`CleanSlate`"];
CleanSlate["Global`", Verbose->False];
fy = exy[bm, c, am] + exy[bm, c, ap] + exy[bp, c, am] + exy[bp, c, ap];
yrf = yrf + prod[fy, rf];
ClearAll[fy];
ClearSystemCache[];
Needs["Utilities`CleanSlate`"];
CleanSlate["Global`", Verbose->False];
fz = exy[c, bm, am] + exy[c, bm, ap] + exy[c, bp, am] + exy[c, bp, ap];
```

```
zrf = zrf + prod[fz, rf];
ClearAll[fz, rf, am, ap, bm, bp, c];
ClearSystemCache[];
Needs["Utilities`CleanSlate`"];
CleanSlate["Global`", Verbose->False];
Print["Memory7 = ", MemoryInUse[]];
];
For[q = 1, q<=Length[electrodenamedc],
SetDirectory[NotebookDirectory[] <> "\\Potentials\\" <> electrodenamedc[[q]]];
DumpSave[p <> electrodenamedc[[q]] <> ToString[i] <> ".mx",
Evaluate[p <> electrodenamedc[[q]]]];
q++];
SetDirectory[NotebookDirectory[] <> "\\Potentials\\rf"];
DumpSave["xrf" <> ToString[i] <> ".mx", xrf];
DumpSave["yrf" <> ToString[i] <> ".mx", yrf];
DumpSave["zrf" <> ToString[i] <> ".mx", zrf];
ClearAll[xrf, yrf, zrf];
For[q = 1, q<=Length[electrodenamedc],
ToExpression["ClearAll[p" <> electrodenamedc[[q]] <> "]"];
q++];
ClearSystemCache[];
Needs["Utilities`CleanSlate`"];
CleanSlate["Global`", Verbose->False];
Print["Memory8 = ", MemoryInUse[]];
];
];
TimeUsed[]
pot[lp, lz, lx, {{1, 0}, {0, 1}}, {1, 0}]; //AbsoluteTiming
TimeUsed[]
ClearSystemCache[];
ClearAll[int, a, b, c, segments, seg, x, pot, lp, exy, ez, prod, sum, f, fx, fy,
fz, lp, xrf, yrf, zrf, rf, am, ap, bm, bp, q];
For[q = 1, q<=Length[electrodenamedc],
ToExpression["ClearAll[" <> electrodenamedc[[q]] <> "]"];
ToExpression["ClearAll[p" <> electrodenamedc[[q]] <> "]"];
q++];
Needs["Utilities`CleanSlate`"]
```

```
CleanSlate["Global`"]
Print["Memoryend = ", MemoryInUse[]]

timeend = AbsoluteTime[];
(timeend - timestart)/3600
```

A.4 Trap analysis

The user specifies the trap voltages in V, rf voltage frequency in Hz, and the ion mass in amu. The code computes the dc node and rf node positions in mm (they must match for the trap to be compensated), trap depth in eV, the secular frequencies in Hz, and the trap a and q parameters.

```
(*interpolates the grid voltages*)
Needs["Utilities`CleanSlate`"]
CleanSlate["Global`"]
$HistoryLength = 0
ClearSystemCache[]
SetDirectory[NotebookDirectory[] <> "\\Segments"];
Get["memorysize.mx"];
SetDirectory[NotebookDirectory[]];
SetDirectory[ParentDirectory[] <> "\\Potentials\\Positions"];
Get["M.mx"];
lp = Quotient[Length[M], memorysize] + 1;
ClearSystemCache[]
Px = {}; Py = {}; Pz = {};
SetDirectory[NotebookDirectory[]];
SetDirectory[ParentDirectory[] <> "\\Segments"];
Get["electrodename.mx"];
electrodenamedc = Complement[electrodename, {"rf"}];
For[q = 1, q ≤ Length[electrodenamedc],
ToExpression[P <> electrodenamedc[[q]] <> "={}"];
q++];
Erf2 = {};
For[i = 1, i ≤ lp, i++,
SetDirectory[NotebookDirectory[]];
```

```
SetDirectory[ParentDirectory[] <> "\\Potentials\\Positions"];
Get["px" <> ToString[i] <> ".mx"];
Px = Join[Px, px];
Get["py" <> ToString[i] <> ".mx"];
Py = Join[Py, py];
Get["pz" <> ToString[i] <> ".mx"];
Pz = Join[Pz, pz];
For[q = 1, q ≤ Length[electrodenamedc],
SetDirectory[NotebookDirectory[]];
SetDirectory[ParentDirectory[] <> "\\Potentials\\" <> electrodenamedc[[q]]];
Get[p <> electrodenamedc[[q]] <> ToString[i] <> ".mx"];
ToExpression[P <> electrodenamedc[[q]] <> "=Join[P" <> electrodenamedc[[q]] <>
",p" <> electrodenamedc[[q]] <> "]"];
q++];
SetDirectory[NotebookDirectory[]];
SetDirectory[ParentDirectory[] <> "\\Potentials\\rf"];
Get["xrf" <> ToString[i] <> ".mx"];
Get["yrf" <> ToString[i] <> ".mx"];
Get["zrf" <> ToString[i] <> ".mx"];
Erf2 = Join [Erf2, xrf^2 + yrf^2 + zrf^2] ;
];
SetDirectory[NotebookDirectory[]];
SetDirectory[ParentDirectory[] <> "\\Potentials\\Positions"];
DumpSave["Px.mx", Px];
DumpSave["Py.mx", Py];
DumpSave["Pz.mx", Pz];
For[q = 1, q ≤ Length[electrodenamedc],
SetDirectory[NotebookDirectory[]];
SetDirectory[ParentDirectory[] <> "\\Potentials\\" <> electrodenamedc[[q]]];
DumpSave[P <> electrodenamedc[[q]] <> ".mx",
Evaluate[P <> electrodenamedc[[q]]]];
q++];
SetDirectory[NotebookDirectory[]];
SetDirectory[ParentDirectory[] <> "\\Potentials\\rf"];
DumpSave["Erf2.mx", Erf2];
ClearAll[px, py, pz, xrf, yrf, zrf, mw];
For[q = 1, q ≤ Length[electrodenamedc],
ToExpression["ClearAll[p" <> electrodenamedc[[q]] <> "]"];
```

```
q++];
Erf2wpos = Table[{{0, 0, 0}, 0}, {Length[M]}];
Erf2wpos[[All, 1]] = M;
Erf2wpos[[All, 2]] = Erf2;
Erf2interp = Interpolation[Erf2wpos, InterpolationOrder → 10]

(*computes the pseudopotential, rf node, and dc node;
gives a cross − section through the pseudopotential*)
NMinimize[{Erf2interp[0, 0, z], 0.001 ≤ z ≤ 1.361}, {z}]
e = 1.60217646 * 10^-19;
amu = 1.66053886 * 10^-27;
m = 88;
freq = 7.22 * 10^6;
Vrf = 250;
Vmid = −6;
Vend = 5;
Vquad = 0;
Vgnd = 0;
pseudopot = Vmid * Pmid + Vend * Pend + Vgnd * Pgnd + Vquad * Pquad+
e*Vrf^2 / (4*amu*m*(2*π*freq)^2*10^-6) * Erf2;
pseudopotwpos = Table[{{0, 0, 0}, 0}, {Length[M]}];
pseudopotwpos[[All, 1]] = M;
pseudopotwpos[[All, 2]] = pseudopot;
pseudopotquadinterp = Interpolation[pseudopotwpos, InterpolationOrder → 5]
pseudosymmxy = pseudosymmx = pseudosymmy = pseudopotwpos;
pseudosymmxy[[All, 1, 1;;2]] = −pseudosymmxy[[All, 1, 1;;2]];
pseudosymmx[[All, 1, 1]] = −pseudosymmx[[All, 1, 1]];
pseudosymmy[[All, 1, 2]] = −pseudosymmy[[All, 1, 2]];
pseudopotwpos = Union[pseudosymmx, pseudosymmy, pseudosymmxy, pseudopotwpos];
pseudopotinterp = Interpolation[pseudopotwpos, InterpolationOrder → 10]
trapmin = NMinimize[{pseudopotinterp[0, 0, z], 0.001 ≤ z ≤ 1.361}, {z}]
pm = trapmin[[1]]
ClearAll[z]
t0 = z/.trapmin[[2]]
ClearAll[z]
Show[{ContourPlot[pseudopotinterp[x, 0, z] + "0.128075",
{x, −0.35, 0.35}, {z, 0.4, 1}, AspectRatio → Automatic, Contours → 12,
AspectRatio → Automatic,
```

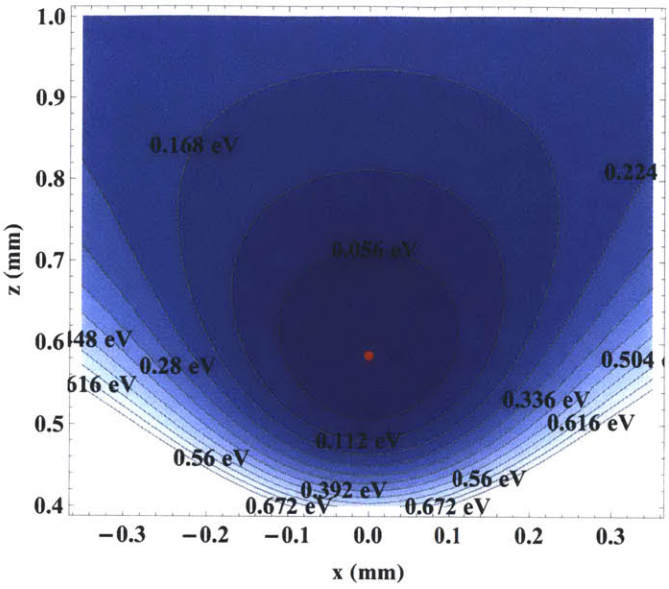

ContourLabels → Function[{x, y, z},

Text[Style[ToString[$N[z]$] <> " eV", 16, Bold], {x, y}]],

FrameLabel → {"x (mm)", "z (mm)"}, LabelStyle → {Bold, 16}],

Graphics[{PointSize[Large], Red, Point[{0, t0}]}]}]

(*computes the coordinates of the saddle point on the last closed

pseudopotential surface, and finds the trap depth*)

ClearAll[nx, ny, nz]

nx = 6;

ny = 3;

nz = 10;

DistributeDefinitions[nx, ny, nz, E2, pseudopotquadinterp];

E2[x_, y_, z_] = D[pseudopotquadinterp[x, y, z], x]^2+

D[pseudopotquadinterp[x, y, z], y]^2 + D[pseudopotquadinterp[x, y, z], z]^2;

DistributeDefinitions[E2]

dp =

ParallelTable[

NMinimize[{E2[x, y, z], $i \le x \le i + 0.714/\text{nx}, j \le y \le j + 3.604/\text{ny}$,

$k \le z \le k + (1.361 - 0.001)/\text{nz}$}, {$x, y, z$}, Method → "DifferentialEvolution"],

{i, 0, $0.714 - 0.714/\text{nx}, 0.714/\text{nx}$}, {$j$, 0, $3.604 - 3.604/\text{ny}, 3.604/\text{ny}$},

{k, 0.001, $1.361 - (1.361 - 0.001)/\text{nz}, (1.361 - 0.001)/\text{nz}$}];

dp = Flatten[dp, 2];

sol = SortBy[dp, First];

```
sol[[1;;10]]
ClearAll[nx, ny, nz]
pseudopotinterp[x, y, z]/.{x → "0.383859", y → "0.", z → "1.01192"}
0.0789579
(*displays the trapping potential*)
Show[{ContourPlot3D[pseudopotinterp[x, y, z] == "0.0789579",
{x, -"0.383859", "0.383859"}, {y, -3.604, 3.604},
{z, 0.4, 1.261}, Mesh → False, ContourStyle → Opacity[0.55](*, PlotPoints → 20*)],
Graphics3D[{
Green, Opacity[1], Cuboid[{-0.3, -3.645, 0}, {0.3, 3.645, 0}],

Orange, Opacity[1], Cuboid[{0.315, -3.645, 0}, {1.015, 3.645, 0}],
Orange, Opacity[1], Cuboid[{-0.315, -3.645, 0}, {-1.015, 3.645, 0}],

Orange, Opacity[1], Cuboid[{1.015, 3.545, 0}, {4.5, 3.645, 0}],
Orange, Opacity[1], Cuboid[{1.015, -3.545, 0}, {4.5, -3.645, 0}],
Orange, Opacity[1], Cuboid[{-1.015, 3.545, 0}, {-4.5, 3.645, 0}],
Orange, Opacity[1], Cuboid[{-1.015, -3.545, 0}, {-4.5, -3.645, 0}],

Lighter[Blue], Opacity[1], Cuboid[{1.03, -0.5, 0}, {4.5, 0.5, 0}],
Lighter[Blue], Opacity[1], Cuboid[{-1.03, -0.5, 0}, {-4.5, 0.5, 0}],

Blue, Opacity[1], Cuboid[{1.03, 0.515, 0}, {4.5, 2.015, 0}],
Blue, Opacity[1], Cuboid[{1.03, -0.515, 0}, {4.5, -2.015, 0}],
Blue, Opacity[1], Cuboid[{-1.03, 0.515, 0}, {-4.5, 2.015, 0}],
Blue, Opacity[1], Cuboid[{-1.03, -0.515, 0}, {-4.5, -2.015, 0}],

Darker[Blue], Opacity[1], Cuboid[{1.03, 2.03, 0}, {4.5, 3.53, 0}],
Darker[Blue], Opacity[1], Cuboid[{1.03, -2.03, 0}, {4.5, -3.53, 0}],
Darker[Blue], Opacity[1], Cuboid[{-1.03, 2.03, 0}, {-4.5, 3.53, 0}],
Darker[Blue], Opacity[1], Cuboid[{-1.03, -2.03, 0}, {-4.5, -3.53, 0}],

Red, Opacity[1], PointSize[0.0075], Point[{0, 0, t0}]}],
PlotRange → All, BoxRatios → {2 * 3.645, 9, 1.261},
AxesLabel → {"x (mm)", "y (mm)", "z (mm)"}, LabelStyle → {Bold, 30}]

(*computes the pseudo electrical fields in which the ions move*)
ClearAll[x, y, z, t, i, j, k, a, b, c]
```

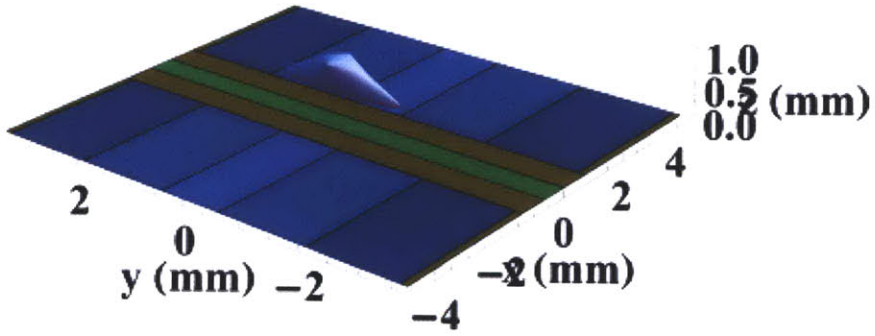


```
DistributeDefinitions[x, y, z, i, j, k, pseudopotinterp]
ext = ParallelTable[−D[pseudopotinterp[x, y, z], x]/.{x → i, y → j, z → k},
{i, −0.714, 0.714, 0.017}, {j, −3.604, 3.604, 0.068}, {k, 0.001, 1.361, 0.034}];
Ex = ListInterpolation[ext, {{−0.714, 0.714}, {−3.604, 3.604}, {0.001, 1.361}},
InterpolationOrder → 5]
eyt = ParallelTable[−D[pseudopotinterp[x, y, z], y]/.{x → i, y → j, z → k},
{i, −0.714, 0.714, 0.017}, {j, −3.604, 3.604, 0.068}, {k, 0.001, 1.361, 0.034}];
Ey = ListInterpolation[eyt, {{−0.714, 0.714}, {−3.604, 3.604}, {0.001, 1.361}},
InterpolationOrder → 5]
ezt = ParallelTable[−D[pseudopotinterp[x, y, z], z]/.{x → i, y → j, z → k},
{i, −0.714, 0.714, 0.017}, {j, −3.604, 3.604, 0.068}, {k, 0.001, 1.361, 0.034}];
Ez = ListInterpolation[ezt, {{−0.714, 0.714}, {−3.604, 3.604}, {0.001, 1.361}},
InterpolationOrder → 5]
(*solves the equations of motion for the ions; gives the secular frequencies,
and a and q trap parameters*)
Clear[q, fx, fz, fy, a]
temp = 0.0001 + pm;
periodx =
NDSolve [{x"[t]==e/(m*amu*10^−6) * Ex[x[t], y[t], z[t]],
y"[t]==e/(m*amu*10^−6) * Ey[x[t], y[t], z[t]],
z"[t]==e/(m*amu*10^−6) * Ez[x[t], y[t], z[t]], x[0] == y[0] == 0, z[0] == t0,
x'[0]==10^3 * Sqrt[2*e*(temp−pm)/(m*amu)], y'[0] == z'[0] == 0}, {x, y, z}, {t, ∞},
Method → {"EventLocator", "Event" → x[t], "Direction" → −1}, AccuracyGoal->12,
PrecisionGoal->12];
periody = NDSolve [{x"[t]==e/(m*amu*10^−6) * Ex[x[t], y[t], z[t]],
y"[t]==e/(m*amu*10^−6) * Ey[x[t], y[t], z[t]],
z"[t]==e/(m*amu*10^−6) * Ez[x[t], y[t], z[t]], x[0] == y[0] == 0, z[0] == t0,
y'[0]==10^3 * Sqrt[2*e*(temp−pm)/(m*amu)], x'[0] == z'[0] == 0}, {x, y, z}, {t, ∞},
```

Method → {"EventLocator", "Event" → $y[t]$, "Direction" → -1}, AccuracyGoal → 12,

PrecisionGoal->12];

periodzup =

NDSolve $\left[\left\{x"[t]==\frac{e}{m*\text{amu}*10^{-6}} * \text{Ex}[x[t], y[t], z[t]],\right.\right.$

$y"[t]==\frac{e}{m*\text{amu}*10^{-6}} * \text{Ey}[x[t], y[t], z[t]],$

$z"[t]==\frac{e}{m*\text{amu}*10^{-6}} * \text{Ez}[x[t], y[t], z[t]], x[0] == y[0] == 0, z[0] == \text{t0},$

$\left.\left.z'[0]==10^3 * \sqrt{\frac{2*e*(\text{temp}-\text{pm})}{m*\text{amu}}}, y'[0] == x'[0] == 0\right\}, \{x, y, z\}, \{t, \infty\}\right.$,

Method → {"EventLocator", "Event" → $z[t] - \text{t0}$, "Direction" → -1},

AccuracyGoal->12, PrecisionGoal->12];

periodzdown =

NDSolve $\left[\left\{x"[t]==\frac{e}{m*\text{amu}*10^{-6}} * \text{Ex}[x[t], y[t], z[t]],\right.\right.$

$y"[t]==\frac{e}{m*\text{amu}*10^{-6}} * \text{Ey}[x[t], y[t], z[t]],$

$z"[t]==\frac{e}{m*\text{amu}*10^{-6}} * \text{Ez}[x[t], y[t], z[t]], x[0] == y[0] == 0, z[0] == \text{t0},$

$\left.\left.z'[0] == -10^3 * \sqrt{\frac{2*e*(\text{temp}-\text{pm})}{m*\text{amu}}}, y'[0] == x'[0] == 0\right\}, \{x, y, z\}, \{t, \infty\}\right.$,

Method → {"EventLocator", "Event" → $z[t] - \text{t0}$, "Direction" → 1},

AccuracyGoal->12, PrecisionGoal->12];

temp − pm

fx = 1/(2 * periodx[[1, 1, 2, 1, 1, 2]])

fy = 1/(2 * periody[[1, 1, 2, 1, 1, 2]])

fz = 1/(1 * (periodzup[[1, 1, 2, 1, 1, 2]] + periodzdown[[1, 1, 2, 1, 1, 2]]))

$q = \frac{2*\sqrt{\text{fx}^2+\text{fz}^2}}{\text{freq}}$

$a = \left(\frac{2*\text{Max}[\text{fx},\text{fz}]}{\text{freq}}\right)^2 - q^2/2$

Plot[Evaluate[$x[t]$/.periodx], {t, "0.", periodx[[1, 1, 2, 1, 1, 2]]}, PlotRange → All]

Plot[Evaluate[$y[t]$/.periody], {t, "0.", periody[[1, 1, 2, 1, 1, 2]]}, PlotRange → All]

Plot[Evaluate[$z[t]$/.periodzup], {t, "0.", periodzup[[1, 1, 2, 1, 1, 2]]},

PlotRange → All]

Plot[Evaluate[$z[t]$/.periodzdown], {t, "0.", periodzdown[[1, 1, 2, 1, 1, 2]]},

PlotRange → All]

0.0001

527335.

113109.

578658.

0.216869

0.00217779

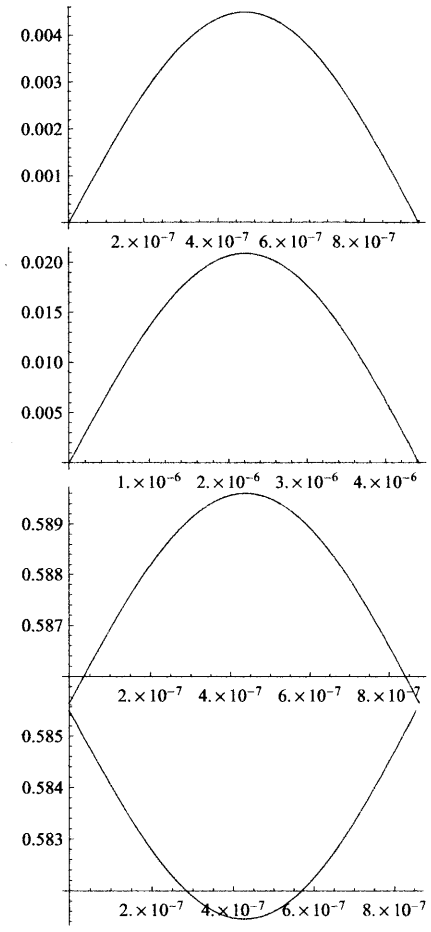
0.004
0.003
0.002
0.001
2.×10^-7 4.×10^-7 6.×10^-7 8.×10^-7
0.020
0.015
0.010
0.005
1.×10^-6 2.×10^-6 3.×10^-6 4.×10^-6
0.589
0.588
0.587
2.×10^-7 4.×10^-7 6.×10^-7 8.×10^-7
0.585
0.584
0.583
2.×10^-7 4.×10^-7 6.×10^-7 8.×10^-7

Appendix B

Numerical evaluation of collisional enhanced heating rates

The following is Mathematica 7 code for the numerical solution to the collisional assisted heating rates as presented in Section 3.3.

(*set up physical constants and problem parameters*)

Clear[etai, etaf, ti, f]

ts = AbsoluteTime[]

kb = $1.38 * 10^{-23}$

hb = $1.054 * 10^{-34}$

ev = $8.854 * 10^{-12}$

$c = 3 * 10^{8}$

$a = 1/137$

el = $1.602 * 10^{-19}$

amu = $1.660 * 10^{-27}$

me = $9.1093826 * 10^{-31}$

debye = $3.33564 * 10^{-30}$

$$d = 9.806 * \text{debye}$$

$$m = \frac{88*123}{88+123} * \text{amu}$$

$$Q = \frac{\text{el}*d*m}{4*\pi*\text{ev}*\text{hb}^2}$$

$$\text{k0} = \frac{\text{el}^2*m}{4*\pi*\text{ev}*\text{hb}^2}$$

$$\text{etran} = 6.52 * 10^9 * 2 * \pi * \text{hb}$$

$$\text{xi} = \frac{\text{el}^2}{4*\pi*\text{ev}*\text{hb}*\sqrt{\frac{2*\text{ti}}{m}}}$$

$$\text{xf} = \frac{\text{el}^2}{4*\pi*\text{ev}*\text{hb}*\sqrt{\frac{2*(\text{ti}-\text{etran})}{m}}}$$

(*computes the collisional cross section s*)

$$f[\text{etai\_}, \text{etaf\_}] = -\frac{32\pi^3}{9} * \frac{\text{etai}*\text{etaf}}{(\text{etaf}-\text{etai})} * \frac{1}{\text{Exp}[2*\pi*(\text{etaf}-\text{etai})]-1} *$$

$$\text{Im}\left[\frac{\text{Hypergeometric2F1}\left[i*\text{etai}, i*\text{etai}, 1-i*(\text{etaf}-\text{etai}), -\frac{(\text{etaf}-\text{etai})^2}{4*\text{etai}*\text{etaf}}\right]}{\text{etai}} *\right.$$

$$(\text{Hypergeometric2F1}[1 - i * \text{etai}, -i * \text{etai}, 1 + i * (\text{etaf} - \text{etai}),$$

$$\left.-\frac{(\text{etaf}-\text{etai})^2}{4*\text{etai}*\text{etaf}}\right] +$$

$$\text{Exp}\left[i * \left(2 * \text{Arg}\left[\frac{\text{Gamma}[i*(\text{etaf}-\text{etai})]*\text{Gamma}[i*\text{etai}]}{\text{Gamma}[i*\text{etaf}]}\right] +\right.\right.$$

$$\left.\left.(\text{etaf} - \text{etai}) * \text{Log}\left[\text{Abs}\left[-\frac{4*\text{etai}*\text{etaf}}{(\text{etaf}-\text{etai})^2}\right]\right]\right)\right] *$$

$$\text{Hypergeometric2F1}[1 - i * \text{etaf}, -i * \text{etaf}, 1 - i * (\text{etaf} - \text{etai}),$$

$$\left.-\frac{(\text{etaf}-\text{etai})^2}{4*\text{etai}*\text{etaf}}\right]) +$$

$$\frac{1}{\text{etaf}}\text{Hypergeometric2F1}[i\text{etaf}, i\text{etaf}, 1 - i(-\text{etaf} + \text{etai}),$$

$$\left.-\frac{(-\text{etaf}+\text{etai})^2}{4\text{etafetai}}\right]$$

$$(\text{Hypergeometric2F1}[1 - i\text{etaf}, -i\text{etaf}, 1 + i(-\text{etaf} + \text{etai}),$$

$$-\frac{(-\text{etaf}+\text{etai})^2}{4\text{etafetai}}] +$$

$$e^{i\left(2\text{Arg}\left[\frac{\text{Gamma}[i\text{etaf}]\text{Gamma}[i(-\text{etaf}+\text{etai})]}{\text{Gamma}[i\text{etai}]}\right]+(-\text{etaf}+\text{etai})\text{Log}\left[4\text{Abs}\left[\frac{\text{etafetai}}{(-\text{etaf}+\text{etai})^2}\right]\right]\right)}$$

$$\text{Hypergeometric2F1}[1 - i\text{etai}, -i\text{etai}, 1 - i(-\text{etaf} + \text{etai}),$$

$$\left.-\frac{(-\text{etaf}+\text{etai})^2}{4\text{etafetai}}\right])\Big] ;$$

$$\text{fdex}[\text{etai\_}, \text{etaf\_}] = \frac{32\pi^3}{9*\sqrt{3}} * \left(1 + 0.218 * \text{Abs}[\text{etaf} - \text{etai}]^{-2/3}\right) ;$$

$$\text{fex}[\text{etai\_}, \text{etaf\_}] = \frac{32\pi^3}{9*\sqrt{3}} * \left(1 + 0.218 * \text{Abs}[\text{etaf} - \text{etai}]^{-2/3}\right) *$$

$$\text{Exp}[-2\pi\text{Abs}[\text{etaf} - \text{etai}]];$$

$s[ji\_, jf\_, etai\_, etaf\_] =$

$\frac{3*(2*jf+1)}{4*\pi} * (Q * etai)^2 * ThreeJSymbol[\{ji, 0\}, \{jf, 0\}, \{1, 0\}]^2 *$

$fdex[etai, etaf] / k0^2$;

$Clear[ti, t, v]$

$omega = \frac{d*1500}{\sqrt{3}*hb}$

(*computes the collisional excitation reaction rate*)

$g12[t\_]:=$

$Re[$

$NIntegrate[8.611665937676688*\text{^}-32$

$\left(1 + \frac{0.218}{Abs\left[\frac{4.515717253913732*\text{^}-7}{\sqrt{-8.635710417152 54*\text{^}-24+ti}} - \frac{4.515717253913732*\text{^}-7}{\sqrt{ti}}\right]^{2/3}}\right) * 4 * \pi *$

$\sqrt{\frac{1}{2*\frac{88*123}{88+123}*amu}} * \frac{1}{(\pi*1.38*10^{-23})^{3/2}} * Exp\left[-\frac{ti}{t*1.38*10^{-23}}\right],$

$\{ti, 2 * etran, 5000kb\}, MaxRecursion \to 500] * \left(\frac{1}{20*10^{-6}}\right)^3\Big]$

$g01[t\_]:=$

$Re[$

$NIntegrate[1.291749890651503*\text{^}-31$

$\left(1 + \frac{0.218}{Abs\left[\frac{4.515717253913732*\text{^}-7}{\sqrt{-4.317855208576 27*\text{^}-24+ti}} - \frac{4.515717253913732*\text{^}-7}{\sqrt{ti}}\right]^{2/3}}\right) * 4 * \pi *$

$\sqrt{\frac{1}{2*\frac{88*123}{88+123}*amu}} * \frac{1}{(\pi*1.38*10^{-23})^{3/2}} * Exp\left[-\frac{ti}{t*1.38*10^{-23}}\right],$

$\{ti, etran, 5000kb\}, MaxRecursion \to 500] * \left(\frac{1}{20*10^{-6}}\right)^3\Big]$

(*computes the heating rate rhm and population inversion n01rat*)

$g10[t\_]:=g01[t] * Exp\left[\frac{etran}{t*1.38*10^{-23}}\right] / 3$

$Z[t\_]:=\sum_{k=0}^{5000}(2 * k + 1) * Exp\left[-\frac{6.52*10^9*\pi*hb*k*(k+1)}{t*kb}\right]$

$S[t\_, v\_]:=\frac{(g01[t]+g10[t]+g12[t])*omega^2}{4*\left(\frac{2\pi}{0.62}*v\right)^2+(g01[t]+g10[t]+g12[t])^2}$

$f[t\_, v\_]:=\frac{3g01[t](g10[t]+g12[t])+(2g01[t]+3(g10[t]+g12[t]))S[t,v]}{3g10[t](g10[t]+g12[t])+(3g10[t]+g12[t])S[t,v]}$

$rh[t\_, v\_]:=etran * \frac{g01[t](f[t,v]g10[t]-g01[t])}{g10[t]f[t,v](Z[t]-1)+g01[t]} / el$

DistributeDefinitions[g01, g10, g12, Z, S, f, rh, etran, kb, amu, t, ti, v, el]

SetDirectory["C:"]

rhout = ParallelTable[rh[x, v], {x, 0.5, 10, 0.1}]

SetDirectory["C:\\Users\\Moi\\Desktop\\slides 2"]

DumpSave["rhout.mx", rhout];

$$\text{n10rat} = \text{ParallelTable}\left[\frac{f[x,0]}{3} * \text{Exp}\left[\frac{\text{etran}}{x*1.38*10^{-23}}\right], \{x, 0.5, 10, 0.1\}\right];$$

DumpSave["n10rat.mx", n10rat];

ClearAll[rhout, n10rat]

ClearAll[rh, v, l]

SetDirectory["C:"]

Get["rhout.mx"]

l = Length[rhout]

rh[v_] = Simplify[rhout]

rhm =

$$\text{Table}\left[\{(0.5 + 0.1 * (k-1)),\right.$$
$$\text{NIntegrate}\left[2 * \sqrt{\frac{88*\text{amu}}{2\pi\text{kb}(0.5+0.1*(k-1))}} * \text{Exp}\left[-\frac{88*\text{amu}*v^2}{2*\text{kb}(0.5+0.1*(k-1))}\right] *\right.$$
$$\left.\left.\left.\text{rh}[v][[k]], \left\{v, 0, \sqrt{\frac{2*5000\text{kb}}{88*\text{amu}}}\right\}, \text{MaxRecursion} \to 500\right]\right\}, \{k, 1, l\}\right]$$

(*plots the heating rate per molecular ion*)

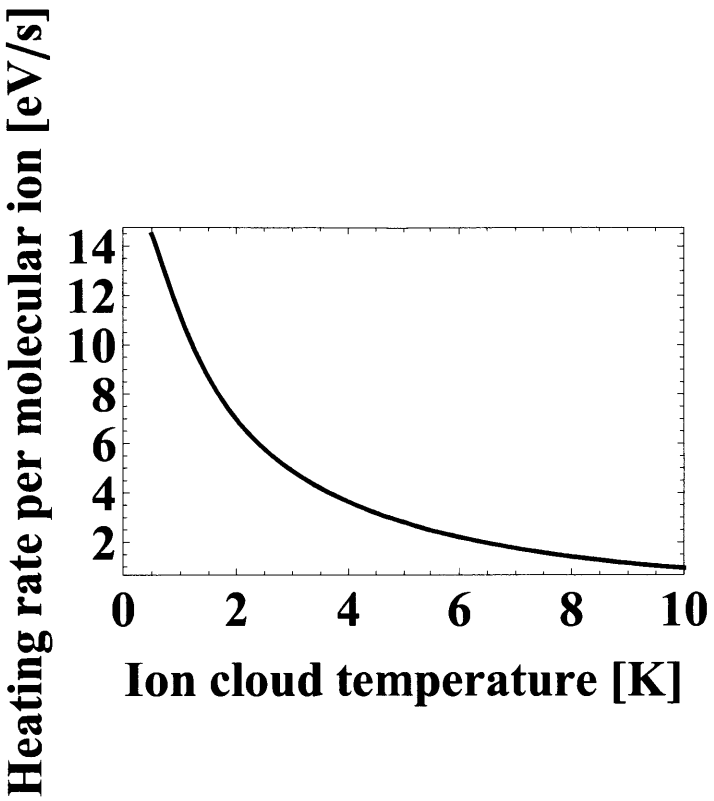


```
(*plots the the population inversion*)

ClearAll[rh, v, l]

SetDirectory["C:"]

Get["n10rat.mx"]

l = Length[n10rat]

func = Interpolation[n10rat, InterpolationOrder → 10]

Plot[func[x], {x, 0.5, 10}, Frame → True, Axes → False,

FrameLabel → {Style["Ion cloud temperature [K]", FontSize → 24, Bold],

Style["J:0-1 Population invertion", FontSize → 24, Bold]},

PlotStyle → Thick, PlotRange → {{0, 10}, All},

BaseStyle->{FontWeight->"Bold", FontSize → 24}]
```

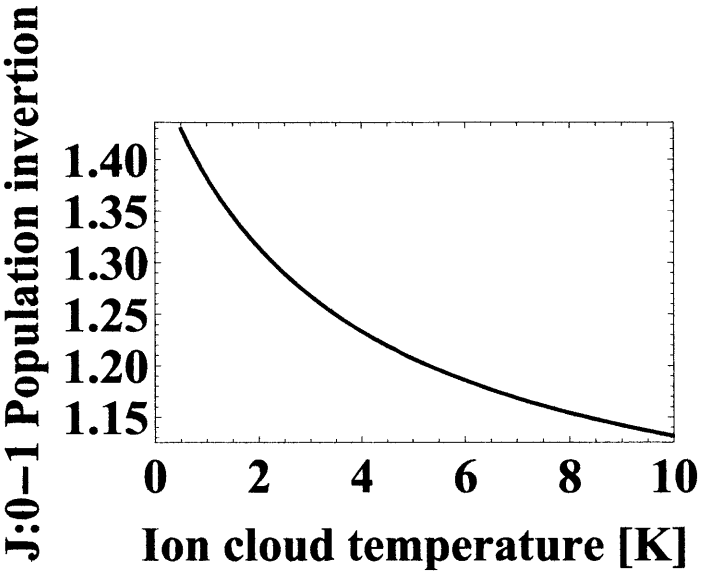
J:0−1 Population invertion
1.40
1.35
1.30
1.25
1.20
1.15
0
2
4
6
8
10
Ion cloud temperature [K]

Appendix C

Numerical evaluation of cavity assisted side band heating rates

The following is Mathematica 7 code for the numerical solution to the microwave cavity assisted heating rate coefficient as presented in Section 3.4.

(*set up the numerical parameters of the problem*)

$\mathbf{modecm} = 2\pi 10^6;$

$\mathbf{modebm} = \mathbf{modecm} * \sqrt{\frac{1+\sqrt{1-\frac{3\mu}{M}}}{1-\sqrt{1-\frac{3\mu}{M}}}};$

$\mathbf{g0} = \text{“16574.4”};$

$\omega_C = 2\pi 6.52 * 10^9;$

$\omega_0 = 2\pi 6.52 * 10^9;$

$Q = 10^6;$

$T = 500\ 10^{-3};$

$\mathbf{y0} = 2\ 10^{-6};$

$\kappa = 2\,\omega_C / Q;$

$\alpha = 88/123;$

$M = (88 + 123)1.660 * 10^{-27};$

$$\mu = 88 * 123 * \left(1.660 * 10^{-27}\right)^2 \Big/ M;$$

(*define the equations enetering the heating rate coefficient*)

$$n_{\text{th}} = \frac{1}{\text{Exp}\left[\frac{1.054*10^{-34}\omega_C}{1.38*10^{-23}T}\right]-1};$$

$$\Omega = \frac{\Omega 0}{\sqrt{2}}\left(1 + \frac{\text{y0}}{6.52*10^9 18\ 10^{-3}}\omega_{\text{MW}}\right);$$

$$g = \frac{\text{g0}}{\sqrt{2}}\left(1 - \frac{\text{y0}}{6.52*10^9 18\ 10^{-3}}\omega_C\right);$$

$$\text{vcm} = \frac{1}{\sqrt{M}}\sqrt{\frac{1+\alpha}{\alpha+\left(1-\alpha+\sqrt{\alpha^2-\alpha+1}\right)^2}}\left(1-\alpha+\sqrt{\alpha^2-\alpha+1}\right);$$

$$\text{vbm} = \frac{1}{\sqrt{M}}\sqrt{\frac{1+\alpha}{\alpha+\left(1-\alpha-\sqrt{\alpha^2-\alpha+1}\right)^2}}\left(1-\alpha-\sqrt{\alpha^2-\alpha+1}\right);$$

$$\text{etamwcm} = \frac{\Omega 0}{\sqrt{2}}\left(\frac{1}{6.52*10^9 18\ 10^{-3}}\omega_{\text{MW}}\right)\text{vcm}\sqrt{\frac{1.054*10^{-34}}{2\text{Abs}[\omega_i]}};$$

$$\text{etacbm} = \frac{\text{g0}}{\sqrt{2}}\left(\frac{1}{6.52*10^9 18\ 10^{-3}}\omega_C\right)\text{vbm}\sqrt{\frac{1.054*10^{-34}}{2\text{Abs}[\omega_{\text{bm}}]}};$$

$$\text{etaccm} = \frac{\text{g0}}{\sqrt{2}}\left(\frac{1}{6.52*10^9 18\ 10^{-3}}\omega_C\right)\text{vcm}\sqrt{\frac{1.054*10^{-34}}{2\text{Abs}[\omega_{\text{cm}}]}};$$

S1 =

etamw^2

$$\left(\frac{1}{4}\right.$$

$$\left(\left(\left(g^2\text{Re}\left[\frac{\frac{2\Omega^2}{\frac{\kappa}{2}+i\left(\omega_C-\omega_{\text{MW}}\right)}+\frac{\left(-\omega_0+\omega_{\text{MW}}+\sqrt{\Omega^2+\left(-\omega_0+\omega_{\text{MW}}\right)^2}\right)^2}{\frac{\kappa}{2}-i\left(-\omega_C+\omega_{\text{MW}}-\sqrt{\Omega^2+\left(-\omega_0+\omega_{\text{MW}}\right)^2}\right)}+\frac{\left(-\omega_0+\omega_{\text{MW}}-\sqrt{\Omega^2+\left(-\omega_0+\omega_{\text{MW}}\right)^2}\right)^2}{\frac{\kappa}{2}-i\left(-\omega_C+\omega_{\text{MW}}+\sqrt{\Omega^2+\left(-\omega_0+\omega_{\text{MW}}\right)^2}\right)}}{\Omega^2+\left(-\omega_0+\omega_{\text{MW}}\right)^2}\right]\right.\right.$$

$$\left.\left.\left.(1+2n_{\text{th}})\left(1-\frac{\Omega^2}{\Omega^2+\left(-\omega_0+\omega_{\text{MW}}\right)^2}\right)\left(2-\frac{\Omega^2}{\Omega^2+\left(-\omega_0+\omega_{\text{MW}}\right)^2}\right)\right.\right.\right.$$

$$\left.\left.\left.\left(\frac{n_{\text{th}}}{1+2n_{\text{th}}}+\frac{1}{2(1+2n_{\text{th}})\left(2-\frac{\Omega^2}{\Omega^2+\left(-\omega_0+\omega_{\text{MW}}\right)^2}\right)}\right)\right)\right) \Big/ \left(4\left(\omega_i^2+\frac{1}{64}g^4\right.\right.$$

$$\text{Re}\left[\left(\frac{2\Omega^2}{\frac{\kappa}{2}+i\left(\omega_C-\omega_{\text{MW}}\right)}+\frac{\left(-\omega_0+\omega_{\text{MW}}+\sqrt{\Omega^2+\left(-\omega_0+\omega_{\text{MW}}\right)^2}\right)^2}{\frac{\kappa}{2}-i\left(-\omega_C+\omega_{\text{MW}}-\sqrt{\Omega^2+\left(-\omega_0+\omega_{\text{MW}}\right)^2}\right)}+\right.\right.$$

$$\left.\left.\frac{\left(-\omega_0+\omega_{\text{MW}}-\sqrt{\Omega^2+\left(-\omega_0+\omega_{\text{MW}}\right)^2}\right)^2}{\frac{\kappa}{2}-i\left(-\omega_C+\omega_{\text{MW}}+\sqrt{\Omega^2+\left(-\omega_0+\omega_{\text{MW}}\right)^2}\right)}\right) \Big/$$

$$\left.\left.\left(\Omega^2+\left(-\omega_0+\omega_{\text{MW}}\right)^2\right)\right]^2(1+2n_{\text{th}})^2\left(2-\frac{\Omega^2}{\Omega^2+\left(-\omega_0+\omega_{\text{MW}}\right)^2}\right)^2\right)\right)+$$

$$\left(g^2\right.$$

$$\mathrm{Re}\Bigg[\frac{\frac{2\Omega^2}{\frac{\kappa}{2}+i(\omega_C-\omega_{MW})}+\frac{\left(-\omega_0+\omega_{MW}+\sqrt{\Omega^2+(-\omega_0+\omega_{MW})^2}\right)^2}{\frac{\kappa}{2}-i\left(-\omega_C+\omega_{MW}-\sqrt{\Omega^2+(-\omega_0+\omega_{MW})^2}\right)}+\frac{\left(-\omega_0+\omega_{MW}-\sqrt{\Omega^2+(-\omega_0+\omega_{MW})^2}\right)^2}{\frac{\kappa}{2}-i\left(-\omega_C+\omega_{MW}+\sqrt{\Omega^2+(-\omega_0+\omega_{MW})^2}\right)}}{\Omega^2+(-\omega_0+\omega_{MW})^2}\Bigg]$$

$$(1+2n_{th})\left(1-\frac{\Omega^2}{\Omega^2+(-\omega_0+\omega_{MW})^2}\right)\left(2+\frac{\Omega^2}{\Omega^2+(-\omega_0+\omega_{MW})^2}\right)$$

$$\left(\frac{n_{th}}{1+2n_{th}}+\frac{\left(1+\sqrt{\mathrm{Abs}\left[1-\frac{\Omega^2}{\Omega^2+(-\omega_0+\omega_{MW})^2}\right]}\right)^2}{2(1+2n_{th})\left(2-\frac{\Omega^2}{\Omega^2+(-\omega_0+\omega_{MW})^2}\right)}\right)\Bigg/$$

$$(4$$

$$\left(\frac{1}{64}g^4\mathrm{Re}\left[\left(\frac{2\Omega^2}{\frac{\kappa}{2}+i(\omega_C-\omega_{MW})}+\frac{\left(-\omega_0+\omega_{MW}+\sqrt{\Omega^2+(-\omega_0+\omega_{MW})^2}\right)^2}{\frac{\kappa}{2}-i\left(-\omega_C+\omega_{MW}-\sqrt{\Omega^2+(-\omega_0+\omega_{MW})^2}\right)}+\right.\right.$$

$$\left.\frac{\left(-\omega_0+\omega_{MW}-\sqrt{\Omega^2+(-\omega_0+\omega_{MW})^2}\right)^2}{\frac{\kappa}{2}-i\left(-\omega_C+\omega_{MW}+\sqrt{\Omega^2+(-\omega_0+\omega_{MW})^2}\right)}\right)\Bigg/$$

$$\left.(\Omega^2+(-\omega_0+\omega_{MW})^2)\right]^2(1+2n_{th})^2\left(2+\frac{\Omega^2}{\Omega^2+(-\omega_0+\omega_{MW})^2}\right)^2+$$

$$\left.\left(\omega_i-\sqrt{\Omega^2+(-\omega_0+\omega_{MW})^2}\right)^2\right)\Bigg)+$$

$$(g^2$$

$$\mathrm{Re}\Bigg[\frac{\frac{2\Omega^2}{\frac{\kappa}{2}+i(\omega_C-\omega_{MW})}+\frac{\left(-\omega_0+\omega_{MW}+\sqrt{\Omega^2+(-\omega_0+\omega_{MW})^2}\right)^2}{\frac{\kappa}{2}-i\left(-\omega_C+\omega_{MW}-\sqrt{\Omega^2+(-\omega_0+\omega_{MW})^2}\right)}+\frac{\left(-\omega_0+\omega_{MW}-\sqrt{\Omega^2+(-\omega_0+\omega_{MW})^2}\right)^2}{\frac{\kappa}{2}-i\left(-\omega_C+\omega_{MW}+\sqrt{\Omega^2+(-\omega_0+\omega_{MW})^2}\right)}}{\Omega^2+(-\omega_0+\omega_{MW})^2}\Bigg]$$

$$(1+2n_{th})\left(1-\frac{\Omega^2}{\Omega^2+(-\omega_0+\omega_{MW})^2}\right)\left(2+\frac{\Omega^2}{\Omega^2+(-\omega_0+\omega_{MW})^2}\right)$$

$$\left(\frac{n_{th}}{1+2n_{th}}+\frac{\left(1-\sqrt{\mathrm{Abs}\left[1-\frac{\Omega^2}{\Omega^2+(-\omega_0+\omega_{MW})^2}\right]}\right)^2}{2(1+2n_{th})\left(2-\frac{\Omega^2}{\Omega^2+(-\omega_0+\omega_{MW})^2}\right)}\right)\Bigg/$$

$$(4$$

$$\left(\frac{1}{64}g^4\mathrm{Re}\left[\left(\frac{2\Omega^2}{\frac{\kappa}{2}+i(\omega_C-\omega_{MW})}+\frac{\left(-\omega_0+\omega_{MW}+\sqrt{\Omega^2+(-\omega_0+\omega_{MW})^2}\right)^2}{\frac{\kappa}{2}-i\left(-\omega_C+\omega_{MW}-\sqrt{\Omega^2+(-\omega_0+\omega_{MW})^2}\right)}+\right.\right.$$

$$\left.\frac{\left(-\omega_0+\omega_{MW}-\sqrt{\Omega^2+(-\omega_0+\omega_{MW})^2}\right)^2}{\frac{\kappa}{2}-i\left(-\omega_C+\omega_{MW}+\sqrt{\Omega^2+(-\omega_0+\omega_{MW})^2}\right)}\right)\Bigg/$$

$$\left.(\Omega^2+(-\omega_0+\omega_{MW})^2)\right]^2(1+2n_{th})^2\left(2+\frac{\Omega^2}{\Omega^2+(-\omega_0+\omega_{MW})^2}\right)^2+$$

$$\left.\left.\left(\omega_i+\sqrt{\Omega^2+(-\omega_0+\omega_{MW})^2}\right)^2\right)\right)\Bigg)\Bigg);$$

$$S2 = etac^2 \left(\frac{\Omega^2 \left(\frac{\kappa n_{th}}{\frac{\kappa^2}{4}+(\omega_C+\omega_i-\omega_{MW})^2} + \frac{\kappa(1+n_{th})}{\frac{\kappa^2}{4}+(-\omega_C+\omega_i+\omega_{MW})^2} \right)}{4(\Omega^2+(-\omega_0+\omega_{MW})^2)} + \right.$$

$$\frac{\kappa n_{th} \left(-\frac{\Omega^4}{2(1+2n_{th})(\Omega^2+2(-\omega_0+\omega_{MW})^2)} + \frac{(1+n_{th})\left(-\omega_0+\omega_{MW}-\sqrt{\Omega^2+(-\omega_0+\omega_{MW})^2}\right)^2}{1+2n_{th}} \right)}{4(\Omega^2+(-\omega_0+\omega_{MW})^2)\left(\frac{\kappa^2}{4}+\left(\omega_C+\omega_i-\omega_{MW}-\sqrt{\Omega^2+(-\omega_0+\omega_{MW})^2}\right)^2\right)} +$$

$$\frac{\kappa(1+n_{th}) \left(\frac{\Omega^4}{2(1+2n_{th})(\Omega^2+2(-\omega_0+\omega_{MW})^2)} + \frac{n_{th}\left(-\omega_0+\omega_{MW}+\sqrt{\Omega^2+(-\omega_0+\omega_{MW})^2}\right)^2}{1+2n_{th}} \right)}{4(\Omega^2+(-\omega_0+\omega_{MW})^2)\left(\frac{\kappa^2}{4}+\left(-\omega_C+\omega_i+\omega_{MW}-\sqrt{\Omega^2+(-\omega_0+\omega_{MW})^2}\right)^2\right)} +$$

$$\frac{\kappa n_{th} \left(-\frac{\Omega^4}{2(1+2n_{th})(\Omega^2+2(-\omega_0+\omega_{MW})^2)} + \frac{(1+n_{th})\left(-\omega_0+\omega_{MW}+\sqrt{\Omega^2+(-\omega_0+\omega_{MW})^2}\right)^2}{1+2n_{th}} \right)}{4(\Omega^2+(-\omega_0+\omega_{MW})^2)\left(\frac{\kappa^2}{4}+\left(\omega_C+\omega_i-\omega_{MW}+\sqrt{\Omega^2+(-\omega_0+\omega_{MW})^2}\right)^2\right)} +$$

$$\left. \frac{\kappa(1+n_{th}) \left(\frac{\Omega^4}{2(1+2n_{th})(\Omega^2+2(-\omega_0+\omega_{MW})^2)} + \frac{n_{th}\left(-\omega_0+\omega_{MW}-\sqrt{\Omega^2+(-\omega_0+\omega_{MW})^2}\right)^2}{1+2n_{th}} \right)}{4(\Omega^2+(-\omega_0+\omega_{MW})^2)\left(\frac{\kappa^2}{4}+\left(-\omega_C+\omega_i+\omega_{MW}+\sqrt{\Omega^2+(-\omega_0+\omega_{MW})^2}\right)^2\right)} \right);$$

$$S3 = \frac{etaccm^2}{4}\left(\frac{\kappa}{\kappa^2/4+(\omega_{cm}-\omega_0+\omega_{MW})^2} - \frac{\kappa}{\kappa^2/4+(\omega_{cm}+\omega_0-\omega_{MW})^2}\right) +$$

$$\frac{etacbm^2}{4}\left(\frac{\kappa}{\kappa^2/4+(\omega_{bm}-\omega_0+\omega_{MW})^2} - \frac{\kappa}{\kappa^2/4+(\omega_{bm}+\omega_0-\omega_{MW})^2}\right);$$

$$Sa[x\_, y\_, \Omega 0\_] = S1/.\{\omega_{MW} \to x, \omega_i \to y\};$$

$$Sb[x\_, y\_, \Omega 0\_] = S2/.\{\omega_{MW} \to x, \omega_i \to y\};$$

$$Sc[x\_, y\_, z\_] = S3/.\{\omega_{MW} \to x, \omega_{cm} \to y, \omega_{bm} \to z\};$$

$$A[x\_, \Omega 0\_] = Sb[x, mode, \Omega 0] - Sb[x, -mode, \Omega 0];$$

(*plot the heating rate coefficeint versus microwave frequency*)

Plot $\left[-Sc\left[x * 10^6 + \omega_C, modecm, modebm\right], \{x, -4\pi, 4\pi\}, PlotPoints \to 100,\right.$

$PlotRange \to \{-0.6, 0.6\}, Frame \to True,$

$FrameLabel \to \{$"Microwave detuning Δ=$\omega_{MW} - \omega_0$ (MHz)",

"Cooling/Heating rate (s^{-1})"$\}$, $LabelStyle \to \{Bold, 20\},$

$FrameStyle \to Thick, PlotStyle \to \{Thick\}]$

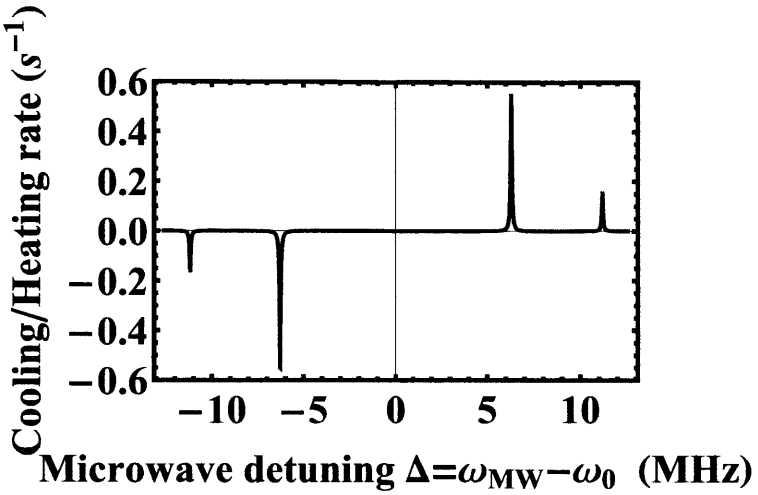
Cooling/Heating rate (s^{-1})
0.6
0.4
0.2
0.0
−0.2
−0.4
−0.6
−10
−5
0
5
10
Microwave detuning $\Delta=\omega_{MW}-\omega_0$ (MHz)